Development of a Bone Tissue-Engineered Construct to Enhance New Bone Formation in Revision Total Hip Replacement

Elena García Gareta

Submitted for the degree of Doctor of Philosophy

Department of Biomedical Engineering
University College London

SEPTEMBER 2011

John Scales Centre for Biomedical Engineering
Institute of Orthopaedics and Musculoskeletal Science
University College London
Royal National Orthopaedic Hospital
Stanmore HA7 4LP
United Kingdom

I, Elena García Gareta, confirm that the work presented in this thesis is my own. Where information has been derived from other sources, I confirm that this has been indicated in the thesis.

ABSTRACT

The main issue associated with revision total hip replacements (rTHRs) is how to generate new bone and restore bone stock for fixation of the revision stem. Bone tissue engineering (BTE) seeks the generation of constructs *ex vivo* in order to replace damaged or lost bone. The aim of this thesis was to develop a bone tissue-engineered construct with a calcium-phosphate (CaP) coated porous metal scaffold seeded throughout its structure with mesenchymal stem cells (MSCs) in order to enhance new bone formation at rTHRs. The study had *in vitro* and *in vivo* phases.

For the *in vitro* phase, CaP coatings by biomimetic and electrochemical methods on the surface of titanium and tantalum discs were investigated and seeded with MSCs under static culture conditions. Different coating methods produced different morphologies and compositions with biomimetic coatings enhancing MSCs growth while the electrochemical ones enhanced their osteogenic potential. An electrochemically CaP coated porous titanium cylinder was seeded with MSCs and dynamically cultured in a perfusion bioreactor, showing an increased MSCs proliferation and osteogenic differentiation and an even distribution of cells throughout the scaffolds compared to statically cultured constructs.

Tissue-engineered constructs in the perfusion bioreactor were evaluated *in vivo* by implantation in the medial femoral condyle of sheep with and without gap. Their osseointegration and implant-bone fixation strength were compared to non tissue-engineered constructs. The results showed that the addition of MSCs to the scaffolds did not significantly increase osseointegration or implant-bone fixation strength. However, in the defects with gap the tissue-engineered constructs showed a higher implant-bone contact area and therefore higher forces were necessary to push the tissue-engineered implants out of the bone in the defects with gap than for the non tissue-engineered ones.

In conclusion, BTE can be applied in order to develop constructs with a clinical application in rTHRs where a lack of bone stock is problematic.

ACKNOWLEDGEMENTS

I would like to thank Dr Jia Hua for his always wise and kind supervision. His infinite patience and constant questioning made me do my best every day and if I have become a better scientist much of the credit is due to him. Thank you for making my PhD experience so challenging, I feel privileged for having you as my supervisor.

This thesis would not have been possible without the opportunity Professor Blunn gave me to be part of this excellent department. Thank you very much Professor Blunn for your support, vast knowledge, supervision and inspiration throughout this thesis. I will always feel proud of introducing myself as one of your students.

Thank you to Mark Harrison and Keith Rayner for technical support, I could have never completed my work without all those bits and pieces you made for me. Thank you to everybody at the Institute of Orthopaedics for being good friends and colleagues, particularly Rebecca Porter for rescuing me and my baby cells in countless occasions. Thank you to everybody at the Royal Veterinary College who made possible the last part of my thesis, particularly to Gillian Hughes for her professionalism and cool music.

Thank you Josie, Sophie, Annie and Michelle for your loveliness, help and never-ending smiles.

Thank you Sorousheh and Kevin for being the best of friends and taking me for lunch, dinner or drinks whenever needed, you will always be in my heart. Thank you Siva for making me feel part of this place from day one. Thank you Lindsey for being so lovely since the first minute I arrived in the Zimmer lab. Thank you Jonathan and Carolina for your intelligent humour. Thank you Michelle for all those improvised breakfasts and cool videos. Thanks to all the MD students for showing me a different perspective of this research field. Finally, thank you Robert and Henry for standing me while writing up my thesis.

Thank you to my friends for listening and supporting me, your advice and patience have been invaluable.

Thank you mamá, papá and niña for your love, support and faith in me. Without your love and pride in me my life does not make any sense. This thesis is for you.

And thank you my husband, my love, for being by my side every day throughout this experience, for listening to my presentations over and over again, for weeping my tears when things were tough, for celebrating my achievements with me and for loving me like only you do: sin ti no soy nada.

TABLE OF CONTENTS:

LIST OF FIGURES:

LIST OF TABLES:

CHAPTER 1:

Introduction

1.1 OVERVIEW

Revision total hip replacements (THRs) due to aseptic loosening, account for 10% of the total hip replacement procedures, with over 7,000 operations per year in England and Wales (National Joint Registry for England and Wales: 7th Annual Report, 2010). Aseptic loosening is caused by osteolysis, which is induced by wear particles from the joint bearing surface materials. It results in bone defects and a reduction of the bone stock necessary for implant fixation in revision THRs (Cooper *et al*. 1992; Harris 1995; Harris 2001; Amstutz *et al*. 1992; Heisel *et al*. 2003; Shen *et al*. 2006). As a result, the clinical results for revision THRs are usually inferior to the primary THRs. Therefore, one of the main issues associated with revision THR is the generation of new bone and restoration of the bone stock for fixation of the revision stem.

Several techniques are used today in order to reconstitute the bone stock at revision operations, such as bone impaction grafting using allograft or autograft (Vaccaro 2002; Moore *et al*. 2001; Delloye *et al*. 2007; Gie *et al*. 1993a; Bohner 2000; Habibovic and de Groot 2007). However, these techniques present some disadvantages. For instance, the supply of bone and donor site morbidity limit the use of autograft (Goulet *et al*. 1997; Moore *et al*. 2001), while the disadvantages associated with the use of allograft are disease transmission and differences in graft preparation techniques which lead to inconsistency and immune response (Delloye *et al*. 2007; Moore *et al*. 2001).

Tissue engineering is a research field based on understanding how tissue formation and regeneration work and its aim is to induce new functional tissues (Langer and Vacanti, 1993; Lanza *et al*. 2000). Specifically bone tissue engineering (BTE) uses constructs generated *ex vivo* in order to replace damaged or lost bone (Rose and Oreffo 2002; Salgado *et al*. 2004; Karageorgiou and Kaplan 2005; Fröhlich *et al*. 2008). Bone is a specialised three dimensional (3D) connective tissue, dynamic and highly vascularised involved in a constant cycle of renewal, undergoing continuous remodelling throughout life. Therefore a scaffold with a 3D structure that mimics bone is necessary to grow new tissue. In this structure cells can proliferate and produce matrix which forms a 3D structure.

Scaffolds for BTE should mimic bone morphology and mechanical properties. They must be biocompatible, porous with an optimum pore size, possess certain surface properties, osteoconductive and osteoinductive (Salgado *et al*. 2004; Fröhlich *et al*. 2008; Yang *et al*. 2001; Lanza *et al*. 2000; Schieker *et al*. 2006; Rose and Oreffo 2002). It is very important to select an appropriate material for the scaffold used for BTE purposes since its characteristics will affect the scaffold application. So far, several materials from both natural and synthetic origins have been investigated. They include biodegradable polymers, ceramics and metals. Combinations of these materials or composites, such as calcium-phosphate coating of metals, have also been proposed for BTE applications (Karageorgiou and Kaplan 2005).

In the field of BTE there is a special interest in the adult stem cells located in the bone marrow, known as mesenchymal stem cells (MSCs) as they can differentiate into lineages of the mesenchymal tissues such as bone or tendon (Pittenger *et al*. 1999; Caplan 1991; Lanza *et al*. 2000).

The biological environment within the bone tissue is a dynamic interaction between active cells that experience mechanical forces and a 3D matrix architecture that is in continuous change. Therefore, in order to engineer bone tissue constructs *ex vivo* it is necessary to develop culture systems that mimic the dynamics of the *in vivo* biological environment (Lanza *et al*. 2000; Kale *et al*. 2000). The current standard tissue culture techniques are not adequate for BTE purposes due to a lack of efficient transport of nutrients and removal of waste products. They are static and thus they do not mimic the dynamics found *in vivo* (Bancroft *et al*. 2003; Martin *et al*. 2004). A solution to overcome these issues is the design and development of bioreactors, which would provide an efficient mass transfer of nutrients and metabolites and mechanical stimulation to the cells by way of fluid shear stress for the engineering of bone tissue (Martin *et al*. 2004; Salgado *et al*. 2004; Ikada 2006). For example, perfusion bioreactor systems have been successfully used for the development of bone tissue-engineered constructs as they provide an enhanced transport of nutrients to the interior of 3D scaffolds as well as mechanical stimulation to the cells by the fluid shear stress due to perfusion of the media (Bancroft *et al*. 2003; Sikavitsas *et al*. 2003).

Finally, the development of bone tissue-engineered constructs requires the evaluation of their performance on preclinical studies prior to evaluation in human subjects. The criteria associated with the choice of an experimental model must be related to the functional application of the construct: the animal model must be biologically analogous and recognizable as a suitable challenge to human physiology (Goldstein 2002).

This thesis proposes a novel tissue engineering approach to address the problem associated with poor bone stock and fixation of implants in patients undergoing revision operations.

1.2 BONE TISSUE

1.2.1 Bone Definition and Function

Bone is a specialised connective tissue which forms the basis of the skeleton. It serves to protect vital internal organs and provides a framework for physical support, locomotion and related movement. Bone tissue has a very important function as reservoir of inorganic ions, which are recruited by various and complex physiological systems when required. Bone provides a source of hematopoietic and mesenchymal stem cells. Bone is a dynamic and highly vascularised tissue involved in a constant cycle of renewal, undergoing continuous remodelling throughout life (Weiner and Wagner 1998; Palmer *et al*. 2008; Hayes and Bouxsein 1997).

1.2.2 Bone Physiology

Normal, mature bones in the human skeleton are composed of two types of bony tissue: cortical or compact bone and cancellous or trabecular bone (Figure 1.1). Both share an identical chemical composition but are macroscopically and microscopically different (Hayes and Bouxsein 1997).

Cortical or compact bone is found along the shaft of the long bones and is the principal component of the flat bones. It has a very dense physical structure comprised of osteons, concentric cylinders of lamellae. Harvasian canals, which are responsible for providing cellular nutrition, can be found at the centre of these structures (Figure 1.1). Approximately 80% of skeletal mass is cortical bone.

On the other hand, *cancellous or trabecular bone* is made of interconnected struts called trabeculae, and therefore this bony tissue is considerable finer in appearance (Figure 1.1). Its physical arrangement of struts interspersed with voids provides for maximum support with a minimum of material. The trabeculae adopt a preferential alignment along the direction of principal mechanical forces. A marrow reservoir and a medullary blood supply are interspersed between the trabeculae. Trabecular bone is found at the epiphyses of the long bones and in the vertebrae of the spinal column.

As observed from Figure 1.1, the periosteum covers the external surface of long bones. The periosteum consists of a fibrous layer and an inner cambial layer and its

functions are to supply nerves as well as blood and lymphatic vessels to the bone. The periosteum is also a source of osteoblasts.

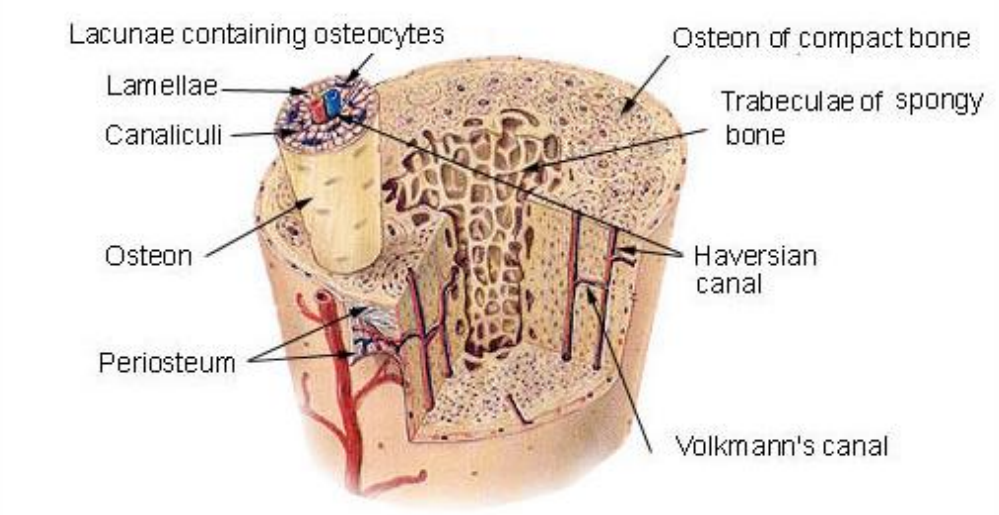

Figure 1.1 Physiology of bone
(http://www.web-books.com/eLibrary/Medicine/Physiology/Skeletal/Skeletal.htm)

1.2.3 Bone Cells

There are four cell types which have a specific function in bone formation, maintenance and removal: osteoblasts, osteocytes, bone lining cells and osteoclasts.

Osteoblasts are mononuclear cells of mesenchymal origin which are responsible for the formation of the organic matrix of bone, the osteoid. Osteoblasts are also believed to be involved in the mineralization process through regulation of the local calcium and phosphate concentrations (Palmer *et al*. 2008). As the organic matrix becomes mineralised, some osteoblasts are trapped, differentiating into *osteocytes*. These cells appear to be responsible for detecting mechanical stress, then signalling for matrix formation or resorption as necessary (Palmer *et al*. 2008).

Bone lining cells cover the surface of all bones and are involved in bone matrix production and degradation (Palmer *et al*. 2008).

Osteoclasts are developed from a hematopoietic lineage; they are multinucleated, macrophage-like cells which are responsible for bone resorption. This process is

essential for bone remodelling, growth and healing as well as regulating some ions concentration, such as calcium, available to the body (Athanasou 1996; Palmer *et al*. 2008).

1.2.4 Molecular Level of Bone

At a molecular level, bone is a complex mineralised matrix composed of biopolymer and biomineral.

The *biopolymer* mostly consists of collagen type 1, the most abundant protein in the human body. Non-collagenous proteins (NCPs), including bone sialoprotein, osteonectin, osteopontin and osteocalcin, contribute to the biopolymer. NCPs may have a role in crystal nucleation and growth, cell signaling and ion homeostasis, although their specific functions are not well understood yet. Minor amounts of lipids and osteogenic factors, such as bone morphogenetic proteins (BMPs), are also found in this collagenous biopolymer (LeGeros 2008; Palmer *et al*. 2008; Weiner and Wagner 1998).

The *biomineral* present in bone is a calcium phosphate that was identified as an apatite by X-ray diffraction analysis (Figure 1.2). Apatite is a group of phosphate minerals that are found naturally in the Earth's crust. These minerals have an empirical formula: $Ca_5(PO_4)_3(OH,F,Cl)$. Their crystal structure is flexible and they are able to accommodate chemical substitutions (LeGeros 1993; Wopenka and Pasteris 2005). Hydroxyapatite, $Ca_5(PO_4)_3(OH)$ with a Ca/P ratio of 1.67, is the apatite mineral of biological importance due to its similarity with the biomineral present in bone (Harper and Posner 1966; Posner 1969). More specifically, the bone mineral has been identified as a carbonate-substituted hydroxyapatite containing minor and trace substitutions with a Ca/P ratio below or above 1.67, depending on age, specie and type of bone (LeGeros 1993; Wopenka and Pasteris 2005; LeGeros 2008). Apart from carbonate (CO_3^{2-}), the most important minor substitutions are magnesium (Mg^{2+}) and sodium (Na^{+}). These substitutions occur because bone is used by the body as an ion reservoir to maintain homeostasis of elements such as calcium, phosphate or magnesium (LeGeros 1993; Wopenka and Pasteris 2005; LeGeros 2008). The crystals of bone mineral are plate-shaped and their dimensions are in the order of nanometers (30-50nm width and 1.5-5nm thick). This platelet morphology effectively interfaces

with collagen fibrils (Wopenka and Pasteris 2005; Weiner and Wagner 1998). The fact that they are in the nano-meter scale suggests there may be a biological advantage to nanocrystals, which may be the easiest to precipitate at body temperature. The number of substitutions found in bone mineral as well as its nano-sized crystals explain the poor resolution of peaks observed in the lower spectra of Figure 1.2, indicating the biomineral found in bone is not crystalline and it is composed of very small crystals:

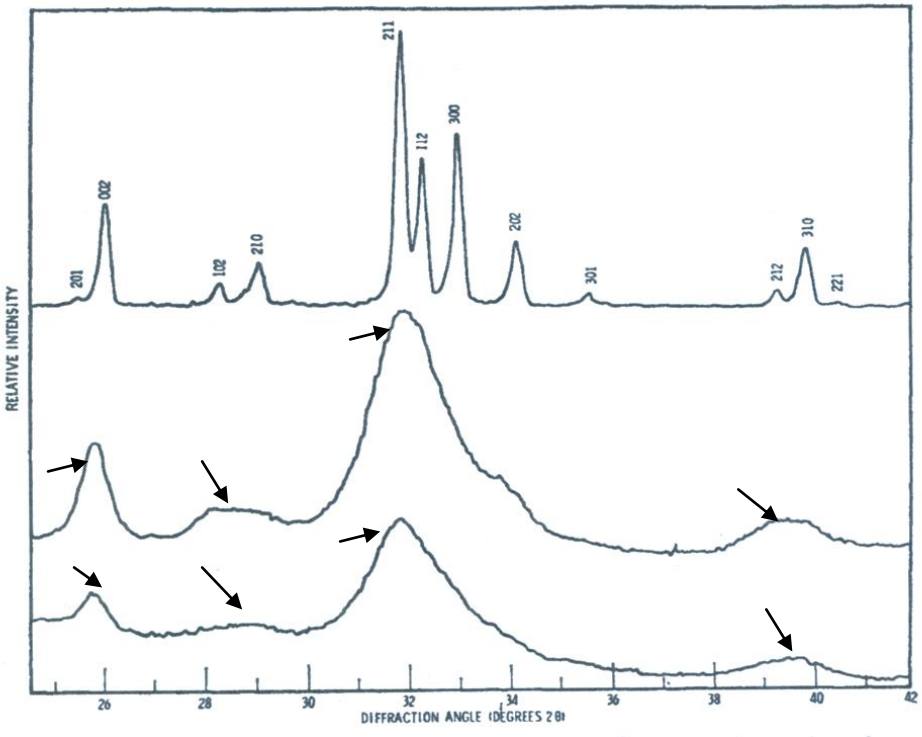

Figure 1.2 X-ray diffraction patterns of powdered bone from human femur diaphysis (lower pattern); 100% crystalline synthetic hydroxyapatite with crystal size comparable to bone biomineral (middle pattern); and crystalline synthetic hydroxyapatite with peaks indexed (upper pattern) (Harper and Posner 1966).
Black arrows point to peaks with poor resolution.

In conclusion, bone is formed of a biomineral, a collagenous biopolymer and cells, which combine to give this tissue its hardness, toughness and self-renewal capacity. (Weiner and Wagner 1998; Hayes and Bouxsein 1997; Posner 1969; Harper and Posner 1966; Wopenka and Pasteris 2005; Athanasou 1996; Palmer *et al*. 2008; LeGeros 1993; LeGeros 2008).

1.3 THE HIP JOINT: ANATOMY AND PATHOLOGY

The anatomy of the hip joint constitutes a ball, known as the femoral head, and a socket, called the acetabulum. The femoral head is the proximal extension of the femur and fits closely into the acetabulum, a depression in the pelvic bone (Figure 1.3). A thin layer of cartilage covers the articulating surfaces of both the femoral head and the acetabulum, allowing them to glide against one another.

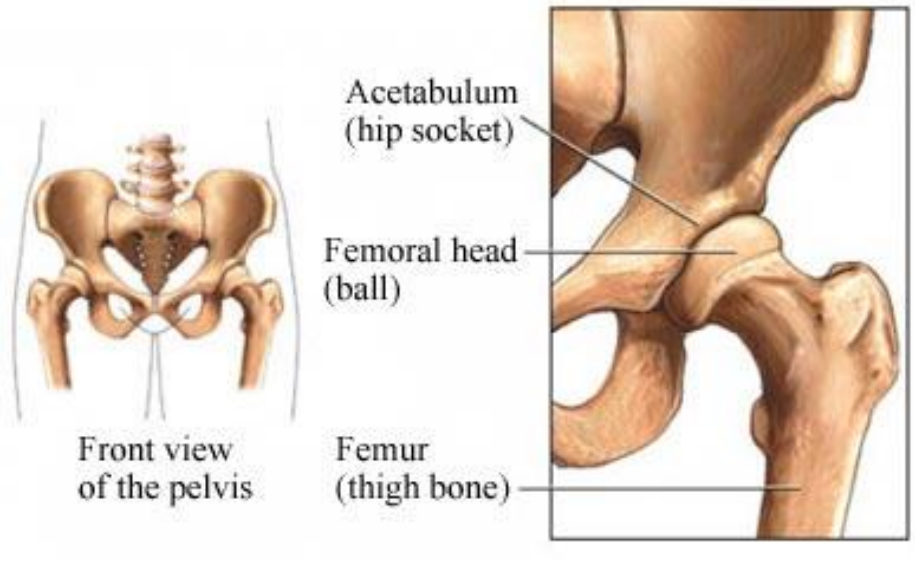

Figure 1.3 Anatomy of the hip joint
(http://www.empowher.com/media/reference/hip-dislocation)

The two main reasons to undergo hip surgery are pain relief and improvement in hip function. Hip pain and poor mobility is usually associated with diseases such as osteoarthritis, rheumatoid arthritis, trauma or osteonecrosis (Van Dijk *et al*. 2006). In a total hip replacement (THR) the damaged hip joint is removed and replaced with an artificial hip. The aim of this procedure is to eliminate pain, restore the resilience and range of movement as closely as possible to those of a fully functional natural hip joint.

1.3.1 Primary THR

In this procedure the damaged parts of the hip joint, including the cartilage covering the articulating surfaces of the joint, are removed and replaced with a prosthetic implant. The prosthetic implant used in THR consists of the femoral component, composed of a stem and femoral head, and the acetabular component or cup usually comprised of a shell and liner (Figure 1.4).

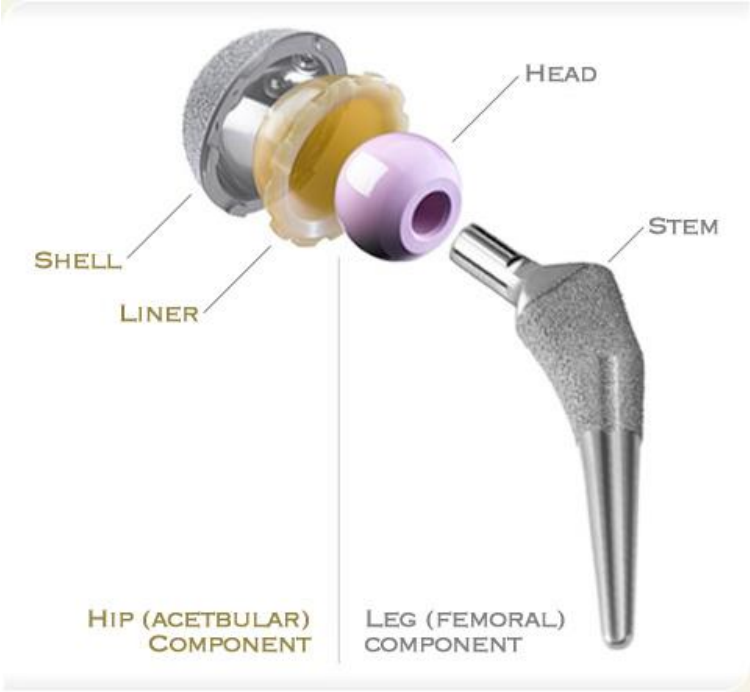

Figure 1.4 Components of the prosthetic implant used in total hip replacement: on the left side of the scheme the acetabular component or cup, composed of a shell and liner, is shown while the femoral component, consisting of a stem and femoral head, is observed on the right side of the scheme (http://evertsmith.com/innovations).

The acetabular cup is the component placed into the hip socket. They can be monobloc or modular. Monobloc cups are either polyethylene, cemented in place, or metal, coated on its surface for direct bone apposition. Modular cups consist of two pieces: a shell and an inside liner. The shell is made of metal with a porous coating on the outside and a locking mechanism in the inside to accept a liner. The liner can be made of polyethylene, metal or ceramic (Heisel *et al*. 2003).

The femoral component fits in the femur, where the femoral head is removed and the femoral canal shaped to accept the femoral stem with modular femoral head. There are two types of fixation, cemented or uncemented. In cemented fixation acrylic bone cement is used to form a mantle between the stem and bone. In uncemented fixation the femoral stem has surface coatings that promote bone ingrowth so called osteointegration (Geesink 2002).

The materials used for the stems are titanium, cobalt-chromium or stainless steel. The femoral component can be monolithic, with the femoral head and stem as one piece. More commonly the femoral component is modular, with an attached femoral head which can be made of metal or ceramic. The commonest combinations of bearing surfaces are metal on polyethylene, metal on metal, ceramic on ceramic and ceramic on polyethylene (Heisel *et al*. 2003; Amstutz and Grigoris 1996).

Figure 1.5 shows a post-operative radiograph of a THR where the left hip has been replaced by a cementless modular implant. The femoral stem is made of metal while the femoral head is made of ceramic and articulates against a ceramic acetabular cup:

Figure 1.5 Post-operative radiograph of a total hip replacement: the left hip has been replaced by a cementless prosthetic implant consisting of a metal femoral stem and ceramic head articulating against a ceramic acetabular cup. (http://manchesterhiparthroscopy.com/complex-hip-replacements/protusio).

1.3.2 Failure of THRs by Osteolysis

Osteolysis is induced by wear particles from the joint bearing surface materials' prosthesis and results in a reduction of the bone stock necessary for implant fixation in THRs (Cooper *et al*. 1992; Harris 1995; Harris 2001; Amstutz *et al*. 1992; Heisel *et al*. 2003).

Osteolysis is triggered by particles of polyethylene, cement and metal released by the articulating movement of the femoral head against the acetabular cup. These wear particles are able to travel between the implant interfaces coming into contact with biological tissues. Inflammatory cells such as macrophages and giant cells engulf these wear particles, thus activating the release of bone resorbing mediators interleukin-1 (IL-1) and tumour necrosis factor (TNF-α). These mediators stimulate monocytes and macrophages to differentiate into osteoclasts, which are multinucleated, macrophage-like cells responsible for bone resorption (Amstutz *et al*. 1992; Athanasou 1996).

There is also evidence in the literature that osteolysis is triggered by hydrostatic pressure around the prosthetic hip components after THR. Skoglund and Aspenberg 2003 compared the resorptive effect of cement wear particles with pressure in a rat tibial dyaphisis model, and reported that the osteolytic process was more greatly influenced by biomechanical stimuli (pressurised fluid) than the cement wear particles.

Erosive inflamed bone resorption is the most aggressive form of osteolysis where the loosened implant is eventually surrounded by a fibrous membrane. This fibrous membrane can be detected on radiographs by the formation of a progressive radiolucent line around the implant (Buma and Gardeniers 1996). Figure 1.6 displays a radiograph of a hip prosthesis showing aseptic loosening, where the radiolucent lines around the implant are indicated by the black arrows:

Figure 1.6 Radiograph of a total hip replacement showing aseptic loosening by osteolysis, indicated by the presence of radiolucent lines around the implant (black arrows).
(Shen *et al*. 2006)

Osteolysis can be observed in both cemented and uncemented femoral components indicating that the released wear particles can access the bone implant interface in spite of improvements in fixation techniques and surface coatings (Coathup *et al*. 2005; Buma and Gardeniers 1995; Amstutz *et al*. 1992; Amstutz and Grigoris 1996).

1.3.3 Revision THR

In revision THRs the previously loosened stem is replaced in order to restore function. The main objectives in revision THRs are to achieve immediate fixation, long term stability and the restoration and maintenance of bone stock (Clohisy *et al*. 2004). The main issue associated with revision THR is insufficient bone stock available for fixation of the revision stem. Moreover, further loss of bone occurs when the primary prosthesis is removed during revision surgery, which constitutes an additional challenge for the surgeon in reconstituting bone stock. Several techniques are applied today in order to reconstitute the bone stock at revision operations: bone transplant of autograft or allograft, impaction grafting and use of bone substitutes (Leopold *et al*. 2000; Goldberg 2000).

Autograft

Autograft is transplanted fresh cortical or trabecular bone or a combination of both bony tissues from one site in the body, such as the iliac crest, to another within the same patient. Autograft is considered the "gold standard" and the most effective method for bone regeneration as it provides osteoconduction, to promote direct bonding with bone tissue, and osteoinduction, to induce local stem cells to differentiate into bone cells, without any associated immune response (Vaccaro 2002; Moore *et al*. 2001). However, this technique offers several disadvantages such as limited bone supply and donor site morbidity (Goulet *et al*. 1997; Moore *et al*. 2001).

Allograft

Allograft is transplanted cortical/trabecular bone or demineralised bone matrix from a living/cadaver donor to a patient. They are usually harvested from the removed femoral heads of patients undergoing primary THR or from sections of the pelvis from cadaveric donors. Allograft possesses osteoconductive properties and when used as fresh frozen or in a demineralised form also has osteoinductive properties (Delloye *et al*. 2007; Moore *et al*. 2001). The disadvantages associated with the use of allograft are disease transmission, bacterial infection, differences in graft preparation techniques which lead to inconsistency, immune response, fracture and non-union due to differences in bone quality between the donors and the patient (Delloye *et al*. 2007; Moore *et al*. 2001).

Impaction Grafting

Impaction grafting in the femur consists of implantation of bone graft by impaction into the endosteal cavity aiming at creating a neo-medullary canal in the femoral shaft. The loose prosthesis along with all cement, debris, granulomata and fibrous membrane is removed. The shaping of the neo-medullary canal comes from a series of tapers that allow the autograft or allograft to be impacted against the walls of the femoral canal by using force. The cemented component is then introduced (Gie *et al*. 1993a; Gie *et al*. 1993b; Leopold *et al*. 2000; Sloof *et al*. 1984; Ling *et al*. 1993). In some instances uncemented implants are used. The main drawbacks with the use of this technique are major complications of bone fracture and massive early subsidence of the femoral stem (Gie *et al*. 1993a; Ling *et al*. 1993; Ullmark and Linder 1998).

Bone Substitutes

The use of bone substitutes aims at overcoming the disadvantages of using autograft and allograft. The mineral composition of natural bone and the structure of interconnected struts of trabecular bone have provided the model for the development of bone substitute materials.

Calcium phosphate materials are the most popular bone substitutes due to their chemical similarity with bone mineral, low cost and plentiful amounts (Bohner 2000; Brandoff *et al*. 2008). Synthetic hydroxyapatite (HA), tricalcium phosphate (TCP) and combinations of them are widely used due to their biocompatibility and osteoconductive properties (Knaack *et al*. 1998; Moore *et al*. 2001). However, calcium phosphate materials are stiff compared to bone, brittle and present unpredictable dissolution rates in vivo (Moore *et al*. 2001; Salgado *et al*. 2004).

Demineralised bone matrix (DBM) is a natural bone substitute which presents osteoinductive potential (Urist 1965; Urist 2002), although its materials properties make it not suitable as bone substitute in load bearing applications, such as revision THR.

Growth factors or cytokines are found naturally in the bone matrix and are signalling molecules between cells (Rose and Oreffo 2002). Growth factors found in bone include bone morphogenetic proteins (BMPs) within the transforming growth factor β (TGF-β) superfamily, insulin-like growth factors (IGF-1, IGF-2) which are found in fracture healing sites and have a role in collagen synthesis, interleukins (IL-1, IL-6) which are associated with bone resorption or fibroblasts growth factors (FGFs) which are involved in bone remodelling (Rose and Oreffo 2002; Yoon and Boden 2002). BMPs have already been used in clinical trials with promising results: 82% of patients showed clinical and radiological union after application of BMP-7 in persistent fracture non-unions and other orthopaedic complications (Giannoudis and Tzioupis 2005). However, better bone healing has often been observed in animal models than in human clinical trials (Einhorn 2003). Moreover, the application of large doses of BMPs has been linked to osteoclast recruitment which may lead to bone resorption (Lane 2001). In addition there is an issue over BMPs commercial availability and expenses (Lane 2001; Yoon and Boden 2002; Yoon and Boden 2004).

Novel Alternative Proposed in this Thesis

All the techniques already discussed present some disadvantages. Therefore, in this thesis we propose a novel alternative for the reconstitution of bone stock at revision THRs: the incorporation of mesenchymal stem cells (MSCs) into the implant thus enabling the reconstitution of the adjacent bone. This approach will be used in order to engineer an implant into which MSCs are incorporated.

1.4 TISSUE ENGINEERING

In 1993 Langer and Vacanti defined tissue engineering (TE) as "an interdisciplinary field of research that applies the principles of engineering and the life sciences towards the development of biological substitutes that restore, maintain, or improve tissue function". Indeed, the tissue engineering field is based on understanding how tissue formation and regeneration work and its aim is to induce new functional tissues (Langer and Vacanti, 1993; Lanza *et al*. 2000).

The three key components for generating any given tissue are suitable cells, growth factors and an appropriate scaffold (Langer and Vacanti, 1993; Lanza *et al*. 2000). Figure 1.7 shows the TE process as well as its components. Cells, in this case autologous as they are taken from the patient, are grown *in vitro* under optimum conditions until desired numbers are achieved. They are then combined with growth factors and seeded on the scaffold, thus obtaining a tissue-engineered construct. The construct is further incubated *in vitro* until it is implanted back in the patient.

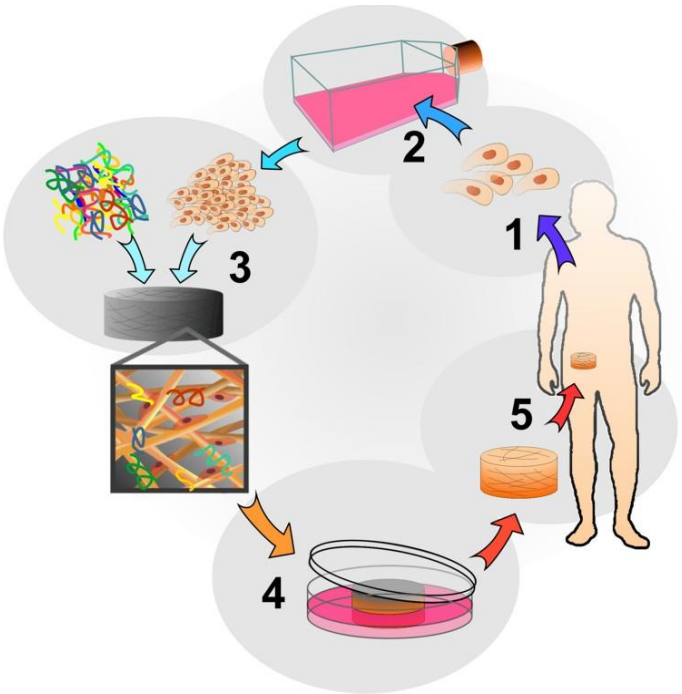

Figure 1.7 The tissue engineering process and its components (http://biomed.brown.edu/Courses/BI108/BI108_2007_Groups/group12/Homepage.html)

1.4.1 Bone Tissue Engineering

Bone tissue engineering (BTE) seeks the generation of constructs *ex vivo* in order to replace damaged or lost bone (Rose and Oreffo 2002; Salgado *et al*. 2004; Karageorgiou and Kaplan 2005; Fröhlich *et al*. 2008). To successfully create a bone construct it is very important to understand what it is required to grow new bone.

First of all, bone is a 3D tissue. Therefore, a scaffold with a 3D structure that mimics bone is necessary to grow new tissue in 3D. In this 3D structure cells, extracellular matrix and growth factors can interact to grow new bone tissue. Secondly, suitable cells that can form new bone tissue are needed to generate a bone construct. Finally, growth factors are essential. They are signalling molecules that initiate intracellular events to promote cell adhesion, proliferation or differentiation (Lanza *et al*. 2000).

1.4.2 Scaffolds Properties for BTE

Scaffolds for BTE should mimic bone morphology and mechanical properties. They must be biocompatible, porous with an optimum pore size, possess certain surface properties, osteoconductive and osteoinductive. They can be either permanent or biodegradable (Salgado *et al*. 2004; Fröhlich *et al*. 2008; Yang *et al*. 2001; Lanza *et al*. 2000; Schieker *et al*. 2006; Rose and Oreffo 2002).

Biocompatibility

The material scaffold must not elicit an immune response in the host (Yang *et al*. 2001). The biocompatibility of implanted biomaterials is controlled by the interaction between the host tissue and the biomaterial (Anderson and Miller 1984). However, biomaterials such as titanium implants, that do not elicit an immune response, do not interact with the host tissue (Niinomi 2008; Karageourgiou and Kaplan 2005). Therefore, it can be concluded that an interaction between the host tissue and the biomaterial is not necessary to elicit an immune response.

Porosity and Pore Size

Porosity is the percentage of void space in a solid. It is a morphological property independent of the material. Porosity is necessary for cell seeding and migration, nutrient transport, tissue ingrowth and vascularisation. Moreover, a porous material enhances mechanical connexion between the implanted tissue-engineered construct

and the host bone (Karageorgiou and Kaplan 2005). Kuboki and colleagues demonstrated the necessity for porosity in their work published in 1998. Solid and porous particles of hydroxyapatite were used for BMP-2 delivery in a rat ectopic model. It was observed that no new bone was formed on the solid particles while direct osteogenesis was seen in the porous hydroxyapatite particles (Kuboki *et al*. 1998). Further support for this is found in published studies about metal implants with a porous coating compared to the non-coated implants. In these studies maximised bone ingrowth and enhanced mechanical properties of the porous-coated metal implants were observed (Chang *et al*. 1998; Harvey *et al*. 1999; Svehla *et al*. 2000).

Pore size is an important issue to consider when choosing a material as scaffold for BTE purposes. If the pores are too small, the seeded cells on the implants will block them. As a result, tissue ingrowth and vascularisation will not occur. However, if the pores are too large the mechanical properties will become compromised, which is critical in regeneration in load bearing bones (Karageorgiou and Kaplan 2005; Salgado *et al*. 2004). Hulbert *et al*. in 1970 established that the minimum pore size in order to regenerate mineralised bone should be 100μm. In this study 46% porosity high-fired calcium aluminate cylindrical implants with different pore sizes were implanted in canine femora. The smaller pores tested, 10-44 and 44-75μm, were only penetrated by fibrous tissue. Pores between 75 and 100μm showed ingrowth of unmineralised osteoid tissue. On the other hand, the larger pores 100-150 and 150-200μm resulted in substantial bone ingrowth. The authors correlated the observations with the approximate diameter of normal Harversian canals, which is between 100 and 200μm (Hulbert *et al*. 1970). It is well accepted that materials as scaffolds for BTE should have a pore size between 200 and 900μm (Maquet *et al*. 1997; Burg *et al*. 2000; Yang *et al*. 2001).

Surface Properties

Chemical and topographical surface properties affect adhesion, proliferation and phenotype of cells (Burg *et al*. 2000; Lanza *et al*. 2000; Curtis and Wilkinson 1997; Oh *et al*. 2006). Chemical properties are essential for protein adhesion, which is very important for cell attachment, growth and differentiation (LeGeros 2008; Vitte *et al*. 2004; Hing 2005). Properties such as surface hydrophobicity or surface free energy

have been shown to affect cell attachment and spreading (Ponsonnet *et al*. 2003; De Bartolo *et al*. 2002).

Topographical properties such as surface roughness are well known to affect ingrowth and fixation of implants, with rough implants showing better bone integration than smooth ones made of the same material (Predecki *et al*. 1972; Hilborn and Bjursten 2007). Larsson and colleagues studied the bone formation around four different types of titanium implants that had different surfaces with essentially the same chemical composition: i) rough surface with thin oxide layer, ii) smooth, electropolished surface with thin oxide layer, iii) smooth, electropolished surface with an oxide layer of intermediate thickness and iv) smooth, electropolished surface with a thick oxide layer. They were implanted in the cortical bone of rabbits. The results showed that the smooth, electropolished implants with a thin oxide layer had significantly lower bone growth around the implants than the other types of implants in the early phase (Larsson *et al*. 1996). However, one year after implantation no significant differences were reported between the different groups. The study concluded that a reduction of surface roughness, that had a negative effect in the early phase, had no influence on the amount of bone formed after one year (Larsson *et al*. 1997).

Osteoconductivity

An osteoconductive surface promotes direct bonding with bone tissue (Albrektsson and Johansson 2001). An osteoconductive material allows the ingrowth of cells and capillaries from the host tissue in order to form new bone (Burg *et al*. 2000). Calcium-phosphate ceramics are an example of osteoconductive materials as they have been shown to form a direct bond with bone tissue (Blokhuis et al. 2000; LeGeros 2008).

Osteoinductivity

A material is osteoinductive when it induces undifferentiated and pluripotent cells to differentiate down the bone-forming cell lineage (Albrektsson and Johansson 2001). An osteoinductive material placed in an injured site that would not heal by itself will allow bone repair (Burg *et al*. 2000). In order to demonstrate the osteoinductivity of a material bone formation after implantation in non-osseous sites is studied (Harris and Cooper 2004).

Biodegradability

If a material is resorbable, the rate at which it degrades must be synchronised with the growth rate of the newly formed bone: the scaffold should be totally degraded when the site of injury is totally regenerated (Langer and Vacanti 1993).

1.4.3 Materials as Scaffolds for BTE

It is very important to select an appropriate material for the scaffold used for BTE purposes since its characteristics will dictate the scaffold properties. So far several materials from both natural and synthetic origins have been proposed. They include biodegradable polymers, ceramics and metals. Combinations of these materials or composites have also been proposed for BTE applications. Table 1.1 summarises the various materials used in BTE and their properties:

MATERIALS	ADVANTAGES	DISADVANTAGES
NATURAL BIODEGRADABLE POLYMERS Collagen, Fibrin, Chitosan	Biocompatibility Biodegradability Bioactivity Unlimited source (some of them)	Insufficient mechanical strength High rates of degradation
SYNTHETIC BIODEGRADABLE POLYMERS Poly(α-hydroxyacids) Poly(ε-caprolactone)	Versatility Biocompatibility Biodegradability	Low mechanical properties High local concentration of acidic degradation products
CERAMICS Coralline HA, Synthetic HA β-TCP BIOGLASSES	Biocompatibility Biodegradability Bioactivity Osteoconductivity Osteoinductivity (subject to physical and chemical properties)	Brittleness Low mechanical stability Degradation rates difficult to predict
METALS Titanium and its alloys, Tantalum, Stainless Steel	Excellent mechanical properties Biocompatibility	Lack of tissue adherence Risk of toxicity
COMPOSITES PLA/HA, CaP coating of metals	Combination of the above	Combination of the above

Table 1.1 Materials used in BTE and their properties
(Karageorgiou and Kaplan 2005; Schieker *et al*. 2006)

Natural Biodegradable Polymers

Natural biodegradable polymers such as collagen, fibrin, starch, hyaluronic acid and chitosan have the advantage of good biocompatibility and biodegradability as they compose the structural materials of tissues. These materials are also bioactive as they have the potential to interact with the host's tissue. Some materials such as starch or chitosan also offer the advantage of an almost unlimited source (Karageorgiou and Kaplan 2005; Schieker *et al*. 2006; Salgado *et al*. 2004; Hayashi 1994).

Collagen is one of the most useful biomaterials with many biomedical applications such as drug delivery systems, nanoparticles for gene delivery and basic matrices for cell culture systems (Lee *et al*. 2001). Osteoconductivity of collagen scaffolds have been reported: anionic collagen matrices were able to heal bone defects in rats therefore demonstrating bone formation (Rocha *et al*. 2002).

However, natural biodegradable polymers present the great disadvantages of insufficient mechanical strength and high rates of degradation. Thus, they are often used in composites, in combination with other materials, or are chemically modified in order to improve mechanical properties and degradation rates (Karageorgiou and Kaplan 2005; Schieker *et al*. 2006; Sachlos and Czernuszka 2003; Salgado *et al*. 2004).

Synthetic Biodegradable Polymers

Synthetic biodegradable polymers are more commonly used for TE applications than the natural ones. They offer great versatility as they can have different porosities, pore sizes, degradation rates, mechanical properties and forms (Karageorgiou and Kaplan 2005; Schieker *et al*. 2006; Sachlos and Czernuszka 2003; Salgado *et al*. 2004; Hayashi 1994). The most commonly used are poly(α-hydroxyacids), such as polyglycolic acid (PGA) and polylactic acid (PLA), and poly(ε-caprolactone). The degradation products of these polymers are glycolic acid and lactic acid, which are naturally found in the human body and therefore are removed by natural metabolic pathways.

Poly(lactide-*co*-glycolide), which is a copolymer formed by the poly(α-hydroxyacids) PLA and PGA, was used to fabricate scaffolds with 200μm mean pore size by Yang et

al. Human osteoprogenitor cells were able to grow and differentiate on these scaffolds, which was increased by protein and peptide surface modification on the scaffold, therefore showing their suitability as material for BTE scaffolds (Yang *et al*. 2001). The effect of fabrication parameters on the scaffold properties of three different synthetic poly(α-hydroxyacids) was studied by Hu and colleagues. Poly(D,L-lactide), with 92% porosity and an average pore size of 118μm, and poly(lactide-*co*-glycolide), with 90% porosity and an average pore size of 78μm, were further investigated in regard to their cell properties *in vitro*. It was found that both polymers were able to support proliferation and differentiation of osteoprecursor cells (Hu *et al*. 2002).

The main disadvantage of these materials is their poor mechanical properties, even when they are in the form of rods or solid screws, and have therefore been applied in low mechanical stress applications. Another potential disadvantage is high local concentrations of acidic degradation products that can affect cell differentiation on the scaffolds *in vitro* and could induce an inflammatory response *in vivo.* Moreover, dissolution of the polymer is often accompanied by breakup into smaller particles which then dissolve inducing an inflammatory reaction (Kohn *et al*. 2002; Santavirta *et al*. 1990).

Ceramics

Ceramics have been widely used in the biomedical engineering field and for clinical applications for many years. As biodegradable polymers they can be from a natural or a synthetic origin and can be synthesized to different forms, porosities, pore sizes or topographies. An example of natural ceramics is coralline hydroxyapatite (HA) while synthetic HA or β-tricalcium phosphate (β-TCP) are among the synthetic ceramics more commonly used (Blockhuis *et al*. 2000; Oh *et al*. 2006; Schieker *et al*. 2006; Karageorgiou and Kaplan 2005).

Ceramics are calcium-phosphate (CaP) materials that are naturally found in the body as part of bone or teeth and are used to synthesize bone-like scaffolds. The main properties that these CaP materials offer are excellent biocompatibily, biodegradability and osteoconductivity (Blockhuis *et al*. 2000; Oh *et al*. 2006; Schieker *et al*. 2006; Karageorgiou and Kaplan 2005; LeGeros 1993; LeGeros 2008).

CaP materials have been shown to be able to form an apatite layer on their surfaces thus enhancing osseointegration (Ducheyne and Qiu 1999; Blockhuis *et al*. 2000; LeGeros 2008). Another reason for the good osseointegration shown by these materials *in vivo* is that natural cytokines and adhesive proteins such as fibronectin are able to bind to CaP materials. The proteins and cytokines adsorbed to a scaffold surface provide a matrix for cell attachment (Kilpadi *et al*. 2001; Hing 2005). As HA is known to be efficient at adsorbing many proteins it has been used for many years to purify proteins from solutions by adsorption in chromatographic columns (Tiselius *et al*. 1956; Bernardi and Kawasaki 1968).

A very important property of bone is its osteoinductivity that allows this tissue to repair and regenerate. Generally, CaP materials are regarded as not osteoinductive as they are not able to form bone *de novo* (LeGeros 2008). However, Zhang et al. demonstrated that more bone formation in non-osseous as well as osseous sites was obtained using HA with 75-550µm pore size and 60% porosity (Zhang *et al*. 1992). Similarly, Yuan and colleagues reported bone formation in CaP materials with microporous structure when implanted in muscles of dogs. These results suggested that CaP materials can show osteoinductive properties when they exhibit specific chemical and structural characteristics (Yuan *et al*. 1998). Thus, it can be concluded that when CaP materials present certain topographies, geometries, pore sizes, percentages of porosity and composition they can show osteoinductive properties (LeGeros 2008; Ripamonti *et al*. 2008).

Addition of mesenchymal stem cells (MSCs) to ceramics can improve bone formation. Petite et al. used a coral scaffold with added MSCs to treat lesions above a critical size of 25mm in sheep metatarsus. Coral alone, coral loaded with fresh bone marrow and coral loaded with MSCs were used to regenerate bone in a large segmental defect model in sheep. The results showed morphogenesis leading to complete recorticalization by the coral with MSCs combination (Petite *et al*. 2000). Further studies have agreed with these results (Eslaminejad *et al*. 2008).

As bone mineral contains various ionic substitutions (i.e. magnesium, potassium, chlorine, silicon) they have been proposed for BTE. An example of these materials is silicate-substituted hydroxyapatite scaffolds (Si-HA) (Porter 2006), which improve

bone healing (Hing *et al*. 2006) and enhance the cellular activity of human MSCs (Samizadeh 2010). When implanted in paraspinous muscle of sheep Si-HA obtained higher new bone formation than HA, thus showing osteoinductive properties (Samizadeh 2010).

In spite of the good properties for BTE purposes exhibited by ceramics, they present two major drawbacks. First, these materials are brittle and have a low mechanical stability, which prevent their use in load-bearing applications. Second, their degradation rates are difficult to predict and therefore if the material degrades too quickly once implanted the mechanical stability of the tissue-engineered construct would be compromised. Moreover, a fast degradation of the CaP material scaffold would dramatically increase the extracellular concentrations of calcium and phosphate, which may result in cell death as shown by Adams et al. (Adams *et al*. 2001).

Metals

Titanium, titanium alloys (i.e. TiAl6V4) and stainless steel are the materials more commonly used in metal implants for bone surgical repairs. The main advantage of metal materials is their excellent mechanical properties which make them ideal candidates for load-bearing applications (Karageorgiou and Kaplan 2005).

Titanium and its alloys are attractive materials for biomedical applications because of their biocompatibility, strength, lightness and high resistance to corrosion (Niinomi 2008; Disegi 2000). The biocompatibility of the titanium materials is based on a thin titanium dioxide (TiO_2) layer formed on the surface of the bulk material. Titanium is a very reactive element so, even at room temperature, a newly polished titanium surface will have a thin layer of TiO_2. Thus coating of titanium implants with a TiO_2 is of interest within the orthopaedic materials research field in order to improve cell adhesion and osseointegration (Yang *et al*. 2009). Porous titanium materials have been developed in order to achieve material properties compared to bone (Schuh *et al*. 2007; Niinomi 2008) and new families of titanium alloys are constantly under research (Guillemot *et al*. 2004).

A biomaterial made of porous tantalum, trabecular metal, has recently been developed for potential application in orthopaedics. Trabecular metal is highly porous, 80%, and was approved by the Foods and Drugs Administration for use in acetabular cups in 1997. The potential of this new material is its structural and mechanical resemblance with trabecular bone (Unger *et al*. 2005). The ingrowth potential of this material was demonstrated by Bobyn et al. (Bobyn *et al*. 1999). Porous tantalum has been used in primary and in revision total hip arthroplasty components with excellent early clinical results (Levine *et al*. 2006). Despite of these excellent preliminary results, the functionality and durability of acetabular cup components made of trabecular metal in revision total hip arthroplasty remain unknown.

The main disadvantage of metals is the lack of tissue adherence, which may result in implant loosening with a necessary second surgery to remove it (Hulbert *et al*. 1970). If the implant gets permanently implanted in the body a risk of toxicity may arise due to accumulation of metal ions from corrosion (Jacobs *et al*. 2003; Hallab *et al*. 2001; Rubin and Yaremchuck 1997).

Composites

Each individual material discussed in this introduction chapter has its advantages and drawbacks. By combining different materials some of these drawbacks can be overcome.

Kasuga et al. fabricated a composite consisting of the synthetic polymer PLA and calcium carbonate. The resulting composite showed no brittleness and an improved modulus of elasticity compared to that of PLA alone. Moreover, the composite was able to form a bone-like apatite layer on its surface when soaked in simulated body fluid, thus showing an osteoconductive potential (Kasuga *et al*. 2003). Poly(lactide-*co*-glycolide)/HA composites has been shown to be osteoconductive (Kim *et al*.2006) and fibrin based scaffolds with incorporated nanocrystalline HA supported bone formation when used in a mouse calvarial defect model (Osathanon *et al*. 2008). Fibrin scaffolds have also been proposed as delivery systems for human MSCs. Bensaïd and colleagues observed that human MSCs were able to migrate out of the fibrin gel where they had been seeded on and invade a ceramic scaffold (Bensaïd *et al*. 2003).

Another example of composites is ceramic coatings in order to increase the biocompatibility and osseointegration of other biomaterials. Specifically, calcium-phosphate coating of metal implants is a subject of extensive research as the resulting material combines the excellent mechanical properties of metals with the excellent biocompatibility and osteoconductivity showed by ceramics (Karageorgiou and Kaplan 2005; Salgado *et al*. 2004). Plasma-spraying is the most common commercial method. However, other calcium-phosphate coating methods are currently under research such as the biomimetic (Habibovic *et al*. 2002; Ma *et al*. 2003) and the electrochemical depositions (Redepenning and McIsaac 1990; Han *et al*. 2001; Lopez-Heredia *et al*. 2007). Barrère et al. showed significantly higher bone contact for biomimetic calcium-phosphate coated dense and porous metal implants compared to non-coated implants when implanted in the femoral diaphysis of goats (Barrère *et al*. 2003). Electrochemically HA coated porous plugs implanted in the distal femoral metaphysis of pigs were shown to significantly increase bony ingrowth when compared with the uncoated implants (Redepenning *et al*. 1996). Biomimetic coatings are being used in order to incorporate growth factors into medical devices (Liu *et al*. 2005). Finally, chitosan/HA composite coatings have been deposited on the surface of titanium substrates by electrochemical deposition (Redepenning *et al*. 2003; Wang *et al*. 2004).

Materials Used as Scaffold in this Thesis and their Properties

As the reconstruction used for repairing and regenerating bony defects in revision THR is likely to be load-bearing, the excellent mechanical properties offered by metal materials make them ideal candidates. Specifically, TiAl6V4, a titanium alloy extensively used in orthopaedic implants, and tantalum will be investigated (Karageorgiou and Kaplan 2005; Niinomi 2008; Disegi 2000; Unger *et al*. 2005). The metal materials will be coated with a calcium-phosphate layer to add biocompatibility and osteoconduction to the scaffold (Karageorgiou and Kaplan 2005; Salgado *et al*. 2004; Blockhuis *et al*. 2000). Moreover, calcium-phosphate materials present good chemical properties for protein adhesion which is important for cell attachment, growth and differentiation (Kilpadi *et al*. 2001; Hing 2005; Ohgushi *et al*. 1993). The scaffold will be porous for bone ingrowth, with a pore size between 200 and 900μm (Maquet *et al*. 1997; Burg *et al*. 2000; Yang *et al*. 2001).

1.4.4 Cells for BTE

Once an appropriate scaffold with adequate properties has been chosen the next step is to select an appropriate source of cells that is easily expandable to high numbers, non-immunogenic and with a protein expression pattern similar to that of the bone tissue.

Osteoblasts

Osteoblasts are the most obvious choice for BTE because of their immunogenicity. They can be isolated from biopsies from the patients and expanded *in vitro*, thus they are autologous cells. However, this source of cells offers an important disadvantage: relatively low numbers are yielded after the dissociation of the tissue and their expansion rates are relatively low. Therefore the number of cells available to be seeded on the scaffolds is limited. Moreover, there are certain bone related diseases in which osteoblasts may not be used due to an insufficient protein expression pattern (Heath 2000).

The use of xenologous osteoblasts, which are obtained from non-human donors, would solve the problem of low cell numbers just mentioned. However, the advantage of immunogenicity offered by the autologous osteoblasts would be lost. Furthermore, there would be a risk of transmission of infectious agents as well as ethical and social issues associated with the use of these cells (Heath 2000; Platt 1996).

Stem Cells

Stem cells are undifferentiated cells, capable of self-renewal and production of a large number of undifferentiated progeny. They have a high proliferation capability and multi-lineage differentiation potential, therefore they are involved in the regeneration of tissues (Blau *et al*. 2001; Lanza *et al*. 2000).

Embryonic stem cells (ES) are pluripotent as they can differentiate into a wide range of cell types, a plasticity that is essential in the early development of the embryo (Wobus 2001; Heath 2000; Lanza *et al*. 2000). The extraordinary pluripotency exhibited by ES cells was beautifully shown in the experiments conducted by Dewey and colleagues. In these experiments teratocarcinoma cells, produced by ectopic injection of blastocysts into adult mice, were isolated, genetically marked and implanted into the blastocyst of a foster mother (Figure 1.8). Although the resulting

progeny was normal, chimeric mixtures of teratocarcinoma and wild type cells were found in virtually every tissue of their body as illustrated in Figure 1.8 (Dewey *et al*. 1977).

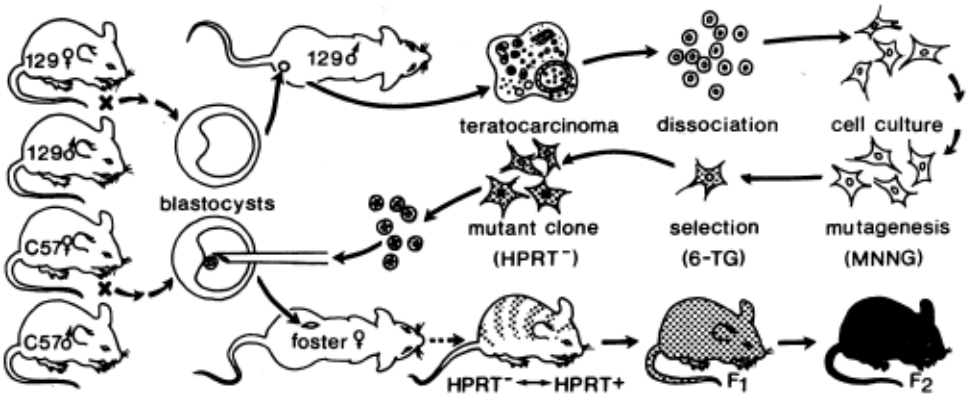

FIG. 1. The plan of the experiment, spanning almost a decade, is diagrammed, starting at the upper left. A blastocyst from a mating of 129-strain mice was grafted under the testis capsule of a syngeneic host (14). The graft formed a malignant teratocarcinoma. After dissociation, tumor cells were explanted and the stem cells were established as an *in vitro* culture line (ref. 12, and unpublished data). Following exposure to the mutagen *N*-methyl-*N'*-nitro-*N*-nitrosoguanidine (MNNG), HPRT⁻ cells (stippled) were selected for their resistance to 6-thioguanine (6-TG). Cells from a resistant *clone* were then microinjected into the cavity of genetically marked blastocysts (e.g., of the C57BL/6 strain). The injected embryos were transferred to the uterus of a pseudopregnant foster mother (previously mated to a sterile vasectomized male) and live mice were born. Some were mosaics comprising HPRT⁻ cells derived from the mutant teratocarcinoma lineage, along with blastocyst-derived cells, in their coats (striped) and/or internal somatic tissues. Tissue-specific effects of the deficiency are analyzable in the mosaics. If mutant cells are of X/O (as in this case) or X/X sex chromosome type and contribute to the germ line of females, affected "Lesch–Nyhan" males would be obtained in the F_1 generation; if the mutant cells are X/Y, in mosaic (non-Lesch–Nyhan) males, affected males would occur in the F_2. (Based upon figure 17, ref. 6.)

Figure 1.8 Experiments conducted by Dewey et al. showing the extraordinary pluripotency of ES cells (Dewey *et al*. 1977).

The main issue associated with the use of ES cells for biomedical and TE applications is the potential tumorogenicity of these cells as it has been shown that when implanted *in vivo* undifferentiated ES cells give rise to teratomas and teratocarcinomas. This tumorogenicity potential is due to their unlimited proliferation potential. Moreover, there are ethical and social questions to answer in order to use ES cells in regenerative medicine (Wobus 2001).

Adult stem cells (AS) are found in the fully differentiated tissues and are responsible for the regeneration of damaged tissue and the maintenance of tissue homeostasis. AS cells have been found in the bone marrow, periosteum, muscle, fat, brain or skin (Blau *et al*. 2001; Lanza *et al*. 2000). It was thought that AS cells were committed to

differentiate only into the cell lineages from the tissue in which they were found but recent reports have challenged this belief. Bjornson et al. showed that neural stem cells could give rise to lineage committed haematopoietic precursors (Bjornson *et al*. 1999). Furthermore, Toma et al. reported that AS cells isolated from the dermis could be differentiated into brain, muscle and fat cells (Toma *et al*. 2001). Although AS cells need to be further investigated, many studies have shown the broad range of potential applications of these cells (Verfaillie 2002; Ferrari *et al*. 2007).

Mesenchymal Stem Cells

In the field of BTE there is a special interest in the adult stem cells located in the bone marrow, known as mesenchymal stem cells (MSCs). MSCs can differentiate into lineages of the mesenchymal tissues such as bone, thus the interest in these cells for BTE purposes (Pittenger *et al*. 1999; Caplan 1991; Lanza *et al*. 2000).

The studies of Petrakova et al. suggested the idea that bone marrow contained some kind of osteogenic precursor cells. In these studies it was possible to obtain an osseous tissue when pieces of bone marrow were implanted under the renal capsule (Petrakova *et al*. 1963). Following this preliminary work, Friedenstein and co-workers published in the 1970s a series of studies *in vitro* in which they showed the possible existence of osteogenic stem cells in the bone marrow. They observed that these cells adhered to tissue culture plates and resembled fibroblasts *in vitro* (Friedenstein *et al*. 1970; Friedenstein *et al*. 1974).

In 1991, almost 20 years later, Caplan gave these cells their current name (Caplan 1991). The same author in 1994 described that, when placed under the appropriate culture conditions, MSCs were able to differentiate into cells with mesenchymal origin and lately give origin to bone, cartilage, fat, tendon and other mesenchymal tissues. He named this differentiating process as "The Mesengenic Process" (Caplan 1994). Figure 1.9 below here shows a scheme of the mesengenic process. According to it, adult MSCs can differentiate into bone, cartilage, muscle, marrow stroma, tendon, ligament and other connective tissues through a series of lineage transitions (Caplan 2009).

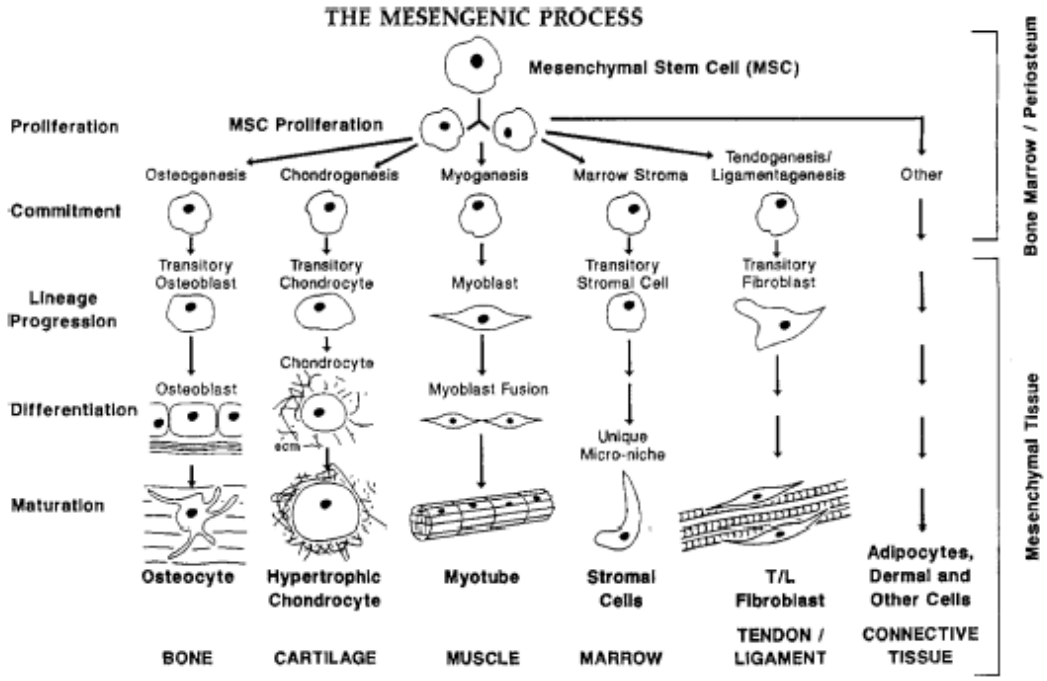

Figure 1.9 The mesengenic process (Caplan 2009)

Bone marrow cultures are heterogenic as hematopoietic and endothelial stem cells are also found in bone marrow (Rubin and Strayer 2007). Therefore, methods of MSCs isolation from bone marrow are important. Their isolation is generally based on their adhesive properties and their fibroblastic morphology (Friedenstein *et al*. 1970; Friedenstein *et al*. 1974; Haynesworth *et al*. 1992; Pittenger *et al*. 1999). Figure 1.10 shows the morphology of a typical monolayer culture of MSCs:

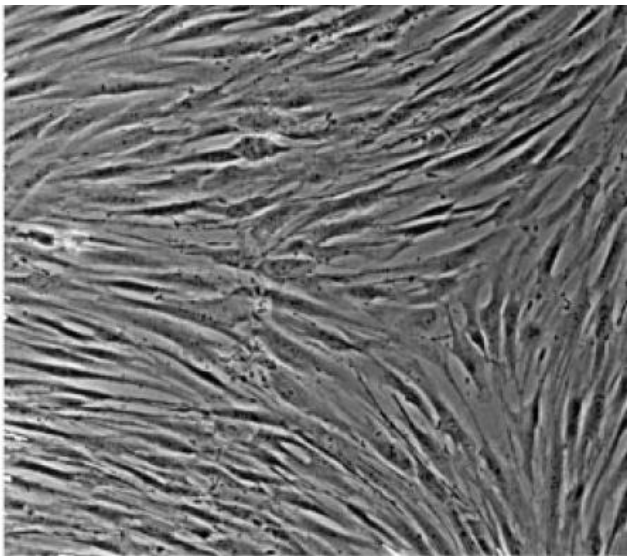

Figure 1.10 MSCs in monolayer culture under light microscopy (Pittenger *et al*. 1999)

Due to the lack of specific markers to distinguish MSCs from other cells in bone marrow, these cells are often characterised by their potential to differentiate into lineages of the mesenchymal tissues, as elegantly shown by Pittenger and colleagues in 1999. Figure 1.11 shows the results of specific stainings for the differentiation of MSCs into the adipogenic, chondrogenic and osteogenic lineages (Pittenger *et al*. 1999):

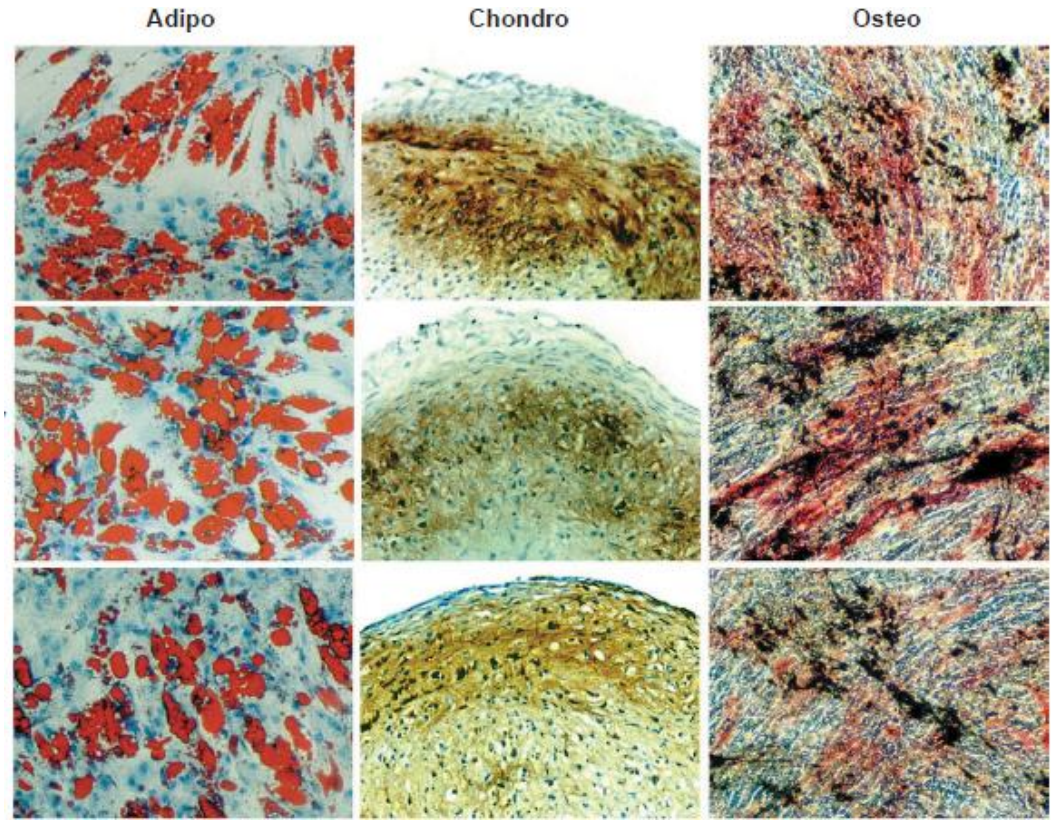

Figure 1.11 Staining results by Pittenger et al. showing the differentiation of MSCs down the adipogenic (left, red indicates lipid deposits), chondrogenic (middle, C4F6 monoclonal antibody to type II collagen) and osteogenic (right, black indicates calcium deposition) pathways (Pittenger *et al*. 1999).

Finally, MSCs not only have potential for engineering of musculoskeletal tissues but also can be used in cardiac tissue repair, as MSCs are also able to differentiate into a cardiac phenotype. MSCs have already been used in clinical trials for certain applications, including BTE (Le Blanc and Pittenger 2005; Caplan 2009).

Cells Used in my Thesis

Autologus MSCs will be seeded throughout the porous scaffold. They will be isolated from bone marrow aspirates retrieved from the iliac crest. As they are autologous no immune response will be elicited when implanted back in the host (Lanza *et al*. 2000). In addition, MSCs have been shown to differentiate down the osteogenic lineage when cultured on calcium-phosphate materials (Ohgushi *et al*. 1993; Oreffo *et al*. 1998; Nishio *et al*. 2000), like the coatings deposited on the surface of the metal scaffolds used in this thesis.

1.4.5 Growth Factors in BTE

Growth factors are cytokines secreted by many cell types that function as signalling molecules. They promote and/or prevent cell adhesion, proliferation, migration and differentiation. These events are affected by up-regulating or down-regulating the synthesis of proteins, growth factors and receptors. These molecules are essential for tissue formation and therefore play an important role in tissue engineering (Lanza *et al*. 2000; Rose and Oreffo 2002; Yoon and Boden 2002; Ikada 2006).

Bone tissue posses a plethora of growth factors, including bone morphogenetic proteins (BMPs) within the transforming growth factor beta (TGF-β) superfamily, fibroblast growth factors (FGFs), insulin growth factor I and II (IGF I/II) and platelet derived growth factor (PDGF). These growth factors have been proposed for BTE applications, although the most heavily studied cytokines are BMPs (Yoon and Boden 2002; Salgado *et al*. 2004).

Bone Morphogenetic Proteins (BMPs)

BMPs are grouped into the TGF-β superfamily due to their similarities in protein structure and sequence with TGF-β. Back in 1965, Urist discovered that demineralised bone matrix could induce bone formation when implanted ectopically in subcutaneous tissue (Urist 1965). This capability was later attributed to a protein called bone morphogenetic protein, which was purified in 1984 based on its potential to induce bone formation (Urist *et al*. 1983; Urist *et al*. 1984). In 1988, Wozney and colleagues cloned these molecules and since then over 30 different BMPs have been identified with promising efficacy as therapeutic molecules for bone formation (Wozney *et al*. 1988; Kang *et al*. 2004; Rose and Oreffo 2002).

However, the failure to identify a suitable carrier for BMPs as well as dosage and maintenance of biological activity has hampered the potential benefits these molecules could offer for bone formation. Therefore, extensive research has been carried out in incorporating BMPs into tissue engineering scaffolds and delivery systems (Rose and Oreffo 2002; Yoon and Boden 2002; Suh *et al*. 2002). Another approach to eliminate the problems associated with the delivery of BMPs to the required site is gene therapy. Genetic modification of isolated and expanded cells is possible due to developments in gene technology. Populations of progenitor cells over-expressing selected signalling molecules can be engineered using this technology. Moreover, gene therapy offers the advantage of continuous delivery of cytokines during a prolonged period rather than just one dose of protein at the time of implantation (Rose and Oreffo 2002; Yoon and Boden 2002; Yoon and Boden 2004; Ho 2011; Kang *et al*. 2004; Conget and Minguell 2000).

Growth Factors Used in this Thesis

In my thesis I propose a self-regulating tissue-engineered construct (Lanza *et al*. 2000) with chemical cues arising from the scaffold itself, as calcium-phosphate materials promote MSCs differentiation down the osteogenic lineage (Ohgushi *et al*. 1993; Oreffo *et al*. 1998; Nishio *et al*. 2000).

1.4.6 The Role of Bioreactors in BTE

As mentioned early in this introduction, bone is a mechanically active tissue arranged in a 3D manner. The biological environment within the bone tissue is a dynamic interaction between active cells that experience mechanical forces and a 3D matrix architecture that is in continuous change. Therefore, in order to engineer bone tissue constructs *ex vivo* it is necessary to develop culture systems that mimic the dynamics of the *in vivo* biological environment (Lanza *et al*. 2000; Kale *et al*. 2000).

The current standard tissue culture techniques are not adequate for BTE purposes due to a lack of efficient transport of nutrients and removal of waste products. As a result, there is a lack of nutrients in the centre of the scaffold which leads to cell migration to the surface where fresh nutrients are more available. Ultimately, a non-even distribution of cells throughout the scaffold is obtained. Moreover, the current tissue

culture techniques are static and do not mimic the dynamics found *in vivo* (Bancroft *et al*. 2003; Martin *et al*. 2004).

A solution to overcome these problems is the design and development of bioreactors. A bioreactor is generally defined as a device in which biological and/or biochemical processes take place under tightly controlled environmental and operating conditions. A bioreactor would provide an efficient mass transfer of nutrients and metabolites and the dynamic requirements for the engineering of bone tissue (Martin *et al*. 2004; Salgado *et al*. 2004; Ikada 2006). So far, three bioreactor systems have been used in BTE applications: spinner flasks, rotating wall vessel bioreactors and flow perfusion bioreactors.

Spinner flasks (Figure 1.12) are very basic bioreactors where scaffolds seeded with cells are attached to needles hanging from the lid of the flask. The scaffolds are covered by medium that is mixed with a magnetic stirrer at the bottom of the flask. The convective forces generated by this magnetic stirrer improve the nutrient concentration gradients at the surface of the scaffolds (Martin *et al*. 2004; Bancroft *et al*. 2003; Ikada 2006). Vunjak-Novakovic and co-workers reported that when cell/polymer constructs for tissue regeneration were cultured in spinner flasks for five weeks they were larger and had more cells than the constructs cultured under static conditions in petri dishes (Vunjak-Novakovic *et al*. 1996). More recently, Mygind and colleagues found that dynamic culture of human MSCs on coralline hydroxyapatite scaffolds using a spinner flask resulted in increased proliferation, differentiation and distribution of cells in scaffolds (Mygind *et al*. 2007).

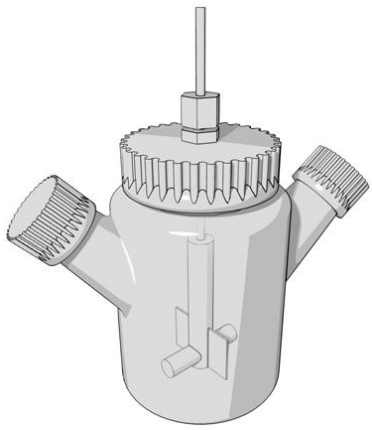

Figure 1.12 Spinner flask scheme (www.currentprotocols.com)

Rotating wall vessel bioreactors (Figure 1.13) were originally designed to simulate microgravity effects. The most common type of rotating wall vessel bioreactor is composed of two concentric cylinders. The seeded scaffolds are placed in the annular space between them. The outer cylinder is impermeable and rotates in a controlled manner while gas exchange is allowed through the stationary inner cylinder. By carefully selecting the appropriate rotational rates the free falling of the scaffolds inside the bioreactor due to gravity can be balanced by the centrifugal forces originated due to the rotation of the outer cylinder. Thus, microgravity-like culturing conditions with laminar rotational flow fields and a low fluid shear stress are established (Martin *et al*. 2004; Bancroft *et al*. 2003; Ikada 2006). Botchwey and colleagues showed an increased alkaline phosphatase activity and mineralization when osteoblast-like cells seeded on lighter than water polymer scaffolds were cultured in a rotating wall vessel bioreactor (Botchwey *et al*. 2001). Sikavitsas, Bancroft and Mikos directly compared the performance of spinner flasks and rotating wall vessel bioreactors to static cultures. PLGA scaffolds were seeded with MSCs from the marrow of femurs and tibias of rats and cultured in six-well plates (static culture), spinner flasks and rotating wall vessel bioreactors for up to 21 days. The results showed that the constructs cultured in spinner flasks obtained higher proliferation rates and increased osteogenic differentiation. These results were attributed to a mitigation of external mass transport limitations in the spinner flask. On the other hand, constructs cultured in the rotating wall vessel displayed minimal osteogenic differentiation which the authors attributed to collisions of the constructs with the walls of the rotating bioreactor. In all three culture systems, a dense cellular layer on the surface of the scaffolds and a considerably lower cell distribution in the inside of the scaffold was revealed by histology, suggesting that the transport of nutrients to the interior of the scaffolds was limited to diffusion in all the cultures. The authors concluded that improved tissue culture conditions were needed in order to permit cellular growth throughout tissue-engineered constructs (Sikavitsas *et al*. 2002).

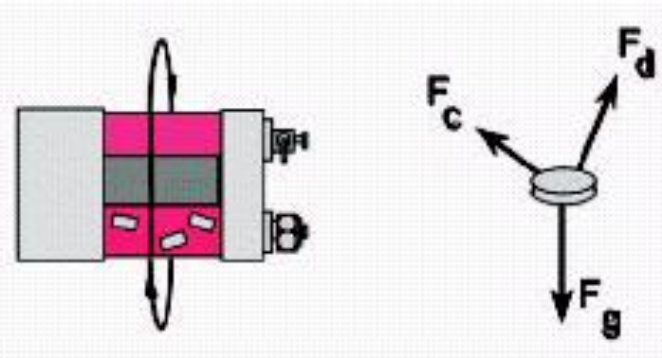

Figure 1.13 Rotating wall vessel bioreactor scheme and forces (www.landesbioscience.com/curie/)

Flow Perfusion Bioreactors

The third bioreactor type used for BTE applications, flow perfusion, offers an improved as well as enhanced transport of nutrients to the interior of 3D scaffolds. This advantage comes from the fact that this bioreactor delivers medium through the interconnected pores of the scaffold. In these bioreactors, the seeded scaffolds are confined inside a chamber with the appropriate dimensions in order to force the continuously pumped culture medium flow through the interconnected porous network and not around it, as illustrated in Figure 1.14 (Bancroft *et al*. 2003; Martin *et al*. 2004). Due to this particular flow culture, an improved cellular distribution is achieved.

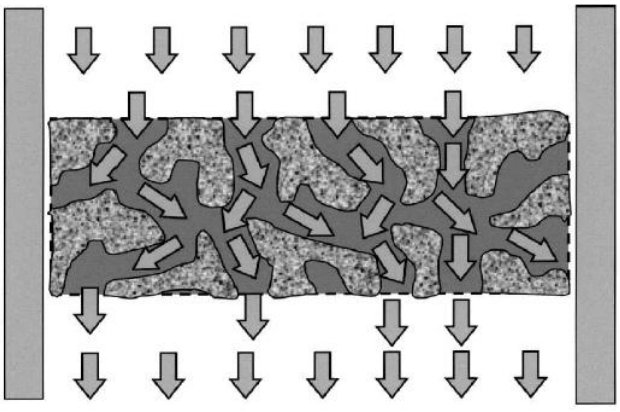

Figure 1.14: Flow perfusion culture, where the culture medium is forced through the internal interconnected pores of the scaffold (Bancroft *et al*. 2003).

Another important advantage offered by these perfusion systems is that they provide mechanical stimulation to the cells by way of fluid shear stress (Bancroft *et al*. 2003). Since bone cells are known to be stimulated by mechanical signals (Hillsley and Frangos 1994; Sikavitsas *et al*. 2001) this is a very important advantage as it mimics the mechanical environment in which bone cells live. Sikavitsas et al. reported direct involvement of fluid shear stresses inside a perfusion bioreactor on the osteogenic differentiation of marrow stromal cells. They also showed that increased shear forces resulted in enhanced mineralised extracellular matrix deposition and improved spatial cellular distribution (Sikavitsas *et al*. 2003). By increasing the flow rate of the culture medium perfused through the constructs fluid shear forces are also increased, which presumably results in greater mechanostimulatory effect of these shear forces on the cells. This greater mechanostimulation may enhance the osteogenic differentiation of MSCs (Sikavitsas *et al*. 2003; Bancroft *et al*. 2002; Sikavitsas *et al*. 2005; Bancroft *et al*. 2003; Cartmell *et al*. 2003; Gomes *et al*. 2006a; Gomes *et al*. 2006b; Zhao *et al*. 2007).

Different designs can be found in the literature. However, all of them present the same components: a pump to deliver the flow of culture medium, a bioreactor chamber in which the construct is fitted, media containers and a tubing system (Bancroft *et al*. 2003). Some of them incorporate a seeding loop for dynamic cell seeding of the scaffolds (Zhao and Ma 2005; Janssen *et al*. 2006; Zhao *et al*. 2007).

Several types of scaffolds have been seeded with different cell types and cultured in flow perfusion systems for BTE purposes. Zhao and Ma used non-woven poly(ethylene terepthalate) fibrous matrices with human MSCs, the same cells that Bjerre et al. seeded on silicate-substitute tricalcium phosphate scaffolds (Zhao and Ma 2005; Bjerre *et al*. 2008). Other ceramics, such as porous biphasic calcium phosphate, have been used by other authors (Holtorff *et al*. 2005; Wang *et al*. 2003). In all these examples increased proliferation, osteogenic differentiation and cell distribution were achieved under flow perfusion culture, setting flow perfusion systems as valuable tools for applications in BTE.

Janssen and colleagues designed a perfusion system for the production of clinically relevant volumes of tissue-engineered bone. Goat bone marrow stromal cells were

dynamically seeded on macroporous biphasic calcium phosphate granulated scaffolds and cultured in the perfusion system for up to 19 days. A homogeneous and viable cell layer could be observed after 19 days of culture. However, subcutaneous implantation of the constructs yielded similar amounts of newly formed bone as the static controls (Janssen *et al*. 2006). The same authors found very similar results with human bone marrow stromal cells seeded on the same scaffold and cultured in the same perfusion system. Dynamically and statically cultured constructs showed no statistical difference in terms of new bone formation when subcutaneously implanted in nude mice (Janssen *et al*. 2010). On the other hand, other *in vivo* studies have shown significantly enhanced bone formation when constructs developed in a perfusion bioreactor were also implanted subcutaneously in rats (Wang *et al*. 2003), showing that the generation of artificial bone tissue could be achieved with a perfusion bioreactor system.

To conclude, perfusion bioreactor systems are also being used in intestinal TE (Kim *et al*. 2007), maxillofacial TE (Depprich *et al*. 2008) or cardiac tissue regeneration (Dvir *et al*. 2006).

Bioreactor System Used in this Thesis

A perfusion bioreactor system will be used in my thesis in order to enhance transport of nutrients to the interior of the porous scaffold seeded with MSCs (Bancroft *et al*. 2003). Moreover, an effective removal of waste products is also achieved by using a perfusion bioreactor system (Bancroft *et al*. 2003). As a result, an even distribution of cells is achieved throughout the scaffold (Holtorff *et al*. 2005). The fluid shear forces generated inside a perfusion bioreactor will add to the effect of the calcium-phosphate coatings on the osteogenic differentiation of MSCs (Sikavitsas *et al*. 2003; Bancroft *et al*. 2002; Sikavitsas *et al*. 2005; Bancroft *et al*. 2003; Cartmell *et al*. 2003; Zhao *et al*. 2007).

1.4.7 Animal Models in BTE

The development of bone tissue-engineered constructs requires the evaluation of their performance on preclinical studies prior to evaluation in human subjects. The first step usually taken in order to test the *in vivo* performance of newly developed constructs in to conduct preclinical trials in smaller animals to evaluate the proof of

concept. If the results of these trials on smaller animals are positive the next step is to proceed to larger animals. The option of working with larger animals is also closely related to the necessity of evaluating responses of the tissue-engineered construct under conditions that better resemble a physiological match with the human clinical conditions (Goldstein 2002).

The appropriate choice of an experimental animal model is critical to the success of the preclinical studies. The criteria associated with the choice of an experimental model must be related to the functional application of the construct: the animal model must be biologically analogous and recognizable as a suitable challenge to human physiology.

Ectopic Models

Ectopic models are used when the aim of the project is to study whether the tissue-engineered construct has an adequate porosity for osseoinduction of bone tissue and blood vessel ingrowth.

The subcutaneous ectopic model is the most popular where rats are more often the chosen animals. Constructs are normally implanted in the back of the animal. Other ectopic sites often used are the muscle, peritoneal cavity or mesentery (An and Friedman 1998). Ectopic models are also chosen when the osteoconductivy and osteoinductivity of biomaterials are assessed (Fujita *et al*. 1991; Mankani *et al*. 2001; Harris and Cooper 2004).

Critical Size Defect Models

In a critical defect model the bone defect must fail to heal unless it is treated with the tissue-engineered construct under study. There are mainly four types of defects: calvarial, long bone or mandibule segmental, partial cortical and trabecular bone defects. The animals usually used with these models are rabbits, rats, dogs, sheep and non-human primates (An and Friedman 1998).

Critical size defects in large animal models are also used in the biomaterials research field in order to evaluate the *in vivo* behaviour of the proposed materials (Constantz *et al*. 1997; Nakamura *et al*. 1998; Hing *et al*. 2005; Ripamonti *et al*. 2008).

Animal Model Chosen for this Thesis

An ovine model was chosen for this thesis because a large animal model is more relevant than a small one in order to represent the human clinical situation (Goldstein 2002). In this thesis, tissue-engineered constructs will be evaluated in a bony *in vivo* environment by implantation in the medial femoral condyle of sheep in a trabecular defect model (An and Friedman 1998). Their performance will be compared to non tissue-engineered constructs, which consist of calcium-phosphate coated porous metal scaffolds not seeded with cells.

1.5 AIM AND HYPOTHESES

The aim of this thesis is to develop a bone tissue-engineered construct with a porous metal scaffold coated with a calcium-phosphate layer and seeded throughout its structure with MSCs, using a perfusion bioreactor system, in order to enhance rapid formation of bone within the implant, repair adjacent defect areas and increase fixation strength at revision total hip replacements. This approach could be used in porous metal acetabular cups as they could be coated with a CaP layer and cultured throughout with MSCs using a perfusion bioreactor system.

The hypotheses explored in this thesis are:

1. **The addition of MSCs to a porous metal scaffold coated with a calcium-phosphate layer can generate significantly increased new bone formation in gaps adjacent to implants and within the porous structure than using the scaffold alone.**

2. **Tissue-engineered implants will achieve greater osseointegration and implant-bone interface fixation than non tissue-engineered implants.**

CHAPTER 2:

Calcium-Phosphate Coating

of Polished and Sand-Blasted Metal Discs

by Biomimetic and Electrochemical Methods

2.1 INTRODUCTION

Metals such as titanium alloys or tantalum are widely used in orthopaedic implants due to their excellent mechanical properties and biocompatibility (Matter and Burch 1990; Grübl *et al*. 2002; Unger *et al*. 2005; Levine *et al*. 2006). However, these materials are not osteoconductive as they do not promote direct bonding with bone tissue.

On the other hand, calcium-phosphate (CaP) ceramics have been shown to form a direct bond with bone tissue through formation of an apatite layer when used for bone substitution, augmentation and repair (Blokhuis *et al*. 2000; LeGeros 2008). Therefore, by coating the surface of metal implants with a CaP layer the implant becomes bioactive and osteoconductive. Tisdel and co-workers, in 1994, demonstrated direct new bone apposition on CaP coated titanium fibre rods in rabbit femora compared with uncoated ones, to which no directly apposed new bone was found. They concluded that an enhancement of attachment of bone-forming cells to the CaP coatings may result in an increased bone formation (Tisdel *et al*. 1994).

The most common commercial method for CaP coating of metal implants is plasma-spraying, which is a line-of-sight process that takes place at high temperatures. Disadvantages of this method are the formation of easily dissolved phases that decrease bond strength, it does not allow the incorporation of bioactive molecules and cannot be applied to implants with complex morphology. Other methods of CaP coating have been developed to overcome these disadvantages, such as the biomimetic and electrochemical depositions. Both of these methods are based on precipitation from aqueous solutions (wet methods), take place at low temperature, allow the coating of complex shapes and are economical (Habibovic *et al*. 2002; Bharati *et al*. 2005; Lopez-Heredia *et al*. 2007; Han *et al*. 2001).

The biomimetic method, originally developed by Kokubo and colleagues in the 1990s (Kokubo *et al*. 1990; Kokubo 1998), uses simulated body fluids (SBF) that mimic the inorganic ions present in physiological solutions. SBFs have inorganic concentrations similar to those of human blood plasma and many procedures and recipes can be found in the literature (Habibovic *et al*. 2002; Cuneyt Tas and Bhaduri 2004; Bharati

et al. 2005). Moreover, as SBFs mimic the physiological conditions found *in vivo* they have been widely used as an *in vitro* model to study apatite formation on the surface of different biomaterials, thus assessing their bioactive and osteconductive potential (Kokubo *et al*. 1990; Li *et al*. 1997; Zhang *et al*. 2003; LeGeros 2008).

In a typical electrochemical deposition, a CaP precursor is first formed that is converted into hydroxyapatite (HA) through an ageing process (heat or alkaline treatment). Thus, this method offers more control over deposit crystallinity (Redepenning and McIsaac 1990; Redepenning *et al*. 1996; Pongkao Kashima and Rakngarm 2008). In order to be able to deposit a CaP layer by this technique the surface of the material must be electronically conductive as the deposition takes place on the cathode of an electrochemical cell.

The aim of this study was to produce, characterise and compare CaP coatings on the surface of polished and sand-blasted tantalum and TiAl6V4 discs deposited by biomimetic and electrochemical methods.

The hypotheses were:

1. **Biomimetic and electrochemical methods can be applied in order to deposit a CaP layer on TiAl6V4 or tantalum surfaces.**
2. **Biomimetic and electrochemical methods will produce different CaP coatings on the surface of TiAl6V4 or tantalum discs in terms of morphology and composition.**
3. **Surface topography and type of metal will not affect the morphology and composition of CaP coatings deposited on TiAl6V4 or tantalum discs by the same method.**
4. **CaP coatings deposited on the surface of TiAl6V4 or tantalum discs by biomimetic and electrochemical methods will develop an apatite layer when immersed in SBF.**

2.2 MATERIALS AND METHODS

2.2.1 Sample Preparation

Pure Tantalum (Ta) and TiAl6V4 (Ti) discs used in this study were 10mm diameter × 2mm thickness.

The surfaces were initially polished using silicon carbide grinding papers (Buehler, Germany) in a grinding machine (EXACT, Germany). In order to create a rough surface, half of them were sandblasted by alumina particles (Al_2O_3) to obtain an average roughness of *Ra*=4.0μm (Plasma Biotal Limited, UK). Sandblasting is a generic term for the process of shaping, smoothing or cleaning hard surfaces by accelerating and forcefully directing solid particles against a hard surface (definition from Oxford English Dictionary). The differences between the polished and sand-blasted surfaces can be seen in Figure 2.1.

Samples were ultrasonically cleaned in acetone, 70% ethanol and distilled water for 15 minutes and air dried prior to coating.

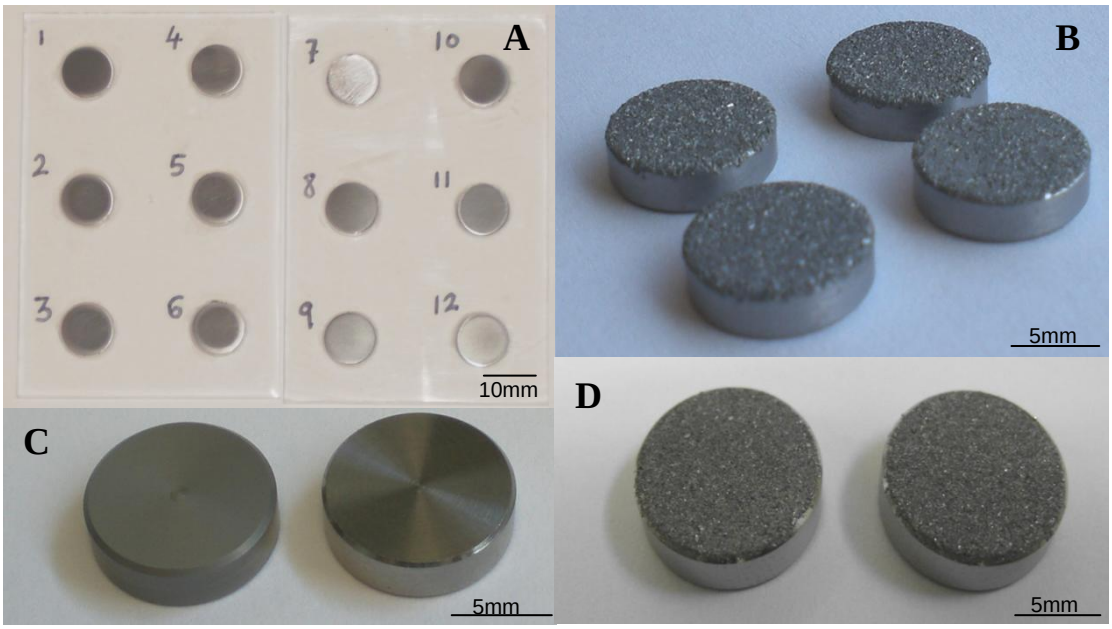

Figure 2.1 A) Polished tantalum discs; **B)** sand-blasted tantalum discs; **C)** polished TiAl6V4 discs and **D)** sand-blasted TiAl6V4 discs.

2.2.2 Biomimetic Coating Process

The biomimetic coating process was adapted from Habibovic *et al*. 2002, who used a two step biomimetic coating procedure on metal implants. Firstly, samples are soaked in a solution that is five times more concentrated than regular simulated body fluid (SBF-1). In this first step the authors reported a thin and uniform amorphous CaP layer was deposited on the metal surface. Secondly, samples are immersed in the SBF-2 solution, which has similar composition to that of SBF-1 but with decreased contents of crystal growth inhibitors (Mg^{2+} and HCO_3^-). During this second coating step, a fast precipitation of a 30μm thick crystalline CaP coating was observed. The biomimetic coating produced by this two step procedure was found to closely resemble bone mineral (Habibovic *et al*. 2002).

Coating solutions SBF-1 and SBF-2 were prepared according to Table 2.1. Both solutions were prepared using reagent grade salts: NaCl (10241AP, BDH, UK), $NaHCO_3$ (102474V, BDH, UK), Na_2HPO_4 (102494C, DBH, UK), $MgCl_2 \cdot 6H_2O$ (101494V, BDH, UK) and $CaCl_2 \cdot 2H_2O$ (100703H, BDH, UK). The appropriate quantities of the salts were dissolved in distilled water at 37ºC with a constant 5%CO_2 supply and stirring.

Discs were firstly soaked in SBF-1 for 24h at 37ºC with constant stirring and 5%CO_2 supply. Secondly, discs were soaked in SBF-2 for 48h (Ta) or 18h (Ti) at 50ºC with constant stirring and 5%CO_2 supply. Discs were not washed in between the two steps. Both steps were carried out inside a 37ºC with 5%CO_2 incubator. For the second step, temperature was raised to 50ºC by using a hot plate and controlled with a thermometer. Finally, discs were cleaned in distilled water for 1min and air dried.

Ion Concentration (mM)								
Component	**Na^+**	**K^+**	**Ca^{2+}**	**Mg^{2+}**	**Cl^-**	**HPO_4^{2-}**	**HCO_3^-**	**SO_4^{2-}**
HBP	142.0	5.0	2.5	1.5	103.0	1.0	27.0	0.5
SBF	142.0	5.0	2.5	1.5	148.8	1.0	4.2	-
SBF-1	714.8	-	12.5	7.5	723.8	5.0	21.0	-
SBF-2	704.2	-	12.5	1.5	711.8	5.0	10.5	-

Table 2.1 Inorganic composition of Human Blood Plasma (HBP), Simulated Body Fluid (SBF) and Coating Solutions SBF-1 and SBF-2.
(Habibovic *et al*. 2002)

2.2.3 Electrochemical Coatings Process

The electrochemical coatings process was adapted from Redepenning *et al*. 1996. The electrochemical coating method described by Redepenning and colleagues in 1996 is routinely used to coat metal implants with a HA layer at the John Scales Centre for Biomedical Engineering. The procedure involves a combination of different chemical reactions that lead to the deposition of a HA layer on the metal implant:

1) Electrochemical reaction, where the pH is controlled by the electrical current passed through the solution:

$2H_2O + 2e^- \leftrightarrow H_2 + 2OH^-$

2) Acid-Base reaction, determined by the pH:

$OH^- + H_2PO_4^- \leftrightarrow H_2O + HPO_4^{2-}$

3) Precipitation reaction, influenced by the concentration of HPO_4^{2-} :

$Ca^{2+} + HPO_4^{2-} + 2H_2O \leftrightarrow CaHPO_4\text{-}2H_2O\downarrow$ (Brushite)

4) Conversion into HA by immersion in NaOH for 72h:

$5CaHPO_4\text{-}2H_2O + 6OH^- \leftrightarrow Ca_5(PO_4)_3OH + 2PO_4^{3-} + 15H_2O$

A difference in morphology before and after the conversion can be observed with little overall change in the crystals sizes.

Summing up, the deposition rate as well as the chemistry and the morphology of the deposited CaP can be controlled by controlling the electrical current.

A CaP saturated solution was prepared by adding 30g of reagent grade $Ca(H_2PO_4)_2$ (C8017, Sigma-Aldrich, UK) to 1L of distilled water at room temperature. The solution was stirred vigorously for 1hour. Finally, the solution was filtered using Whatman 540 filter paper in order to remove suspended monobasic calcium phosphate crystals and obtain a clear solution.

Discs were immersed in the CaP solution and attached to the negative terminal of a DC Dual Power Supply pack (Peak Tech, Telonic instruments Ltd, UK) to act as the cathode. A platinum ring (20mm diameter × 1.5mm thickness) acted as the anode.

Two different electrical currents of 20 and 6.5mA/cm^2 of surface area were tested. 20mA/cm^2 was found to be optimum for current efficiency by Redepenning *et al*. 1996. 6.5mA/cm^2 was chosen so a thinner HA layer on the surface of discs could be produced, as the lower the electrical current the lower the deposition rate and therefore the thinner it is the deposited CaP precipitate (Redepenning *et al*. 1996). A FLUKE 867B Graphical Multimeter (Fluke Corporation, USA) was used to control the current. The electrical current was passed through the solution for 250 seconds. The deposition of a mineral layer could be observed over time. Figure 2.2 shows the equipment and setting used in the electrochemical depositions.

In order to convert the initial CaP precipitate ($CaHPO_4$-$2H_2O$ or Brushite) in HA [$Ca_5(PO_4)_3OH$] the discs were soaked in 0.1M NaOH solution for 72 hours. In alkaline conditions brushite is converted into HA by deprotonation, expulsion of phosphate groups and rearrangement of the lattice. The alkaline solution was made by adding 2g of NaOH (480878, Sigma-Aldrich, UK) to 500ml of distilled water and vigorously stirred for 20 minutes. Finally, the coated discs were cleaned in distilled water and air dried.

Figure 2.2 Equipment and setting for the electrochemical depositions of a CaP layer on the surface of titanium or tantalum discs.

2.2.4 Groups and Number of Discs

Description of groups of samples tested are summarised in Table 2.2.

12 groups were tested with n=3 per group:

GROUP	DESCRIPTION
1	**PTa-BioM**: Polished tantalum discs CaP coated by the biomimetic method
2	**PTi-BioM**: Polished titanium discs CaP coated by the biomimetic method
3	**SBTa-BioM**: Sand-blasted tantalum discs CaP coated by the biomimetic method
4	**SBTi-BioM**: Sand-blasted titanium discs CaP coated by the biomimetic method
5	**PTa-E20**: Polished tantalum discs CaP coated by the electrochemical method at 20mA/cm^2
6	**PTi-E20**: Polished titanium discs CaP coated by the electrochemical method at 20mA/cm^2
7	**SBTa-E20**: Sand-blasted tantalum discs CaP coated by the electrochemical method at 20mA/cm^2
8	**SBTi-E20**: Sand-blasted titanium discs CaP coated by the electrochemical method at 20mA/cm^2
9	**PTa-E6.5**: Polished tantalum discs CaP coated by the electrochemical method at 6.5mA/cm^2
10	**PTi-E6.5**: Polished titanium discs CaP coated by the electrochemical method at 6.5mA/cm^2
11	**SBTa-E6.5**: Sand-blasted tantalum discs CaP coated by the electrochemical method at 6.5mA/cm^2
12	**SBTi-E6.5**: Sand-blasted titanium discs CaP coated by the electrochemical method at 6.5mA/cm^2

Table 2.2: Description of groups of samples for the study of CaP coating of metal discs with different topographic surface.

In order to compare the first CaP mineral deposited on the metal discs to the converted CaP mineral after the ageing treatment, groups 5 to 12 were also prepared without immersion in 0.1M NaOH for 72h.

2.2.5 Characterisation of Coatings

Morphology and crystal size of the coatings were characterised by scanning electron microscopy (SEM). Elemental analysis, phase composition and crystallinity were studied by energy dispersive X-ray spectroscopy (EDAX) and X-ray diffraction (XRD). Thickness of the CaP coatings was quantified by SEM. Finally, an apatite layer formation study was carried out by immersion of CaP coated discs in SBF and analysis by SEM and EDAX.

2.2.5.1 Morphology and Crystal Size: Scanning Electron Microscopy (SEM)

SEM is a useful technique for inspecting topographies of specimens at very high magnifications. Therefore, morphology and crystal sizes were analysed by observing the CaP coated metal discs by SEM.

CaP coated Ta and Ti discs were mounted on stubs and gold/palladium sputtered coated (EMITECH K550, Emitech, UK) before observation by SEM (JEOL JSM 5500 LV). Images were obtained at 15 to 20kV.

2.2.5.2 Elemental Analysis: Energy Dispersive X-Ray Spectroscopy (EDAX)

EDAX is a technique used to perform compositional analysis as well as to estimate relative concentrations of the elements on the surface of the specimens. In the present work, elemental composition of the CaP coatings as well as their calcium to phosphorous ratio (Ca/P) were investigated using this technique.

The EDAX detector was filled up with liquid Nitrogen 30 to 60 minutes before the analysis. After observation of the CaP coated discs by SEM, the EDAX analysis was done (EDAX, EDAX Inc. USA). EDAX Genesis® software (EDAX UK, Cambs. UK) was used to acquire and analyse the data. EDAX spectra and analysis were printed out and scanned (CanoScan FB1200S, Canon UK) in order to convert them into a JPEG file.

2.2.5.3 Phase Composition and Crystallinity: X-Ray Diffraction (XRD)

XRD techniques are used to study the phase composition and crystallographic structure of crystalline materials. In this thesis, XRD was chosen to find out the CaP phases formed on the surface of the metal discs as well as their crystallinity. This information was obtained from the XRD patterns of the samples, which are unique for each compound.

XRD analysis was kindly performed by Professor Jonathan C. Knowles at the UCL Eastman Dental Institute. A Brüker D8 Advance Diffractometer (Brüker, UK) operated with Ni-filtered Cu Kα radiation was used. Data were collected from 2θ = 10º to 100º with a step size of 0.02º and a count time of 12s per point with a Brüker Lynx Eye detector.

In order to indentify the peaks in the samples' diffraction patterns, pure Ti, Ta and HA discs were also analysed by XRD. A pure brushite XRD pattern was obtained from ICSD database.

HA discs were kindly donated by Doctor Sorousheh Samizadeh. They were prepared using HA (Batch no. A00P0B06500) powder that was provided by ApaTech Ltd. 1 gram of the powder was pressed at 1.5 tones/mg force using a mechanically operated press machine and metallic dyes specially designed for making dense discs of 11 x 3 mm. The HA discs were then sintered in a furnace at 1250°C: the temperature of the sintering furnace was set to increase at a rate of 5°C/min up to the sintering temperature followed by 2 hours of dwell time. The temperature was then reduced down to 26°C at the rate of 10°C/min.

2.2.5.4 Thickness of the CaP Coatings: SEM Analysis

In order to quantify the thickness of the CaP coatings, discs were embedded in hard grade acrylic resin (LR White Resin, Agar Scientific) and transversely cut using EXACT diamond band saw (EXACT, Germany). They were then polished using silicon carbide grinding papers at increasing grades (240, 600, 1200, 2500 and 4000; Buehler, Germany) in a grinding machine (EXACT, Germany). In the last step, samples were polished on polishing cloth using AP-A suspension (5μm agglomerated α-alumina suspension, Struers, Denmark). Next, they were analysed by SEM, as

explained in section 2.2.5.1. Four to five photos per sample were printed out and their thickness was calculated using a ruler. The measurements in centimetres were transformed to micrometres by taking into account the magnification bar of the photos.

2.2.5.5 Apatite Layer Formation Study

As it has been shown that CaP materials promote direct bonding with bone tissue through formation of an apatite layer, *in vitro* models for studying apatite formation on the surface of different biomaterials are used as an assessment of their bioactivity and osteoconductivity. These *in vitro* models use the method developed by Kokubo and co-workers in the 1990s in which SBFs that mimic physiological solutions are used (Kokubo *et al*. 1990; Kokubo 1998; Kokubo *et al*. 2001): biomaterials under study are immersed in SBFs and the mineral layer formed on their surface is subsequently characterised.

In this thesis, an apatite layer formation study was carried out by immersion of CaP coated discs in SBF. Since surface topography and metal type did not affect the morphology and composition of CaP coatings deposited on Ti and Ta discs by the same method, for this study only CaP coated polished Ti discs were used. Uncoated polished Ti and pure HA discs were used as controls. Pure HA discs were the same ones as in section 2.2.5.3.

SBF was prepared according to Table 2.1 (Kokubo *et al*. 1990) using reagent grade salts: NaCl (10241AP, BDH, UK), KCl (101983K, BDH, UK), $NaHCO_3$ (102474V, BDH, UK), K_2HPO_4 (17835, Sigma-Aldrich, UK), $MgCl_2 \cdot 6H_2O$ (101494V, BDH, UK) and $CaCl_2 \cdot 2H_2O$ (100703H, BDH, UK). The appropriate quantities of the salts were dissolved in distilled water with constant stirring. The solution was buffered at pH=7.25 with $(CH_2OH)_3CNH_2$ 50mM/HCl 45 mM buffer and kept at 37ºC.

The buffer mentioned above was prepared by mixing 3.7mL of hydrochloric acid (HCl, 101256J, BDH, UK) and 1.51g of trishydroxymethyl-aminomethane [$(CH_2OH)_3CNH_2$, 103153L, BDH, UK] in 1L of distilled water.

PTi, HA, PTi-BioM, PTi-E20 and PTi-E6.5 discs were immersed for up to 7 days in SBF at 37ºC. Discs surfaces were analysed by SEM and elemental composition by EDAX at days 0, 1 and 7 as already explained in sections 2.2.5.1 and 2.2.5.2.

2.2.6 Statistics

Statistical analysis was performed with SPSS 14.0 software. Non parametric tests were applied to the data as the sample number was small. Comparisons between groups were made using the Mann Whitney U test. A p-value$\leq$0.05 was considered a significant result.

2.3 RESULTS

2.3.1 Morphology and Crystal Size of Coatings

SEM analysis revealed different morphologies and crystal sizes for the different coatings deposited by the three methods described, as seen in Figures 2.3 and 2.4.

From Figure 2.3A it can be seen that biomimetic coating barely covered the discs surfaces. As it can be observed from the photos, patches of mineral are scattered over the discs surfaces, which were not completely covered and therefore were still visible after the biomimetic coating process (Figure 2.3). On the other hand, electrochemical depositions at 20 and 6.5mA/cm^2 completely covered the discs surfaces with a CaP layer, as seen in Figure 2.4A and B.

It can be observed from Figure 2.3 that the biomimetic coatings exhibited globular morphology composed of nanocrystals (a particle is considered to be within the nanometer scale when it measures less than 0.1μm, www.nanodic.com/Nanomaterial/Nanoparticle.htm), arranged in large globules. Globular morphologies for biomimetic coatings have already been described by other authors (Bharati *et al*. 2005; Kokubo *et al*. 2001). Photos in Figure 2.3 also show that the biomimetic coatings had the same morphology and crystal size on all the different discs, suggesting the surface topography and metal type did not have an effect on morphology and crystal size.

The original brushite deposited on the metal discs by the electrochemical depositions at 20 and 6.5mA/cm^2 displayed a typical plate-like morphology (Redepenning *et al*. 1996; Pongkao Kashima and Rakngarm 2008) as shown by Figure 2.4C and D. After the ageing treatment, by immersion in alkaline solution for 72h, the electrochemical coatings had different morphologies with a combination of plate-like and needle-like crystals occurring with tiny globular crystals and also porous structures in some areas (Fig. 2.4E-H). Crystal sizes ranged from the micrometer to the nanometer scale. Surface topography and metal type did not appear to have an effect on morphology and crystal size.

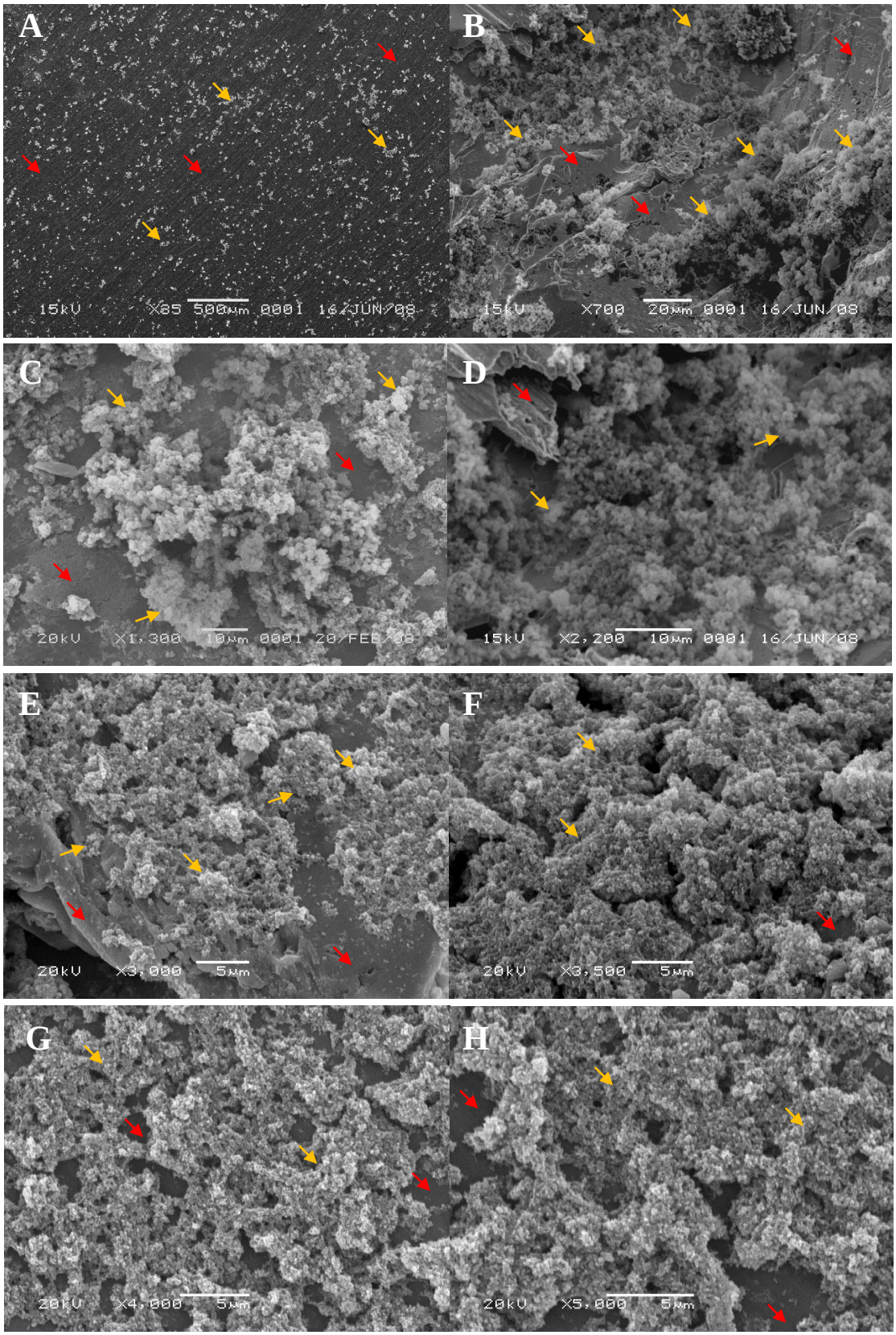

Figure 2.3 SEM photos of biomimetic CaP coating on the surface of **A)** PTa; **B)** SBTa; **C)** PTa; **D)** SBTa; **E)** SBTi **F)** SBTi and **G, H)** PTi discs, showing the globular morphology exhibited by these coatings, with nanocrystals arranged in globules (yellow arrows). Red arrows show bare surface of metal disc.

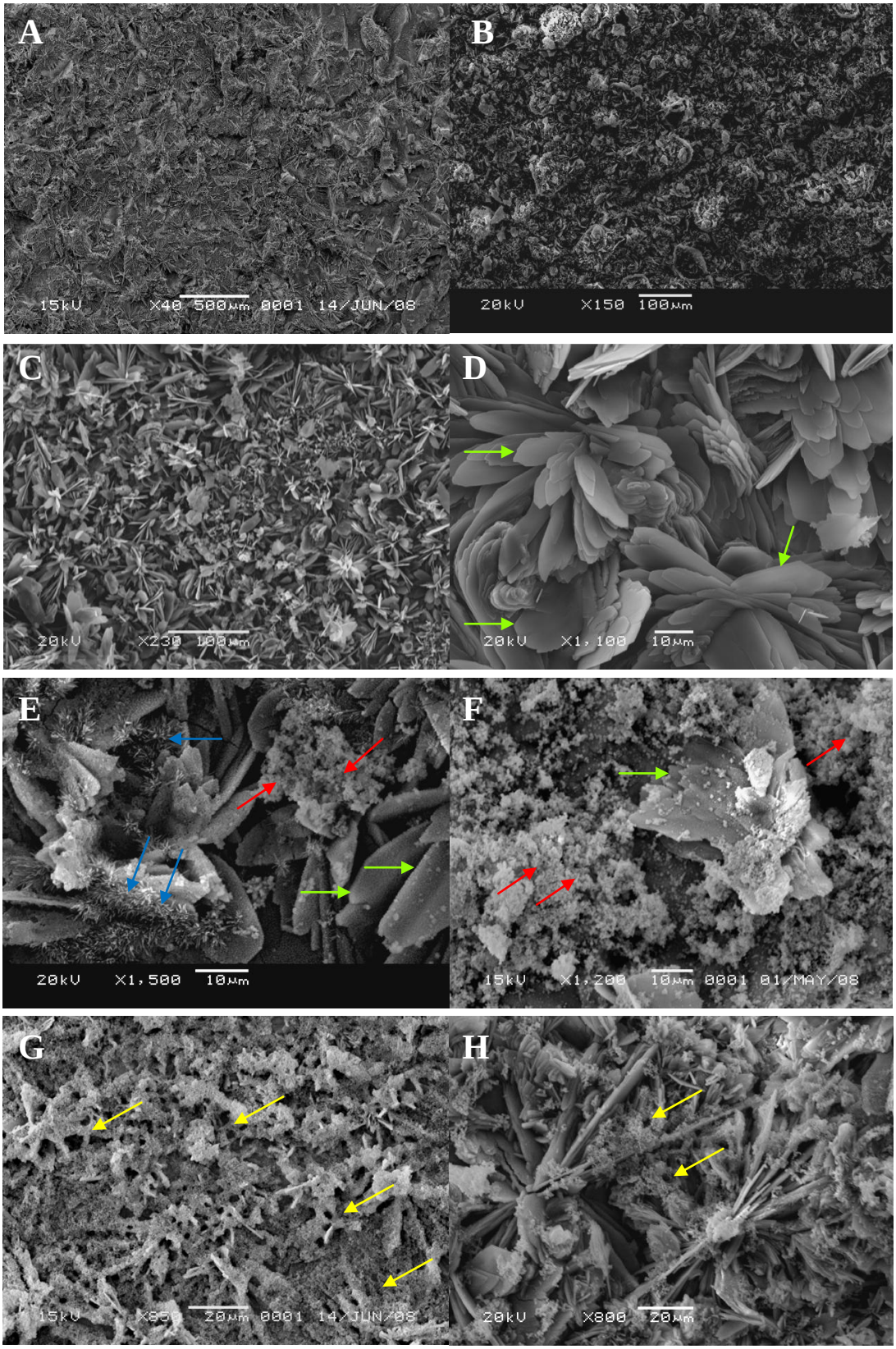

Figure 2.4 SEM photos of electrochemical CaP coatings: **A)** SBTa-E6.5; **B)** SBTi-E20; **C)** PTi-E20 not immersed in 0.1M NaOH; **D)** PTa-E6.5 not immersed in 0.1M NaOH; **E)** PTi-E20; **F)** SBTa-E20; **G)** PTa-E6.5 and **H)** SBTi-E6.5. (Arrows: green, plate-like crystals; blue, needle-like crystals; red, tiny globular crystals and yellow, porous structures).

2.3.2 Elemental Analysis and Ca/P Ratio

EDAX spectra and analysis can be seen from Figures 2.5 to 2.8. 3 discs per group were used and 3 spectra per disc were taken. Therefore, n=9 for each group in EDAX analysis.

The spectra showed that all the coatings deposited by the different methods contained calcium (Ca) and phosphorous (P) as main elements. For all the samples, carbon (C) and oxygen (O) peaks were present in the EDAX spectra. A constant peak for sodium (Na) was found for the electrochemically coated samples while it was not observed for the biomimetically coated ones. In some biomimetic samples spectra, a magnesium (Mg) peak was seen (Figure 2.5B).

Ca/P ratios calculated for the different samples can be seen in Table 2.3. Before immersion in 0.1M NaOH for 72h, Ca/P ratios calculated for electrochemically coated Ta discs were 0.92 ± 0.03 and 1.01 ± 0.06 for Ti discs. In both cases they were very close to 1 which is the Ca/P for brushite. The Ca/P ratio of all coatings was below 1.67, that of pure HA, suggesting they were Ca deficient. No significant differences ($p>0.05$) in Ca/P ratios were found between Ta and Ti discs coated by the same method when statistical analysis was applied to the data. Similarly, no significant differences ($p>0.05$) were found between BioM and E20/E6.5 coatings.

Finally, the spectra showed no differences in the coatings produced by the same method between polished and sand-blasted discs for a given metal surface. They also showed no differences in terms of elemental composition between E20 and E6.5 coatings.

Ca/P			
Coating	**BioM**	**E20/E6.5**	**E no NaOH**
Ta	1.48 ± 0.03	1.47 ± 0.07	0.92 ± 0.03
Ti	1.43 ± 0.08	1.47 ± 0.07	1.01 ± 0.06

Table 2.3 Calculated Ca/P ratios by EDAX analysis for the Ta and Ti discs CaP coated by the biomimetic method (BioM), electrochemical depositions at 20 (E20) and 6.5 mA/cm^2 (E6.5) and without immersion in 0.1M NaOH for 72h (E no NaOH).
Results show averages ± standard deviation.

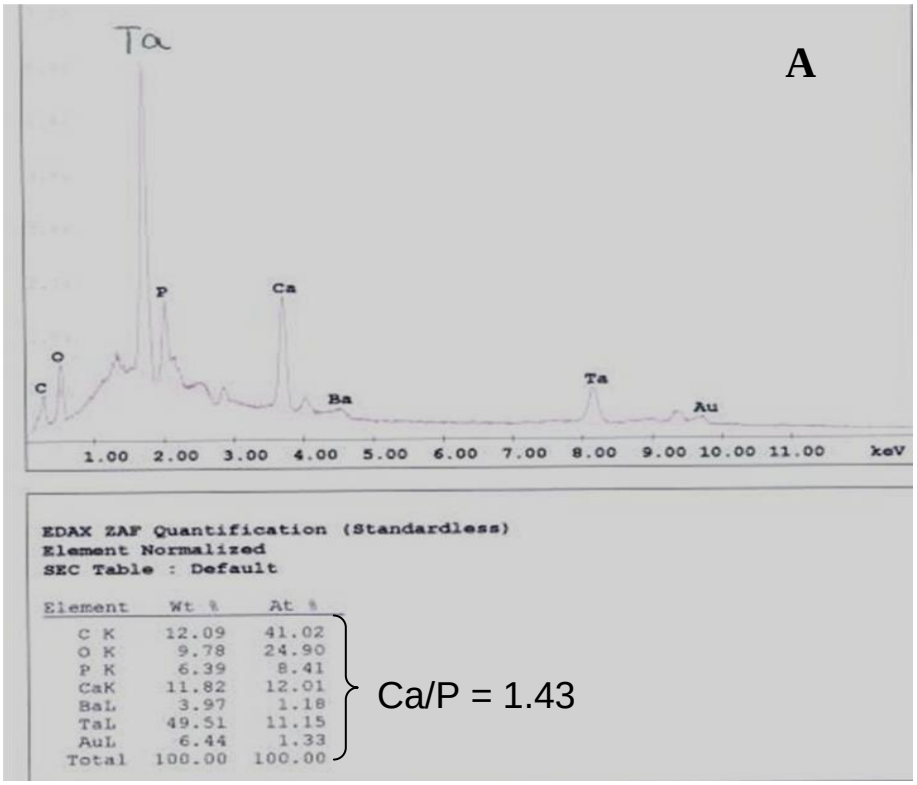

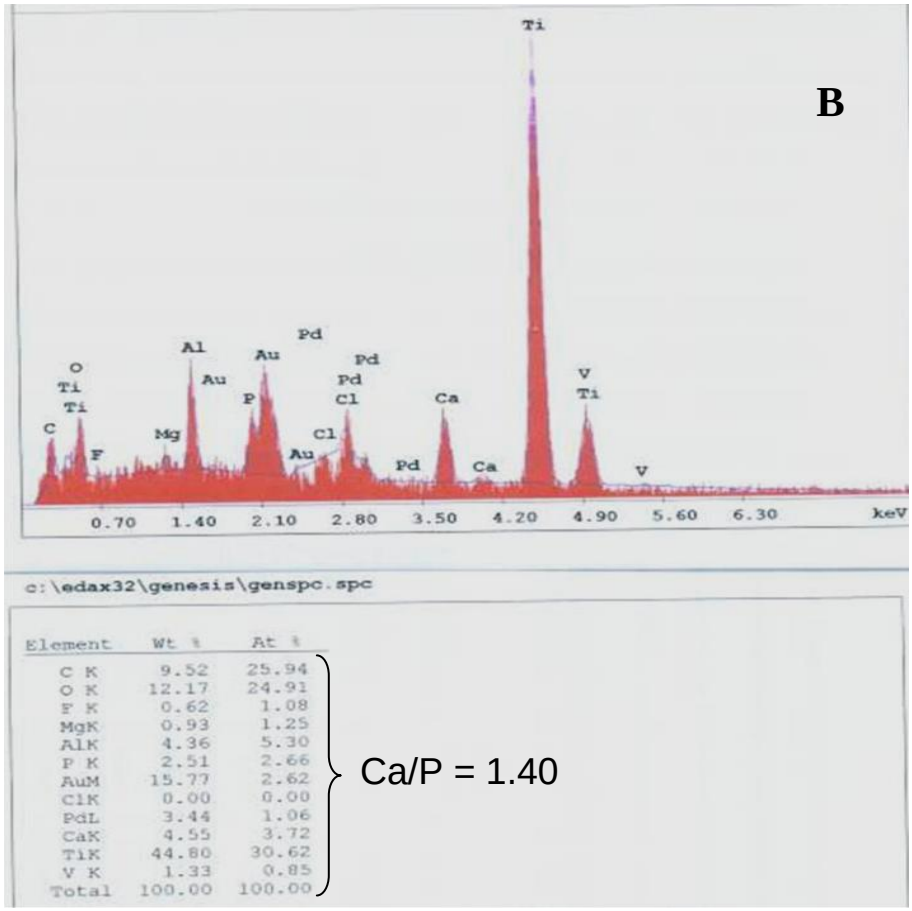

Figure 2.5 EDAX spectra and analysis of biomimetically coated **A)** polished Ta and **B)** sand-blasted Ti discs.

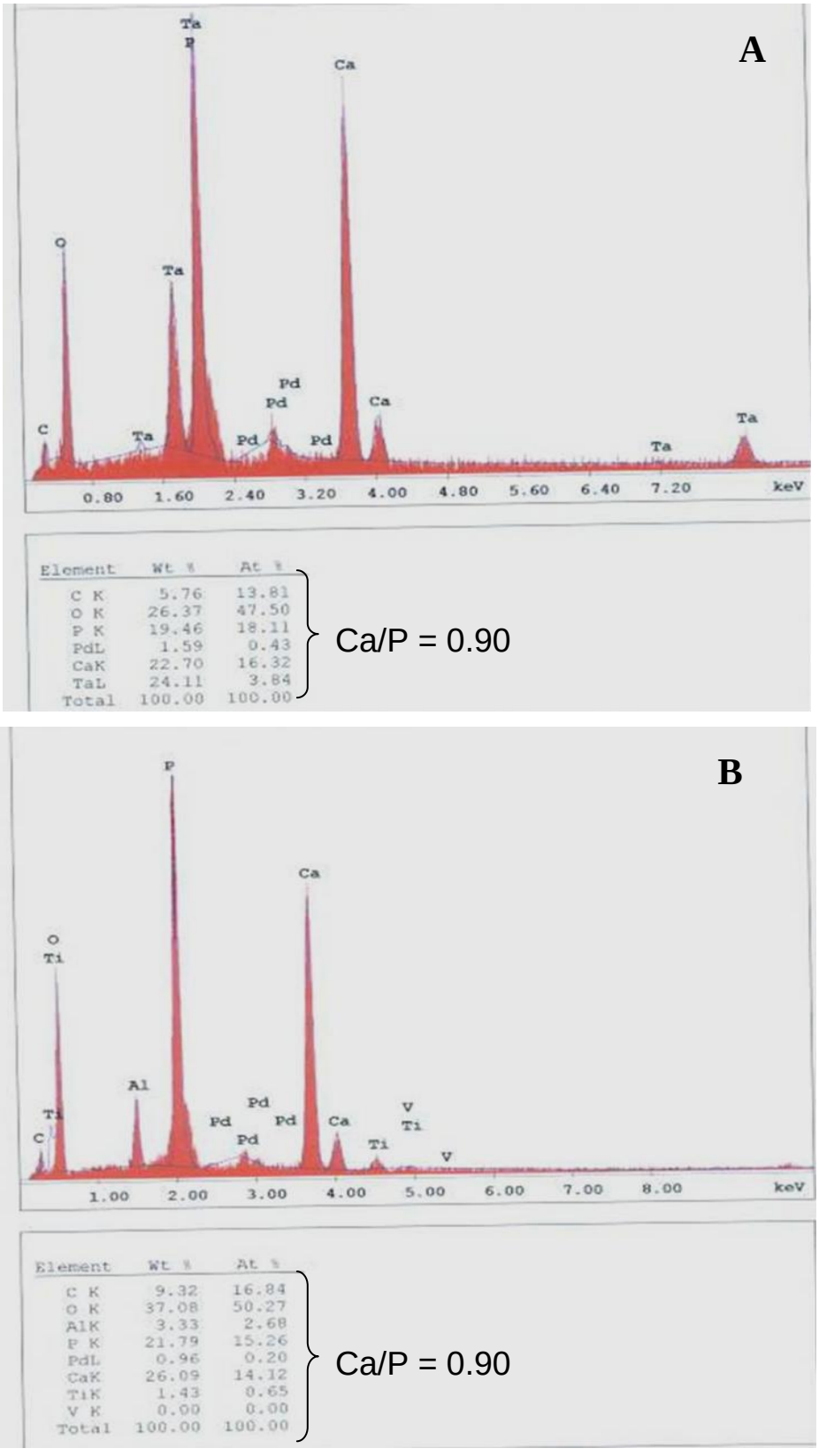

Figure 2.6 EDAX spectra and analysis of

A) polished Ta and **B)** sand-blasted Ti electrochemically coated at 6.5mA/cm^2, without immersion in 0.1M NaOH for 72 hours.

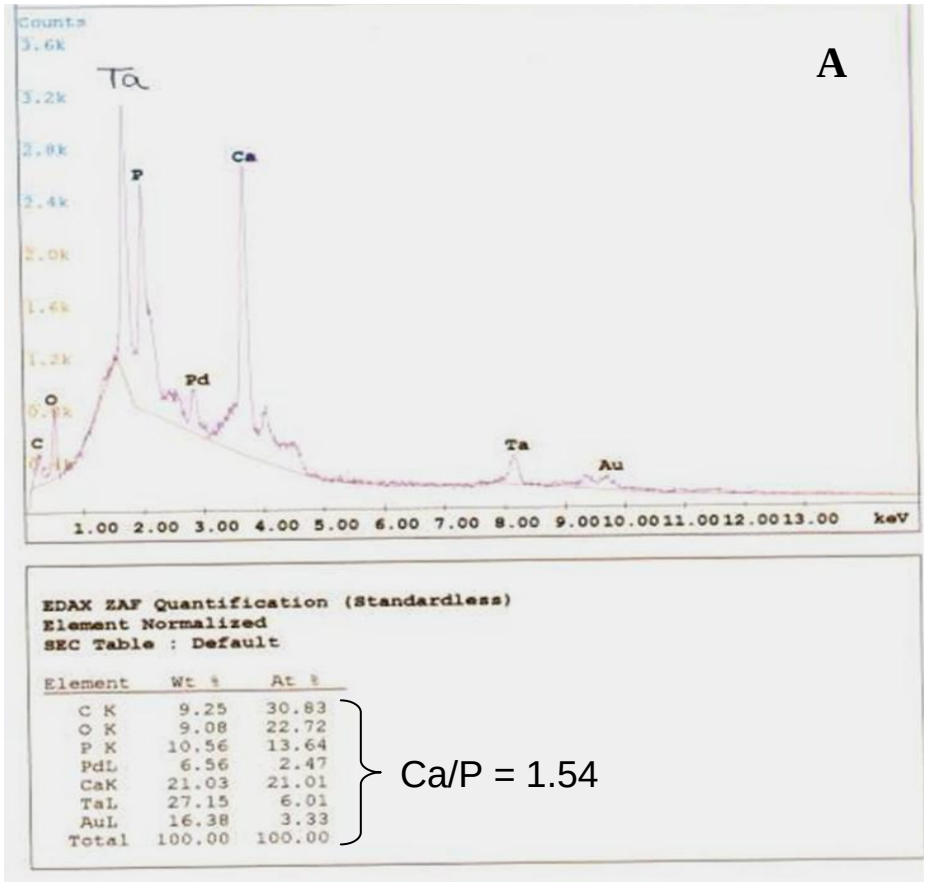

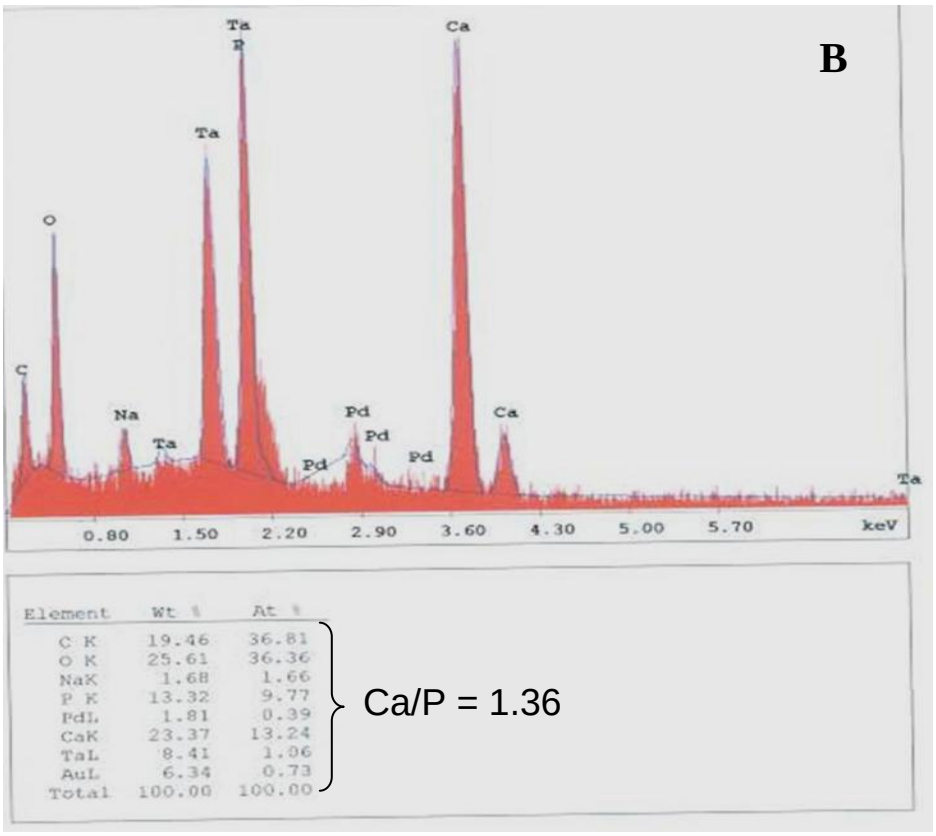

Figure 2.7 EDAX spectra and analysis of **A)** polished Ta electrochemically coated at 20mA/cm^2 and **B)** polished Ta electrochemically coated at 6.5mA/cm^2.

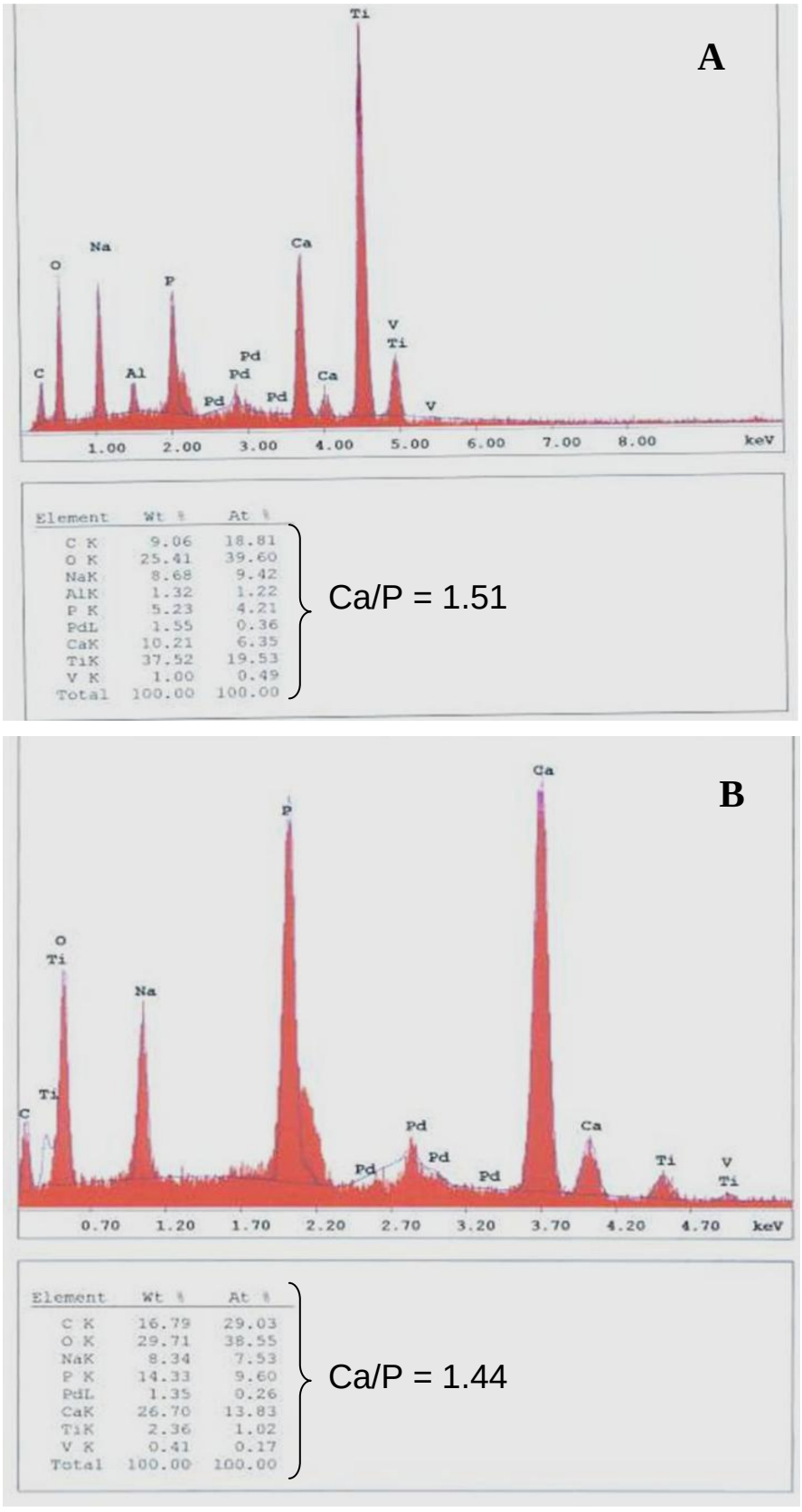

Figure 2.8 EDAX spectra and analysis of **A)** polished Ti electrochemically coated at 20mA/cm^2 and **B)** sand-blasted Ti electrochemically coated at 6.5mA/cm^2.

2.3.3 Phase Composition and Crystallinity

XRD patterns and analysis can be seen from Figures 2.13 to 2.18. In all the XRD patterns a high background noise could be observed indicating the samples contained amorphous phases. They were compared to those of pure Ta, Ti, brushite and HA (Figures 2.9 to 2.12) in order to identify the peaks.

For the biomimetically coated discs (Figures 2.13 and 2.14), no CaP phase was identified and only peaks from the metal discs could be observed, suggesting that the biomimetic CaP layers deposited were amorphous and composed of very small crystals.

Electrochemically coated discs (Figures 2.15 to 2.18) exhibited brushite peaks (B) for those samples not immersed in 0.1M NaOH for 3 days. These brushite peaks were sharp, in contrast to those of the HA into it was converted after immersion in 0.1M NaOH for 3 days, which were broad. In some samples, brushite peaks were still visible after the NaOH treatment.

EDAX and XRD results showed that for the same coating method composition was not affected by metal type or surface topography.

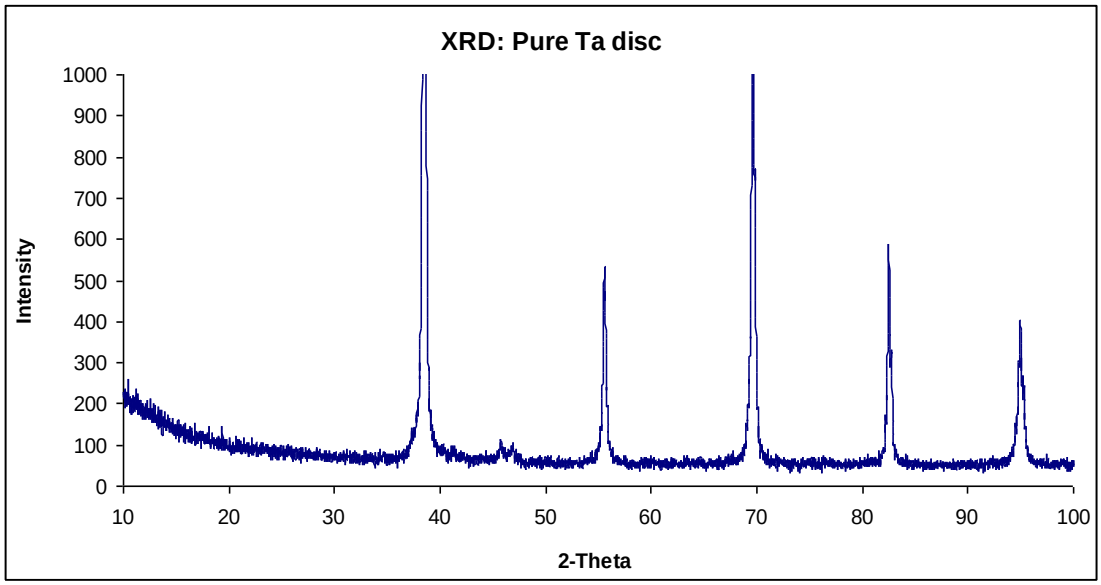

Figure 2.9 XRD pattern of pure Ta disc.

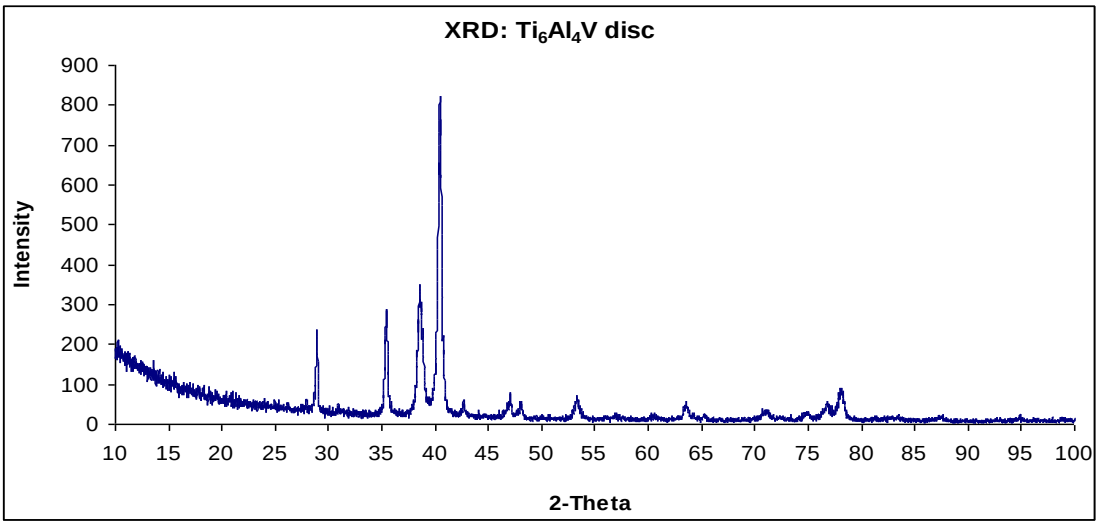

Figure 2.10 XRD pattern of Ti disc.

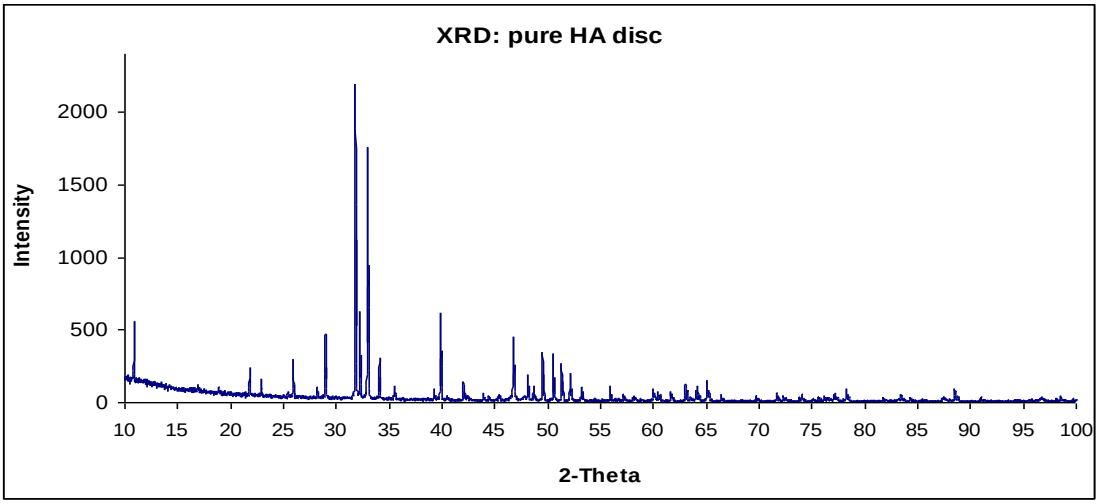

Figure 2.11 XRD pattern of pure hydroxyapatite disc.

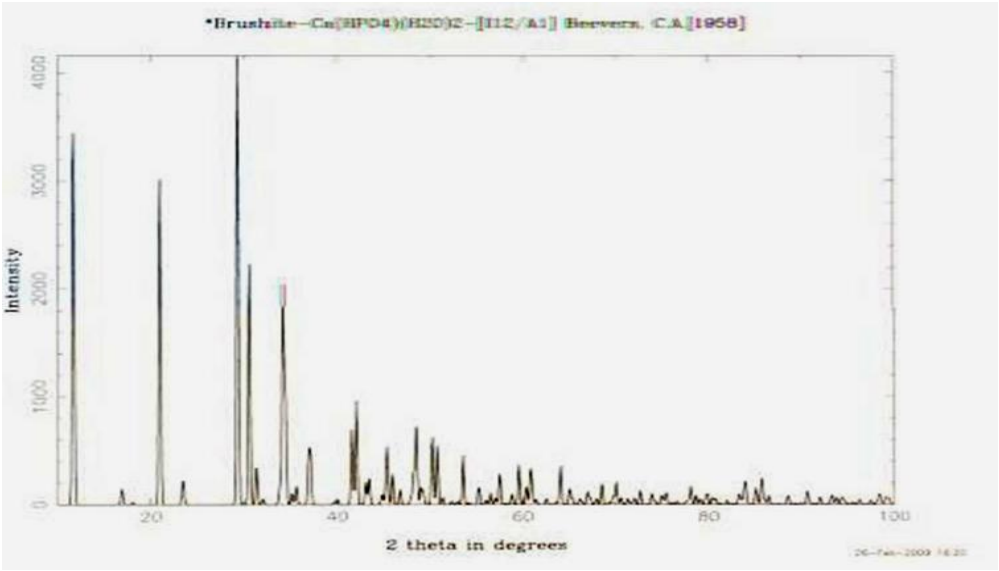

Figure 2.12 XRD pattern of pure brushite.

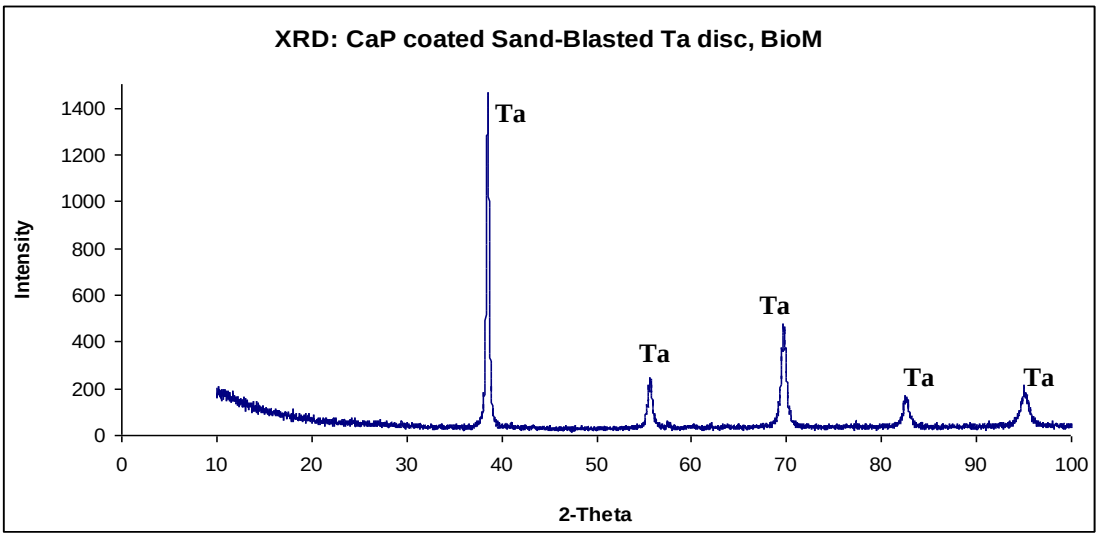

Figure 2.13 XRD pattern of biomimetically CaP coated sand-blasted Ta disc.

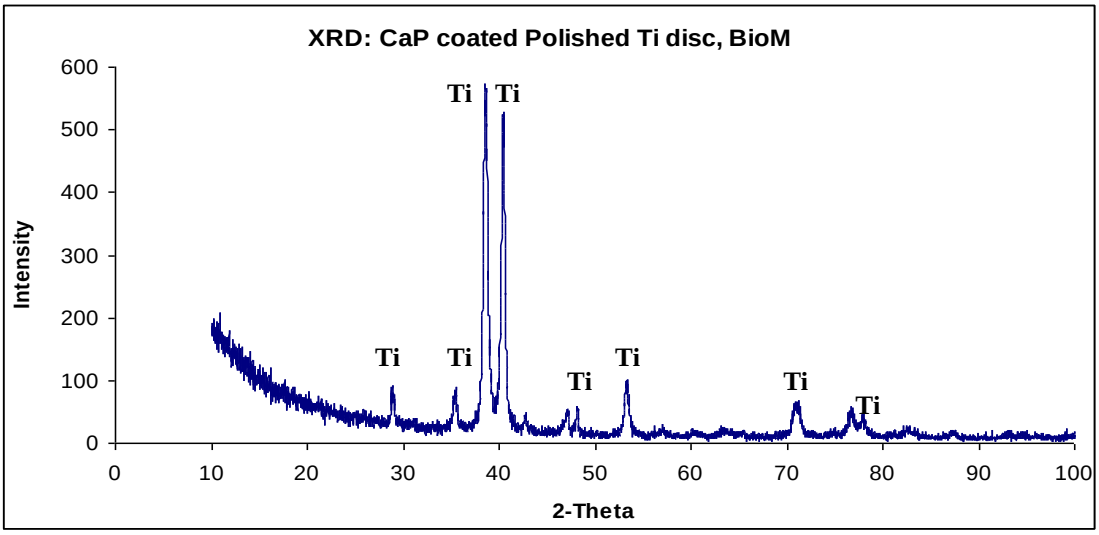

Figure 2.14 XRD pattern of biomimetically CaP coated polished Ti disc.

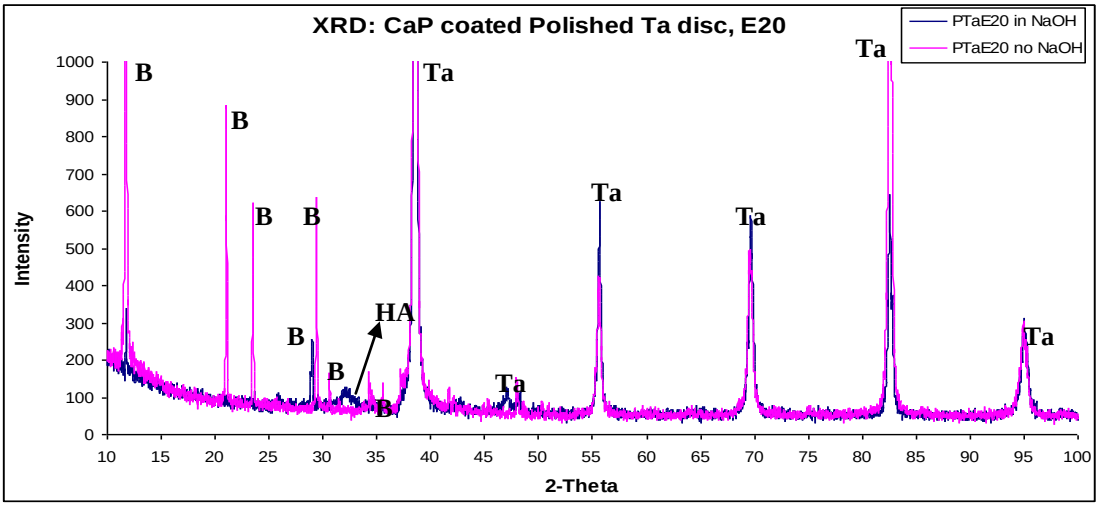

Figure 2.15 XRD pattern of electrochemically CaP coated at 20mA/cm^2 polished Ta disc.

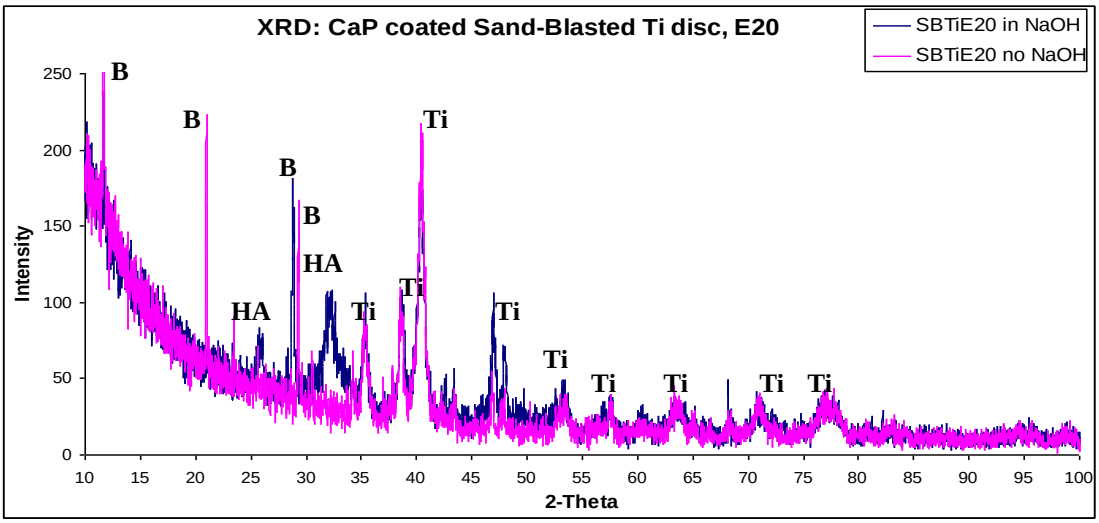

Figure 2.16 XRD pattern of electrochemically CaP coated at 20mA/cm^2 sand-blasted Ti disc.

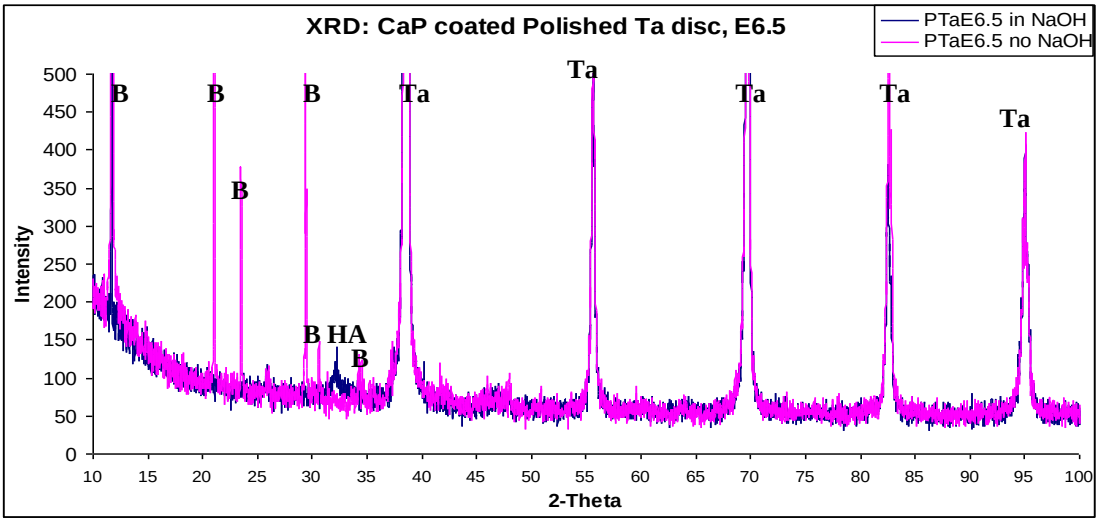

Figure 2.17 XRD pattern of electrochemically CaP coated at 6.5mA/cm^2 polished Ta disc.

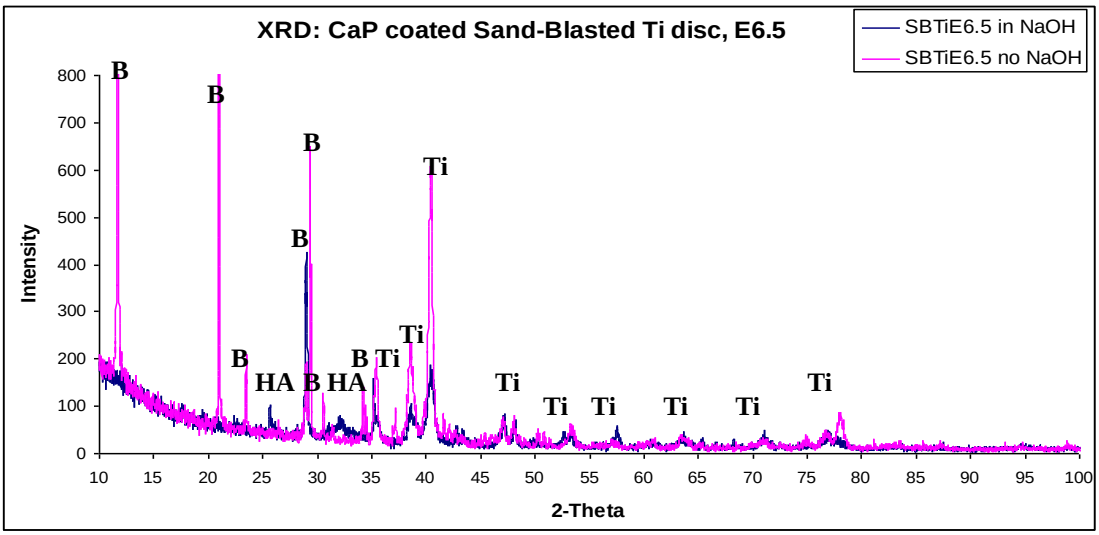

Figure 2.18 XRD pattern of electrochemically CaP coated at 6.5mA/cm^2 sand-blasted Ti disc.

2.3.4 Thickness of Coatings

Table 2.4 showed that E20 produced the thickest coatings, followed by E6.5. BioM coatings were the thinnest. These results were in line with the SEM observations summarised in Figures 2.3 and 2.4. Statistical analysis showed no significant differences ($p>0.05$) between E20 and E6.5 coatings. On the other hand, the thickness of both electrochemical coatings was significantly different ($p<0.05$) when compared to the thickness of BioM coating.

Figure 2.19 displays the SEM analysis for the biomimetic coatings. The photos showed that the surface was not completely covered by a CaP layer. The globular nature of these coatings was also observed from the photos.

Figures 2.20 and 2.21 display the SEM analysis for the electrochemical coatings. As it can be seen from them, the discs surfaces were completely covered with a CaP layer. Some photos reveal the porous nature of these coatings as well as a bigger crystal size compared to the biomimetic coatings.

Variation in thickness for the sand-blasted discs was observed to be slightly higher than for the polished ones. Finally, thickness of CaP layers on either Ta or Ti discs were found to be very similar, with no statistical differences ($p>0.05$) between them, which suggests that metal type does not affect thickness of coating.

Coating Thickness (µm)			
Coating	**BioM**	**E20**	**E6.5**
PTa	3 ± 3	16 ± 5	14 ± 6
PTi	4 ± 4	16 ± 6	14 ± 3
SBTa	3 ± 2	18 ± 10	15 ± 8
SBTi	5 ± 5	18 ± 7	14 ± 7

Table 2.4 Calculated coating thickness by SEM for the Ta and Ti discs CaP coated by the biomimetic method (BioM) and electrochemical depositions at 20 (E20) and 6.5 mA/cm^2 (E6.5).
Results show averages ± standard deviation.

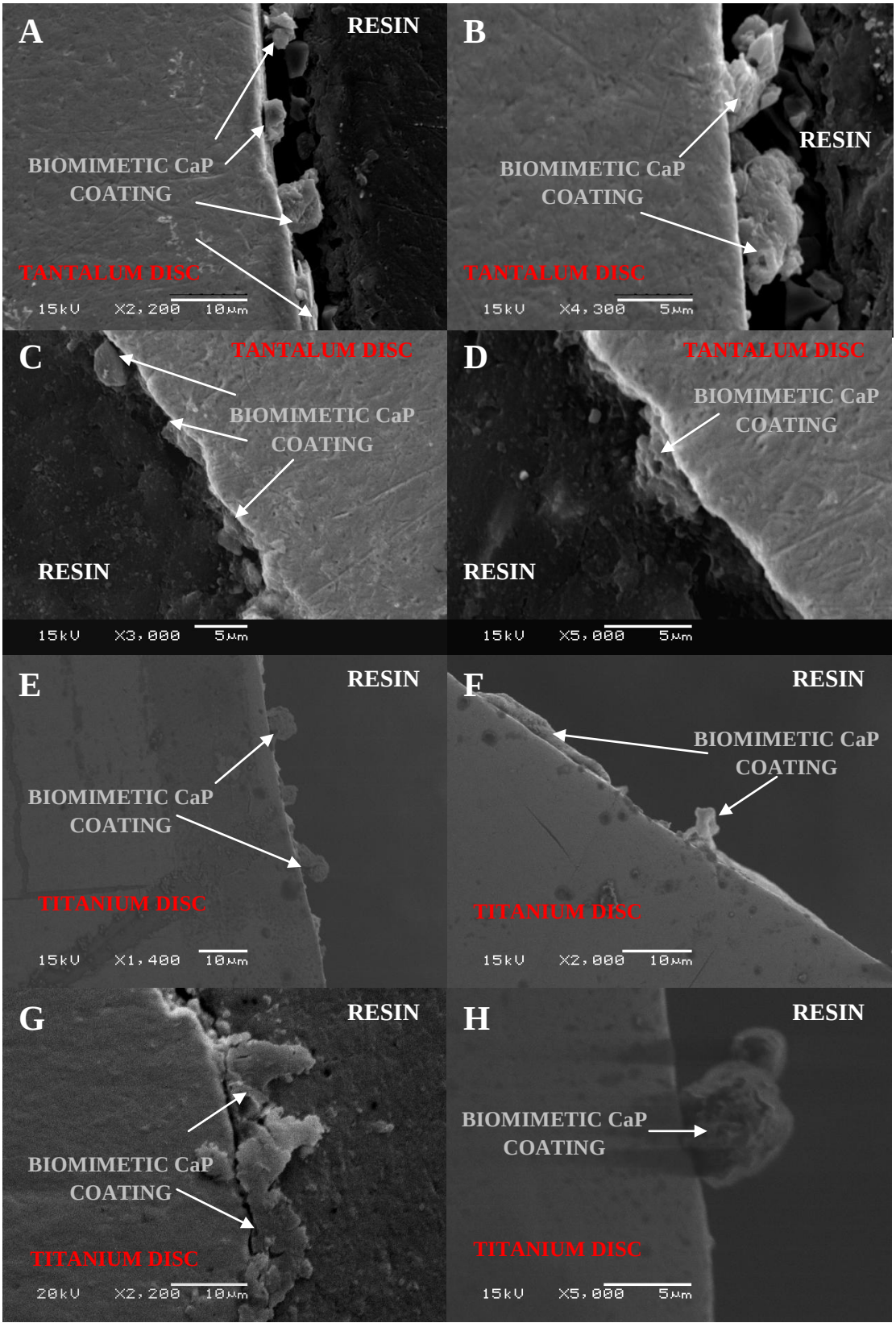

Figure 2.19 Coating thickness SEM analysis for the biomimetic coating: polished Ta disc **(A, B)**, sand-blasted Ta disc **(C, D)**, polished Ti disc **(E, F)** and sand-blasted Ti disc **(G, H)**.

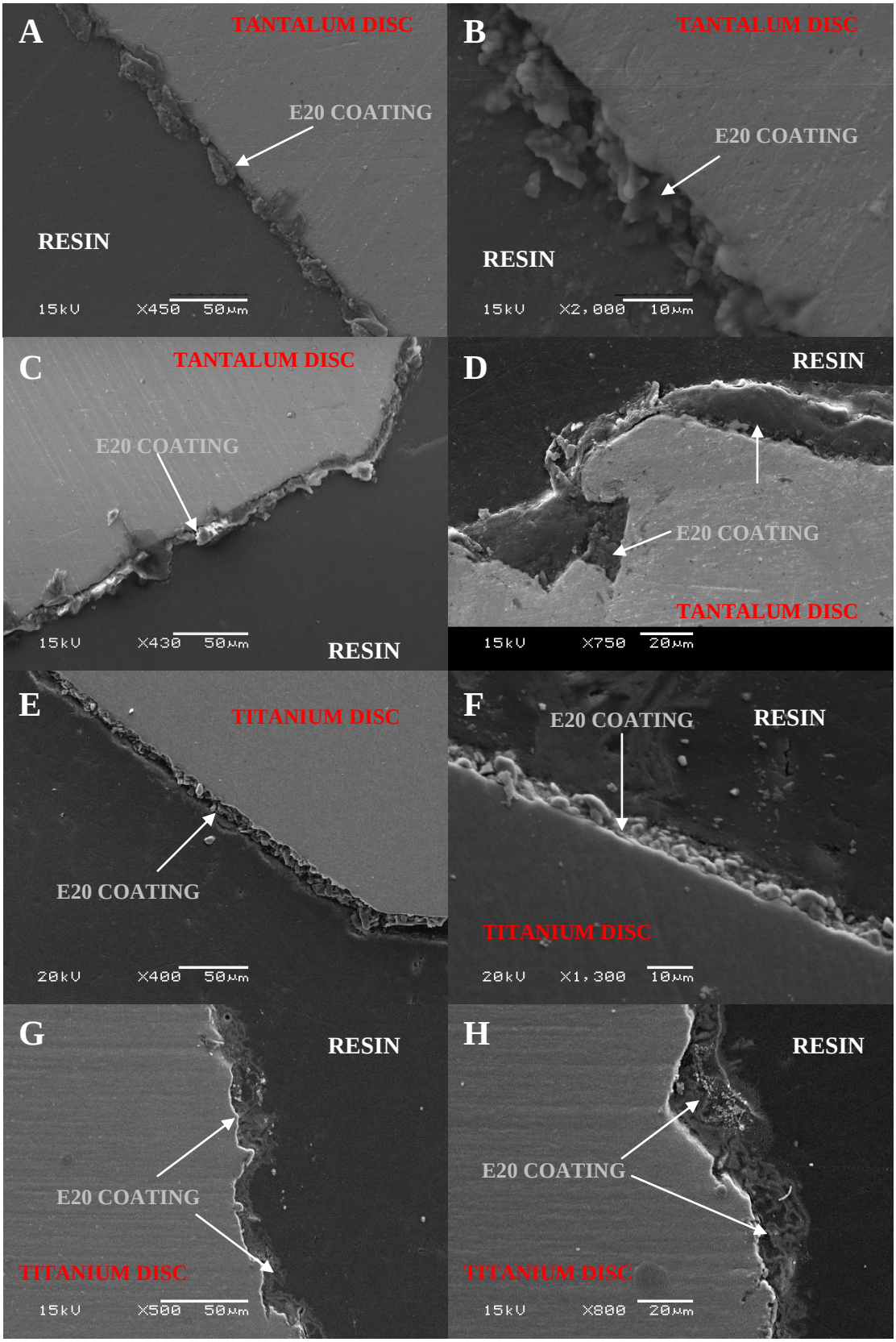

Figure 2.20 Coating thickness SEM analysis for the electrochemical coating at 20mA/cm^2: polished Ta disc **(A, B)**, sand-blasted Ta disc **(C, D)**, polished Ti disc **(E, F)** and sand-blasted Ti disc **(G, H)**.

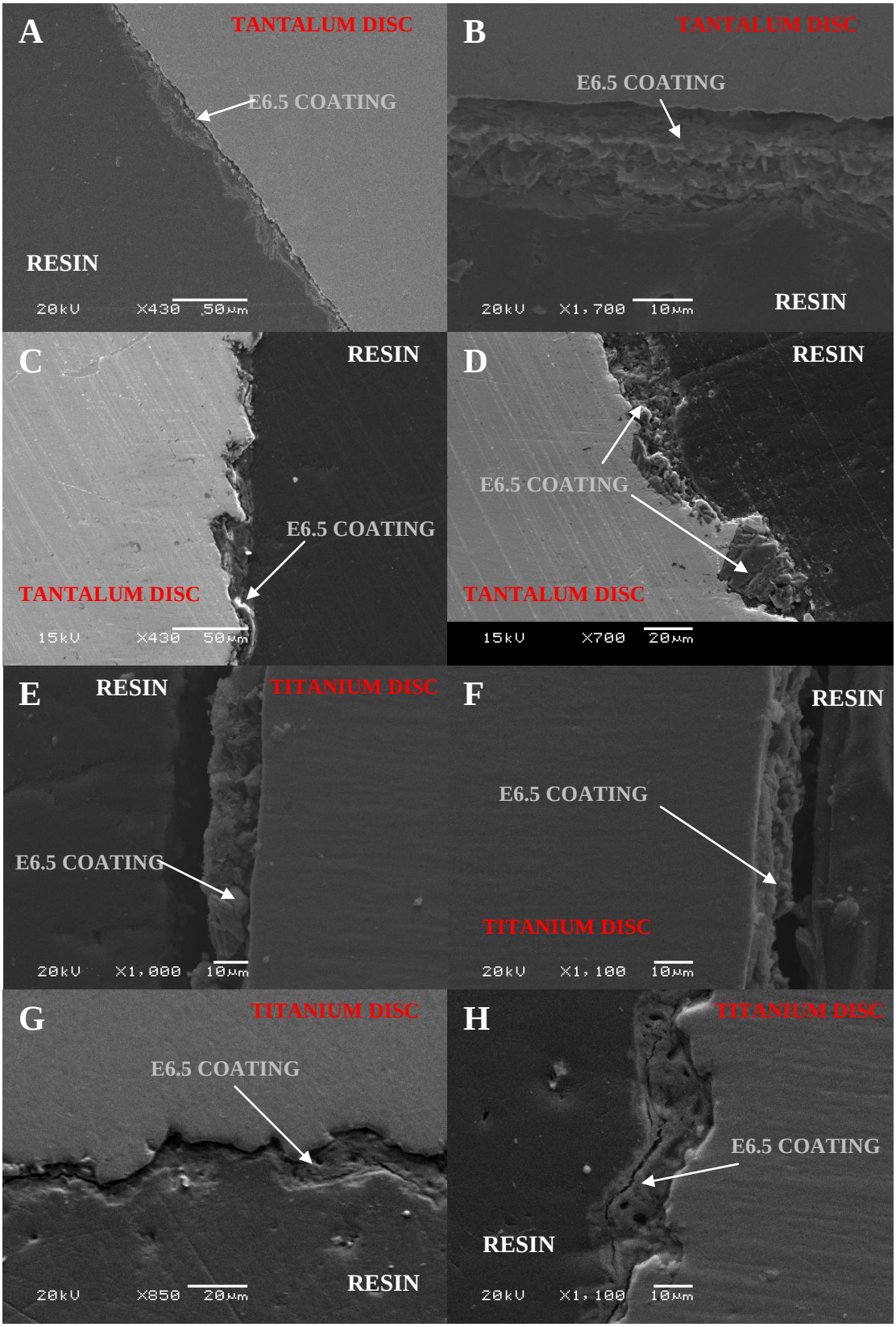

Figure 2.21 Coating thickness SEM analysis for the electrochemical coating at 6.5mA/cm^2: polished Ta disc **(A, B)**, sand-blasted Ta disc **(C, D)**, polished Ti disc **(E, F)** and sand-blasted Ti disc **(G, H)**.

2.3.5 Apatite Layer Formation Study

SEM analysis revealed a mineral layer at day 1 on control polished Ti discs which became denser after 7 days (Figure 2.22), suggesting the process of deposition of a mineral layer on the surface of Ti discs from available ions in solution was continuos over 7 days. Close observation of the particles deposited on the surface of these uncoated Ti discs showed that they were 2 to 3μm diameter globular particles. Likewise, deposition of a mineral layer over time was observed for the HA control discs (Figure 2.23). Globular amorphous crystals in the micrometer scale were observed at day 7 (Figure 2.23).

Biomimetic coating was observed to become denser after immersion in SBF for 7 days. Figure 2.24 shows that the globules formed by the nanocrystals become larger and in some areas the morphology is observed to be different, with globular amorphous crystals in the micrometer scale observed at day 7.

Figures 2.25 and 2.26 show how electrochemical coatings changed their morphology over time after immersion in SBF. Globular amorphous crystals in the micrometer scale, similar to those observed at day 7 on HA control discs and biomimetic coatings, were seen at day 7 for both electrochemical coatings (Figures 2.25 and 2.26).

From Figure 2.27 it can be seen how Ca and P peaks were barely detected by EDAX analysis on control polished Ti discs at day 1. However, they were clearly visible at day 7. A Mg peak was also detected at day 7 on these control discs. Calculated Ca/P ratios were 1.22 ± 0.08. EDAX spectra of HA discs at day 1 contained only Ca and P peaks. At day 7, Na and Cl peaks were also present besides those of Ca and P (Figure 2.28). Ca/P ratios for the HA control disc were 1.63 ± 0.07.

Figures 2.29 to 2.31 display the EDAX spectra and analysis for the coated polished Ti discs. At both time points, Na, Cl and Mg peaks were visible in the spectra as well as Ca and P peaks. Na and Cl peaks were higher in the biomimetically coated discs than in the electrochemically coated ones. Calculated Ca/P ratios were 1.39 ± 0.03 for BioM, 1.43 ± 0.06 for E20 and 1.44 ± 0.07 for E6.5, cery similar to those found for coatings without immersion in SBF, which can be seen summarised in Table 2.3.

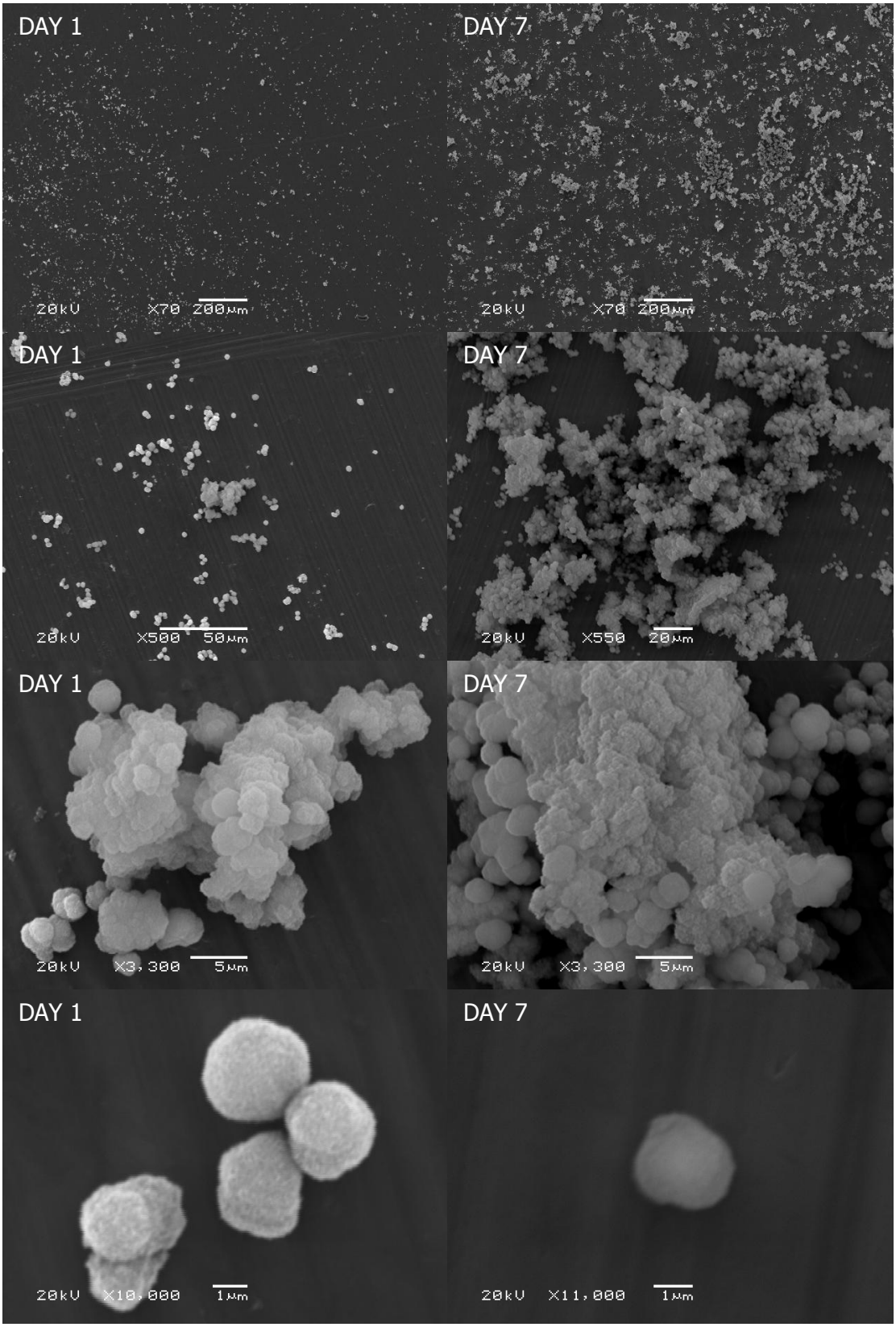

Figure 2.22 Apatite layer formation study:

SEM analysis for the control uncoated polished Ti discs after immersion in SBF for 1 (images on the left) and 7 days (images on the right).

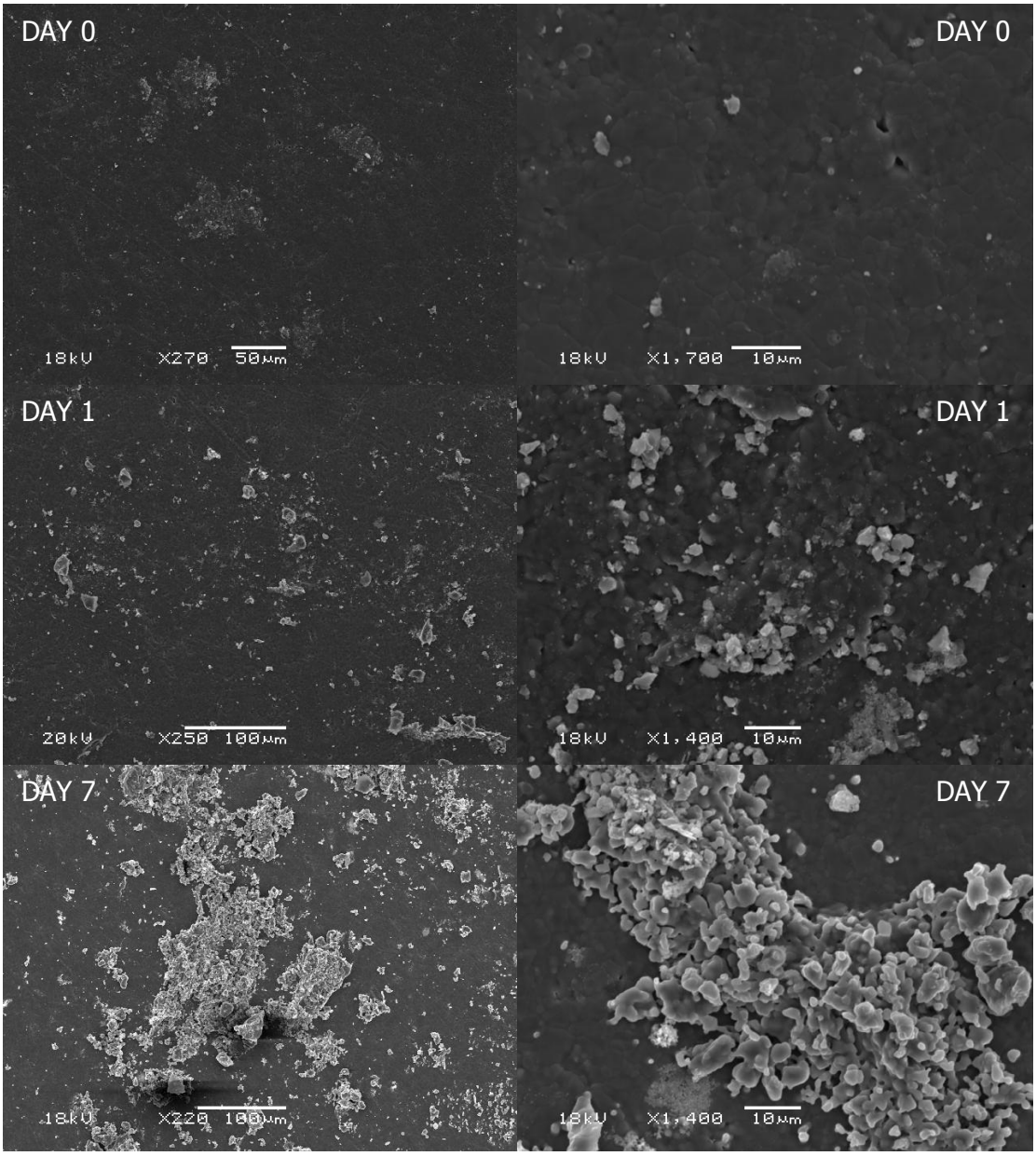

Figure 2.23 Apatite layer formation study: SEM analysis for the control HA discs after immersion in SBF for 0, 1 and 7 days.

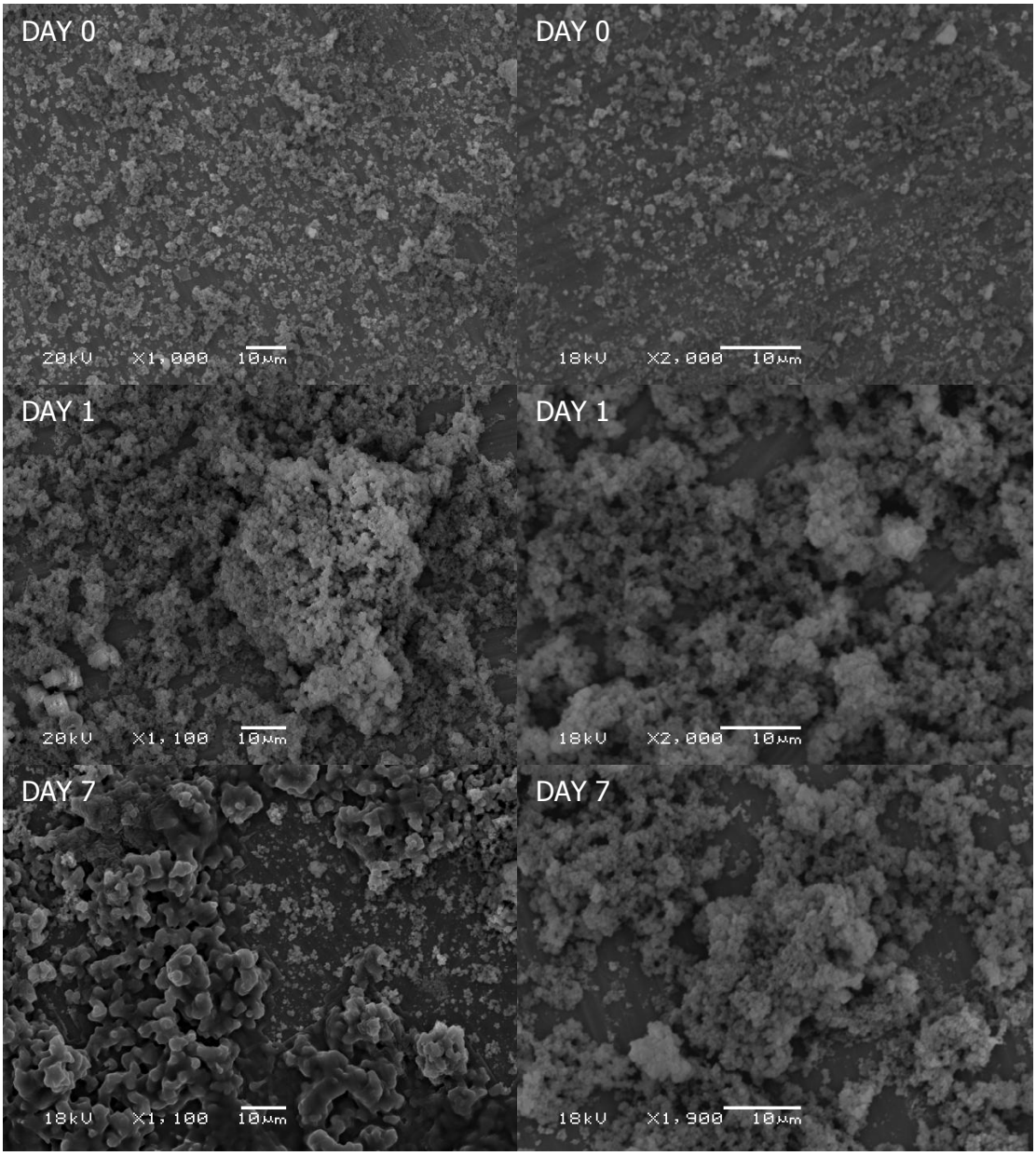

Figure 2.24 Apatite layer formation study: SEM analysis for the biomimetically coated polished Ti discs after immersion in SBF for 0, 1 and 7 days.

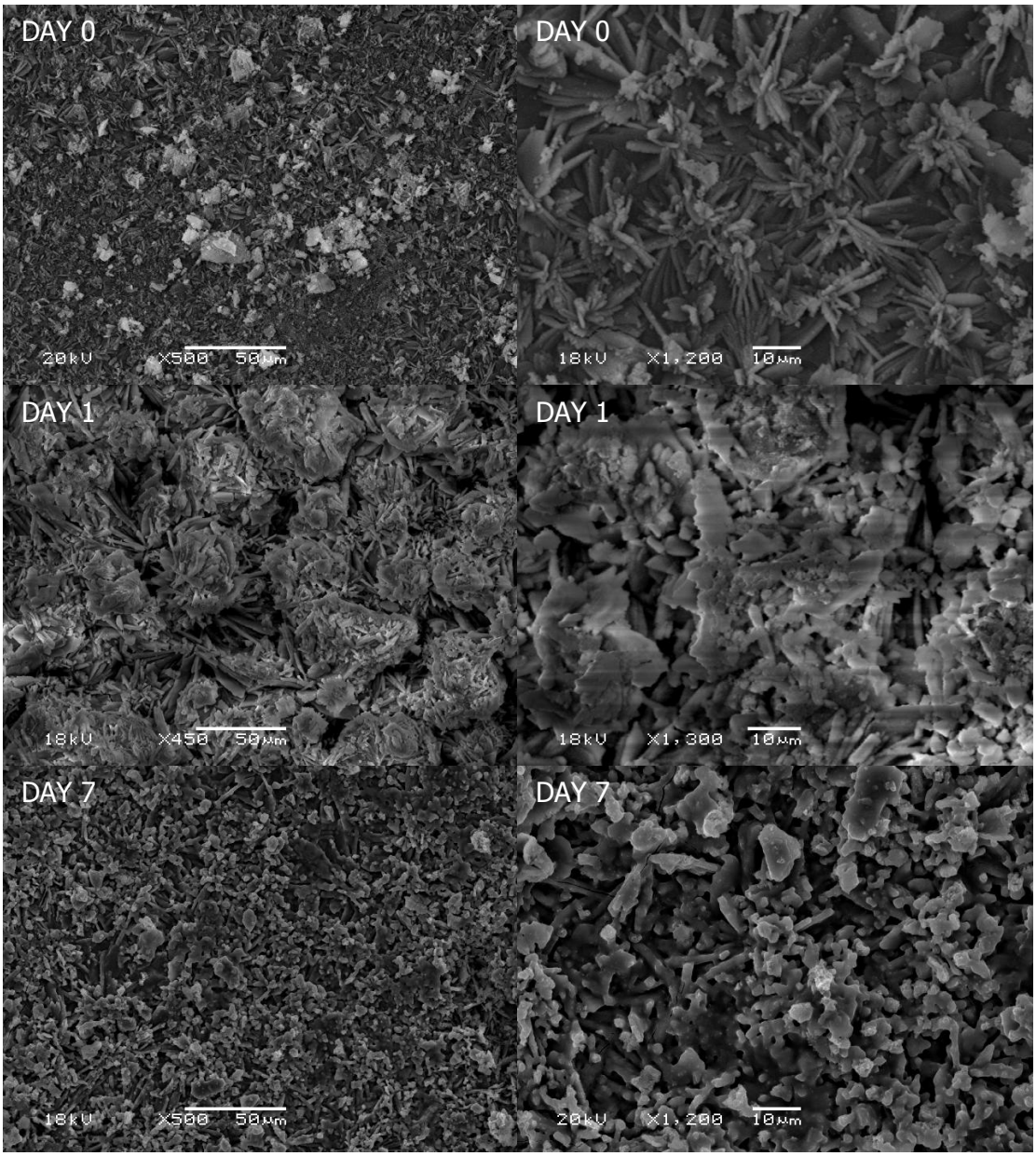

Figure 2.25 Apatite layer formation study: SEM analysis for the electrochemically coated polished Ti discs at 20mA/cm^2 after immersion in SBF for 0, 1 and 7 days.

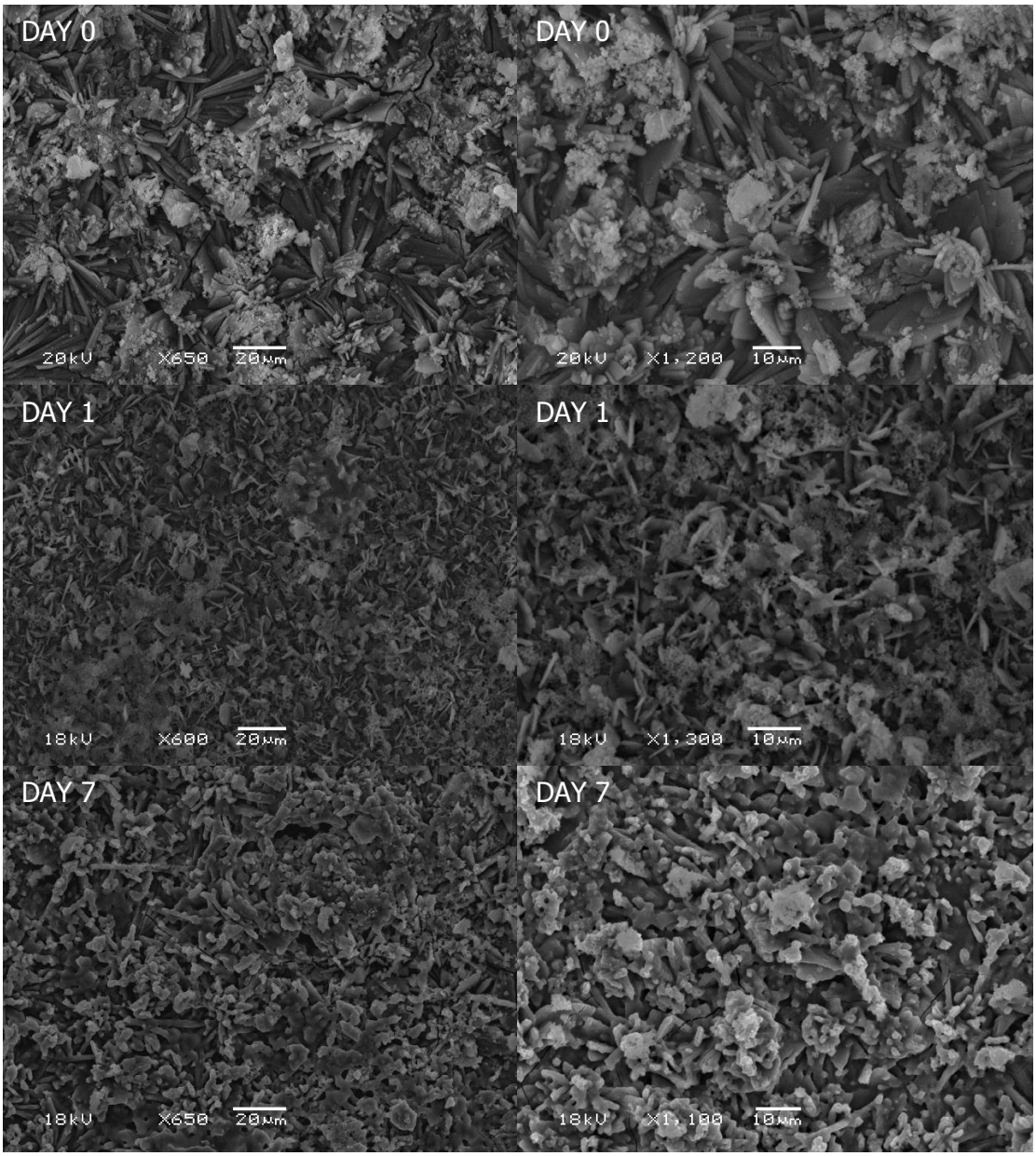

Figure 2.26 Apatite layer formation study: SEM analysis for the electrochemically coated polished Ti discs at 6.5mA/cm^2 after immersion in SBF for 0, 1 and 7 days.

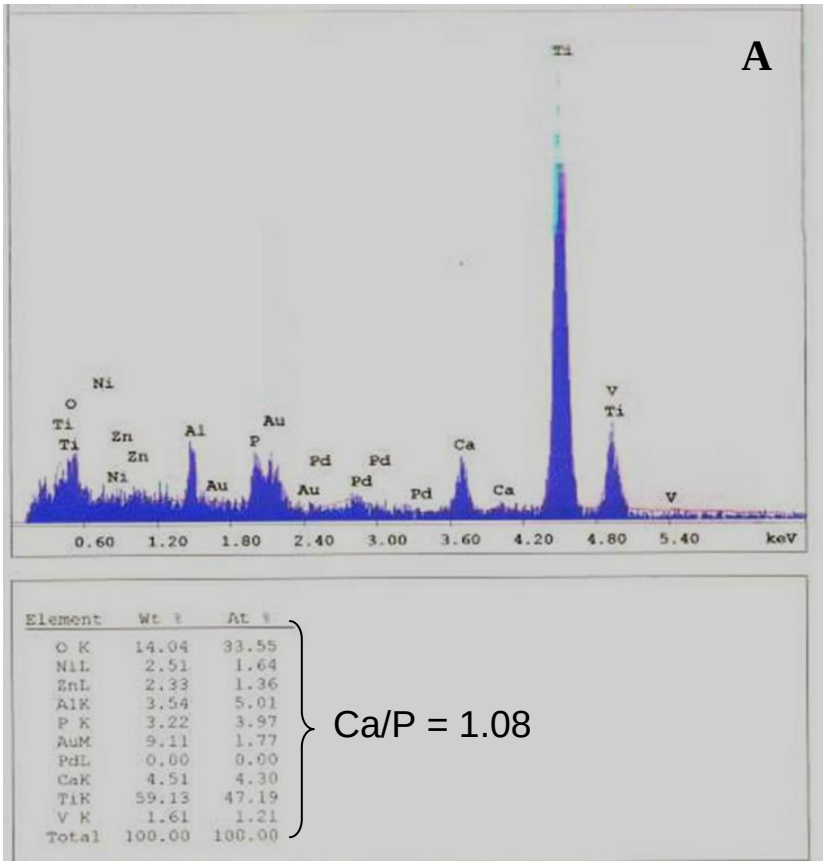

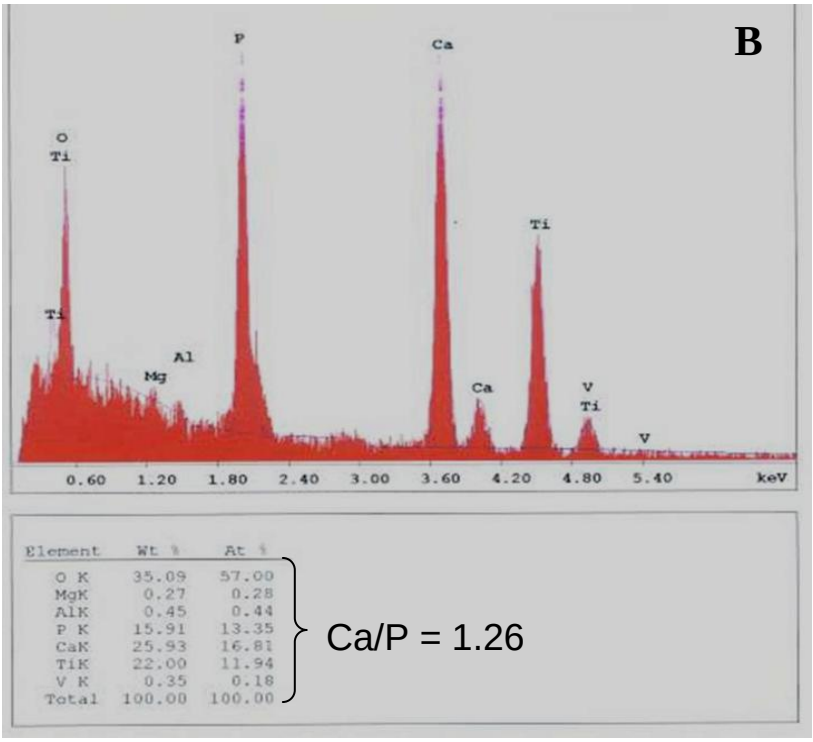

Figure 2.27 Apatite layer formation study: EDAX spectra and analysis of control polished Ti disc at **A)** day 1 and **B)** day 7 of immersion in SBF.

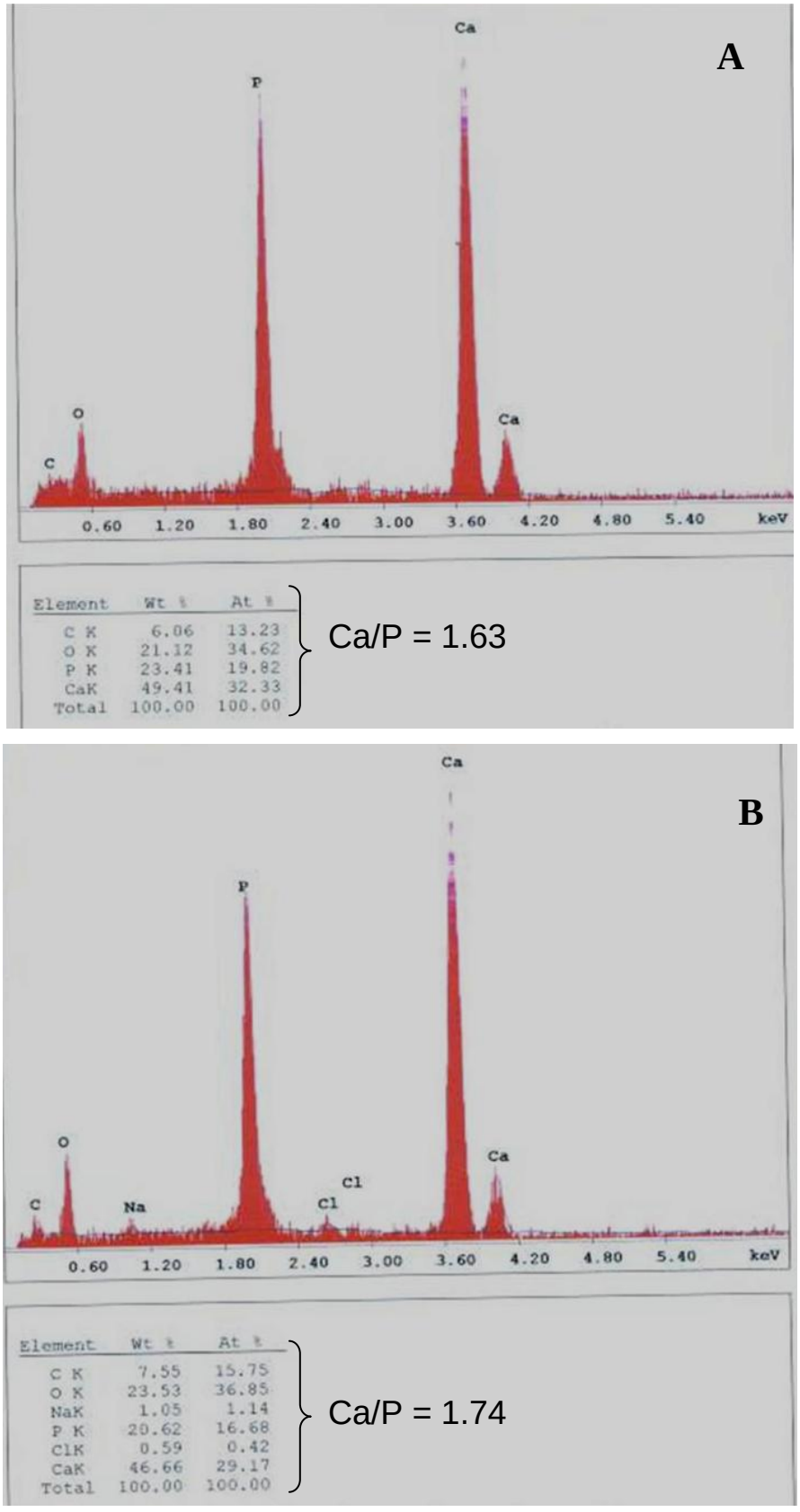

Figure 2.28 Apatite layer formation study: EDAX spectra and analysis of control HA disc at **A)** day 1 and **B)** day 7 of immersion in SBF.

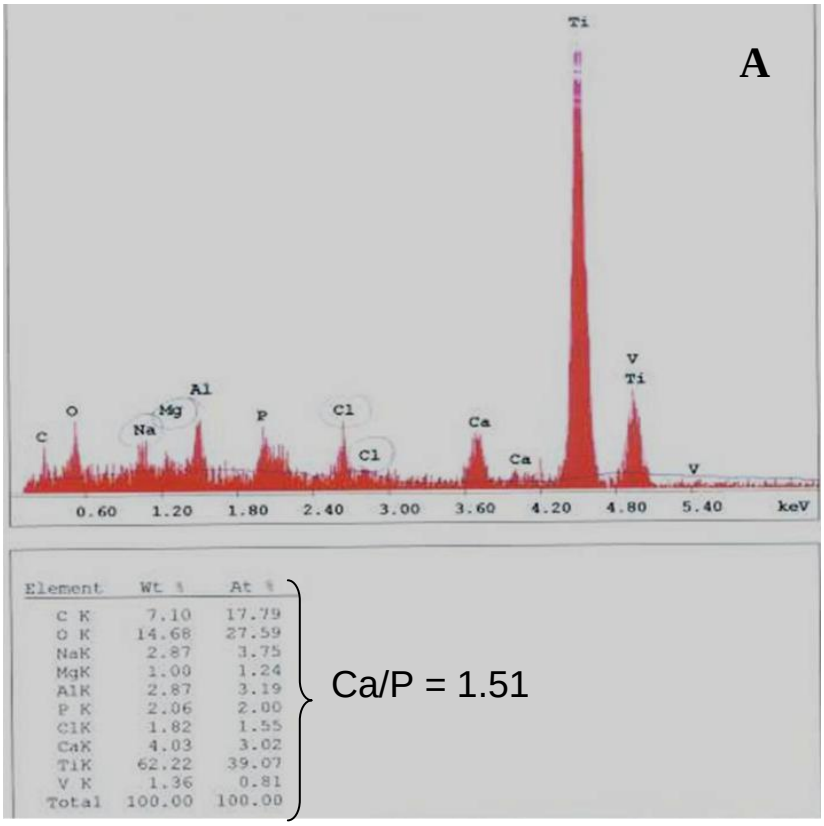

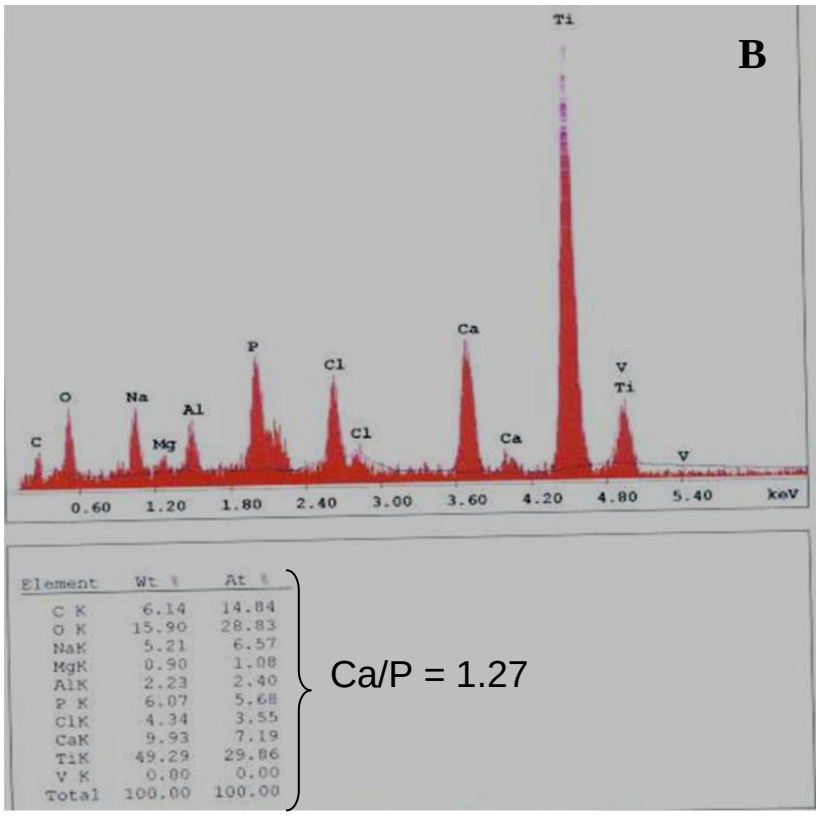

Figure 2.29 Apatite layer formation study: EDAX spectra and analysis of biomimetically coated polished Ti disc at **A)** day 1 and **B)** day 7 of immersion in SBF.

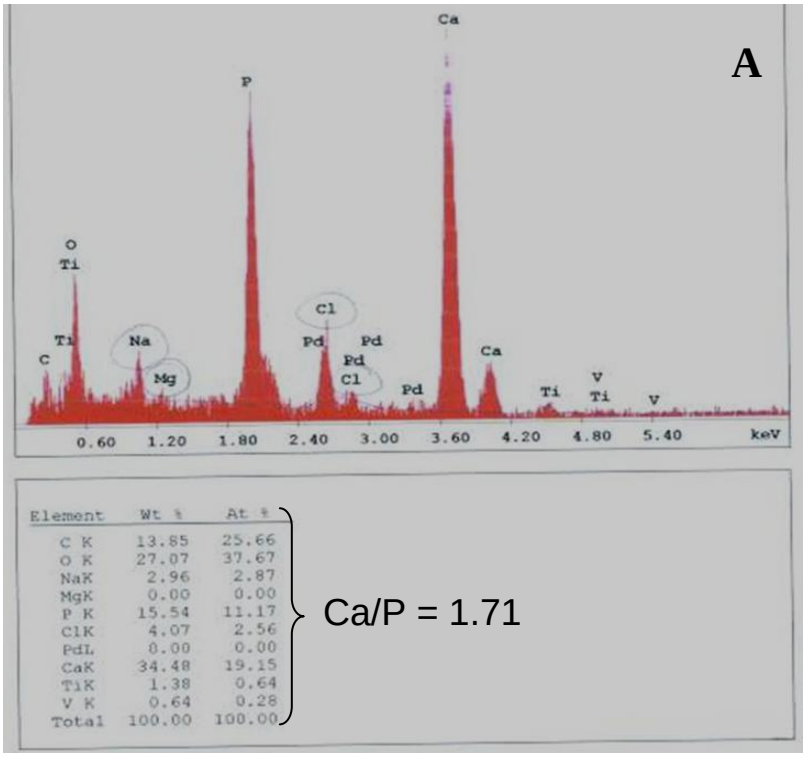

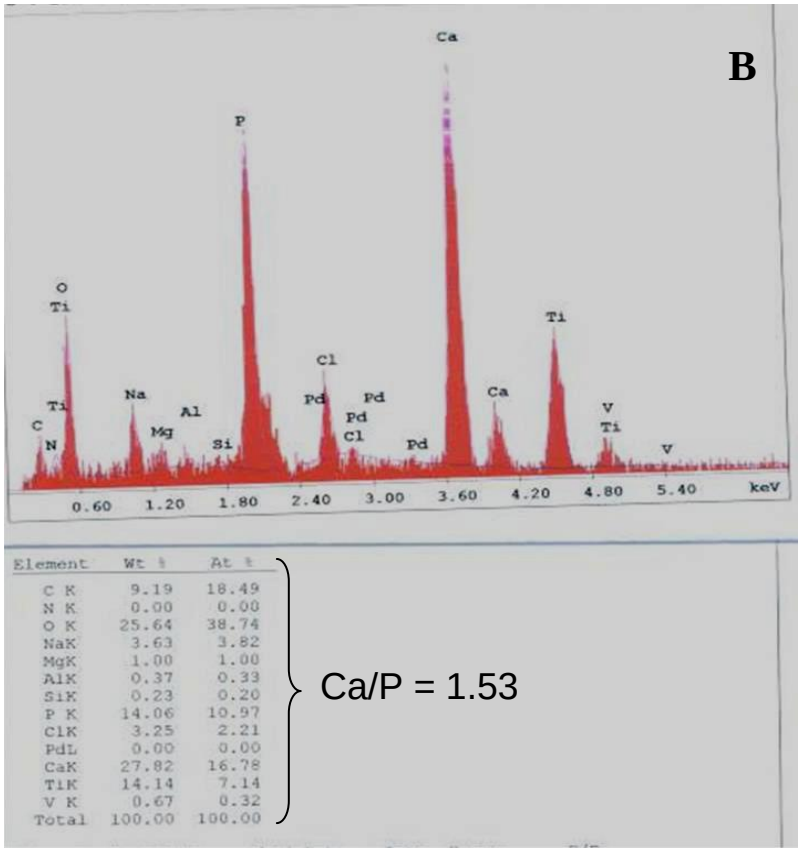

Figure 2.30 Apatite layer formation study: EDAX spectra and analysis of electrochemically coated polished Ti disc at 20mA/cm^2 at **A)** day 1 and **B)** day 7 of immersion in SBF.

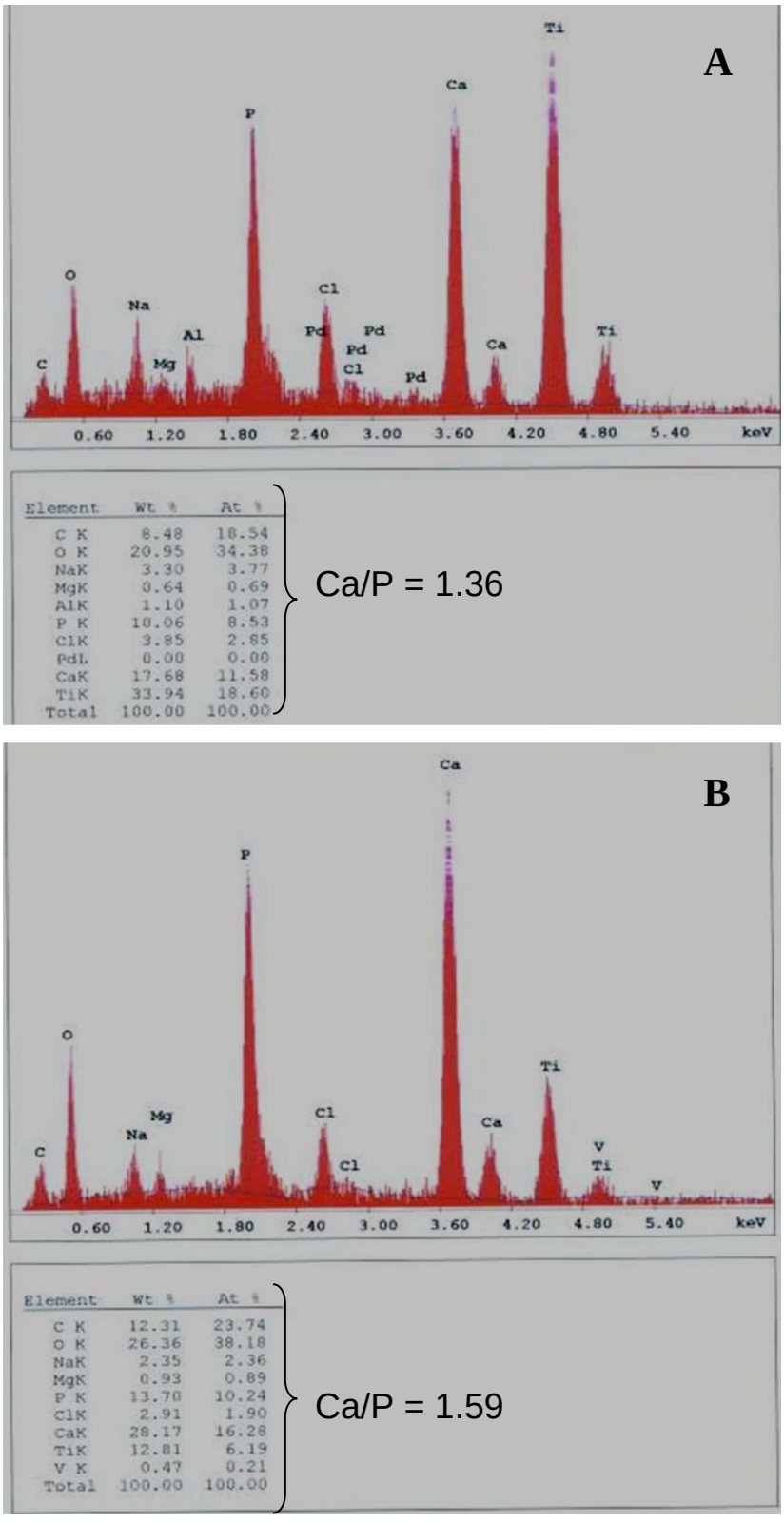

Figure 2.31 Apatite layer formation study: EDAX spectra and analysis of electrochemically coated polished Ti disc at 6.5mA/cm^2 at **A)** day 1 and **B)** day 7 of immersion in SBF.

2.4 DISCUSSION

In the present chapter, three different methods were used to deposit a CaP coating layer on the surface of tantalum and TiAl6V4 discs which had different topography, polished and sand-blasted. The coating methods all used supersaturated solutions at room temperature. However, the coatings resulted in different characteristics, as shown in the results section of this chapter.

Biomimetic coatings were composed of tiny crystals in the nanometer scale arranged in globules. EDAX results showed these coatings were composed of Ca and P as well as C and O. Mg was barely detected in some spectra. Ca/P ratio was below 1.67, that for pure hydroxyapatite, indicating the biomimetic coatings were Ca deficient, like the bone mineral (Wopenka and Pasteris 2005; Narasaraju and Phebe 1996; LeGeros 1993). However, no CaP phase was detected by XRD, which means it is present as very amorphous phases composed of very small crystals (Suryanarayana and Grant Norton 1998; Hammond 2001; Nishio *et al*. 2000). All together, this data suggests that the biomimetic coatings are composed of a CaP phase or phases that are very amorphous, composed of nano-sized crystals and Ca deficient. Mg may be incorporated in the coatings, which is one of the reported substituting ions found in bone mineral (Wopenka and Pasteris 2005; LeGeros 1993; LeGeros 2008).

Back in 1994, Kokubo and de Groot described the coating on a titanium substrate immersed in SBF as "carbonated, calcium-deficient, poorly crystallized hydroxyapatite". This biomimetic coating was defined as "bone-like" due to its resemblance with the mineral found in bone (Li *et al*. 1994). Since then other authors have used the definition bone-like when their biomimetic coatings presented the mentioned characteristics (Yamashita *et al*. 1996; Ma *et al*. 2003; Oliveira *et al*. 2003). The characteristic calcium-deficient and poorly crystallized coating described by Kokubo and de Groot in 1994 were observed in my study. However, the analytical methods used to characterise the biomimetic coatings did not reveal whether they were carbonated. Therefore the biomimetic coatings in my study cannot be classified as bone-like although further analysis may reveal the nature of their composition. For instance, an analytical technique such as Fourier transform infrared spectroscopy

(FTIR) would provide an infrared spectrum which is unique for each compound, thus revealing the carbonate groups in the coatings.

The original brushite deposited on the metal discs by the electrochemical depositions displayed the characteristic plate-like morphology of this CaP mineral as well as Ca/P ratio indicative of brushite (Redepenning *et al*. 1996; Pongkao Kashima and Rakngarm 2008). Moreover, XRD patterns showed the characteristic peaks of this mineral and were sharp indicating its crystalline nature (Suryanarayana and Grant Norton 1998; Hammond 2001).

The morphology of the coating adopted several forms and crystal sizes ranged from the nanometer to the micrometer scale after immersion of samples in NaOH for 3 days. EDAX revealed these coatings were also Ca deficient (Ca/P<1.67), characteristic of the synthetic CaP prepared by wet methods (Narasaraju 1996). XRD patterns displayed a characteristic broad peak for HA, indicating it was amorphous (Suryanarayana and Grant Norton 1998; Hammond 2001). This broad HA peak is similar to that obtained from a bone sample (Narasaraju 1996; LeGeros 1993). The XRD patterns showed the electrochemical coatings were composed of HA as well as brushite, as peaks for this mineral remained after the ageing treatment, which in my thesis was by immersion in 0.1M NaOH for 72h.

As mentioned in the introduction of this chapter, CaP materials promote direct bonding with bone tissue through formation of an apatite layer. SBFs have been used as an *in vitro* model to study apatite formation on the surface of different biomaterials (Kokubo *et al*. 1990; Li *et al*. 1997; Kokubo *et al*. 2001; Zhang *et al*. 2003; LeGeros 2008). In this chapter, to further understand these CaP coatings, their characterisation when immersed in SBF was studied as an indication of how they may behave when used in an *in vivo* environment.

When the control uncoated Ti discs were immersed in SBF, the appearance of globular particles on their surface was observed after just 1 day of immersion. These particles multiplied and aggregated after 7 days (Figure 2.22). The morphologies of these samples resembled those described by Kokubo in 1998 and 2001 on the surfaces of ceramics, metals and polymers when immersed in SBF. Some photos taken at day

7 and displayed in Figure 2.32 showed very similar morphologies to those described for the biomimetically coated metal discs, summarised in Figure 2.3. The deposition of a mineral phase over time was observed on the pure HA control disc. However, the morphology of this mineral phase appeared different to the one on the uncoated Ti disc. Morphologies observed after very immersion of coated discs in SBF for 7 days were similar to those observed by Kokubo and co-workers in 1990. SEM analysis revealed a different appearance for these coatings after 7 days in the supersaturated solution. Biomimetic coatings looked denser and very amorphous morphologies were found in some areas (Figure 2.24), while electrochemical coatings were very different compared to their appearance at day 0: the plate-like crystals occurring with tiny globular ones observed at day 0 changed to globular amorphous crystals, seen at day 7 (Figures 2.25 and 2.26)

EDAX results for this study showed that after immersion in SBF the coated discs were able to incorporate Na, Cl and Mg. On the other hand, control HA discs only incorporated Na and Cl while Mg was the only element apart from Ca and P observed in the EDAX spectra of the uncoated Ti discs after 7 days. SEM and EDAX results suggest the coatings dissolved when immersed in SBF and subsequently mineralised incorporating Na, Cl and Mg as it has been previously described by Zhang and co-workers in 2003 (Zhang *et al*. 2003). Na, Cl and Mg are among the reported substituting ions in bone mineral (Wopenka and Pasteris 2005; LeGeros 1993).

Together, these findings may suggest the three coatings would be bioactive bonding directly with bone when used *in vivo*, via dissolution and subsequent mineralisation incorporating suitable and available ions in the surrounding environment.

The results from this chapter show that the methods applied in order to deposit a CaP layer on the surface of Ti and Ta discs provided CaP coatings that were Ca deficient and would be able to directly bind with bone tissue. These coatings had different morphologies, compositions and thicknesses depending on the method applied. In the next chapter of this thesis the same methods will be used to coat Ti and Ta discs as the ones used in this study. CaP coated Ti and Ta discs will be seeded with ovine MSCs in order to study how these coatings affect proliferation and differentiation of these cells.

2.5 CONCLUSION

Biomimetic and electrochemical methods can be applied in order to deposit a CaP layer on the surface of tantalum and TiAl6V4 discs. Surface topography and metal type did not affect the morphology and composition of the CaP coatings deposited by the same method. Biomimetic coatings were composed of nano-sized globular crystals while electrochemical coatings produced nano to micro crystals with different morphologies. All the coatings were Ca deficient. No CaP phase was detected by XRD for the biomimetic coatings whereas the electrochemical ones contained HA and brushite. The coatings produced and characterised in this chapter altered their morphology and composition when immersed in SBF. In the next chapter of this thesis the three coatings will be seeded with ovine mesenchymal stem cells. The growth and osteogenic differentiation of these cells on the biomimetic and electrochemical coatings will be investigated.

CHAPTER 3:

Growth and Differentiation of Mesenchymal Stem Cells on Polished and Sand-Blasted Metal Discs Calcium-Phosphate Coated by Biomimetic and Electrochemical Methods

3.1 INTRODUCTION

Bone marrow stromal cells or mesenchymal stem cells (MSCs) are ideal candidates for developing bone tissue-engineered constructs as they have been shown to differentiate into bone, as well as other lineages of mesenchymal tissues (Caplan 1991; Jaiswal *et al*. 1997; Pittenger *et al*. 1999; Bosnakovski *et al*. 2005; Csaki *et al*. 2007; Janssen *et al*. 2006). This differentiation potential is often used to characterise MSCs after isolation from bone marrow aspirates (Hara *et al*. 2008; Eslaminejad *et al*. 2008).

When the supplements dexamethasone, ascorbic acid and β-glycerophosphate are added to the culture medium, MSCs change their typical fibroblastic morphology to a cuboidal shape and produce nodules that stain positively for calcium. As MSCs differentiate down the osteogenic lineage, they produce alkaline phosphatase (ALP) on their cell surface: ALP is the enzyme responsible for hydrolysing phosphate esters and inducing bone mineralisation. The ALP activity increases as MSCs differentiate and therefore it is a recognised marker for osteogenic differentiation (Ohgushi *et al*. 1996; Jaiswal *et al*. 1997; Pittenger *et al*. 1999; Rust 2003).

When MSCs are treated with culture medium supplemented with dexamethasone, indomethacin, 1-methyl-3-isobutylxanthine and insulin they differentiate down the adipogenic lineage. The MSCs-derived adipocytes accumulate lipid-rich vacuoles within them that can be detected using stains such as Oil Red O (Pittenger *et al*. 1999; Rust 2003).

In my thesis, bone marrow isolated ovine MSCs were characterised by demonstrating their multipotency differentiating them down the adipogenic and osteogenic lineages.

In the previous chapter, CaP coatings with different characteristics were successfully deposited on the surface of metal discs which had different topographic surface. It is well known that CaP materials promote MSCs differentiation down the osteogenic lineage (Ohgushi *et al*. 1993; Oreffo *et al*. 1998; Nishio *et al*. 2000). Ohgushi and co-workers in 1993 demonstrated osteogenic differentiation of MSCs in porous HA ceramics and when composites of porous HA and MSCs were implanted into ectopic

sites, bone formation occurred within the HA pores. They hypothesised that the bioactive material has the capability of differentiating MSCs and therefore causes the expression of the osteogenic phenotype on the material surface, which leads to integration of the material with the surrounding tissue (Ohgushi *et al*. 1993). In this chapter, the osteogenic potential of MSCs on the CaP coatings produced by the biomimetic and electrochemical methods will be investigated and will be used to indicate the potential of these surfaces to form new bone *in vivo*.

It has been reported that surface topography and particle size have an effect on cell proliferation and differentiation (Anselme *et al*. 2000; Weiβenböck *et al*. 2006; Chen *et al*. 2007). In an interesting paper by Dalby et al. published in 2007, it was demonstrated that nanoscale disorder could be used to stimulate human MSCs to produce bone mineral *in vitro*, without supplementing the culture medium with any osteogenic compounds (Dalby *et al*. 2007). Since one key difference between the CaP coatings characterised in chapter 2 was the crystal size, in this chapter MSCs proliferation and differentiation on these different coatings will be studied. Moreover, as the coatings were deposited on metal discs that had different topographic surface and composition, the influence of the substrate will be also investigated.

The aim of this study was to investigate the effect on MSCs proliferation and osteogenic differentiation of CaP coatings with different crystal size that were deposited on different topographic surfaces of metal discs; and the hypotheses were:

1. **CaP coatings will significantly increase MSCs proliferation compared to uncoated Ta/Ti surfaces.**
2. **CaP coatings will induce MSCs differentiation down the osteogenic lineage.**
3. **Biomimetic coating will significantly enhance MSCs proliferation compared to electrochemical coatings.**
4. **Flatter topographies will significantly increase MSCs proliferation compared to complex and rougher ones.**
5. **Complex and rougher topographies will significantly increase MSCs differentiation compared to flatter ones.**
6. **Ta and Ti will show no significant differences in terms of MSCs proliferation and differentiation.**

3.2 MATERIALS AND METHODS

3.2.1 Expansion and Characterisation of MSCs

3.2.1.1 Cell Culture and Maintenance

Ovine MSCs, isolated from bone marrow which was aspirated from sheep iliac crest using an aseptic technique, were kindly donated by Dr Priya Kalia.

The growth medium for MSCs was Dubelcco's modified eagles medium (DMEM, D6429, Sigma-Aldrich, UK) supplemented with 10% fetal calf serum (FCS, First Link, UK) and 100 Units/mL of the antibiotics penicillin and streptomycin (P/S, Gibco, UK) (DMEM+).

MSCs were resuscitated by placing the cryovials stored in liquid Nitrogen in a water bath at 37ºC until thawed. DMEM+ was also warmed in a water bath at 37ºC. Thawed cells and warmed DMEM+ were placed inside a laminar flow hood which provides a sterile environment for cell culture work. 1mL of growth medium was gently added to the cells. They were left to stand inside the laminar flow hood for 5 minutes before they were transferred to a universal tube. Doubling volumes of DMEM+ were gently added to the universal tube containing the cells, with 5 minutes equilibration periods between each addition, until a total volume of 16mL was reached. The cell suspensions were centrifuged at 2,000rpm for 5 minutes. The supernatant was discarded and the pellet of cells was resuspended in 1mL of growth medium using a gauge needle (0.8 × 40mm, Becton Dickinson UK Ltd, UK) and 1mL syringe (Becton Dickinson UK Ltd, UK). Cells were transferred to T75 (75cm^2 of growth area) polystyrene cell culture flasks (Corning, USA) with 10mL of DMEM+ and designated passage 2 (P2). Culture flasks were kept in incubators at 37ºC with 5% CO_2 and regularly observed under a phase-contrast light microscope. Medium was changed every 3 to 5 days until the cultures were 80 to 90% confluent, ie when cells covered 80 to 90% of the total growth area of the culture flask.

When cultures reached 80 to 90% confluency they were passaged. Growth medium in the flasks was discarded and the cells were washed with cold phosphate buffered saline (PBS) which was also discarded. MSCs grew as adherent monolayers and

therefore need to be released from the flask surface. Enzymatic disaggregation is commonly used in order to break the cell adhesion interactions mediated by proteins such as cadherins which are Ca^{2+} dependent. On addition of trypsin/EDTA, a protease and a chelating agent for Ca^{2+}, and subsequent incubation the cells are released from the flask surface and can be replated (Freshney 2000). Thus, the cells were trypsinised by addition of 1mL of 0.5% trypsin-5.3mM EDTA·4Na solution (Gibco, UK) and incubation at 37ºC with 5% CO_2 for 5 minutes. Once the cells lifted off the surface the reaction was stopped by adding a 1:1 volume of DMEM+. The FCS added to the culture medium contains trypsin inhibitors that stop the reaction. All cells were transferred to a universal tube except a small amount that was used to determine cell viability and cell density. A 1/10 dilution of the cells in trypan blue (T8154, Sigma-Aldrich, UK) was pipetted into a coverslipped haemocytometer which was then placed under a phase-contrast light microscope. Viable cells were rounded and bright while blue cells were considered as non-viable. Both viable and non-viable cells were counted in order to calculate the viability percentage and the number of viable cells in the cell suspension. Cells in the universal tube were centrifuged at 2,000rpm for 5minutes, after which the supernatant was discarded and the pellet of cells resuspended in 1mL DMEM+ using gauge needle (0.8 × 40mm, Becton Dickinson UK Ltd, UK) and 1mL syringe (Becton Dickinson UK Ltd, UK). Approximately 3,000 to 5,000 cells per cm^2 of growth area were seeded in T225 (225cm^2 of growth area) polystyrene cell culture flasks (Corning, USA) with 30mL of DMEM+ and designated passage 3 (P3). Culture flasks were kept in incubators at 37ºC with 5% CO_2. Medium was changed every 3 to 5 days and the cultures passaged when 80 to 90% of confluency was reached. MSCs were expanded until passage number 12 (P12) and routinely observed by phase-contrast light microscopy.

3.2.1.2 Characterisation of MSCs

Ovine MSCs were characterised by demonstrating their multipotency differentiating them down 2 cell lineages: adipogenic and osteogenic (Pittenger *et al*. 1999).

3.2.1.2.1 Adipogenic Differentiation

For the adipogenic differentiation cells at P5 were cultured under adipogenic conditions for 21 days on Thermanox™ coverslips (Nalge Nunc International, USA) in 12 well plates (Orange Scientifique, Belgium). Thermanox™ coverslips offer

optimum cell attachment and growth as its surface is treated to achieve a hydrophilic state for cell adherence and growth (from product technical data sheet: http://www.nuncbrand.com/files/en-626.pdf). 1×10^5 cells per well were plated.

Adipogenic medium was DMEM+ with 1μM Dexamethasone (D2915, Sigma-Aldrich, UK), 200μM Indomethacin (I7378, Sigma-Aldrich, UK), 500μM 1-methyl-3-isobutylxanthine (I5879, Sigma-Aldrich, UK) and 10μg/mL Insulin, (I0516, Sigma-Aldrich, UK) (from Rust 2003). Control cells were cultured in the same way but using DMEM+ instead of adipogenic medium. Media were changed every 3-5 days.

After 21 days of culture in either DMEM+ or adipogenic medium, cellular morphology and presence of lipids by Oil Red O staining were studied. Oil Red O is a fat-soluble dye used for staining of neutral triglycerides and lipids (Young *et al*. 2006).

3.2.1.2.2 Adipogenic Differentiation: Oil Red O Staining

An Oil Red O stock solution was prepared by mixing 0.5g of Oil Red O (S267-2, Raymond A. Lamb, London, UK) with 100mL of absolute isopropyl alcohol (296946H, BDH, UK) and left to stand overnight. A dextrin stock solution was prepared by adding 1g of dextrin (D2256, Sigma-Aldrich, UK) to 100mL of distilled water. Oil Red O working solution was made by mixing 60mL of the Oil Red O stock solution with 40mL of the dextrin stock solution. This working solution was filtered before use using Whatman 540 filter paper.

After 21 days of culture under either DMEM+ or adipogenic conditions, cells were washed with PBS and fixed in formal saline for 5 minutes, then rinsed with distilled water. They were covered with Oil Red O working solution for 20 minutes, rinsed with distilled water to remove excess stain and counterstained with Harris haematoxylin for 3 minutes. Finally, they were rinsed with distilled water and air dried. Thermanox™ coverslips were then observed under a phase-contrast light microscope. Oil Red O stains cell nuclei blue and lipids brilliant red. Photos were taken using an Olympus digital camera C-2020Z.

3.2.1.2.3 Osteogenic Differentiation

For the osteogenic differentiation cells at P5 were cultured under osteogenic conditions up to 28 days on Thermanox™ coverslips (Nalge Nunc International, USA) in either 6, for ALP and DNA assays, or 12 well plates (Orange Scientifique, Belgium), for cell morphology and Von Kossa staining. 3×10^4 cells per well were plated in both 6 and 12 well plates. The von Kossa stain is used to quantify mineralization in cell culture and tissue sections (Young *et al*. 2006).

Osteogenic medium was DMEM+ with 0.1μM Dexamethasone (D2915, Sigma-Aldrich, UK), 500μM Ascorbic Acid (A4544, Sigma-Aldrich, UK) and 10mM β-glycerophosphate (G9891, Sigma-Aldrich, UK) (from Rust 2003). Control cells were cultured in the same way but using DMEM+ instead of osteogenic medium. Media were changed every 3-5 days.

Cell proliferation was measured by DNA assay at days 7, 14, 21 and 28 of culture in either DMEM+ or osteogenic medium. ALP production per μg of DNA were analysed at the same time points. Changes in cellular morphology were regularly observed by phase-contrast light microscopy. Finally, mineral deposition by Von Kossa staining was checked at day 28 of culture.

3.2.1.2.4 Osteogenic Differentiation: DNA Assay

Cell proliferation was studied by quantifying the amount of DNA in the samples. The assay is based on the use of the fluorochrome bisbenzimidazole (Hoerchst 33258). Upon specifically binding cellular DNA its fluorescence is enhanced and emission wavelength shifted, resulting in a linear relationship between fluorescence and DNA concentration (Rago *et al*. 1990).

Cells were washed in PBS and lysed by adding autoclaved distilled water at 37ºC. After frozen at -70ºC and thawed 3 times, samples were transferred to Eppendorf tubes and spun at 10,000 rpm for 10 min. 100μL of the supernatant were loaded in triplicate for each sample into a FluorNunc™ white 96-well plate (Nalge Nunc International, USA). DNA standards, ranging from 20 to 0.3125μg/mL of DNA, were prepared by diluting the 1mg/mL DNA stock (Sigma-Aldrich, UK) in saline sodium

citrate buffer (SSC). 100µL of the standards were also loaded in triplicate into the FluorNunc™ white 96-well plate. Finally, 100µL of 1µg/mL Hoerchst 33258 dye (Sigma-Aldrich, UK) were added to each sample. The original 1mg/mL concentration of Hoerchst 33258 dye stock was diluted in SSC. Fluorescence was read at 460 nm using a plate reader (Fluoroskan Ascent, Labsystems, USA).

The amount of DNA in the samples was calculated as µg of DNA by multiplying the µg/mL value obtained for each sample by the volume of each sample used for the assay.

3.2.1.2.5 Osteogenic Differentiation: ALP Activity Assay

The assay is based on the enzymatic activity of ALP, which cleaves the phosphate group of the compound p-nitrophenol phosphate to produce p-nitrophenol. The production of p-nitrophenol can be monitored at 405nm as it is yellow at alkaline pH (Bowers and McComb 1966).

50µL of the same supernatant used for the DNA assay were loaded into Cobas Bio® blue sample cups (AS Diagnostics, UK). Pre-weighed p-nitrophenol phosphate powder was mixed with 10mL of diethanolamine buffer (both Randox, UK) and pre-heated to 37ºC to produce the working solution, which was loaded along with the samples into the Cobas Bio® analyser (Roche, UK) to run the assay. 250µL of working solution were used for each sample.

The analyser calculates the reaction rate for each sample, i.e. the rate of appearance of the coloured product, by plotting absorbance readings against time. The slope of these graphs determines the enzymatic activity. The ALP activity was calculated as U/L and normalised for the number of cells in the sample using the DNA concentration calculated for each sample. ALP/DNA was expressed as U/µg.

3.2.1.2.6 Osteogenic Differentiation: Von Kossa Staining

After 28 days of culture under either standard or osteogenic conditions, cells were washed with PBS and fixed in methanol. They were covered with 1.5% silver nitrate solution (S2252, Sigma-Aldrich, UK. 1.5g of silver nitrate in 100mL of distilled water) and exposed to bright light for 1 hour. The cells were washed with distilled

water before covering them with 2.5% sodium thiosulphate (10268, BDH, UK. 2.5g of sodium thiosulphate in 100mL of distilled water) for 5 min. Finally, they were counterstained in Neutral Red (N6634, Sigma-Aldrich, UK) for 5 min, washed until clear with distilled water and air dried. The principle of the Von Kossa Staining is a precipitation reaction in which silver ions react with phosphate under acidic conditions. Then, photochemical degradation of silver phosphate to silver occurs under light illumination (Young *et al*. 2006). Thermanox™ coverslips were mounted on slides and observed by light microscopy. Cell nuclei were stained red and mineral deposits black or brown-black. Photos were taken using an Olympus digital camera C-2020Z.

3.2.2 Culture of MSCs on CaP Coated Metal Discs with Different Topographic Surface

3.2.2.1 Seeding and Culture of MSCs on Samples and Controls

Description of groups of controls and samples tested are summarised in Table 3.1. For each group and assay performed n=3:

GROUP	DESCRIPTION
C-	Negative control for MSCs differentiation: Thermanox™ coverslips, DMEM+
C+	Positive control for MSCs differentiation: Thermanox™ coverslips, osteogenic medium
PTa	Control for MSCs proliferation and differentiation on uncoated polished tantalum discs, DMEM+
SBTa	Control for MSCs proliferation and differentiation on uncoated sand-blasted tantalum discs, DMEM+
PTi	Control for MSCs proliferation and differentiation on uncoated polished titanium discs, DMEM+
SBTi	Control for MSCs proliferation and differentiation on uncoated sand-blasted titanium discs, DMEM+
PTa-BioM	Polished tantalum discs CaP coated by the biomimetic method
PTi-BioM	Polished titanium discs CaP coated by the biomimetic method
SBTa-BioM	Sand-blasted tantalum discs CaP coated by the biomimetic method
SBTi-BioM	Sand-blasted titanium discs CaP coated by the biomimetic method
PTa-E20	Polished tantalum discs CaP coated by the electrochemical method at 20mA/cm^2
PTi-E20	Polished titanium discs CaP coated by the electrochemical method at 20mA/cm^2
SBTa-E20	Sand-blasted tantalum discs CaP coated by the electrochemical method at 20mA/cm^2
SBTi-E20	Sand-blasted titanium discs CaP coated by the electrochemical method at 20mA/cm^2
PTa-E6.5	Polished tantalum discs CaP coated by the electrochemical method at 6.5mA/cm^2
PTi-E6.5	Polished titanium discs CaP coated by the electrochemical method at 6.5mA/cm^2
SBTa-E6.5	Sand-blasted tantalum discs CaP coated by the electrochemical method at 6.5mA/cm^2
SBTi-E6.5	Sand-blasted titanium discs CaP coated by the electrochemical method at 6.5mA/cm^2

Table 3.1: Description of groups of controls and samples for the study of MSCs growth and differentiation on CaP coated metal discs with different topographic surface.

CaP coated and uncoated discs were autoclaved before cell seeding which was performed under sterile conditions inside a laminar flow hood. Autoclaved discs were placed in 12 well plates (Orange Scientifique, Belgium) for cell seeding. Ovine MSCs were grown to confluency and used at P4 and P5. Each disc was seeded with 25,000 cells (20,000 for SEM) in a total volume of 50μL of DMEM+ onto the centre of the disc. After incubation for 100min at 37ºC with 5%CO_2, 2-3mL of DMEM+ were added to each well and plates kept in a 37ºC with 5%CO_2 incubator. Medium was changed every 3-5 days.

C- (Thermanox™ discs and DMEM+) and C+ (Thermanox™ discs and osteogenic medium) controls were seeded following the same procedure as for the CaP coated and uncoated discs. Osteogenic medium for control C+ was prepared as described in section 3.2.1.2.3.

3.2.2.2 Analysis of Cytotoxicity, Cell Proliferation, Cell Differentiation, Cell Morphology and Interaction with the Material

At days 4, 7 and 14 of culture cytotoxicity, cell proliferation, cell differentiation into the osteogenic lineage and interaction with the material were studied for all samples and controls.

Cell proliferation was quantitatively measured by AlamarBlue® activity and DNA assays and qualitatively by observation under SEM. AlamarBlue® activity assay was also a measurement of cytotoxicity of the different coatings and materials. ALP production per μg of DNA was measured in order to check cell differentiation into the osteogenic lineage. Changes in cell morphology and the interaction of the cells with the different coatings and materials were studied by SEM.

3.2.2.2.1 AlamarBlue® Activity Assay

AlamarBlue® (AbD Serotec, UK) is a biochemical indicator of metabolic activity that changes its colour from blue to pink when it is reduced as a result of a redox reaction in the cytochrome oxidase chain. This redox reaction is related to metabolic activity and cell growth and therefore this assay is an indicator of cell proliferation as well as cytotoxicity (from online product manual: http://www.abdserotec.com/about/company_profile-483.html).

AlamarBlue® was diluted in phenol free Dubelcco's modified eagles medium (D5921, Sigma-Aldrich, UK) to make a 10% working solution. Wells were washed with PBS and 3mL of the AlamarBlue™ working solution added to them. Plates were incubated at 37ºC with 5%CO2. After 4 hours, 100µL from each sample were loaded in triplicate into a FluoroNunc^{TM} white 96-well plate and absorbance measured at 590 nm using a plate reader (Fluoroskan Ascent, Labsystems, USA). Results were compared to those of an empty well to which 3mL of 10% Alamar Blue® working solution had been added at the beginning of the assay.

3.2.2.2.2 DNA Assay

The DNA assay followed the same procedure as in section 3.2.1.2.4.

3.2.2.2.3 ALP Activity Assay

The ALP activity assay and calculations to find out the ALP activity per µg of DNA followed the same procedures as in section 3.2.1.2.5.

3.2.2.2.4 SEM Analysis

The controls and samples in 12 well plates were washed with PBS and fixed in 2.5% glutaraldehyde (Agar Scientific, UK) overnight. They were then washed for 10 minutes with 0.1M sodium cacodylate (Agar Scientific, UK) buffer and post-fixed in 1% osmium tetraoxide (Agar Scientific, UK) in 0.1M sodium cacodylate buffer for 1 hour. After washing with 0.1M sodium cacodylate buffer for 2×5 minutes, specimens were dehydrated through a graded series of industrial methylated spirit (IMS) (20-60%) and ethanol (70-100%) each for 2×5 minutes. Finally, specimens were treated for 2×4 minutes with hexamethyldisalazane (Agar Scientific, UK), a transition solvent, and left to dry overnight.

Specimens were mounted on stubs and gold/palladium sputtered coated (EMITECH K550, Emitech, UK) before observation under SEM (JEOL JSM 5500 LV).

3.2.3 Statistics

Statistical analysis was performed with SPSS 14.0 software. As the sample number was small non parametric tests were applied to the data. Multiple comparisons were

made using the Kruskal-Wallis test and comparisons between groups were made using the Mann Whitney U test. A p-value≤0.05 was considered a significant result.

3.3 RESULTS

3.3.1 Expansion and Characterisation of MSCs

3.3.1.1 In vitro Observations of MSCs

Monolayer cultures of MSCs consisted of adherent, flat cells which were long and spindle-like in shape. This fibroblastic morphology was observed to persist for 12 passages (Figure 3.1A-C). Cells possessed large nuclei with multiple nucleoli and some of them could be seen to be in contact between them (Figure 3.1D).

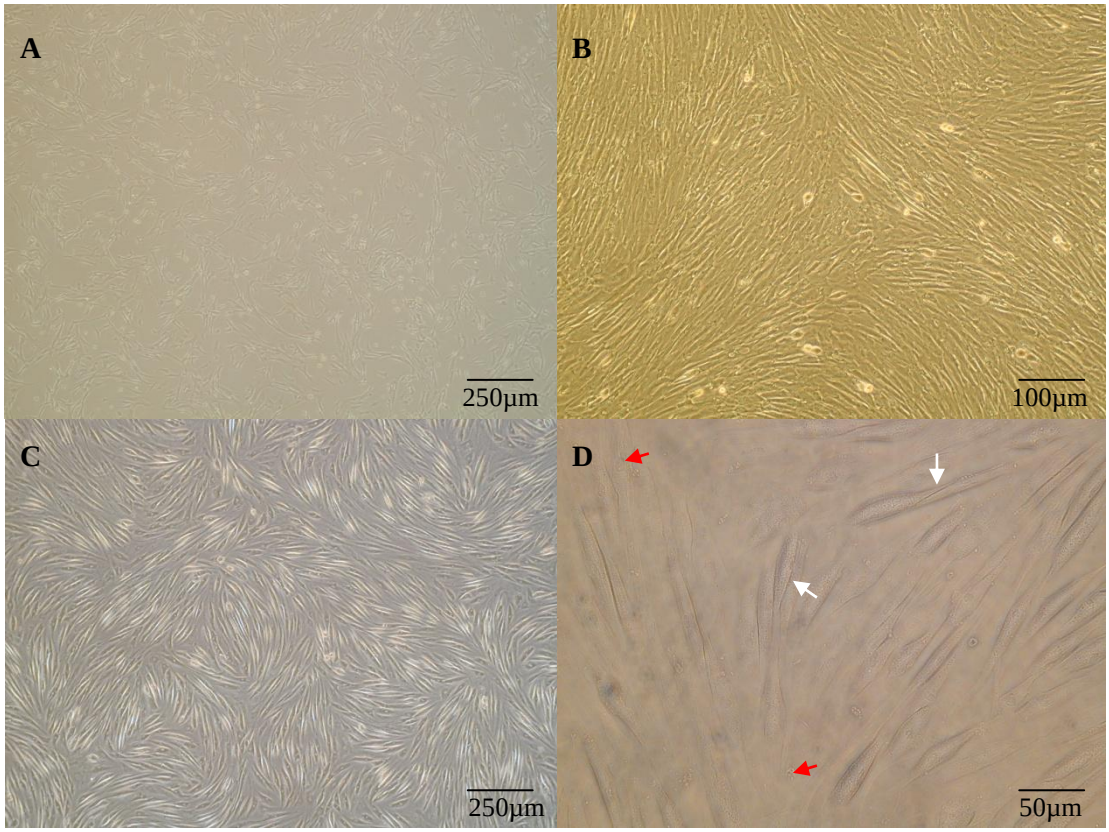

Figure 3.1 Phase-contrast light microscopy photos of monolayer cultures of MSCs at different passage numbers and states of confluency: **A)** P3 (magnification ×4); **B)** P5 (magnification ×10); **C)** P9 (magnification ×4) and **D)** P9 (magnification ×20) where large nuclei containing multiple nucleoli can be observed (red arrows) and cells can be seen in contact (white arrows).

3.3.1.2 Characterisation of MSCs

3.3.1.2.1 Adipogenic Differentiation

Oil Red O staining revealed numerous red spots, indicating the presence of lipids, only in the cultures treated with adipogenic medium for 21 days (Figure 3.2B). Moreover, a clear change in morphology could be observed as cells under adipogenic conditions had become less spindle-like shaped and shorter with long extensions (Figure 3.2).

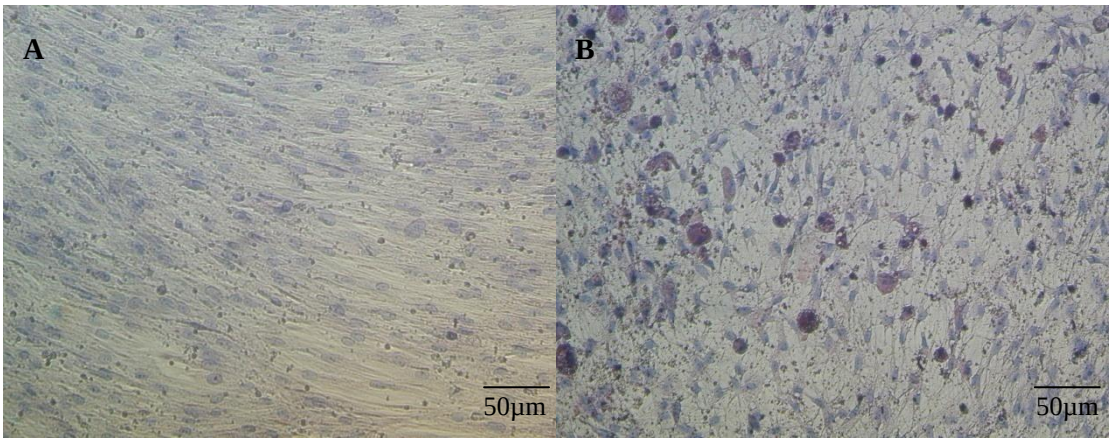

Figure 3.2 Oil Red O staining results after MSCs were cultured for 21 days in **A)** DMEM+ or **B)** adipogenic medium (magnification ×20).

3.3.1.2.2 Osteogenic Differentiation

Changes in cell morphology could be observed as early as day 4 of culture under osteogenic conditions as some individual cells became less spindle-like and more cuboidal (Figure 3.3D-F). From day 9 multiple cuboidal cells could be seen in the osteogenic cultures. By day 21 the osteogenic cultures had become confluent and displayed a different appearance to the confluent control cultures (Figure 3.3C and F).

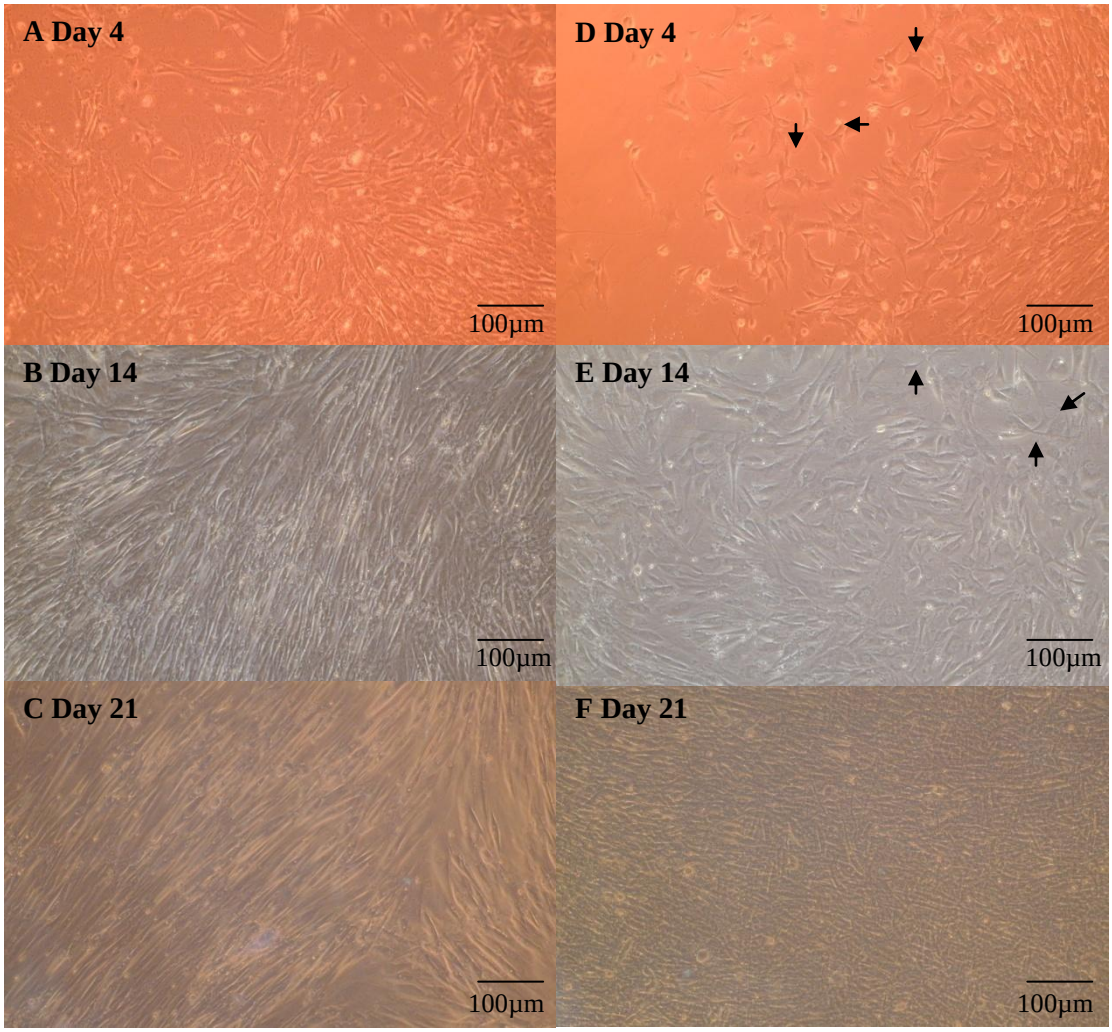

Figure 3.3 Phase-contrast light microscopy photos of MSCs cultured in **A-C)** DMEM+ or **D-F)** osteogenic medium (magnification ×10). Black arrows show cuboidal cells.

Results for Von Kossa staining at day 28 of culture showed black deposits indicating mineral deposition only in the cultures treated with osteogenic supplements (Figure 3.4B). Besides, morphology of the osteogenic cultures appeared different to that of the control cultures (Figure 3.4).

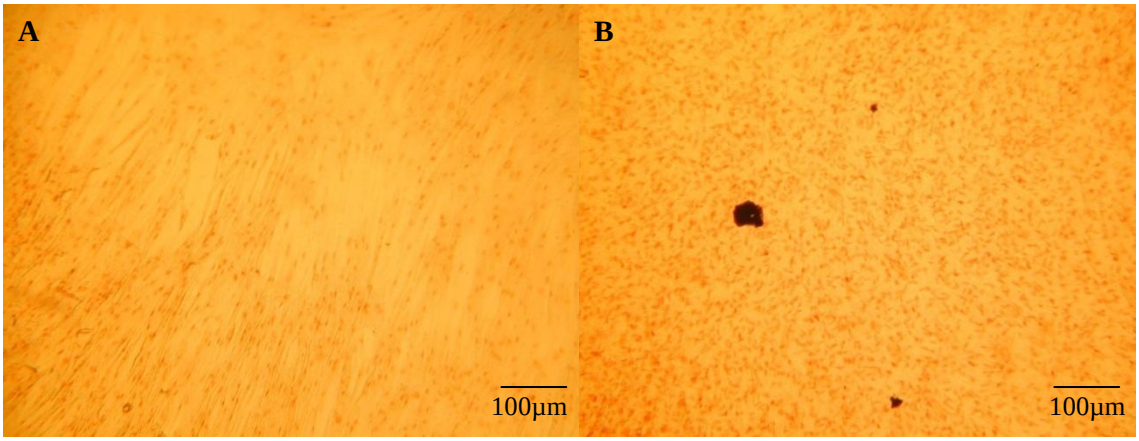

Figure 3.4 Von Kossa staining results after MSCs were cultured for 28 days in **A)** DMEM+ or **B)** osteogenic medium (magnification ×10).

Figure 3.5 shows the results for the DNA assay. The amount of DNA quantified in the osteogenic cultures was always greater than in the control cultures, which was statistically significant at days 7, 21 and 28 (*p≤0.05). The growth curve in the MSCs treated with osteogenic supplements was steady during the time of the study. MSCs in the control cultures grew very slowly until day 21. An increase in cell growth was observed between days 21 and 28. The results displayed below suggest that the osteogenic supplements added to the medium may be mitogenic as well, as they promote cell growth, as already described by other authors (Jaiswal *et al*. 1997; Bruder *et al*. 1997).

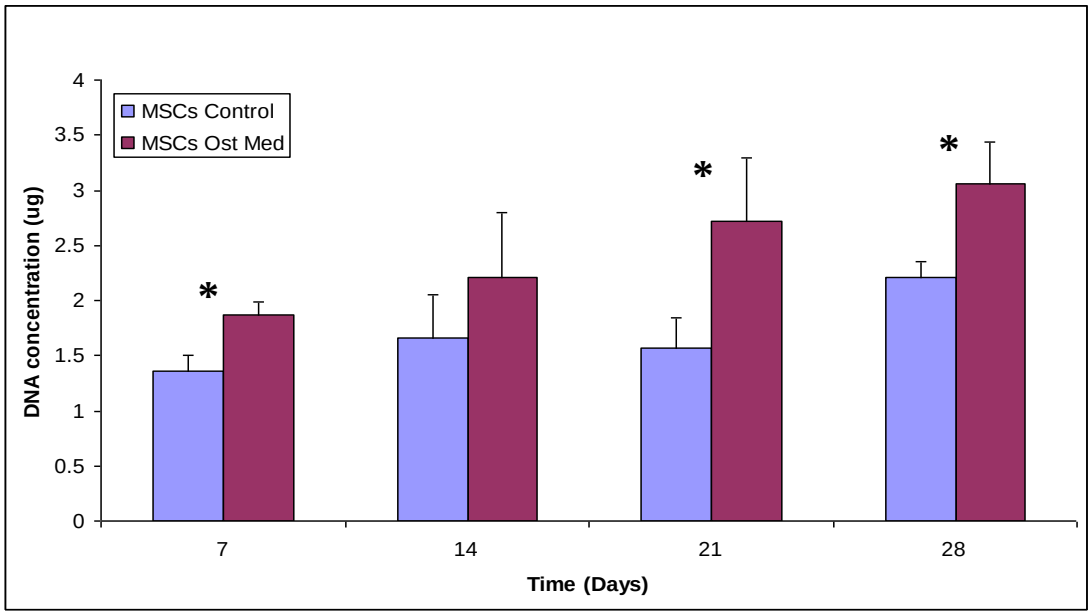

Figure 3.5 Results for the DNA assay in MSCs treated with (MSCs Ost Med) and without (MSCs control) osteogenic medium at days 7, 14, 21 and 28 of culture.

Figure 3.6 displays the results for the ALP assay. The calculated ALP activity was normalised by the amount of DNA in the sample. At all time points the enzyme activity was higher in the osteogenic cultures than in the control samples. The results were statistically significant at days 14, 21 and 28 (*$p \leq 0.05$). The pattern of production of ALP in the osteogenic cultures showed a significant increase between days 7 and 14 followed by a decrease in the enzyme production, which slightly increased between days 21 and 28. The control MSCs, not treated with osteogenic medium, produced relatively low levels of ALP. An increase in the ALP activity between days 7 and 14 and almost no changes between time points from day 14 until the end of the study were observed.

The results show that in osteogenic medium the cells had increased ALP activity therefore suggesting that MSCs underwent osteogenic differentiation. The observed ALP activity trend, with a peak at day 14, has already been described in the literature and it is characteristic of MSCs undergoing osteogenic differentiation (Lian and Stein 1992; Jaiswal *et al*. 1997).

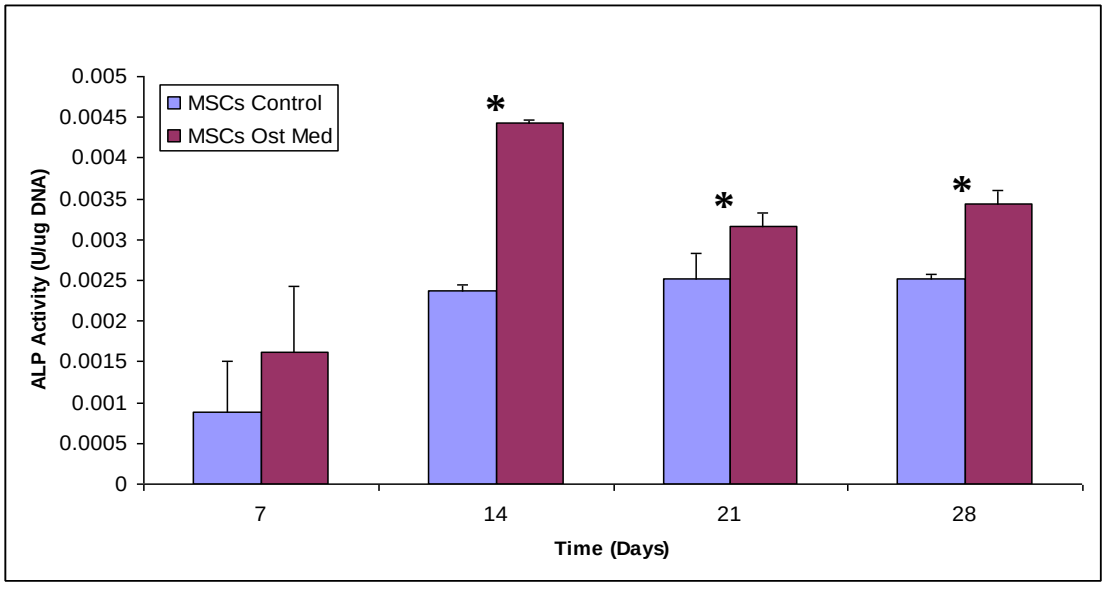

Figure 3.6 Results for the ALP activity assay in MSCs treated with (MSCs Ost Med) and without (MSCs control) osteogenic medium at days 7, 14, 21 and 28 of culture.

3.3.2 Culture of MSCs on CaP Coated Metal Discs with Different Topographic Surface

3.3.2.1 Analysis of Cytotoxicity and Cell Proliferation: AlamarBlue® Activity Assay

Results from the AlamarBlue® activity assay can be seen in Figure 3.7. The positive control for osteogenic differentiation C+ had higher absorbance values than the negative control C-, indicating the cells under osteogenic conditions had an increased metabolism compared to the cells cultured in standard DMEM+. These results are in agreement with the ones previously observed in Figure 3.5, again suggesting that the osteogenic supplements added to DMEM+ may be mitogenic (Jaiswal *et al*. 1997; Bruder *et al*. 1997).

For the uncoated discs, AlamarBlue® activity was higher in the polished discs than in the sand-blasted ones ($p \leq 0.037$ at all time points). Regarding the type of metal, higher absorbances at 590nm for titanium compared to tantalum were measured, although no statistical significance was found.

The highest AlamarBlue® activities were observed for the cells cultured on biomimetically coated discs. These results were statistically significant as $p<0.001$ at all time points when biomimetic coating was compared with the electrochemical coatings or the uncoated discs. Very similar results were found for the two classes of electrochemical coatings. When these two coatings were compared with each other, only a statistically significant difference ($p=0.013$) was found at day 4 where cells on electrochemical coating at 20mA/cm^2 had higher activities than at 6.5mA/cm^2. For all types of coatings, AlamarBlue® activity was higher in polished discs than in sand-blasted ones ($p \leq 0.037$) except for biomimetic coating at day 14 and both electrochemical coatings at day 4. Activities in the titanium discs were higher than in the tantalum samples. However, these results were not statistically significant.

Results from the AlamarBlue® activity assay suggest that the biomimetic coating is the best for MSCs growth. Moreover, they proliferate less on complex topographies, defined as less organised surfaces such as those of the electrochemical coatings and sand-blasted discs, than on flatter topographies.

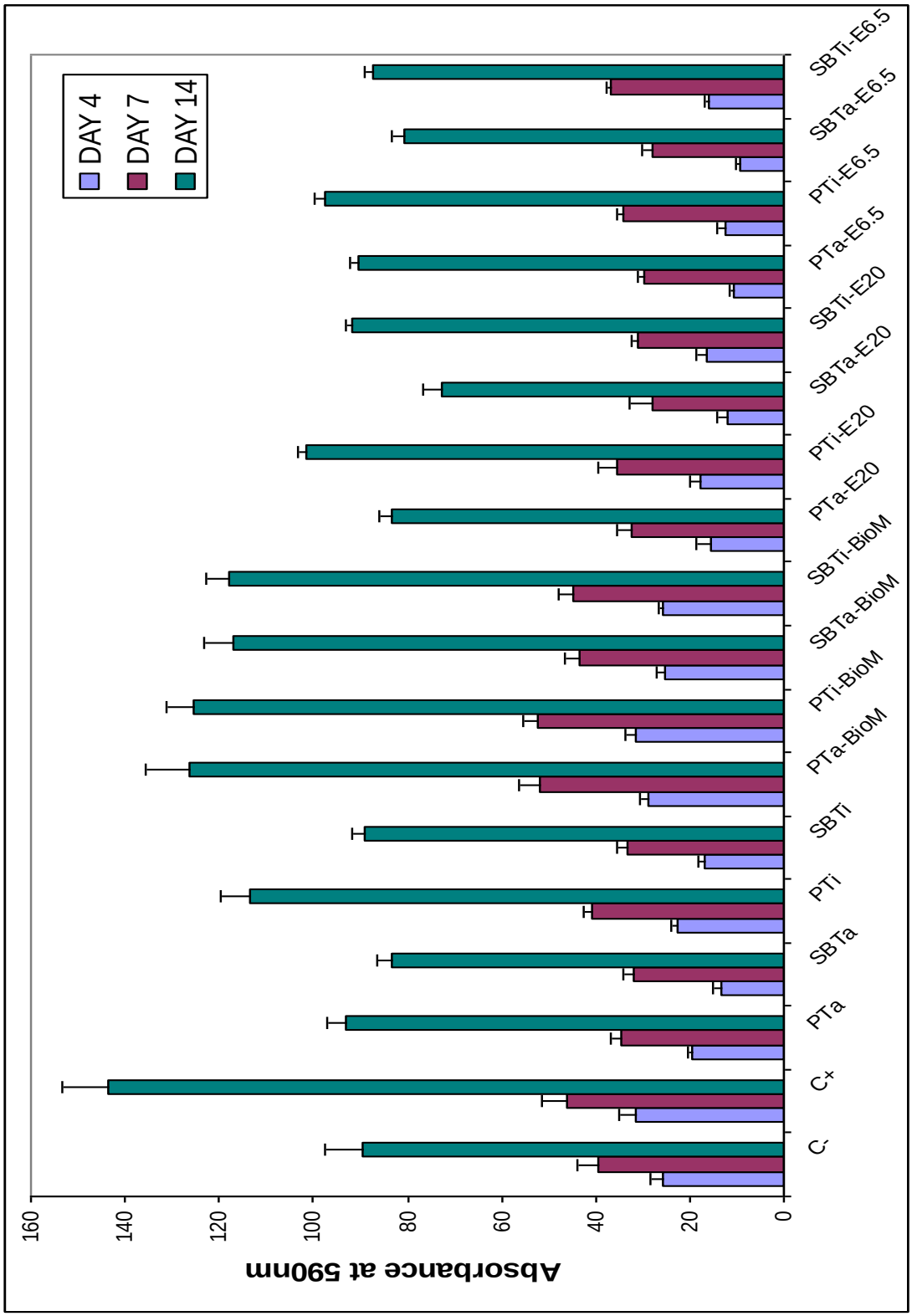

Figure 3.7 AlamarBlue® activity assay results for MSCs cultured on controls for osteogenic differentiation (C- and C+), uncoated tantalum and titanium discs (PTa, SBTa, PTi, SBTi), biomimetically coated discs (BioM), electrochemically coated discs at 20mA/cm^2 (E20) and at 6.5mA/cm^2 (E6.5) at 3 time points (4,7 and 14 days).

3.3.2.2 Analysis of Cell Proliferation: DNA Assay

Results from the DNA assay can be seen in Figure 3.8. As in the AlamarBlue® activity assay, C+, positive control for osteogenic differentiation, had higher amounts of DNA at the three time points of measurement than C-, supporting the suggestion that the osteogenic supplements used in this chapter may be mitogenic (Jaiswal *et al*. 1997; Bruder *et al*. 1997).

For the uncoated discs, the DNA concentration was higher in the polished discs than in the sand-blasted ones. These results were statistically significant ($p \leq 0.025$) at all time points, supporting the findings already discussed for the AlamarBlue® activity assay results: MSCs proliferate more on flatter topographies. Higher amounts of DNA were measured for titanium discs than for tantalum ones, although no statistical significance was found for these results.

The highest amounts of DNA were measured for the biomimetically coated discs, as seen in the AlamarBlue® activity assay. These results were statistically significant when biomimetic coating was compared with the electrochemical coatings ($p \leq 0.001$) or the uncoated discs ($p \leq 0.013$). Comparing the two electrochemical coatings, a higher variance between the 4 samples at day 14 could be observed for the electrochemical coating at 20mA/cm^2 than for the coating at 6.5mA/cm^2. However, no statistical significance was found at any time point when these two coatings were compared. For all types of coatings, the DNA concentration was higher in polished discs than in sand-blasted ones which was statistically significant ($p \leq 0.037$) except for the following groups: biomimetic coating at day 14, electrochemical coatings at day 4 and electrochemical coating at 6.5mA/cm^2 at day 14.

Although the AlamarBlue® results (Figure 3.7) and the level of DNA in cells growing on the titanium discs were generally higher than in the tantalum samples, the results were not statistically significant. This shows that there is no difference in terms of cell proliferation between titanium and tantalum.

Results from the DNA assay support those of the AlamarBlue® activity assay and also show that the biomimetic coating is the best for cell proliferation and that they proliferate less on complex topographies.

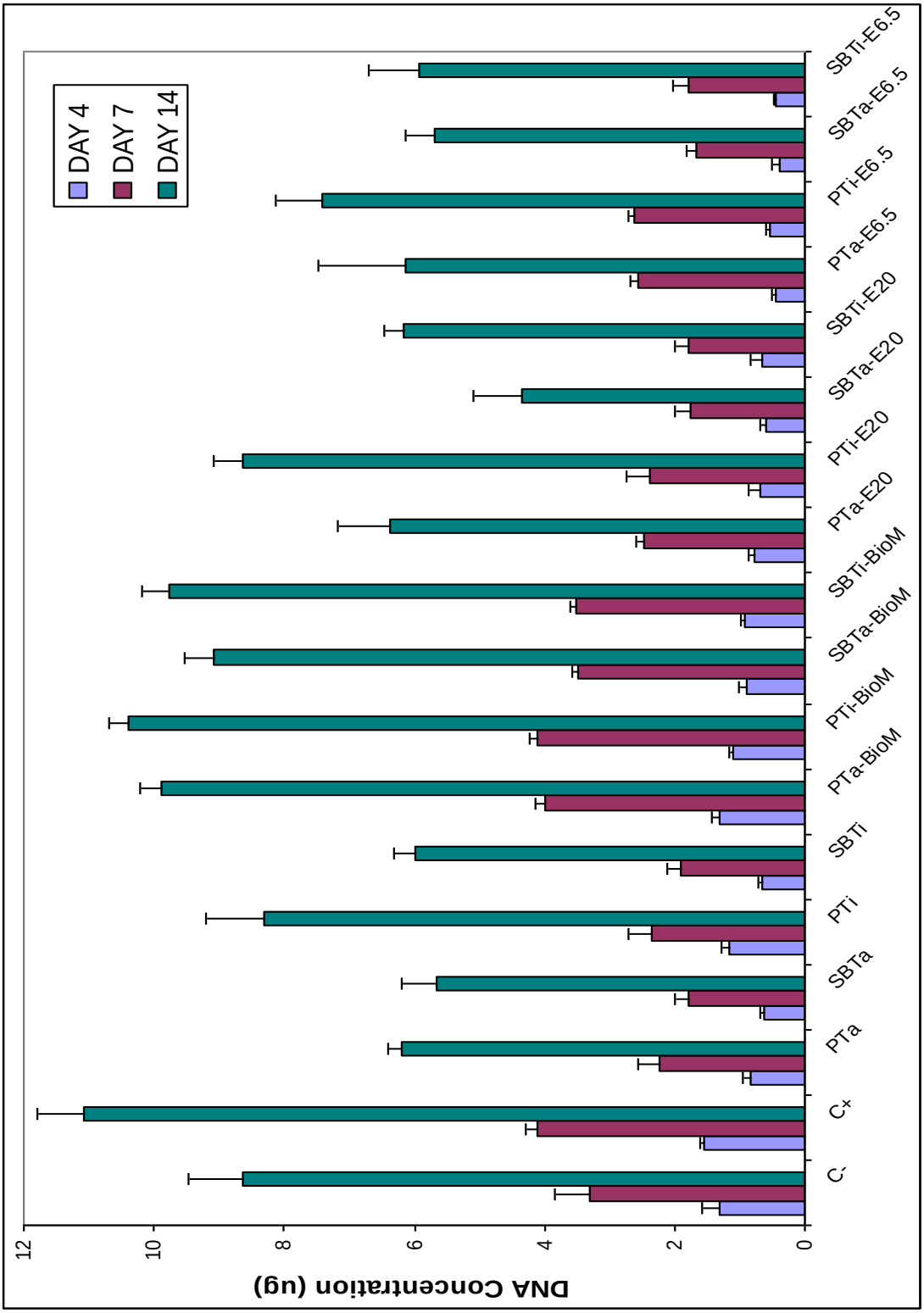

Figure 3.8 DNA assay results for MSCs cultured on controls for osteogenic differentiation (C- and C+), uncoated tantalum and titanium discs (PTa, SBTa, PTi, SBTi), biomimetically coated discs (BioM), electrochemically coated discs at 20mA/cm^2 (E20) and at 6.5mA/cm^2 (E6.5) at 3 time points (4, 7 and 14 days).

3.3.2.3 Analysis of Cell Differentiation down the Osteogenic Lineage: ALP Activity Assay

Figure 3.9 displays the results from the ALP activity assay. As already showed in Figure 3.6, C+ had higher enzyme activity than the negative control for osteogenic differentiation C-. The ALP activity increased throughout the study for both controls. No peak in the enzyme activity was observed for C+, suggesting that it may have happened in between days 7 and 14 or would have happened at a later time point.

Uncoated polished discs had very similar values to those of C-. Although it was not statistically significant, activities for the uncoated sand-blasted discs were found to be slightly higher than for the uncoated polished samples.

The calculated ALP activity per μg of DNA was higher in coated discs than in uncoated ones. Statistical analysis revealed that $p<0.001$ at all time points for each coating group when compared with the uncoated discs.

Figure 3.9 also shows ALP activity was higher in electrochemically coated samples than in biomimetic ones ($p<0.001$). The difference in ALP activity between the last two time points in the electrochemical samples was lower than in the biomimetic discs. The enzyme activity was higher in sand-blasted discs than in polished ones, although these differences were only significant ($p\leq0.01$) for biomimetically coated discs at days 7 and 14 and electrochemical coatings at day 7.

Finally, no statistical differences were found between Ta and Ti in terms of ALP activity.

These results show that MSCs differentiated down the osteogenic lineage when cultured on the biomimetic and electrochemical CaP coatings. As the ALP activity was higher in the electrochemical coatings and sand-blasted discs, the results also suggest that MSCs began to differentiate earlier when cultured on surfaces with more complex topographies.

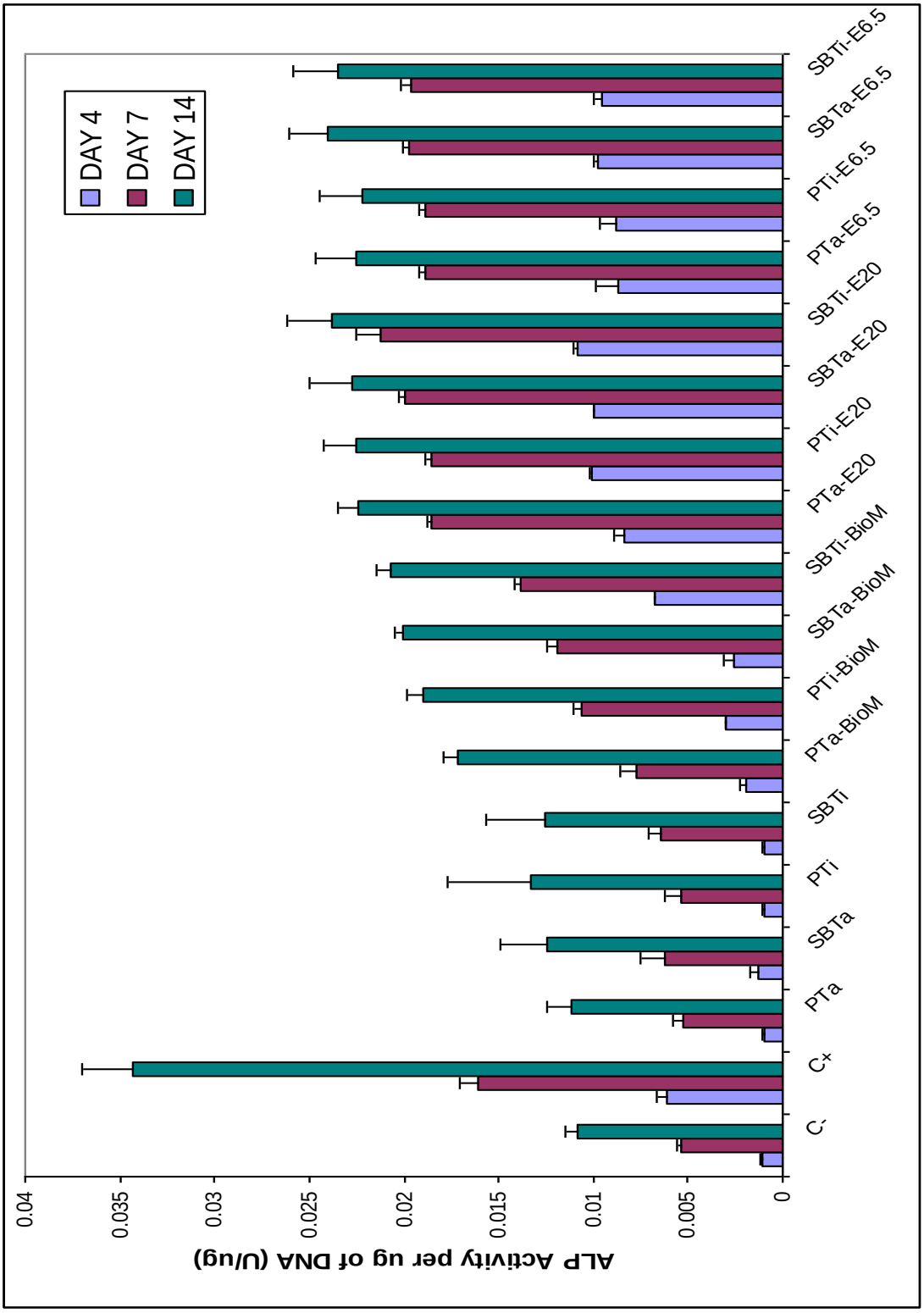

Figure 3.9 ALP activity assay results for MSCs cultured on controls for osteogenic differentiation (C- and C+), uncoated tantalum and titanium discs (PTa, SBTa, PTi, SBTi), biomimetically coated discs (BioM), electrochemically coated discs at 20mA/cm^2 (E20) and at 6.5mA/cm^2 (E6.5) at 3 time points (4, 7 and 14 days).

3.3.2.4 Analysis of Cell Morphology and Interaction with the Material: SEM Analysis

Figure 3.10 shows SEM photos of the controls for osteogenic differentiation C- and C+ at days 4, 7 and 14. As it can be seen from the photos, cells in C- at day 4 displayed a spindle or bipolar morphology, characteristic of MSCs in monolayer culture (Friedenstein *et al*. 1970; Friedenstein *et al*. 1974). Cells in C+ start to look more polygonal by day 4, which has been described as an osteoblast feature (Vrouwenvelder *et al*. 1993). In cells becoming more cuboidal, cytoplasmic organules are more visible than in spindle shaped cells. In both controls, cytoplasmic processes of attachment to the Thermanox™ surface of the discs and to each others can be observed (Figure 3.10A-F).

At day 7, cells in C- retained a spindle morphology, as shown by Figure 3.10G to I. Cells in C+ were cuboidal with very visible cytoplasmic granules (Figure 3.10J-L). Figure 3.10K shows two cuboidal cells interacting through long cytoplasmic processes or filopodia. At day 14, cells covered the disc surface in both controls. In C- cells kept the bipolar morphology while in C+ were cuboidal. In both controls cells were seen to be in contact between them (Figure 3.10M-R). The SEM analysis show that cells in C+, under osteogenic conditions, become cuboidal with visible cytoplasmic granules and interact between them and with the disc surface through long cytoplasmic processes or filopodia.

Figure 3.11 shows SEM photos of MSCs cultured on the control uncoated discs at days 4, 7 and 14. On the polished Ti and Ta discs, cells were orientated to one another and displayed a flattened morphology. Cells could be seen to be in contact between them and with multiple cytoplasmic processes extending at attaching the cell. (Figure 3.11A-F). On the other hand, patches of cells were observed covering the disc surface of the sand-blasted uncoated discs. They can also be seen in contact between them and long cytoplasmic processes of attachment and interaction are visible (Figure 3.11G-L). The SEM analysis shown in Figure 3.11 suggests that when MSCs are cultured on flat surfaces they displayed a flattened morphology and orientate to one another in a parallel way while on complex topographies they form patches of cells.

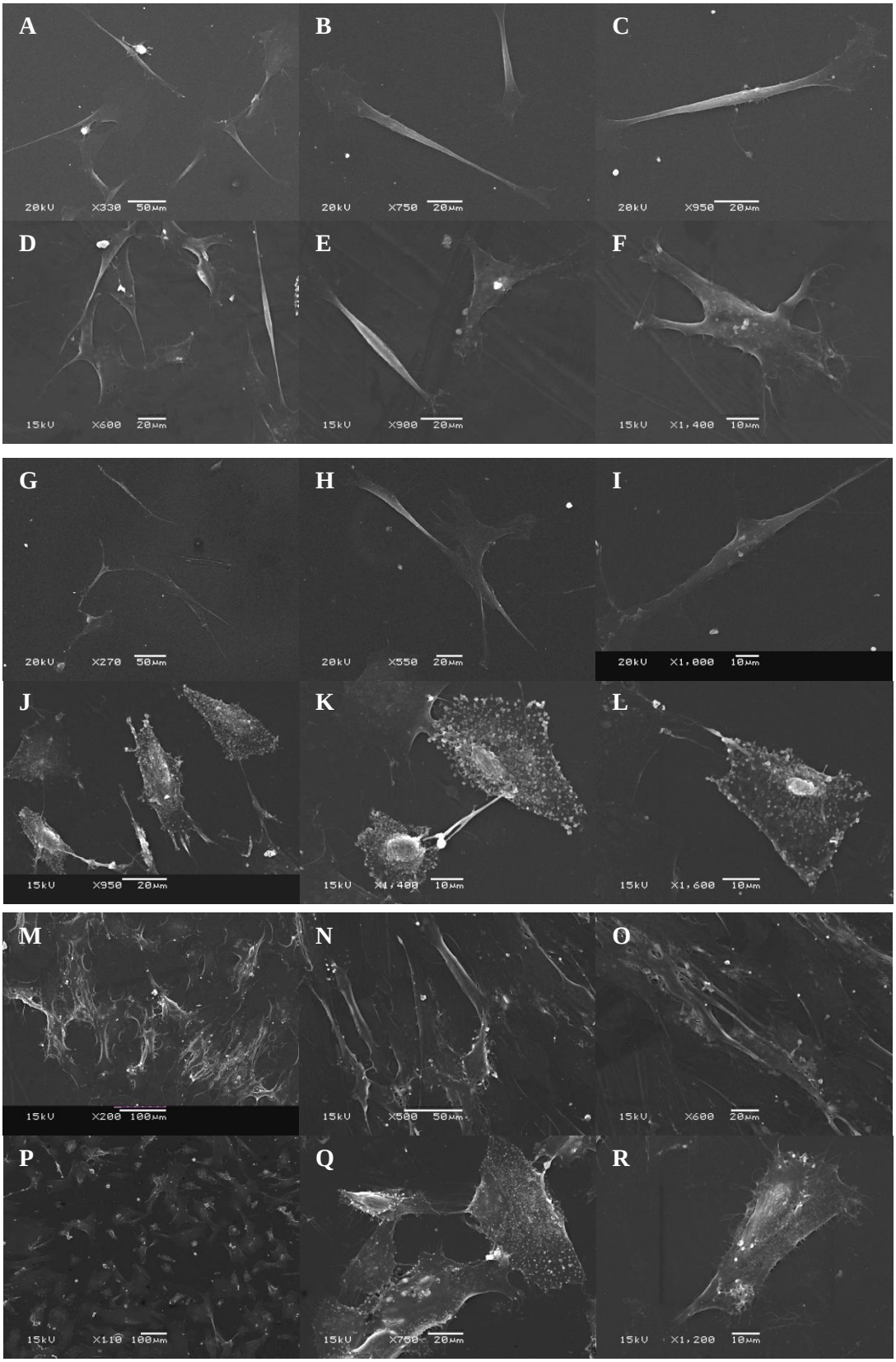

Figure 3.10 SEM analysis of MSCs cultured on Thermanox™ discs in either DMEM+ (C-) or osteogenic medium (C+): C- at day 4 **(A-C)**, C+ at day 4 **(D-F)**, C- at day 7 **(G-I)**, C+ at day 7 **(J-L)**, C- at day 14 **(M-O)** and C+ at day 14 **(P-R)**.

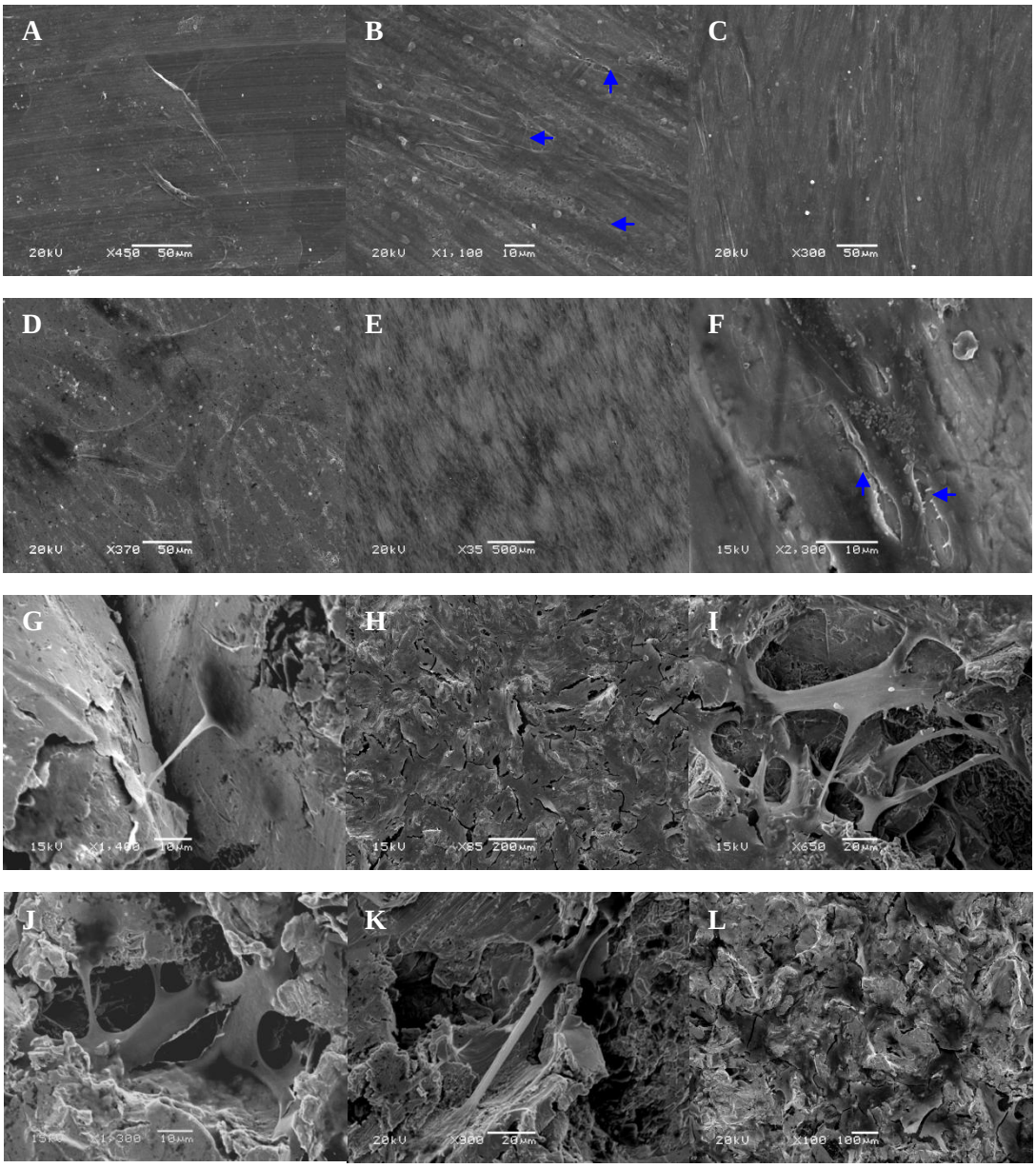

Figure 3.11 SEM analysis of MSCs cultured on uncoated polished (PTi and PTa) and sand-blasted (SBTi and SBTa) discs in DMEM+:

PTi at day 4 **(A)**, 7 **(B)** and 14 **(C)**; PTa at day 4 **(D)**, 7 **(E)** and 14 **(F)**; SBTi at day 4 **(G)**, 7 **(H)** and 14 **(I)**; SBTa at day 4 **(J)**, 7 **(K)** and 14 **(L)**.

Blue arrows show cytoplasmic processes of interaction and cells in contact.

SEM analysis of MSCs cultured on CaP coated Ti and Ta discs showed the growth of MSCs on the three different coatings deposited on the metal surfaces.

Figure 3.12 shows SEM photos of MSCs cultured on CaP coated metal discs at day 4.At this time these cells display, different morphologies -with long and spindle (Figure 3.12A, C, E, F, G), squarer or cuboidal (Figure 3.12D, F,H)- observed on the three different coatings. Figure 3.12B shows a cell adapting its morphology to the complex surface topography of the sand-blasted disc.

Figure 3.13 shows SEM photos of MSCs cultured on CaP coated metal discs at day 7. As before, different morphologies could be observed on different coatings (Figure 3.13D-H). In some regions, a dense cell coverage could be seen (Figure 3.13A-C). Figure 3.13D shows two cuboidal cells interacting through long cytoplasmic processes and a spindle shaped cell next to one of them.

SEM analysis of MSCs cultured on CaP coated metal discs at day 14 is shown in Figure 3.14. A dense cell coverage of the disc surface could be observed for all the samples (Figure 3.14A-C). Different morphologies could still be seen in some areas (Figure 3.14D-H). Figure 3.14D shows a spindle shaped cell interacting with a more polygonal cell.

At the three time points analysed the plasticity of MSCs was revealed as they adapted their morphology to the complex topographies of the sand-blasted discs and electrochemical coatings. However, two main morphologies for these cells could be distinguished: bipolar, long, spindle shaped cells and squarer, cuboidal cells.

The photos showed these cells were able to interact with the different CaP minerals deposited on the discs surfaces through long cytoplasmic processes or filopodia, which they also used to interact with each others.

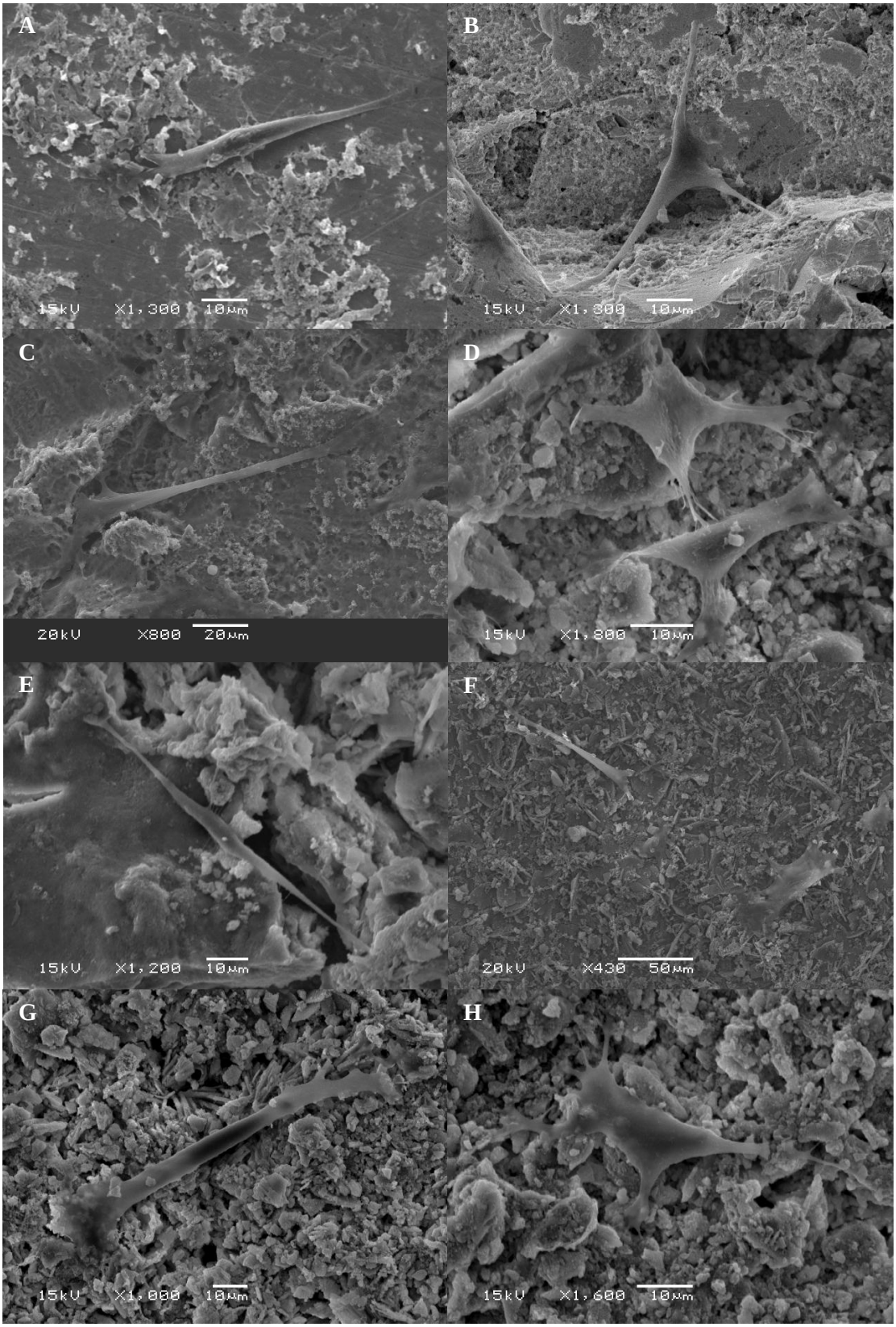

Figure 3.12 SEM analysis of MSCs cultured on CaP coated discs in DMEM+ at day 4: **(A)** PTa-BioM, **(B)** SBTa-BioM, **(C)**; SBTi-BioM, **(D)** PTi-E20, **(E)** PTa-E20, **(F)** PTi-E6.5, **(G)** SBTa-E6.5 and **(H)** SBTa-E6.5.

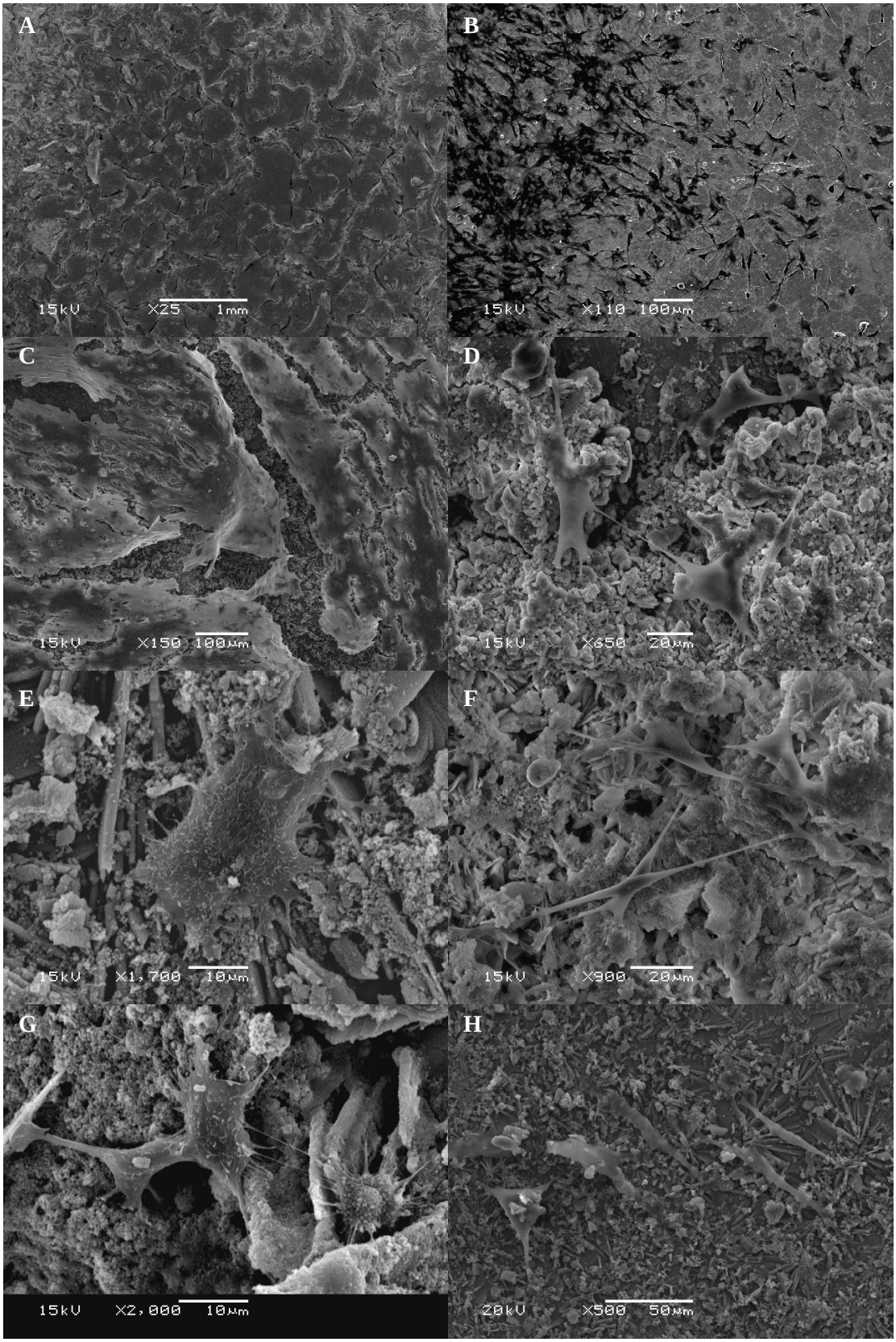

Figure 3.13 SEM analysis of MSCs cultured on CaP coated discs in DMEM+ at day 7: **(A)** SBTa-BioM, **(B)** PTa-BioM, **(C)**; PTi-E20, **(D)** PTi-E20, **(E)** PTa-E20, **(F)** SBTa-E20, **(G)** SBTa-E6.5 and **(H)** PTi-E6.5.

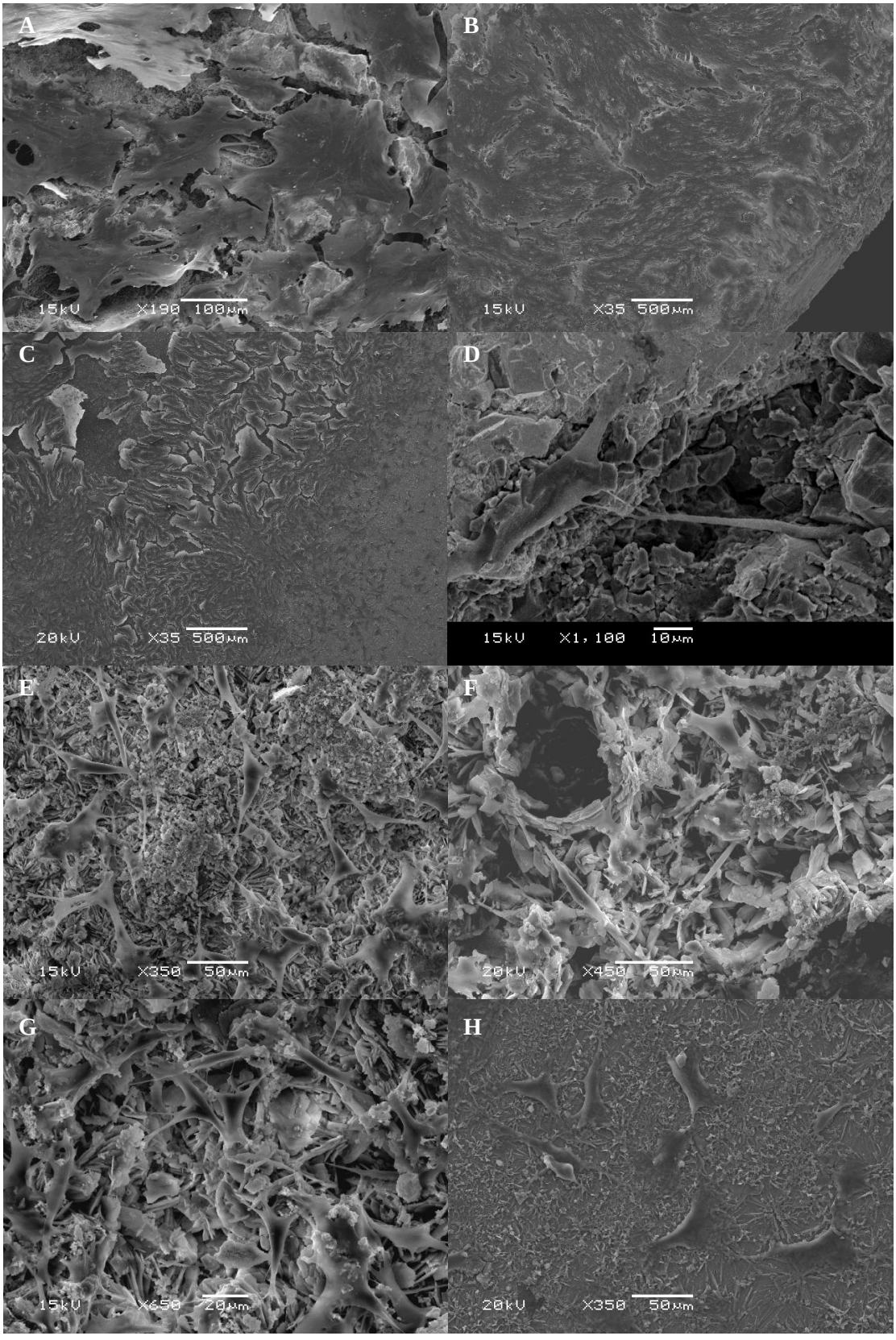

Figure 3.14 SEM analysis of MSCs cultured on CaP coated discs in DMEM+ at day 14: **(A)** SBTa-BioM, **(B)** PTa-E20, **(C)**; PTi-E6.5, **(D)** SBTa-BioM, **(E)** SBTa-E20, **(F)** SBTi-E20, **(G)** SBTa-E6.5 and **(H)** PTi-E6.5.

3.4 DISCUSSION

3.4.1 Expansion and Characterisation of MSCs

MSCs were first described by Friedestein and co-workers in the 1970s, who observed that these cells adhered to tissue culture plates and resembled fibroblasts in vitro (Friedenstein *et al*. 1970; Friedenstein *et al*. 1974). In the present work, routine observations of MSCs in monolayer cultures by phase-contrast light microscopy revealed these characteristics: photos seen in Figure 3.1 show that monolayer cultures of MSCs were composed of cells with a fibroblastic or spindle morphology. The typical spindle shape of these cells was observed to persist for 12 passages, suggesting MSCs were able to replicate as undifferentiated cells and kept their phenotype, as previously described by Jaiswal *et al*. 1997 and Pittenger *et al*. 1999.

As MSCs have the potential to differentiate into lineages of mesenchymal tissues, these cells are often characterised by demonstrating their multipotency differentiating them down two or more mesenchymal lineages (Pittenger *et al*. 1999; Erices *et al*. 2000; Rust 2003; Hara *et al*. 2008). In my study, MSCs were characterised by differentiating them into adipocytes and osteocytes. Other cell lineages of mesenchymal tissues into which they have been shown to differentiate are chondrocytes, fibroblasts and myoblasts (Verfaillie 2002; Pittenger *et al*. 1999).

After 21 days of culture under adipogenic conditions, Oil Red O staining showed the presence of lipids as well as a clear difference in morphology, as seen on Figure 3.2. These results indicate the cells had undergone adipogenic differentiation (Erices *et al*. 2000; Rust 2003).

Changes in morphology were also observed in MSCs cultured under osteogenic conditions with cells becoming polygonal, which has been described as osteoblast feature (Vrouwenvelder *et al*. 1993). Mineral deposits, representative of mineralised matrix formation, another indicator of osteoblastic differentiation, were stained in the osteogenic samples after 28 days (Erices *et al*. 2000). The results displayed in Figure 3.5 showed that the DNA concentration of MSCs in osteogenic medium was higher at all time points than that of the control samples. Jaiswal *et al*. 1997 and Bruder *et al*. 1997 found very similar results in their studies of osteogenic differentiation of human

MSCs and concluded that the osteogenic supplements added to the culture medium stimulated cell proliferation as well as differentiation. Figure 3.6 showed that ALP/DNA of osteogenic cultures was also higher at all time points. MSCs in osteogenic medium showed a characteristic trend already described in the literature (Lian and Stein 1992; Jaiswal *et al*. 1997): ALP activity elevates when MSCs begin to differentiate and peaks between days 8 and 12, which coincides with their commitment to become osteoblasts. Thus, ALP expression is an early marker of osteogenic differentiation. In the present study, this peak could be seen at day 14, although it could have happened sometime in between days 7 and 14 as no measurements were taken in between these two time points. Other markers of osteogenic differentiation could have been analysed in order to show that the MSCs used in this study differentiated along the osteogenic pathway, such as Runx2, a transcriptional activator essential for initial osteoblast differentiation and subsequent bone formation (McCarthy *et al*. 2000), or osteocalcin, a late marker that binds HA and is expressed by osteoblasts just before and during extracellular matrix deposition and mineralisation (Lian and Stein 1992). As mentioned in the introduction chapter of this thesis there is a lack of a specific marker or combination of markers that specifically define MSCs. Pittenger and colleagues in 1999 showed that expanded and attached human MSCs were uniformly positive for the following markers: SH2, SH3, CD29 CD44, CD71, CD90, CD106, CD120a, CD124 and many other surface proteins (Pittenger *et al*. 1999). However, it has been reported that MSCs populations are often heterogeneous between species (Colter *et al*. 2000; Javazon *et al*. 2001; Peister *et al*. 2004). Therefore it is necessary to characterise MSCs through a combination of physical, phenotypic and functional properties such as the differentiation potential into different lineages study found throughout the literature and used in this thesis (Hara *et al*. 2008; Maeda *et al*. 2007; Eslaminejad *et al*. 2008).

Together, all the findings showed that MSCs were able to differentiate into two different cell lineages, thus demonstrating their multipotency (Pittenger *et al*. 1999).

3.4.2 Culture of MSCs on CaP Coated Metal Discs with Different Topographic Surface

In order to create new bone tissue-engineered constructs it is very important to understand how the scaffold properties may affect the cells with which it is being

seeded. Thus, once MSCs and the CaP coatings had been fully characterised, the next step of my thesis was to study the effect of these coatings on MSCs behaviour in terms of proliferation and differentiation. When comparing the different samples between each others, three properties were considered: coating type, surface topography and metal type. From the findings of this study, the best metal type and coating method for cell proliferation and differentiation would be chosen to carry on with the rest of my thesis.

Cytotoxicity is widely used for the initial screening of materials for biocompatibility (Salgado *et al*. 2006; Chen *et al*. 2006). In this work, cytotoxicity was measured by AlamarBlue® activity assay. As AlamarBlue® is a biochemical indicator of metabolic activity the results show that all the samples had viable cells able to proliferate. SEM analysis of the coated discs, shown in Figures 3.12, 3.13 and 3.14, further supported these results.

The DNA assay used in this study quantifies the amount of DNA in the sample and thus it is a measurement of cell proliferation. Results from AlamarBlue® activity and DNA assays agreed and showed that the biomimetic coating was the best at all time points when compared to the uncoated discs and the electrochemically coated samples. However, the electrochemically coated discs were very similar to the uncoated ones. Therefore, the first hypothesis of this chapter was proved to be false: CaP coatings will increase MSCs proliferation compared to uncoated Ta/Ti surfaces. A possible explanation for the observed increase in MSCs proliferation on the biomimetically coated discs could be the nano-scale of these coatings. Nano-scale CaP more closely resembles the size and properties of CaP crystals in natural bone (Wopenka and Pasteris 2005) and it has been shown to increase cell proliferation when compared to micro-scale coatings (Chen *et al*. 2007). Proliferation was also significantly greater on polished discs than on sand-blasted ones. These results suggest that complex topography, defined as less organised surfaces like those of the electrochemical coatings and sand-blasted discs, significantly decreases cell proliferation. Anselme *et al*. in their work published in 2000 observed lower adhesion and proliferation of human osteoblasts on less organised surfaces, which supports the data presented in this chapter.

In the ALP/DNA assay results displayed in Figure 3.9 it can be seen that the uncoated discs had very similar values to the C- ones. Maeda et al. in 2007 showed that titanium surfaces are comparable to tissue culture polystyrene dishes in terms of osteogenic differentiation: MSCs only differentiated on Ti surfaces when treated with osteogenic supplements. At day 4 all the CaP coated samples showed higher activities than C-, indicating that MSCs differentiated down the osteogenic lineage. Moreover, for all the electrochemically coated samples and SBTi-BioM the activities are higher than for C+. As ALP activity elevates when MSCs begin to differentiate these results suggest that MSCs cultured on CaP coated discs began to differentiate before than in C+. At day 7 the electrochemically coated samples had higher activities than C+ while the biomimetically coated discs had activities in between C- and C+, suggesting MSCs were more differentiated on electrochemical coatings than on biomimetic ones. At day 14 all the samples had enzymatic activities in between C- and C+. The fact that the increment in activity between days 7 and 14 was higher for the biomimetic samples than for the electrochemical ones which suggests that MSCs began to differentiate earlier on electrochemically coated discs than in C+ or biomimetic samples and therefore the peak in ALP activity is sometime in between days 7 and 14.

In summary, results for the ALP/DNA assay show that MSCs differentiate down the osteogenic lineage when cultured on CaP coatings (Ohgushi *et al*. 1993; Ohgushi *et al*. 1996; Nishio *et al*. 2000). They also suggest that MSCs begin to differentiate earlier when cultured on surfaces with more complex topographies, as the ALP activity was higher on sand-blasted samples compared with polished surfaces (Jäger *et al*. 2008). Electrochemically coated samples showed significantly more ALP activity per μg of DNA than biomimetically coated samples which could be a combination of both factors described above: electrochemical samples contain more amount of CaP and their surface is less organised than that of the biomimetic samples.

SEM analysis confirmed the coatings were biocompatible and images taken showed a dense coverage of cells on the discs surfaces after 14 days. Spindle-shaped cells as well as with cuboidal morphology could be observed on all the coatings, confirming MSCs underwent osteogenic differentiation on the CaP coated discs. On the uncoated polished discs, cells displayed a flattened morphology (Vrouwenvelder *et al*. 1993) and they grew in a parallel way. However, on the uncoated sand-blasted discs patches

of cells were observed covering the disc surface. This difference in morphology between polished and sand-blasted surfaces was also observed by Anselme *et al*. 2000. From the photos it was observed that MSCs adapted their morphology to the complex topography of sand-blasted and electrochemically coated discs. Finally, cells were seen to be interacting with the material and with each other through long cytoplasmic processes or filopodia, already described in the literature (Vrouwenvelder *et al*. 1993).

Statistical analysis of the results revealed no significant differences between Ta and Ti discs in terms of MSCs proliferation and differentiation for either the uncoated discs or the coated ones. These results indicate that tantalum and titanium offer very similar characteristics for MSCs.

3.5 CONCLUSION

Different crystal-sized CaP coatings were deposited on different topographical metal surfaces using biomimetic and electrochemical methods. When MSCs were cultured on these coatings, the nano-sized crystals of the biomimetic coatings significantly increased cell growth compared to the electrochemical ones and the uncoated discs. MSCs were also shown to proliferate more on polished discs than on sand-blasted ones. All the coatings induced differentiation of MSCs down the osteogenic lineage, which was significantly greater on electrochemical coatings and complex topographies. Finally, no significant differences were found between tantalum and TiAl6V4 discs in terms of MSCs growth and differentiation.

The findings from this study will be used in the next chapter of my thesis in order to create a bone tissue-engineered construct seeded throughout its structure with MSCs. The construct will have a porous metal scaffold coated with a CaP layer throughout.

CHAPTER 4:

Tissue Culture

of Mesenchymal Stem Cells

Seeded on a Calcium-Phosphate Coated

Porous Metal Scaffold

using a Perfusion Bioreactor System

4.1 INTRODUCTION

So far my thesis has investigated different CaP coatings and their effect on MSCs growth and osteogenic differentiation on flat Ta and Ti surfaces. Using electrodeposited and biomimetic CaP coatings is advantageous because it allows the coating of porous structures. However, cell growth into porous structures is difficult to accomplish using static culture systems and for this reason a perfusion bioreactor system was investigated.

As a key component of bone tissue engineering, the perfusion bioreactor system provides an optimised environment for functional 3D tissue development. Important advantages offered by the perfusion system are enhanced delivery of nutrients throughout the entire scaffold, which ultimately results in a construct with an even distribution of cells throughout, and mechanical stimulation to the cells by means of fluid shear stress, which enhances osteoblastic differentiation of mesenchymal stem cells (Bancroft *et al*. 2003; Martin *et al*. 2004; Sikavitsas *et al*. 2003).

In the absence of a vascular blood supply *in vitro*, the delivery of nutrients to cells seeded on 3D scaffolds and cultured under static conditions occurs by diffusion. Due to static culture conditions, cells on the surface of the constructs are typically viable and proliferate readily, while cells within the construct may be less active, necrotic or the inner construct may not be colonised. Therefore, a dynamic culture system is necessary in order to obtain an even distribution of cells throughout 3D scaffolds (Holtorf *et al*. 2005; Sikavitsas *et al*. 2005).

MSCs are mechanosensitive as *in vivo* they are involved in the transduction of mechanical stimulation to bone cells necessary for the continuous bone remodelling process (Sikavitsas *et al*. 2001). Mechanical stimulation provided by a flow perfusion system enhances the osteogenic differentiation potential of these cells (Sikavitsas *et al*. 2003; Bjerre *et al*. 2008). Mechanical stimulation by means of fluid shear stress closely resembles the *in vivo* situation in bone: the mechanical loading of the skeleton causes interstitial fluid flow throughout the lacunar and canalicular spaces in bone, where the bone cells lining these spaces respond to this mechanostimulation. This response is mechanotransducted into alterations in biochemical behaviour, which is

thought to be directly involved in bone remodelling in response to mechanical stress (Hillsley and Frangos 1994; Sikavitsas *et al*. 2001).

In the previous chapter 3 of this thesis Ta and Ti alloy discs with different surface topography (polished and sand-blasted) were CaP coated using different methods (biomimetic and electrochemical depositions) and cultured with MSCs in order to study how these coatings affected the proliferation and osteogenic differentiation potential of these cells. The study was carried out using a 2D experimental model under static culture conditions. From this study it was concluded that MSCs were able to proliferate and differentiate on both Ta and Ti surfaces. For this investigation I chose to use Ti because of its proven biocompatibility, strength, lightness and high resistance to corrosion when used in orthopaedic applications and availability (Niinomi 2008; Disegi 2000).

For this chapter, a porous Ti material coated with CaP was used as scaffold. Porous metals are becoming increasingly popular in orthopaedic surgery because they offer excellent mechanical properties, biocompatibility and bone ingrowth potential (Karageorgiou and Kaplan 2005; Niinomi 2008; Bobyn *et al*. 1999). By coating metal materials with a CaP layer bioactivity and osteconductivity properties are added (Karageorgiou and Kaplan 2005). The porous scaffolds were seeded with MSCs and dynamically cultured in a perfusion bioreactor system. Proliferation, osteogenic differentiation and cellular distribution were compared to those of constructs statically cultured. The outcomes of this chapter will be used in order to design an *in vivo* study where tissue-engineered constructs will be implanted and compared to non tissue-engineered ones.

The aim of this study was to design a perfusion bioreactor system in order to culture MSCs seeded on a porous scaffold and study their proliferation, osteogenic differentiation and distribution throughout the scaffold.

The hypotheses were:

1. **A perfusion bioreactor system will enhance MSCs proliferation when cultured on a CaP coated porous Ti scaffold compared to statically cultured cells on the same scaffold.**

2. **A perfusion bioreactor system will enhance MSCs differentiation down the osteogenic lineage when cultured on a CaP coated porous Ti scaffold compared to statically cultured cells on the same scaffold.**
3. **A perfusion bioreactor system will provide a more even distribution of MSCs throughout a CaP coated porous Ti scaffold when compared to statically cultured MSCs on the same scaffold.**

4.2 MATERIALS AND METHODS

4.2.1 Perfusion Bioreactor System Design

The perfusion bioreactor system used in this thesis was designed following the requirements outlined by Bancroft *et al*. 2003. As explained in section 1.4.6 of this thesis, different designs for perfusion systems can be found in the literature. However, all of them present the same components: a bioreactor chamber in which the construct is fitted, a pump to deliver the flow rate, media containers and a tubing system. Figure 4.1 shows a scheme depicting the design and components of the perfusion bioreactor system used in this thesis:

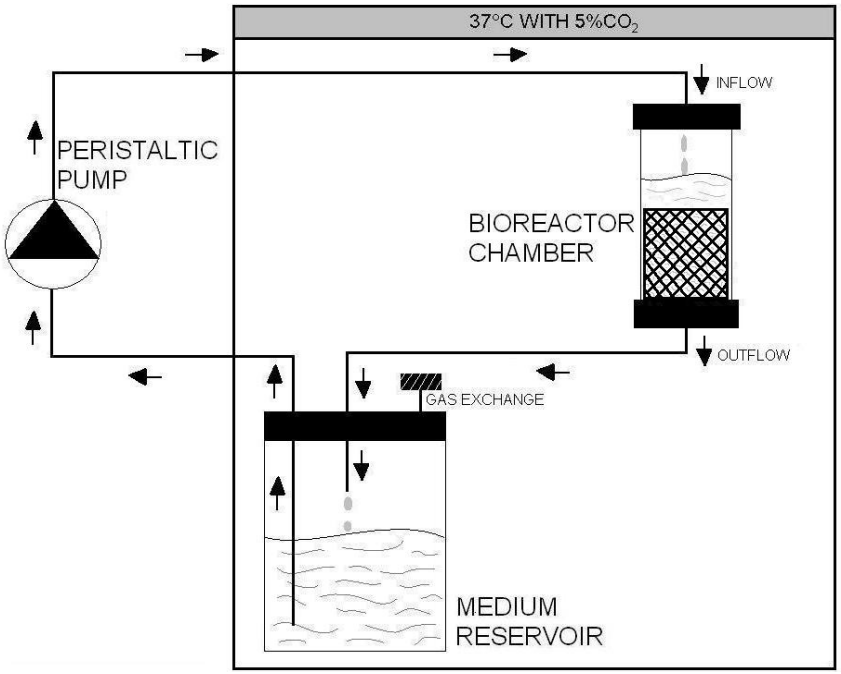

Figure 4.1 Perfusion bioreactor system scheme.

The first requirement outlined by Bancroft *et al*. 2003 is that the flow must be delivered through the scaffolds, trying to avoid non-perfusion flow going around them. Therefore, a bioreactor chamber was made out of polycarbonate, a transparent, durable, tough and autoclavable material, with 45mm length and 10mm inner diameter that optimized the delivery of the flow through the scaffolds (Figure 4.2B).

The second requirement, the flow rate delivered to the scaffolds must be consistent, repeatable and controllable, was met by using a multichannel peristaltic pump (Masterflex L/S 07523-Series, Cole-Parmer®, UK) (Figure 4.2A). To test whether the

flow rate delivered by the pump was consistent, repeatable and controllable an experiment was carried out using distilled water. A 25mL universal tube was filled with distilled water and a 25mL universal tube was left empty for collection of the outflow. A tube (Masterflex® 06409-13, Tygon®, Cole-Parmer®, UK) was immersed in the universal with water, connected to the pump and then to the inflow of a bioreactor chamber containing a scaffold. Another tube was connected to the outflow of the bioreactor chamber and its other end placed inside the empty universal for collection of the outflow. A flow rate of 1mL/min was set and the pump was left to run for 5min, after which the volume of water collected in the outflow tube was measured using a 10mL measuring cylinder. This test was carried out 3 times, always collecting 5mL of distilled water after it, indicating the delivered flow rate was consistent, repeatable and controllable.

Third, the perfusion system must be able to be sterilised and kept in sterile conditions throughout the duration of the culture. To meet this requirement, a medium reservoir and a tubing system that are autoclavable were chosen. The medium reservoir (KIMAX® GL-45 Media/Storage Bottles with Color Polypropylene Caps, General Laboratory Supply, USA) had air ventilation system (two sterile 0.22μm filters per reservoir, Millex®GP, Millipore, Ireland), to allow gas exchange (Figure 4.2C). The tubing system (Masterflex® 06409-13, Tygon®, Cole-Parmer®, UK) connected the different parts and sealed the system so it could be kept sterile (Figure 4.2D). Moreover, it is long-lasting and crack-resistant. The components were easily assembled inside a laminar flow hood.

The last requirement is that the perfusion system must be simple and operable by one person. All the different parts of the system were connected in an easy manner, making the whole system simple to work with. Moreover, four perfusion systems could run in parallel due to the multichannel capability of the peristaltic pump.

Figure 4.2E shows a photo of the chamber containing the construct where the construct tightly fits inside the chamber and that some medium is always above the top of the construct. Figure 4.2F shows the whole system in operation, with 3 chambers and 3 medium reservoirs inside the 37ºC with 5%CO_2 incubator with the peristaltic pump outside the incubator delivering a flow of 0.75mL/min.

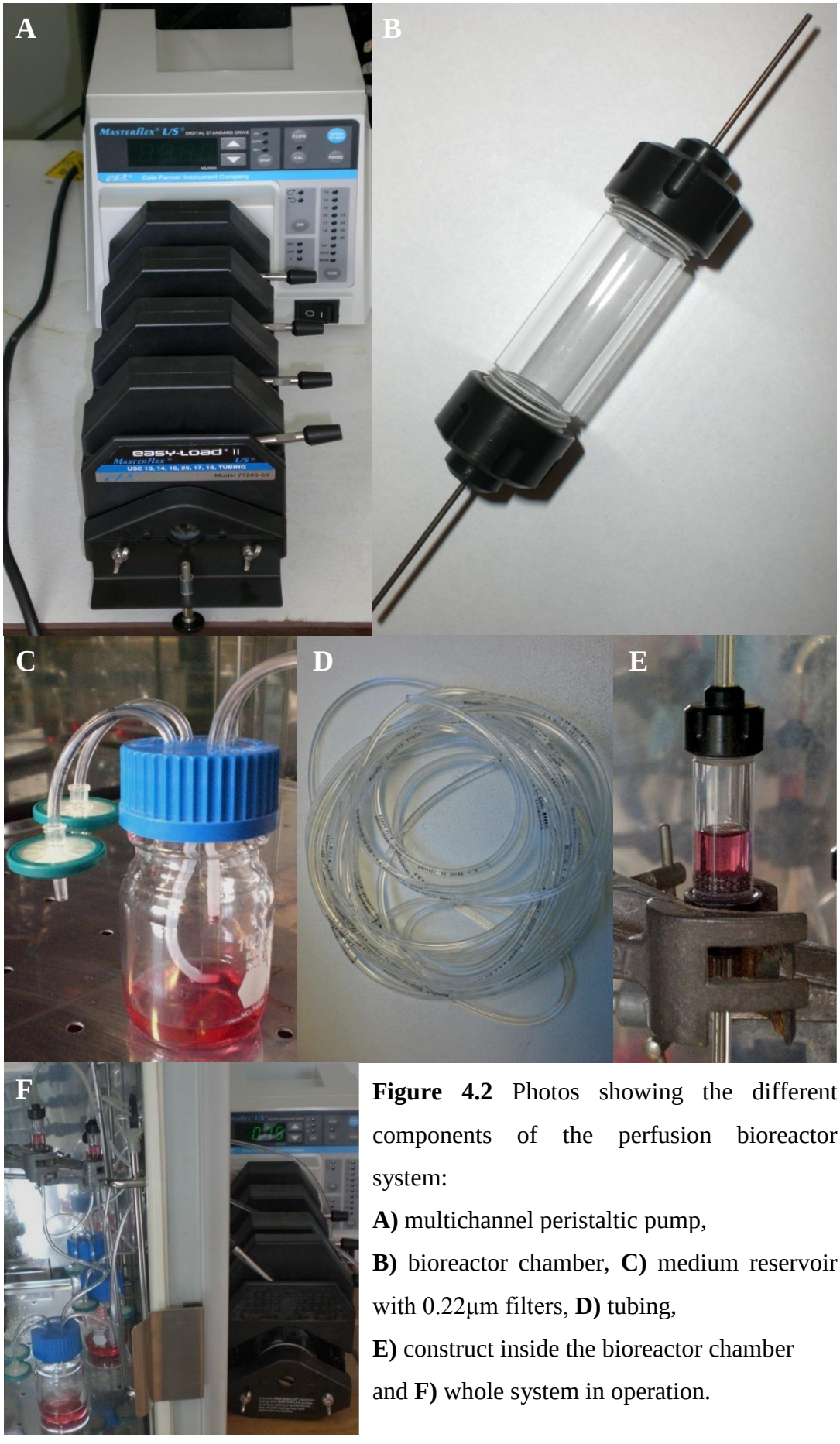

Figure 4.2 Photos showing the different components of the perfusion bioreactor system:
A) multichannel peristaltic pump,
B) bioreactor chamber, **C)** medium reservoir with 0.22µm filters, **D)** tubing,
E) construct inside the bioreactor chamber and **F)** whole system in operation.

4.2.2 Scaffolds

The scaffolds used in this thesis were porous TiAl6V4 (Ti) cylinders coated with a calcium-phosphate (CaP) layer, as explained at the end of section 1.4.3.

The porous Ti cylinders were 9mm diameter and 11mm length (Figure 4.3A), manufactured by Eurocoating S.p.a, Ciré-Pergine, Italy. Figure 4.2B shows the measurements taken for the voids and the struts of the material as supplied by the manufacturer. As it can be seen from it, the voids are ~700-850µm while the struts are ~350-480µm. The material has a porosity of 70%.

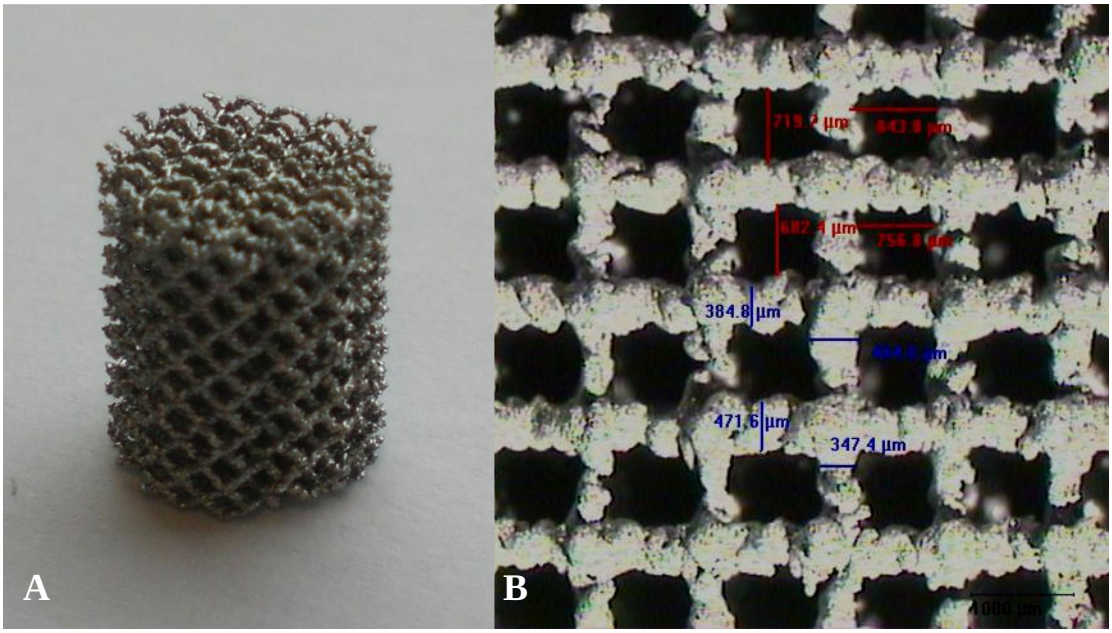

Figure 4.3 Ti cylinders used in this study: **A)** macroscopic and **B)** microscopic views.

4.2.2.1 CaP coating of Ti cylinders

Ti cylinders were coated with a CaP layer using two different methods, biomimetic and electrochemical at 20mA/cm^2. As already mentioned in section 2.2.3, 20mA/cm^2 was found to be optimum for current efficiency by Redepenning *et al*. 1996. In order to make a comparison between the two types of coatings, Ti cubes (~1cm length each side) from the same material shown in Figure 4.3 were used for this purpose (Figure 4.4). The criteria in order to choose one coating method over the other were fully and uniform covering of the outside and inside of the Ti blocks with a CaP layer.

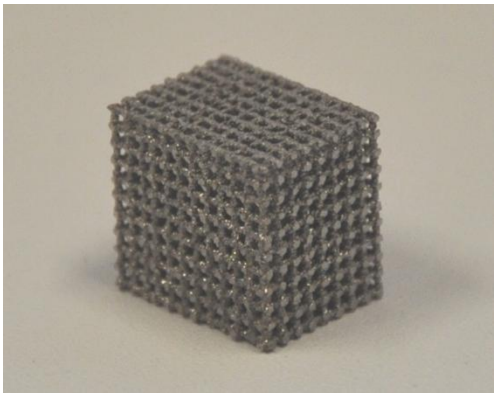

Figure 4.4 Ti cubes used to compare the biomimetic versus the electrochemical coating at 20mA/cm^2.

The biomimetic coating was carried out as previously explained in section 2.2.2 of this thesis, according to the procedure described by Habibovic *et al*. 2002. The electrochemical depositions at 20mA/cm^2 were done according to section 2.2.3, following the procedure described by Redepenning *et al*. 1996. For each type of coating 3 Ti cubes were sued (n=3 for each coating).

Morphology and crystal size of the coatings were characterised by scanning electron microscopy (SEM). In order to find out whether the inside of the material was coated with a CaP layer and how thick this layer was, samples were embedded in hard grade acrylic resin, transversely cut using EXACT diamond band saw and polished as explained in section 2.2.5.4. The sections were then visualised by SEM. Finally, elemental analysis of the successful coating (n=9 as 3 spectra per sample were obtained) was carried out by energy dispersive X-ray spectroscopy (EDAX) as already explained in section 2.2.5.2.

4.2.3 Cells

Cells used for this study were ovine mesenchymal stem cells, aspirated from the iliac crest using an aseptic technique. The cells used in this chapter were the same ones as in previous chapter 3, and therefore their multipotency was demonstrated (see section 3.3.1). Ovine MSCs were chosen for this study because ultimately the construct with cells will be tested in an ovine *in vivo* model.

Cell culture and maintenance was carried out as detailed in section 3.2.1.1. Standard DMEM+ was used for culturing the cells as well as throughout the study described in this chapter. Culture flasks were kept in incubators at 37ºC with 5% CO_2. Medium was changed every 3 to 5 days and the cultures passaged when 80 to 90% of confluency was reached. MSCs were routinely observed by phase-contrast light microscopy.

4.2.4 Cell Seeding Study of MSCs on CaP Coated Porous Ti Scaffolds

In order to test the optimum incubation time for the cells once inoculated on the scaffolds, a cell seeding study was carried out. The ideal incubation time allows the cells to attach to the scaffold without the medium evaporating dry, which would result in cell lysis.

Calcium-phosphate coated porous titanium cylinders were sterilised in an oven at 160ºC for 1 hour prior to cell seeding, which was carried out under sterile conditions inside a laminar flow hood.

The MSCs were trypsinised and a viable cell count was performed using a haemocytometer as described in Chapter 3. 1×10^6 cells (Rust 2003) in a total volume of 0.2mL of medium were seeded onto each scaffold, which had been placed in 24 well plates (Orange Scientifique, Belgium). The cells were incubated with the porous cylinders for 60, 90 and 120 minutes at 37ºC with 5% CO_2. 3 scaffolds per time point were used. After the incubation times, 2mL of DMEM+ were added per well. After further incubation of the cells for 24 hours at 37ºC with 5% CO_2, a cell count with trypan blue was done on the medium in order to count unattached cells. An AlamarBlue® activity assay was done on each sample as a measurement of cell metabolism which relates to cell number.

A 1/2 dilution of the cells in trypan blue was prepared and pipetted into a cover-slipped haemocytometer which was then placed under a phase-contrast light microscope.

For the AlamarBlue® activity assay, the working solution was prepared as specified in Chapter 3 and 2mL of it were added per well. Samples were incubated at 37ºC with

5% CO_2. After 4 hours, 100µL from each sample were loaded in triplicate into a FluoroNunc™ white 96-well plate and absorbance measured at 590 nm using a plate reader (Fluoroskan Ascent, Labsystems, USA). Results were compared to those of an empty well to which 2mL of working solution had been added at the beginning of the assay.

From this seeding study, 90 minutes was chosen as the optimum incubation time for the cells as it obtained the highest AlamarBlue activity (see results section 4.3.4. of this chapter). 90 minutes incubation time was applied for the rest of the work described in this chapter.

4.2.5 Perfusion Flow Rates Study

A study in order to choose an appropriate flow rate for the perfusion bioreactor system designed in this chapter was carried out. The perfusion flow rates study was based on the work conducted by Cartmell and colleagues, where the effect of four different perfusion flow rates on cell viability, proliferation and osteogenic differentiation of immature osteoblasts-like cells was assessed (Cartmell *et al*. 2003). The chosen flow rates, normalised per solid volume of material, were 0.33, 3.3, 6.6 and 33mL/min/cm^3. Since Cartmell and co-workers reported that 33mL/min/cm^3 resulted in substantial cell dead throughout the constructs, this perfusion flow rate was not investigated in the present study.

The autoclaved components of the perfusion bioreactor system were placed inside a laminar flow hood and soaked in 70% industrial methylated spirit (IMS, BDH laboratory supplies, UK) in distilled water prior to assemble and culture. The different parts were left to dry and then very carefully put together, always inside the hood. The remaining alcohol that may be left inside the tubing was washed out by flowing PBS using a syringe and needle. The seeded implants were taken out of the incubator and placed inside the hood. Using sterile tweezers the implants were placed inside the bioreactor chambers and all the connections tightly closed. The perfusion bioreactor system was then transferred to a 37ºC with 5%CO_2 incubator and connected to the peristaltic pump, which was placed outside, through a hole on the wall of the incubator. The flow was perfused through the samples at 0.33mL/min/cm^3

(0.07mL/min), 3.3mL/min/cm^3 (0.7mL/min) and 6.6mL/min/cm^3 (1.4mL/min) for up to 14 days.

The highest flow rate of 1.4mL/min resulted in constant cracking (appearance of thin splits) of the bioreactor chamber after only one day of culture, probably due to an increment in pressure. The lowest flow rate of 0.07mL/min had the same effect on the bioreactor chamber after 3-4 days of perfusion culture. On the other hand, the flow rate of 0.7mL/min allowed the system to run for up to 14 days. A test was carried out in order to determine the volume of medium necessary to just cover the whole scaffold. This volume was of 0.75mL (Figure 4.4) and therefore the flow rate of 0.7mL/min was adjusted to 0.75mL/min in order for the construct to renew the medium every minute. The perfusion bioreactor system was successfully run with a flow rate of 0.75mL/min for up to 14 days and therefore this flow rate was chosen to carry out this study.

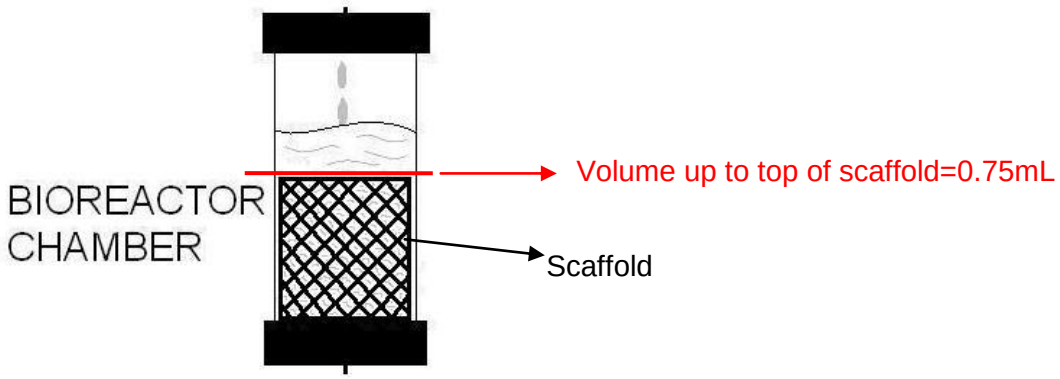

Figure 4.5 Scheme of bioreactor chamber containing the scaffold: measurement of volume up to the top of the scaffold.

4.2.6 Static Cultures (Controls)

After the 24 hours incubation to ensure cell attachment (see section 4.2.4), the seeded implants were transferred to 12 well plates (Orange Scientifique, Belgium). Approximately 5mL of medium were added to each sample and the plates placed inside a 37ºC with 5%CO_2 incubator. Medium was changed every 3 to 5 days.

4.2.7 Bioreactor Culture

The autoclaved components of the perfusion bioreactor system were placed inside a laminar flow hood, soaked in 70% industrial methylated spirit (IMS, BDH laboratory supplies, UK) in distilled water and assembled as already explained in section 4.2.5. The seeded implants (see section 4.2.4) were taken out of the incubator and inside the hood and using autoclaved tweezers placed inside the bioreactor chambers. The connections were tightly closed. The perfusion bioreactor system was then transferred to a 37ºC with 5%CO_2 incubator and connected to the peristaltic pump, which was placed outside, through a hole on the wall of the incubator. The flow was perfused through the samples at 0.75mL/min.

4.2.8 Analysis

At days 4, 7 and 14 the bioreactor was stopped and the constructs were retrieved. Along with the controls, the constructs were analysed for cell proliferation (AlamarBlue® activity and DNA assays, n=3 each), cell differentiation down the osteogenic lineage (ALP assay, n=3), cell interaction with the material (SEM, n=1) and cell distribution throughout the scaffold (Toluidine Blue staining, n=1).

4.2.8.1 AlamarBlue® Activity Assay

AlamarBlue® (AbD Serotec, UK) was diluted in phenol free Dubelcco's modified eagles medium (D5921, Sigma-Aldrich, UK) to make a 10% working solution. Samples and controls were transferred to 24 well plates. Wells were washed with PBS and 2mL of the AlamarBlue™ working solution added to them. Plates were incubated at 37ºC with 5%CO_2 for 4 hours, after which 100µL from each sample were loaded in triplicate into a FluoroNunc^{TM} white 96-well plate. Absorbance was measured at 590nm using a plate reader (Fluoroskan Ascent, Labsystems, USA). Results were compared to those of an empty well to which 2mL of 10% Alamar Blue® working solution had been added at the beginning of the assay.

4.2.8.2 DNA Assay

The constructs from the bioreactors and static controls were placed in 24 well plates and washed in PBS. Cells were lysed by adding 2mL of autoclaved distilled water at 37ºC. After frozen at -70ºC and thawed 3 times, constructs along with the distilled water were transferred to sterile tubes and sonicated for 1min. 0.5mL of each sample

and control were then transferred to Eppendorf tubes and spun at 10,000 rpm for 10 min. 100µL of the supernatant were loaded in triplicate for each sample into a FluorNunc™ white 96-well plate (Nalge Nunc International, USA). DNA standards, ranging from 20 to 0.3125µg/mL of DNA, were prepared by diluting the 1mg/mL DNA stock (Sigma-Aldrich, UK) in saline sodium citrate buffer (SSC). 100µL of the standards were also loaded in triplicate into the FluorNunc™ white 96-well plate. Finally, 100µL of 1µg/mL Hoerchst 33258 dye (Sigma-Aldrich, UK) were added to each sample. The original 1mg/mL concentration of Hoerchst 33258 dye stock was diluted in SSC. Fluorescence was read at 460nm using a plate reader (Fluoroskan Ascent, Labsystems, USA).

The amount of DNA in the samples was calculated as µg of DNA by multiplying the µg/mL value obtained for each sample by the total volume of each sample (2mL).

4.2.8.3 ALP Activity Assay

50µL of the same supernatant used for the DNA assay were loaded into Cobas Bio® blue sample cups (AS Diagnostics, UK). Pre-weighed p-nitrophenol phosphate powder was mixed with 10mL of diethanolamine buffer (both Randox, UK) and pre-heated to 37ºC to produce the working solution, which was loaded along with the samples into the Cobas Bio® analyser (Roche, UK) to run the assay. 250µL of working solution were used for each sample. The ALP activity was calculated as U/L and normalised for the number of cells in the sample using the DNA concentration calculated for each sample. ALP/DNA was expressed as U/µg.

4.2.8.4 Scanning Electron Microscopy (SEM)

The constructs from the bioreactors and static controls were placed in 12 well plates, washed with PBS and fixed in 2.5% glutaraldehyde (Agar Scientific, UK) overnight. They were then processed for SEM analysis as explained in section 3.2.2.2.4. Specimens were mounted on stubs and gold/palladium sputtered coated (EMITECH K550, Emitech, UK) before observation under SEM (JEOL JSM 5500 LV).

4.2.8.5 Histology and Toluidine Blue Staining

The constructs from the bioreactors and static controls were placed in 12 well plates, washed with PBS and fixed in formal saline overnight. They were then dehydrated

through a graded series of industrial methylated spirit (IMS, BDH laboratory supplies, UK) (50-100%) in distilled water, each for one day. 100% IMS step was repeated twice. 50%IMS-50% LR white resin (Agar Scientific Ltd, UK) was next added to the samples for one day. Finally, 100% LR white resin was added to the samples for one day. This final step was repeated twice before embedding. The samples were longitudinally sectioned using the Exakt saw and ground to a thickness of 100μm using the Exakt micro-grinding system and polished on the Motopol 2000 (Buehler, Coventry, UK).

The sections were stained with Toluidine Blue, which stains cell nuclei blue, for 20 minutes and then rinsed with running water. Sections were observed by light microscopy and photos acquired using Axiovision Release 4.5 image analysis system software.

4.2.9 Statistics

Statistical analysis was performed with SPSS 14.0 software. Non-parametric data was analysed using the Mann Whitney U test. A p-value$\leq$0.05 was considered a significant result.

4.3 RESULTS

4.3.1 CaP Coating of Porous Ti Cylinders

Both methods applied, biomimetic and electrochemical deposition at 20mA/cm^2, were able to coat the outside as well as the inside of the Ti blocks. As it can be seen from Figure 4.7C and D the biomimetic coating presented the globular morphology and the nano-sized crystals already discussed in chapter 2 (2.3.1). Similarly, the electrochemical CaP layer observed in Figure 4.7E and F was similar to that seen on the surface of the Ta and Ti discs used in chapter 2, where different morphologies were observed as well as crystal sizes ranging from the nano to the micro scale (2.3.1). When the CaP coated Ti blocks were embedded in hard grade acrylic resin, polished and analysed by SEM it was observed that the biomimetic method did not deposit a continuous CaP layer (Figure 4.7G). On the other hand, the electrochemical method was able to provide a uniform coating with a measured thickness of 3 to 15μm (Figure 4.7H). Therefore, the electrochemical coating was used with this study presented in this chapter.

Further EDAX analysis of the electrochemical coating confirmed that the main elements present were Ca and P, with a calculated Ca/P of 1.50 ± 0.04, in the range of those calculated in Chapter 2 (see Table 2.3). Other elements present in the spectra were C, O and Na (Figure 4.6).

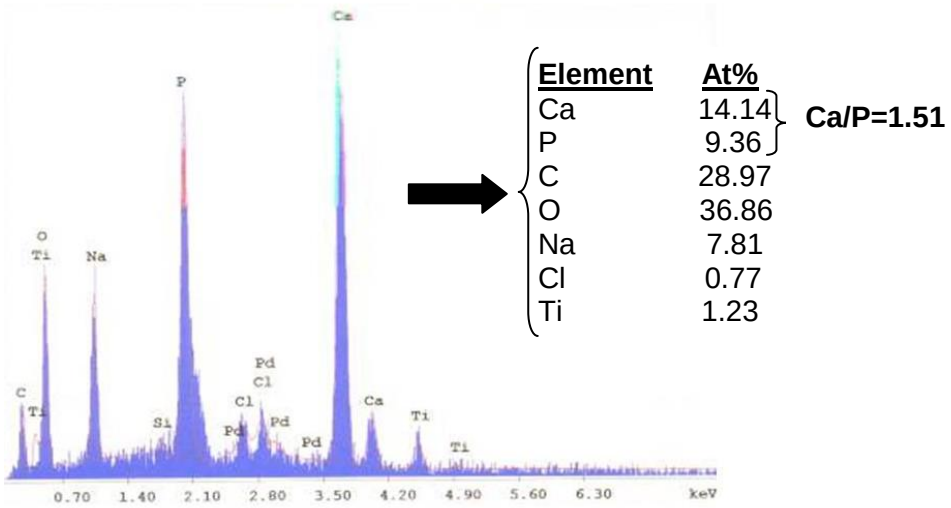

Figure 4.6 EDAX spectra and analysis of porous Ti block electrochemically coated at 20mA/cm^2.

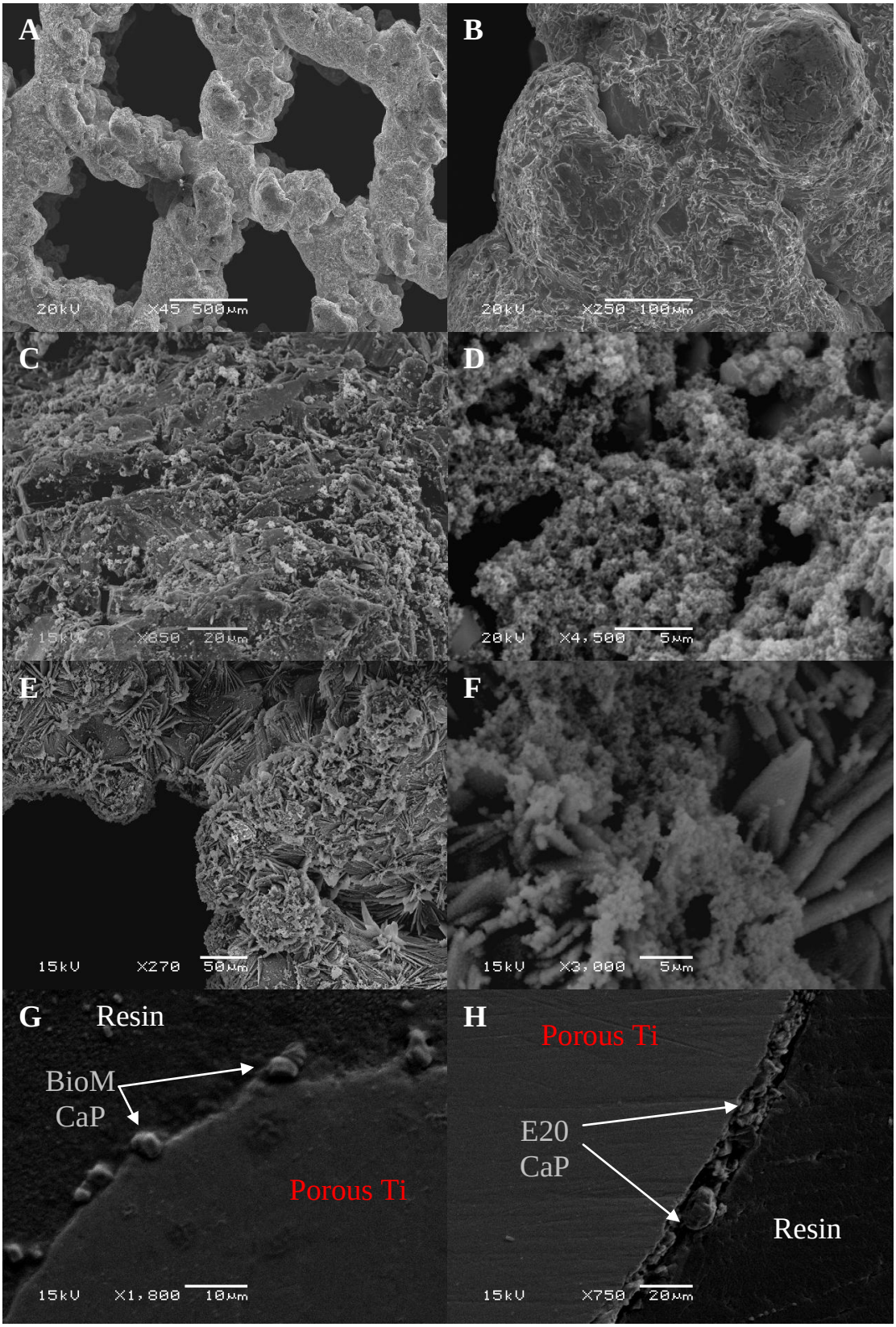

Figure 4.7 SEM analysis of **A, B)** uncoated porous Ti block; **C, D)** BioM-porous Ti block; **E, F)** E20-porous Ti block; **G)** BioM coating thickness and **H)** E20 coating thickness.

4.3.2 Cells

As it was observed in previous chapter 3 (3.3.1.1), monolayer cultures of MSCs consisted of adherent, flat cells which were long and spindle-like in shape (Figure 3.1).

4.3.3 Cell Seeding Study of MSCs on CaP Coated Porous Ti Cylinders

No cells were counted by trypan blue staining in the medium, suggesting that most of the cells adhered to the scaffold as there were too few cells left in the medium to be counted by this method.

AlamarBlue® activity assay results are displayed in Figure 4.8. These results showed that the optimum incubation time for the cells was 1 hour and 30 minutes as AlamarBlue® activity was highest at this time period. 1 hour incubation time resulted in a low AlamarBlue® activity, suggesting this time period was not long enough for the cells to attach to the scaffold. Finally, 2 hours incubation time also showed low AlamarBlue® activity, suggesting the medium evaporated and therefore the cells died.

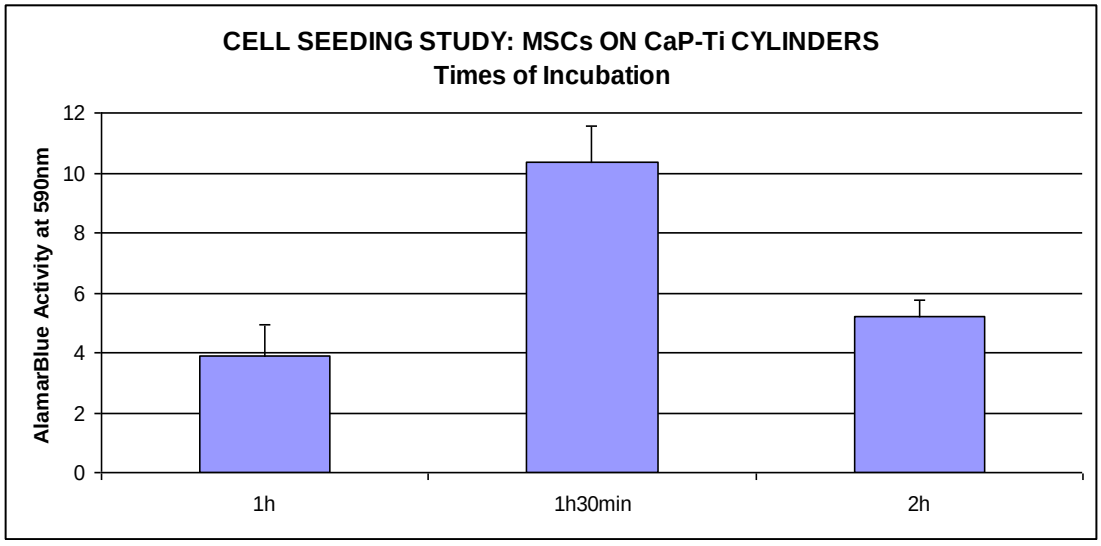

Figure 4.8 Results for the AlamarBlue® activity assay on MSCs seeded on CaP coated Ti cylinders and incubated for different time periods.

4.3.4 Cell Proliferation: AlamarBlue® Activity and DNA Assays

Increased cell proliferation for the samples cultured under flow perfusion conditions was observed by AlamarBlue® activity assay (Figure 4.9). These results were statistically significant (*p=0.05) at all time points.

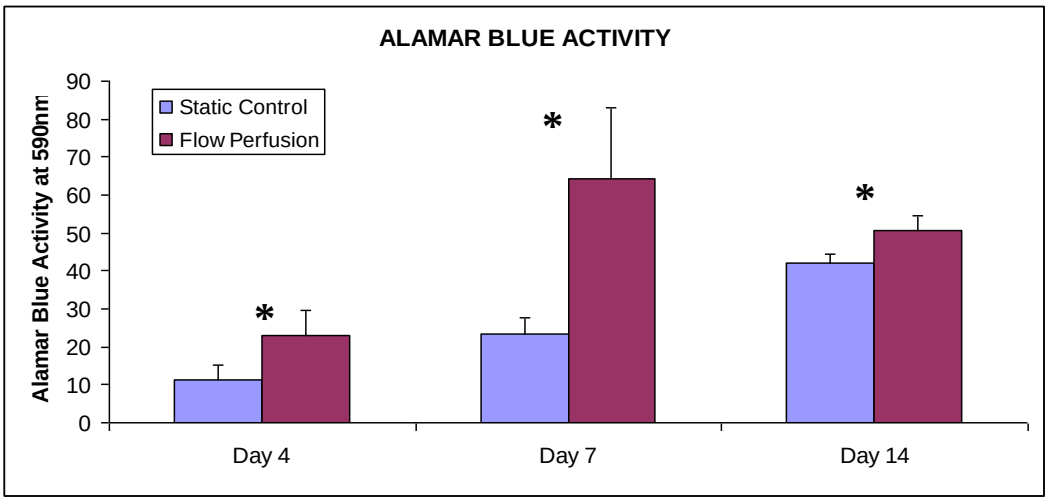

Figure 4.9 AlamarBlue® activity assay results for MSCs cultured either under static conditions or in the perfusion bioreactor system.

By plotting the same results as a scatter plot against time to analyse rate of cell growth Figure 4.10 was obtained. As it can be observed, cells in the static control grew steadily over time. However, cells under perfusion conditions grew abruptly between days 4 and 7 and then decreased growth.

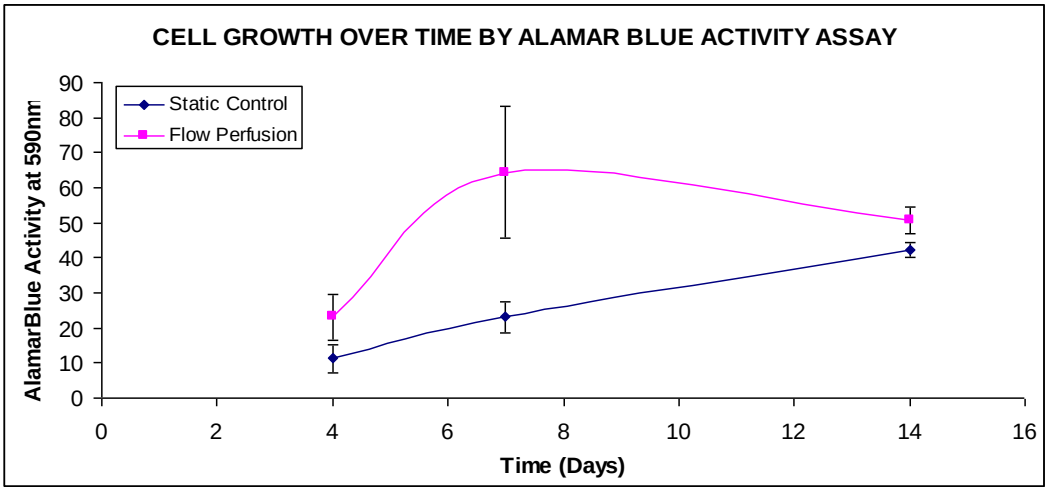

Figure 4.10 Cell growth by AlamarBlue® activity assay over the period of culture monitored in this study.

DNA assay results agreed with those from the AlamarBlue® activity assay and showed increased proliferation for the flow perfusion cultures except at day 4, where proliferation was observed to be almost equal for both types of culture (Figure 4.11). Only at day 7 there was statistical difference (*p=0.05) between static control cultures and those in the perfusion bioreactor.

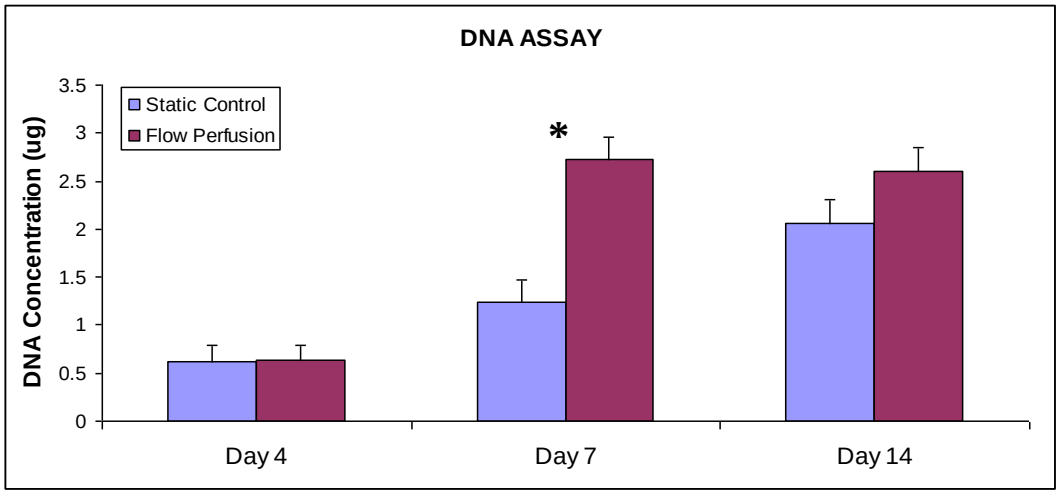

Figure 4.11 DNA assay results for MSCs cultured either under static conditions or in the perfusion bioreactor system.

Rate of cell growth over time showed a similar trend to that observed with cell proliferation as measured by the Alamar blue assay. Cells in the static control cultures grew steadily over the culture period while cells in the bioreactor grew abruptly towards the end of the first week and then decreased their proliferation (Figure 4.12).

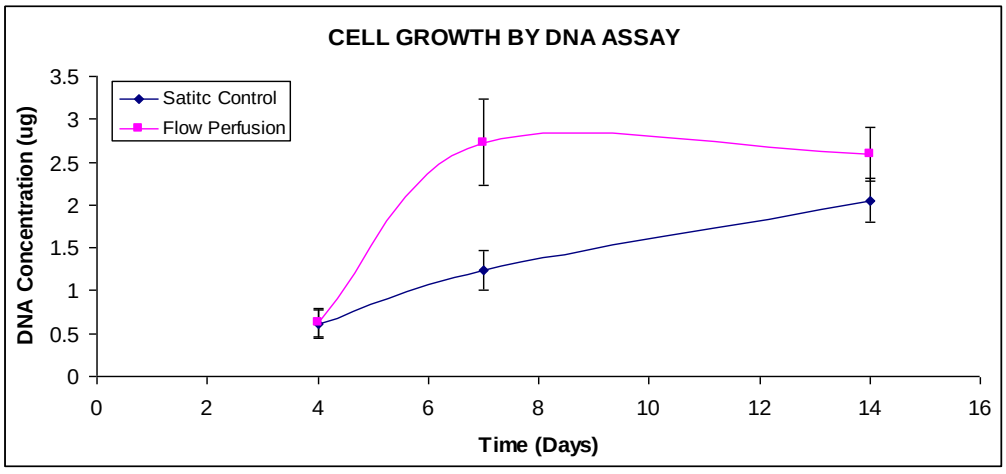

Figure 4.12 Cell growth by DNA assay over the period of culture monitored in this study.

4.3.5 Cell Differentiation down the Osteogenic Lineage: ALP Activity Assay

As it can be seen from Figure 4.13 the ALP activity measured for the flow perfusion samples was higher at all time points than those of the static controls. Differences were only statistically significant at days 4 and 7 (*p=0.05). For the flow perfusion samples ALP was observed to be highest at day 7 and slowly decreased after that. For the static controls ALP activity grows until day 7 and then remains constant.

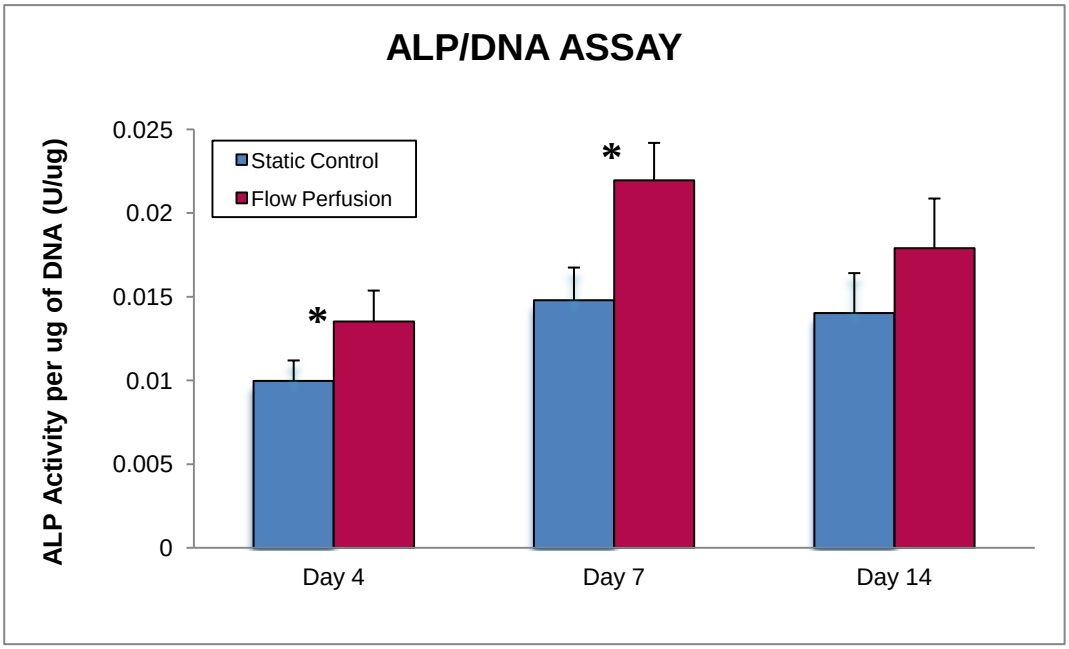

Figure 4.13 Cell differentiation down the osteogenic lineage by ALP activity assay, normalised by the amount of DNA in each sample, over the period of culture monitored in this study for MSCs cultured either under static conditions or in the perfusion bioreactor system.

4.3.6 Cell Interaction with the Material: SEM Analysis

SEM analysis of the samples showed good proliferation of MSCs on the scaffolds, where the development of a cellular layer over time was observed (Figure 4.14A-F). Long cytoplasmic processes attached cells to the scaffold surface and interaction between cells similar to that seen in Chapter 3 (see section 3.3.2.4) were evident as exemplified in Figure 4.15A to F.

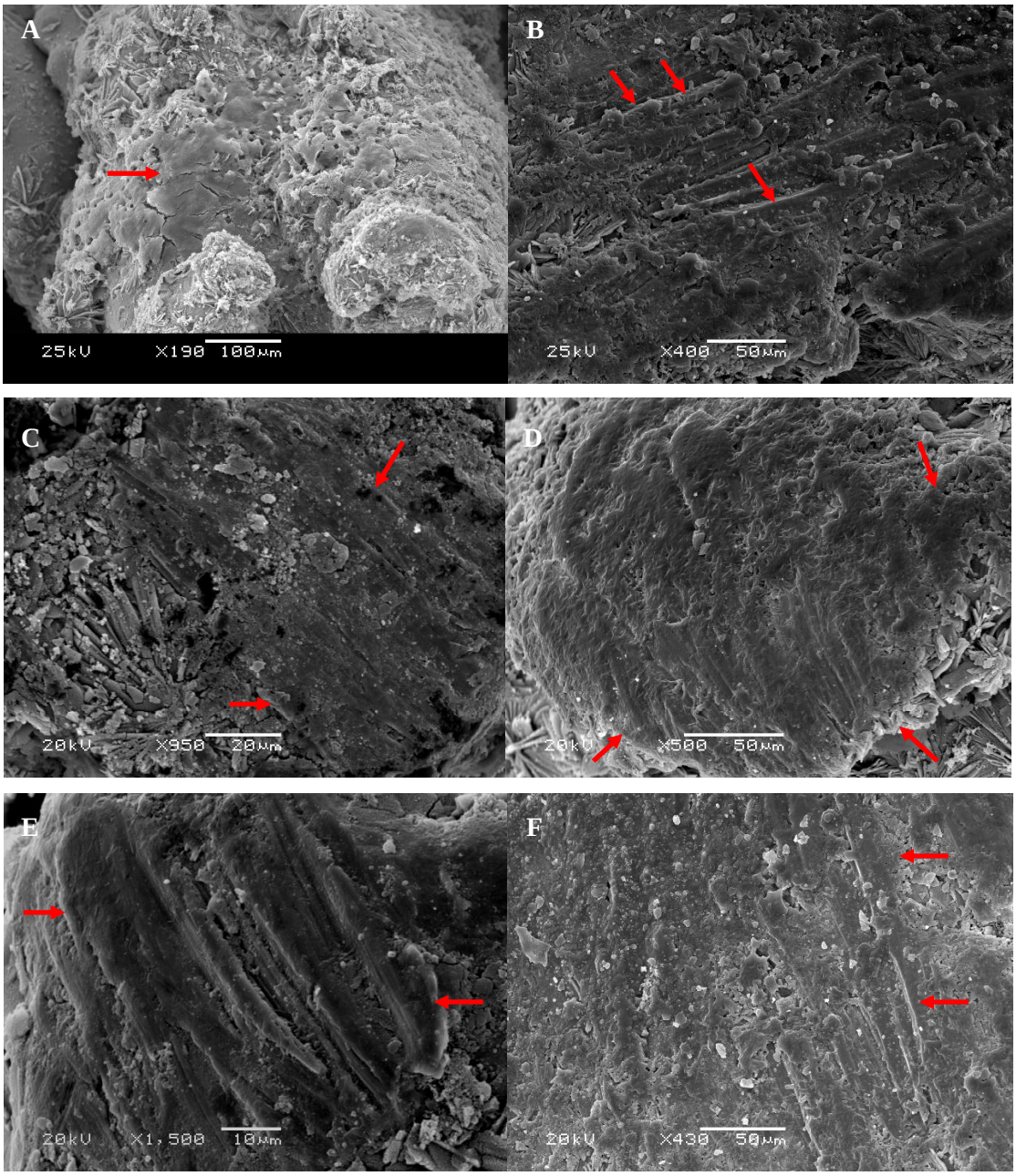

Figure 4.14 SEM analysis showing good proliferation of MSCs on the scaffolds of:

A) static control at day 4, **B)** flow perfusion sample at day 4,

C) static control at day 7, **D)** flow perfusion sample at day 7,

E) static control at day 14 and **F)** flow perfusion at day 14.

(Red arrows point to cellular sheets)

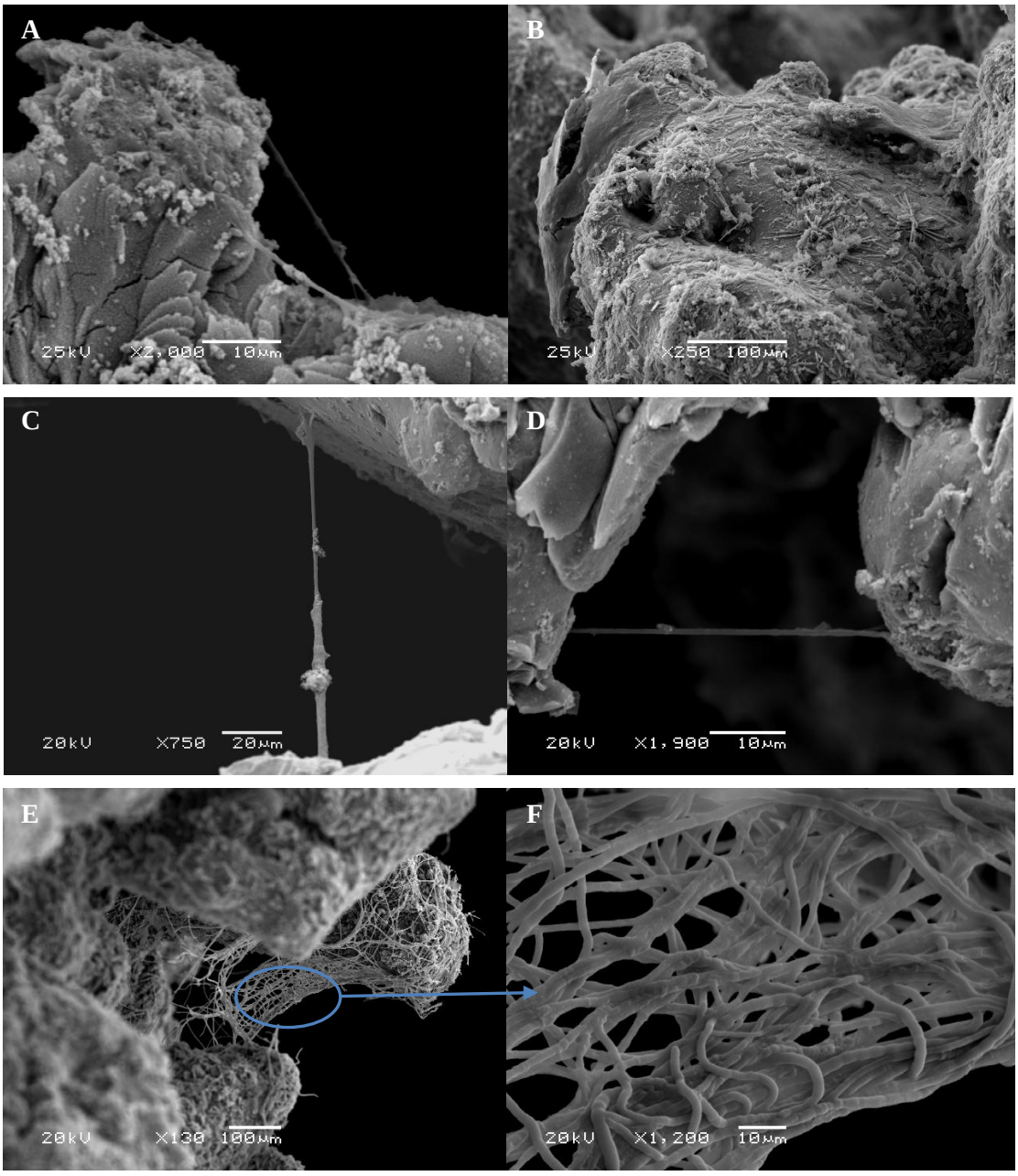

Figure 4.15 SEM analysis showing cytoplasmic processes of MSCs on the surface of the scaffolds of interaction with the material and with other cells:

A) flow perfusion sample at day 4, **B)** static control at day 4,

C) static control at day 7, **D)** flow perfusion sample at day 7,

E) flow perfusion sample at day 14 and **F)** detail of E.

4.3.7 Cell Distribution throughout the Scaffold: Histology and Toluidine Blue Staining

As it can be seen from Figures 4.16 to 4.18, samples cultured in the perfusion bioreactor system developed a uniform cellular layer over time. This cellular layer was observed to be present on the edges as well as inside of the scaffold, indicating cells grew throughout the entire scaffold. The thickness of this cellular layer was of 40-90µm at day 4, 110-200µm at day 7 and 290-400µm at day 14 of flow perfusion culture.

On the other hand, constructs developed under static conditions displayed either no cellular layer or very thin inside the scaffold. On the edges of the scaffolds, the cell layer grew thicker over the culture period with a measured thickness of 30-50µm at day 4, 40-60µm at day 7 and 50-100µm at day 14.

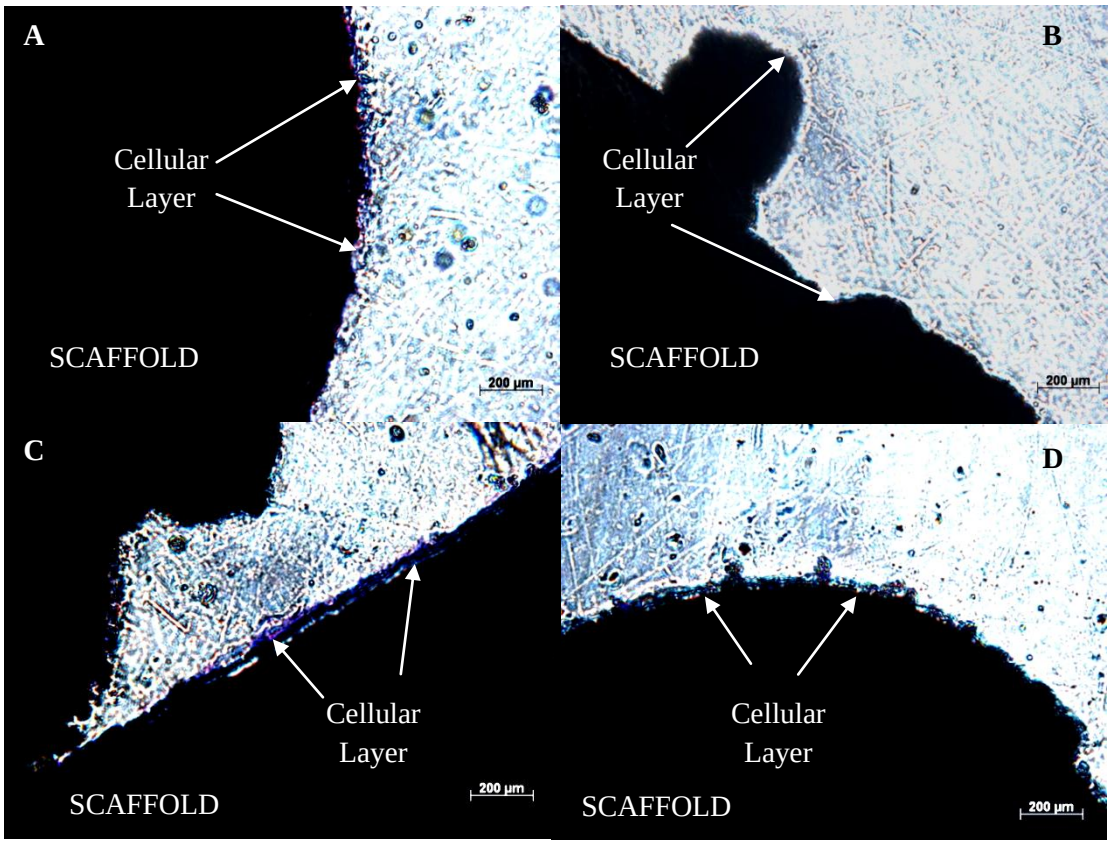

Figure 4.16 Histological analysis at day 4 of culture of:
A) static control at the edge, **B)** static control in the middle,
C) flow perfusion sample at the edge and **D)** flow perfusion sample in the middle.

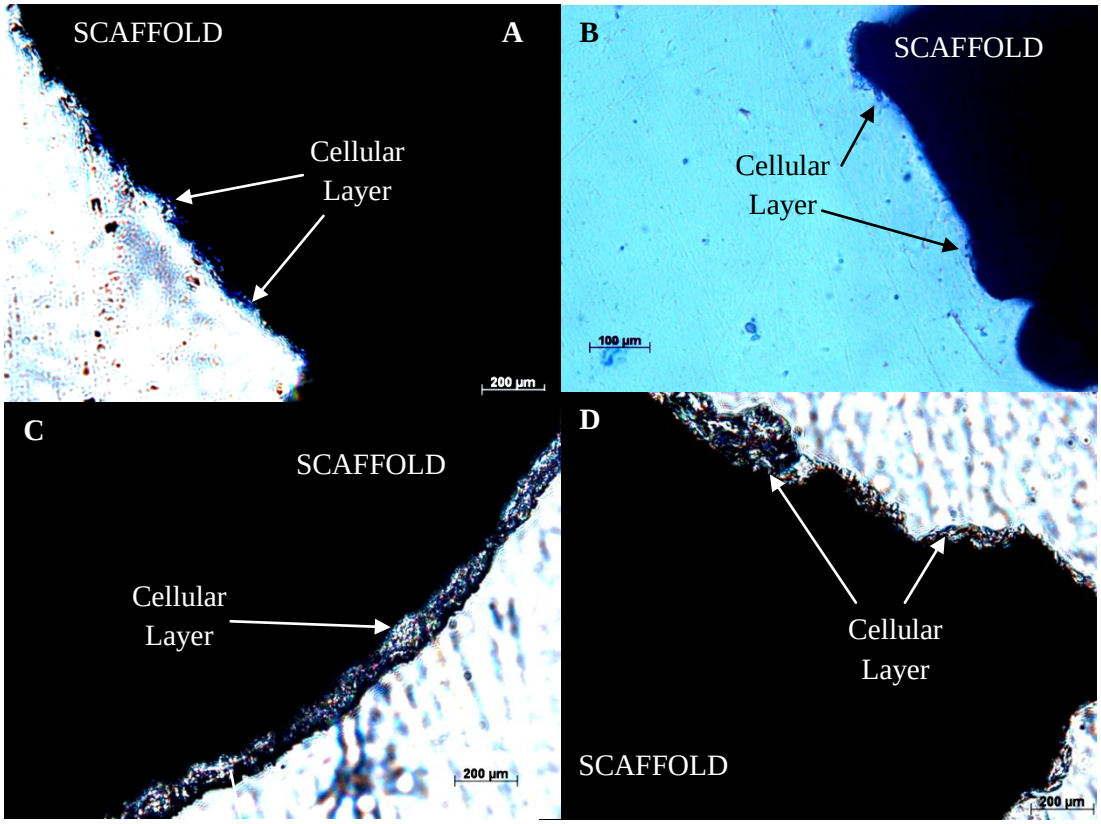

Figure 4.17 Histological analysis at day 7 of culture of:

A) static control at the edge, **B)** static control in the middle,

C) flow perfusion sample at the edge and **D)** flow perfusion sample in the middle.

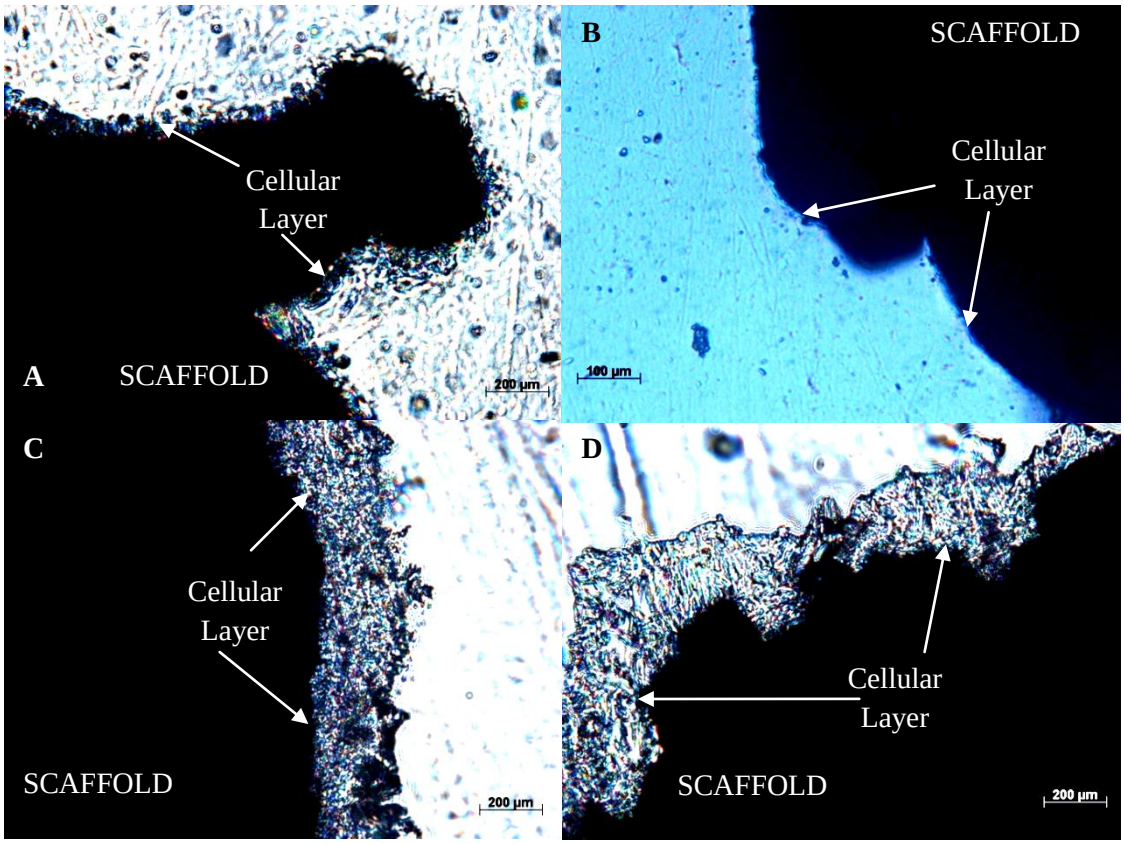

Figure 4.18 Histological analysis at day 14 of culture of:

A) static control at the edge, **B)** static control in the middle,

C) flow perfusion sample at the edge and **D)** flow perfusion sample in the middle.

4.4 DISCUSSION

4.4.1 Perfusion Flow Rates Study

In order to choose an appropriate flow rate for the perfusion bioreactor system designed in this chapter work conducted by Cartmell et al. in 2003 where the effect of flow rates was investigated in a perfusion bioreactor was used. In their work the effect of four different medium perfusion flow rates (0.33, 3.3, 6.6 and 33mL/min/cm^3) on cell proliferation, viability and osteoblastic gene expression was investigated (Cartmell *et al*. 2003). The highest flow rate of 33mL/min/cm^3 resulted in nearly complete cell death throughout the constructs after 7 days of culture. Cell viability and proliferation throughout the constructs was increased by lowering the flow rate, with 0.33mL/min/cm^3 giving a high proportion of viable cells on the surface as well as inside the constructs. No statistical differences in terms of cell proliferation were found between 0.33 and 3.3mL/min/cm^3 flow rates. However, both of these flow rates were statistically significant higher compared to 6.6mL/min/cm^3. The authors concluded that the observed trend in cell viability and proliferation was due to the increased shear stresses at the higher perfusion flow rates which may shear the cells off the constructs. In terms of osteoblastic gene expression the trend was observed to be reversed, with constructs cultured under a flow rate of 6.6mL/min/cm^3 obtaining the highest ALP, Runx2 and osteocalcin gene expression. These results are in agreement with other studies that have reported a direct effect of increased flow rates on the increment of osteogenic differentiation of marrow stromal osteoblasts (Sikavitsas *et al*. 2003; Bancroft *et al*. 2002) and human MSCs (Zhao *et al*. 2007).

In my study, the higher flow rate of 6.6mL/min/cm^3 (1.4mL/min) cracked the bioreactor chamber after just one day of perfusion culture as a result of an increased pressure inside the system. The high shear forces generated by this flow rate may have sheared the cells off the scaffold. These sheared cells blocked the outflow of the chamber resulting in an increment in pressure, which ultimately cracked the polycarbonate cylinder. The lower flow rate of 0.33mL/min/cm^3 (0.07mL/min) had the same effect on the bioreactor chamber after 3-4 days of perfusion culture. In this case the flow rate may not have been efficient enough in removing waste products and supplying fresh nutrients to the cells. Under these conditions, the cells died and blocked the outflow of the bioreactor chamber, which ultimately cracked.

The flow rate of 3.3mL/min/cm^3 allowed the system to run for up to 14 days without the complications observed with the other two flow rates tested and therefore was chosen to carry out the rest of the work presented in this chapter. Further support for this flow rate came from the studies by Zhao and colleagues. Zhao and Ma reported the highest seeding efficiencies when a flow rate of 3.77mL/min/cm^3 (0.79mL/min if used in my system) was assessed for the dynamic cell seeding of human MSCs on poly(ethylene terephthalate) (PET) fibrous matrices (Zhao and Ma 2005). This flow rate was used in their next study to dynamically seed human MSCs on PET matrices, maintained for 20 days and compared to a perfusion flow rate of 56.6mL/min/cm^3. As in the described study by Cartmell et al., Zhao and colleagues observed increased cell numbers at the lower flow rate and increased ALP activity and calcium deposition (markers for osteogenic differentiation) at the higher flow rate (Zhao *et al*. 2007). Further adjustment of the flow rate to 0.75mL/min allows the construct to ideally renew the culture medium every minute and is in between 0.7mL/min (3.3mL/min/cm^3, Cartmell *et al*. 2003) and 0.79mL/min (3.77mL/min/cm^3, Zhao and Ma 2005; Zhao *et al*. 2007).

4.4.2 Cell Proliferation, Differentiation down the Osteogenic Lineage and Distribution throughout the Scaffold

In perfusion bioreactors, as the one used in this chapter, the culture medium flows through the pores of the scaffold enabling local supply of nutrients and removal of waste products (Bancroft *et al*. 2003). Results from the AlamarBlue® and DNA assays show that the constant supply of medium to and through the porous constructs has a beneficial effect on cell proliferation as constructs cultured under flow perfusion had an increased proliferation compared to constructs cultured under static conditions. Several studies have reported the beneficial effects of flow perfusion culture on proliferation, as observed in this study (Sikavitsas *et al*. 2005; Bjerre *et al*. 2008; Bancroft *et al*. 2002).

Similarly, the ALP activity assay results showed an increased activity for the flow perfused constructs with a peak in activity at day 7, while no peak was observed for the static controls. The results suggest that the fluid shear forces experimented by the cells cultured in the bioreactor system had a mechanostimulatory effect on them that

enhanced the osteogenic differentiation potential of MSCs, as already described by other authors (Sikavitsas *et al*. 2003; Sikavitsas *et al*. 2005; Zhao *et al*. 2007; Bancroft *et al*. 2002).

Lian and Stein described that the temporal expression of cell growth and osteogenic phenotype has three distinct periods. First, a period of strong proliferation and formation of collagenous extracellular matrix up to day 13 of culture. Second, a period of extracellular matrix maturation with decreased proliferation and increased ALP expression was observed between days 13 and 21 of culture. Finally, mineralisation with decreased proliferation and ALP expression and increased osteoblastic proteins expression was observed from day 21 until day 35 of culture (Lian and Stein 1992). In my study, during the first week of perfusion culture the cell number increased and then stayed almost constant until the end of the experiment. These results suggest that the cells had an early stage of increased proliferation during the first week of the experiment followed by a period of decreased proliferation and increased ALP expression, with a final stage of decreased proliferation and ALP expression. The peak in ALP activity was observed at day 7, however it could have happened between days 7 and 14. In this study, no analysis of extracellular matrix was conducted, which could have helped to further characterise these periods in the constructs.

On the other hand, the histology results suggest that MSCs were able to proliferate over the perfusion culture period, as a uniform cellular layer developed over time with a final thickness of approximately 290-400μm on the surface and inside the constructs. As toluidine blue stains dead cells as well, the thicker cellular layer observed at day 14 may be composed of viable and non-viable cells. This would explain the lower AlamarBlue® reading at day 14 indicating a decrease in cell viability. However, the fact that DNA concentration stayed constant between days 7 and 14 would not be explained as the DNA assay would also quantify the DNA of the dead cells. As the cellular layer at day 14 was too thick the process of DNA extraction may have not been successful and therefore a lower amount of DNA was measured. For the static controls the proliferation assays and the histology results agree: the cell layer for the static controls at day 14 is thinner and therefore the DNA was correctly extracted from the constructs. Other authors have encountered similar problems when

performing quantitative DNA assays, which were attributed to the large amounts of extracellular matrix deposited by the cells, that may interfere with the recovery of DNA (Holtorf *et al*. 2005; Mygind *et al*. 2007).

Some studies have reported a clear influence of perfusion rate on cell viability. As already discussed in section 4.4.1, Cartmell and co-workers found that constructs under higher flow rates resulted in a mixture of viable and dead cells on the constructs surface with a limited cell viability observed in the centre of the constructs. However, lower flow rates provided a high proportion of viable cells on the surface as well as at the centre of the constructs (Cartmell *et al*. 2003). Similarly, although in a different kind of tissue application, Kalyanaraman and colleagues concluded that perfusion culture of engineered skin substitutes at lower flow rates increased cell viability (Kalyanaraman *et al*. 2008). In my study, the chosen flow rate had a beneficial effect on cell proliferation and viability until day 7, as evidenced by the AlamarBlue® and DNA assays, but resulted in a decrease of cell viability between days 7 and 14 as shown by the AlamarBlue® assay.

4.4.3 Cell Interaction with the Material

To assess cell morphology and interaction with the material SEM was performed on the surfaces of scaffolds. The SEM analysis support the AlamarBlue® assay results as cells proliferated well on the scaffolds. MSCs arranged in cellular sheets, already observed by other authors (Mygind *et al*. 2007; Gomes *et al*. 2006). The long cytoplasmic processes, or filopodia, attached to the scaffold have also been observed in other studies (Mygind *et al*. 2007). Dalby and colleagues reported that human bone marrow cells responded to nanotopography by filopodial interactions which stimulated osteoblastic differentiation, while cells on the flat controls were observed to be well spread with fewer and shorter filopodia (Dalby *et al*. 2006). In my study, the topography of the scaffolds was not flat and the CaP coating deposited on the surface of the porous Ti cylinders contained nanosized crystals.

4.4.4 Choice of Time Point for *in vivo* Study

For the next *in vivo* chapter of this thesis, day 7 will be chosen as the culture time inside the perfusion bioreactor system for the tissue-engineered constructs before implantation. Under the conditions tested in this study, day 7 provides the best results

for MSCs proliferation and differentiation as well as a uniform cellular distribution throughout the scaffold compared to static controls and the other time points. Day 4 resulted in an early time point for cell proliferation, with a thin cellular layer observed. At day 14 the cellular layer was composed of a mixture of viable and dead cells with a mean value thickness of 345µm, which would greatly narrow the pore size of the construct (mean value of 765µm after the CaP coating) and therefore compromise *in vivo* ingrowth.

4.5 CONCLUSION

A perfusion bioreactor system was designed in order to culture MSCs in CaP coated porous TiAl6V4 cylinders. When compared to constructs cultured under static conditions, constructs cultured in the flow perfusion bioreactor had increased proliferation and osteogenic differentiation. An even distribution of cells throughout the scaffolds was observed for the samples cultured under flow perfusion. Under the conditions tested in this study, day 7 provides the best results for MSCs proliferation and differentiation as well as a uniform cellular distribution throughout the scaffold compared to static controls and the other time points. This time point is therefore chosen to carry out the next *in vivo* chapter of this thesis.

CHAPTER 5:

Comparison of Osseointegration and Implant-Bone Interface Fixation *in vivo* Between Tissue-Engineered and Non Tissue-Engineered Constructs

5.1 INTRODUCTION

The clinical problem addressed in this thesis is the reduction of the bone stock necessary for implant fixation in revision THRs (Cooper *et al*. 1992; Harris 1995; Harris 2001; Amstutz *et al*. 1992; Heisel *et al*. 2003), where the main issue is how to generate new bone and restore bone stock for fixation of the revision implant. A novel tissue engineering approach was proposed in this thesis to address this clinical problem: the incorporation of MSCs into a porous implant thus enabling the reconstitution of bone.

The development of bone tissue-engineered constructs requires the evaluation of their performance *in vivo* (Goldstein 2002). In the previous chapter of this thesis a tissue-engineered construct using a perfusion bioreactor system was developed. This tissue-engineered construct consists of a CaP coated porous Ti scaffold seeded throughout with ovine MSCs. In the present chapter this tissue-engineered construct will be evaluated *in vivo* by implantation in the medial femoral condyle of sheep and their performance will be compared to non tissue-engineered constructs, which consist of a CaP coated porous Ti scaffold not seeded with cells.

Sheep was chosen as the animal model to carry out this project because a large animal model is more relevant than a small one in order to represent the human clinical situation. Moreover, Pastoureau and colleagues reported in 1989 a resemblance between the iliac crest of sheep and the human one in terms of access for biopsies (Pastoureau *et al*. 1989). Aerssens and co-workers studied the ash, hydroxyproline, extractable protein and IGF-1 content of trabecular and cortical bone in sheep and humans. It was shown that trabecular bone from sheep was very similar to humans while main differences in the contents of the above parameters were found in cortical bone between both species (Aerssens *et al*. 1998). The femoral condyle was chosen as the site of implantation for this study because it contains the mostly trabecular bone.

When using a defect to evaluate a tissue-engineered construct, as the one used in this study, the bone defect must fail to heal unless it is treated with the tissue engineering strategy under study (Salgado *et al*. 2004). The trabecular bone defect is made by drilling a hole, for example, in the femoral condyle of the sheep. Thus, the tissue-

engineered construct behaviour is evaluated within a bony environment namely the osteoconduction level and the new bone ingrowth and formation.

In order to analyse the outcomes of the *in vivo* tests histological staining followed by histomorphometric analysis is the common methodology used to asses new bone formation (Salgado *et al*. 2004). Mechanical tests are also commonly used to assess implant-bone interface shear stress by pushing out the section of the implant (Svehla *et al*. 2000). In this chapter new bone formation will be analysed by histomorphometric analysis and implant-bone interface fixation by mechanical push out tests.

The aim of this study was to compare osseointegration and implant-bone interface fixation *in vivo* between tissue-engineered and non tissue-engineered implants.

The hypotheses were:

1. **Tissue-engineered implants using a perfusion bioreactor system will achieve greater osseointegration when implanted *in vivo* than non tissue-engineered implants.**
2. **Tissue-engineered implants using a perfusion bioreactor system will achieve greater implant-bone interface fixation when implanted *in vivo* than non tissue-engineered implants.**

5.2 MATERIALS AND METHODS

5.2.1 Study Design

Twenty skeletally mature mule sheep were used in order to compare osseointegration and implant-bone interface fixation between tissue-engineered and non tissue-engineered constructs. As in revision THRs the implant will be either in contact with the host bone or at a gap distance from the host bone, two models were studied: a direct contact model in which the constructs were in direct contact with the host bone and a gap model in which a 2.5mm gap was created between the constructs and the host bone.

For the direct contact model, ten female sheep were implanted with CaP coated porous Ti cylinders either with no cells or cultured with MSCs in a perfusion bioreactor. On both right and left sides of the sheep, defects of 10mm diameter were created in the medial femoral condyle and the constructs inserted. In each sheep one condyle served as a control, with no cells, and the other condyle contained the construct cultured with cells in a perfusion bioreactor (Figure 5.1A).

For the gap model, ten female sheep were implanted with CaP coated porous Ti cylinders with either no cells or cultured with MSCs in a perfusion bioreactor and mounted onto 14.0mm rings at both ends to create a 2.5mm gap (Figure 5.1B). For this model, defects of 14mm were created. As before, in each sheep one condyle served as a control, with no cells, and the other condyle contained the construct cultured with cells in a perfusion bioreactor.

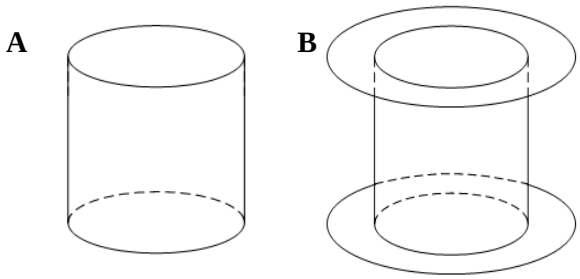

Figure 5.1 Scheme of the implants used in this study:
A) 9mm diameter and 11mm length CaP coated TiAl6V4 cylinders used in the direct contact model, **B)** 9mm diameter and 11mm length CaP coated TiAl6V4 cylinders with 14mm diameter and 2mm length rings used in the gap model.

The animals were euthanized at six weeks. The femoral condyles were removed and processed for either hard grade histology and histomorphometric analysis or mechanical push-out tests.

Table 5.1 summarises the study design and specifies groups and n numbers:

Number of Sheep	Construct Type	Femoral Condyle: Right or Left	Femoral Condyle: Right or Left	Histology and Histomorphometric Analysis	Mechanical Push-out Tests
n=5	CaP-Ti cylinders	Control	MSCs	YES	NO
n=5	CaP-Ti cylinders	Control	MSCs	NO	YES
n=5	CaP-Ti cylinders with rings	Control	MSCs	YES	NO
n=5	CaP-Ti cylinders with rings	Control	MSCs	NO	YES

Table 5.1: Study Design

5.2.2 Harvesting Autologous MSCs

5.2.2.1 Obtaining Bone Marrow

Bone marrow was aspirated from the iliac crest of twenty skeletally mature Mule sheep. All procedures took place at the Royal Veterinary College, North Mymms, in accordance with the Animals (Scientific Procedures) Act 1986. Home Office Licences were held by all those taking part in any surgical procedure. The procedures were carried out 2 months before implantation in the femoral condyles.

Intramuscular Xylazine at 0.1 mg/kg 10 minutes before induction of anaesthesia was used to premedicate the sheep. The animal was then intravenously administered Ketamine (2mg/kg) and Midazolam (2.5mg) to induce anaesthesia. The animal was intubated and maintained on 2% Halothane and oxygen for the duration of the procedure, which was monitored by pulse oximetry, ECG and end tidal carbon dioxide.

The sheep were placed in the lateral position. The fleece above either the right or the left iliac crest was shaved to the skin. Approximately, 10cm^2 area of skin were prepared by treatment with Pevidine scrub and antiseptic solution. The entire area was further sterilised with Hydrex solution-chlorohexidine and covered with a drape.

A small incision was made on top of the iliac crest and a bone marrow gauge needle was used to reach the intramedullary cavity of the iliac crest. A 10mL syringe that had been loaded with 1mL of heparin at 1000 iu/mL was attached to the bone marrow gauge needle. A minimum of 2mL but no more than 6mL of bone marrow were aspirated, gently mixed with the heparin to prevent clotting and transferred into a sterile universal tube. The aspirates were kept at 4ºC until taken to tissue culture facilities. The incisions were sutured using a resorbable zero cirylTM suture. Finally, animals were given 0.6mg Buprenorphine as an analgesic and 15 mg/kg Amoxicillin as a long-acting antibiotic.

5.2.2.2 MSCs Isolation, Culture and Cryopreservation

The bone marrow aspirates were transferred to tissue culture facilities and were always manipulated inside a laminar flow hood. The growth medium for MSCs was Dubelcco's modified eagles medium (DMEM, D6429, Sigma-Aldrich, UK) supplemented with 10% fetal calf serum (FCS, First Link, UK) and 100 Units/mL of the antibiotics penicillin and streptomycin (P/S, Gibco, UK) (DMEM+).

2mL of each aspirate were plated in T225 (225cm^2 of growth area) polystyrene cell culture flasks (Corning, USA) with 30mL of the above medium. Cultures were designated P0. Flasks were kept in incubators at 37ºC with 5% CO_2 and regularly observed under a phase-contrast light microscope. Medium was changed every 3 to 5 days until the cultures were 80 to 90% confluent.

In order to ensure the autologous MSCs were all used at the same passage number, cells were cryopreserved in liquid Nitrogen. When cultures reached 80 to 90% confluency medium was removed from the flasks and the cells were washed with cold PBS. The cells were then trypsinised and incubated at 37ºC with 5% CO_2 for 5 minutes. Once the cells have lifted off the surface the trypsin was neutralised by adding a 1:1 volume of DMEM+. All cells were transferred to a universal tube except

a small amount that was removed to perform a cell count in order to calculate cell density to be stored in each cryovial. A 1/10 dilution of the cells in trypan blue (T8154, Sigma-Aldrich, UK) was done and pipetted into a cover-slipped haemocytometer which was then placed under a phase-contrast light microscope. Viable cells were rounded and bright while blue cells were considered as non-viable. Cells in the universal tube were centrifuged at 2,000rpm for 5minutes, after which the supernatant was discarded. The pellet of cells was resuspended in a 10% dimethyl sulfoxide (DMSO, D5879, Sigma-Aldrich, UK) solution in FCS. 2×10^6 cells in 1mL of 10% DMSO in FCS were added per cryovial and stored overnight at -70ºC in a "Mr Frosty" 5100 Cryo 1ºC freezing container (Fisher Scientific, UK) containing isopropan-2-ol. The vials, containing cells at P1, were then transferred to liquid nitrogen.

5.2.3 Preparation of Constructs

5.2.3.1 Calcium Phosphate Coating of Porous Ti Cylinders

TiAl6V4 porous cylinders (Figure 4.2), 9mm diameter and 11mm length, were coated with a calcium phosphate layer as already explained in sections 2.2.3 and 4.2.2.1.

The scaffolds were sterilised in an oven at 160ºC for 1 hour prior to cell seeding, which was carried out inside a laminar flow hood to ensure sterile conditions.

5.2.3.2 MSCs Resuscitation and Seeding on the Scaffolds

MSCs were resuscitated from liquid Nitrogen as detailed in section 3.2.1.1. Cells were kept in T225 culture flasks at 37ºC with 5% CO_2 until they were about 80% confluent.

The MSCs were then trypsinised and a viable cell count was performed using a haemocytometer as described in Chapter 3. 1×10^6 cells in a total volume of 0.2mL of medium were seeded onto each scaffold, which had been placed in 24 well plates. Therefore, all the cells were seeded at passage number 2. The plates were incubated for 90 minutes at 37ºC with 5% CO_2, after which 2mL of DMEM+ were added per well. After further incubation of the cells for 24 hours at 37ºC with 5% CO_2, the seeded scaffolds were transferred to bioreactor chambers.

5.2.3.3 Dynamic Cell Culture in a Perfusion Bioreactor System

After the seeded scaffold was placed inside the bioreactor chamber, the whole system was assembled as described in section 4.2.5. Flow was perfused through the seeded scaffolds at 0.75mL/min.

After 7 days of dynamic perfusion cell culture, the flow was stopped and the system dismantled inside a laminar flow hood. The construct was transferred to a sealed 12 well plate with approximately 5mL of DMEM+, ready for the surgical procedure.

5.2.3.4 Controls: Unseeded Scaffolds

As mentioned in section 5.2.1, the controls for this study were CaP coated porous Ti cylinders with no cells. Section 4.2.2 of this thesis details the properties and CaP coating of the scaffolds. Control scaffolds were sterilised at 160ºC for 1 hour and transferred to sealed 12 well plates with approximately 5mL of DMEM+ per scaffold, ready for the surgical procedure.

5.2.3.5 Rings

TiAl6V4 rings used in the gap model were 14mm diameter and 2mm length (Figure 5.2). The same steps previously described in section 5.2.3.4 were followed to sterilise the rings and get them ready for the surgical procedure.

Figure 5.2 14mm diameter and 2mm length TiAl6V4 ring used in the gap model

5.2.4 Surgery

All procedures took place at the Royal Veterinary College, North Mymms, in accordance with the Animals (Scientific Procedures) Act 1986. Home Office Licences were held by all those taking part in any surgical procedure.

5.2.4.1. Analgesia

Intramuscular Xylazine at 0.1 mg/kg 10 minutes before induction of anaesthesia was used to premedicate the sheep. The animal was then intravenously administered Ketamine (2mg/kg) and Midazolam (2.5mg) to induce anaesthesia. The animal was intubated and maintained on 2% Halothane and oxygen for the duration of the procedure, which was monitored by pulse oximetry, ECG and entidal carbon dioxide.

5.2.4.2 Insertion of Constructs

Animals were placed in supine position and an area over the medial aspect of both knee joints and an area extending proximally over the medial aspect of the stifle joint and lower abdomen was shaved. Betadine surgical scrub, which is a broad spectrum topical iodophor microbicide, was applied followed by Betadine antiseptic solution. The animal was moved in to the operating theatre. Prior to draping the site was further cleaned with Hydrex Surgical Scrub (MidMeds Ltd, Loughton, UK) which contains chlorohexidine, an alkaline aqueous antimicrobial.

Sterile drapes were used to cover the area around the wound site. 4cm longitudinal incisions were placed over the medial aspect of the distal femoral condyles. The femoral condyles were exposed and the periosteum was then scraped from the surface exposing the underlying bone. The bone was drilled (Figure 5.3A) to create a cylindrical defect of 10mm diameter and 11mm depth (Figure 5.3B and C). In the gap model cylindrical defects of 14mm diameter and 15mm depth were created (Figure 5.4A). The defects were flushed with sterile saline to remove debris. The implants with or without cells were inserted into the created defects in either the right or the left femoral condyle (Figures 5.3B-D and 5.4B-D). The wound was closed in layers with resorbable Vicryl™ sutures. Post-operatively the animals were allowed full mobilisation as tolerated.

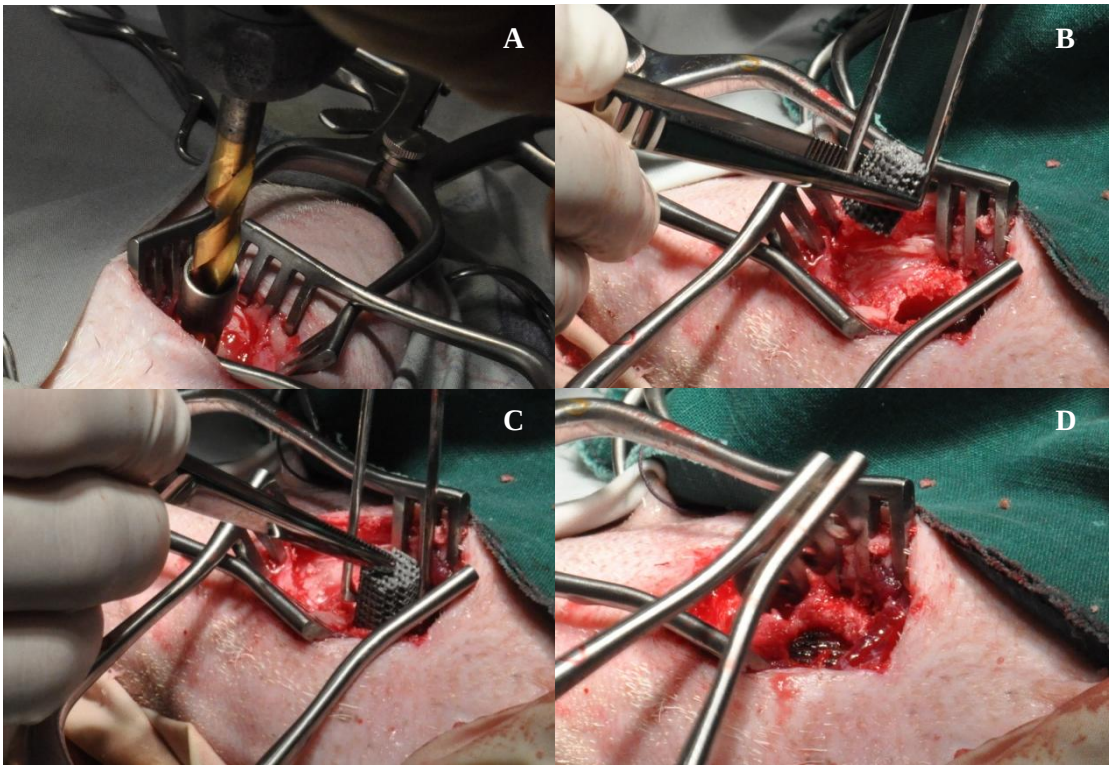

Figure 5.3 illustrates **A)** bone being drilled, **B)** defect created within the femoral condyle, **C)** insertion of construct and **D)** construct fully inserted.

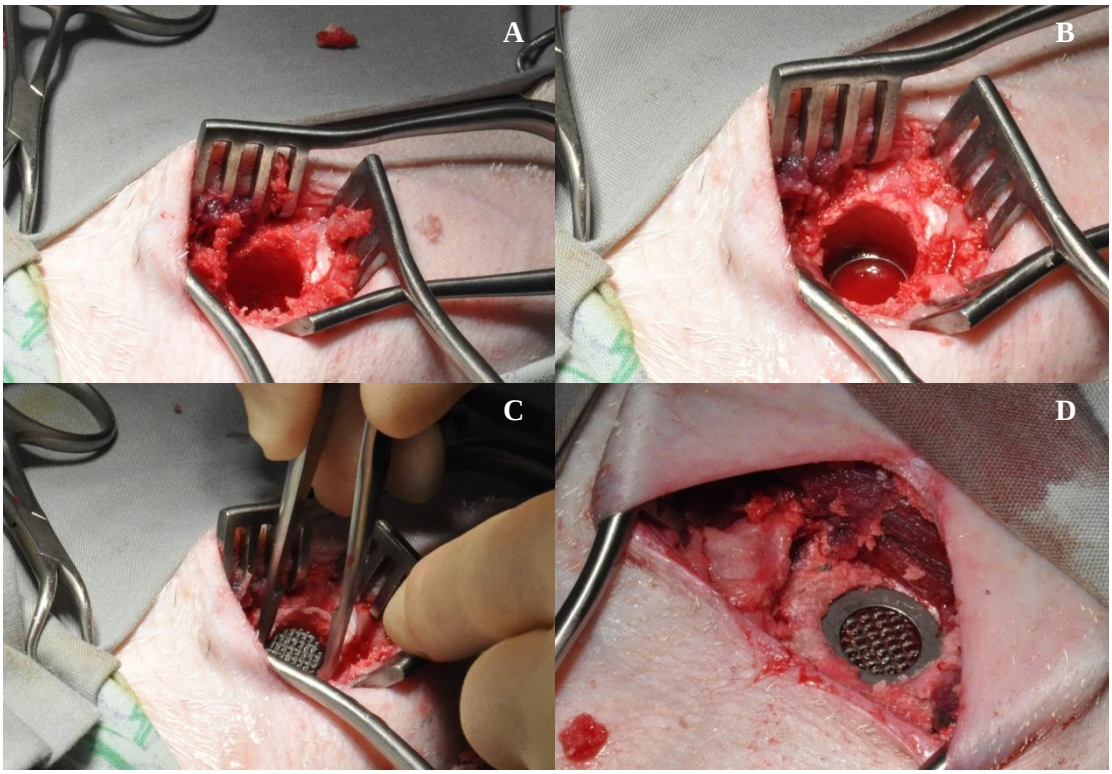

Figure 5.4 illustrates **A)** defect created within the femoral condyle, **B)** first ring inside the defect, **C)** insertion of construct and **D)** construct fully inserted with second ring.

5.2.5. Histology

Six weeks after the surgical procedures the sheep were euthanized with Phenobarbitone (50mL of 20% solution) intravenously. Femurs were removed, debrided of soft tissue and cut down on the bandsaw until the femoral condyles containing the implants remained, which were fixed in 10% buffered formal saline. They were then dehydrated with solutions of ascending concentrations of industrial methylated spirit (IMS, BDH laboratory supplies, UK) in distilled water. After dehydration, the samples were defatted with chloroform to allow adequate penetration of the solutions prior to embedding in LR white resin (Agar Scientific Ltd, UK). Infiltration of the resin into the samples was aided by application of a vacuum. One drop of catalyst (LR White Accelerator, Agar Scientific Ltd, UK) per 10mL of resin was added to initiate polymerisation. The samples were placed in a 4ºC refrigerator to allow slow setting and dissipation of heat produced by the exothermic reaction. Table 5.2 details the histology processing protocol:

Steps	Number of Days
10% buffered formal saline	3
50% IMS 50% distilled water	3
75% IMS 25% distilled water	3
85% IMS 15% distilled water	3
95% IMS 5% distilled water	3
100% IMS (repeat step twice)	3
Chloroform (repeat step twice)	3
100% IMS (repeat step twice)	3
50% IMS 50% LR White resin	3
LR White resin, with one change of resin at day 3 and under vacuum every day (repeat step twice)	7
Cast in LR White resin, using 1 drop of accelerator per 10mL of resin. Leave in fridge	24 hours

Table 5.2: Histology Processing Protocol

The samples were longitudinally sectioned using the Exakt saw (EXACT, Germany) and ground to a thickness of 100μm using the Exakt micro-grinding system (EXACT, Germany) and polished on the Motopol 2000 (Buehler, Coventry, UK). The sections were stained with Toluidine Blue for 20 minutes, which stains cell nuclei blue, and a Paragon stain for 15 minutes, which stains new bone bright pink. The stained sections were analysed by histomorphometry.

5.2.5.1 Histomorphometry

Comparison of the amount of new bone formation within the tissue-engineered and non-tissue engineered constructs was made using histomorphometry techniques. The percentage area occupied with new bone over total available area and the percentage of new bone in contact with the material surface were quantified with the Axiovision Release 4.5 image analysis system (Zeiss, Germany). Three images were taken at 5× magnification, two from the edges and one from the centre, of each stained thin section. Figure 5.5 details the areas where the photos were taken. The images were then overlaid with a grid (14×14units). The line-intercept method was used for quantification of the percentage of new bone area and bone-material contact where each line crossed the type of feature being measured.

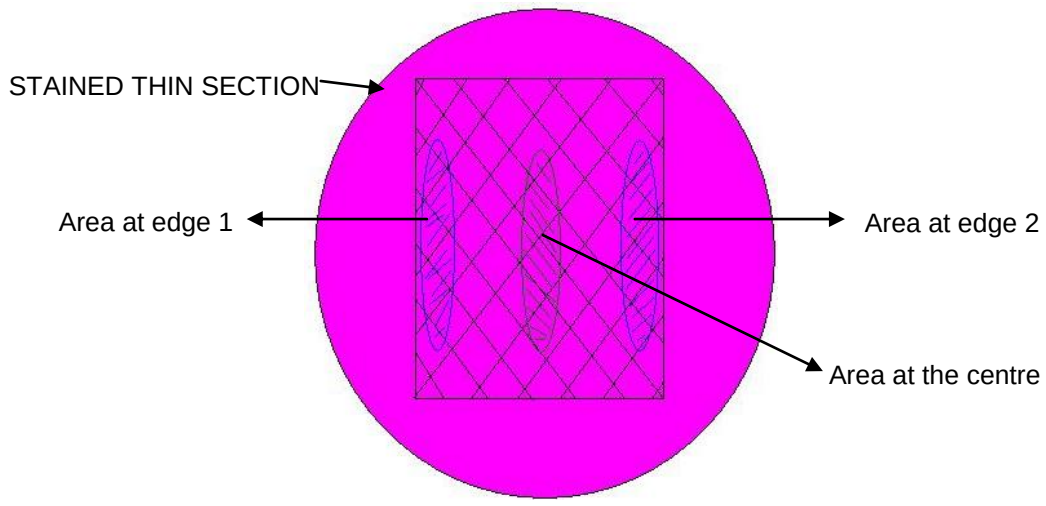

Figure 5.5 Scheme showing the areas of stained thin sections at which photos were taken for histomorphometric analysis.

5.2.6 Mechanical Push-Out Tests

Implants were tested for implant-bone interface shear strength by mechanical push-out test. The experiments were performed on a Zwick-Roell Z005 mechanical test instrument. Specimens were tested at a rate of 10mm/min (Nordström *et al*. 2002; Santoni *et al*. 2009; Fakhouri *et al*. 2011), with a pre-load of 15N at 5mm/min. The maximum load at which the implant was pushed out of the specimen was recorded. Figure 5.6 shows the setting for the mechanical push out tests with a specimen at the end of the test.

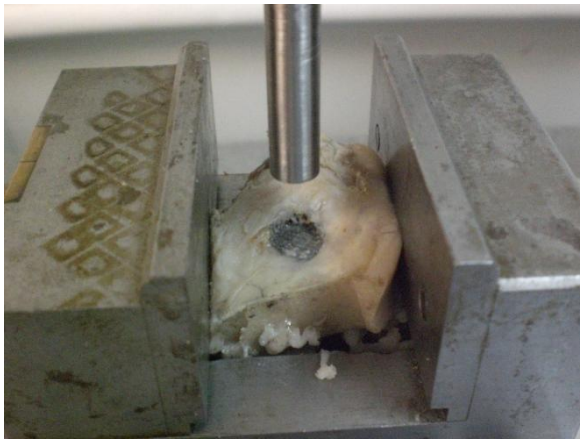

Figure 5.6 Setting for the mechanical push out tests with a specimen from which the implant has been pushed out.

5.2.7 Statistics

Statistical analysis was performed with SPSS 14.0 software. Non-parametric data was analysed using the Mann Whitney U test. A p-value≤0.05 was considered a significant result.

5.3 RESULTS

5.3.1 Mechanical Push-Out Tests

The results showed that the implants were very well fixed and integrated with the surrounding bone and it required 3500N forces in order to push the implants out (Figure 5.7). However, there were no statistical differences between the tissue-engineered and the non-tissue engineered implant ($p>0.05$). The forces required to push the implants out in the gap model were significantly lower (Figure 5.8).

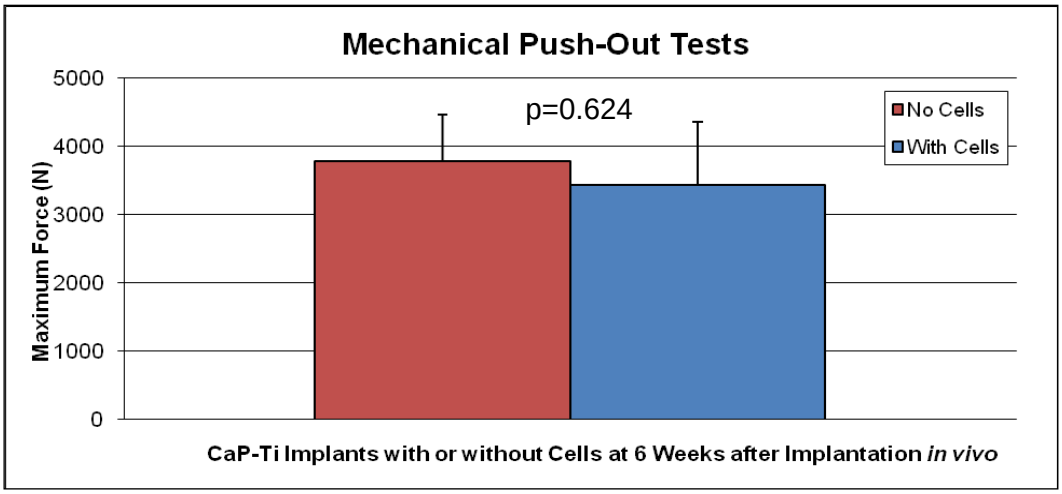

Figure 5.7 Direct contact model mechanical push-out tests results for CaP-Ti implants with or without cells at 6 weeks after implantation *in vivo*.

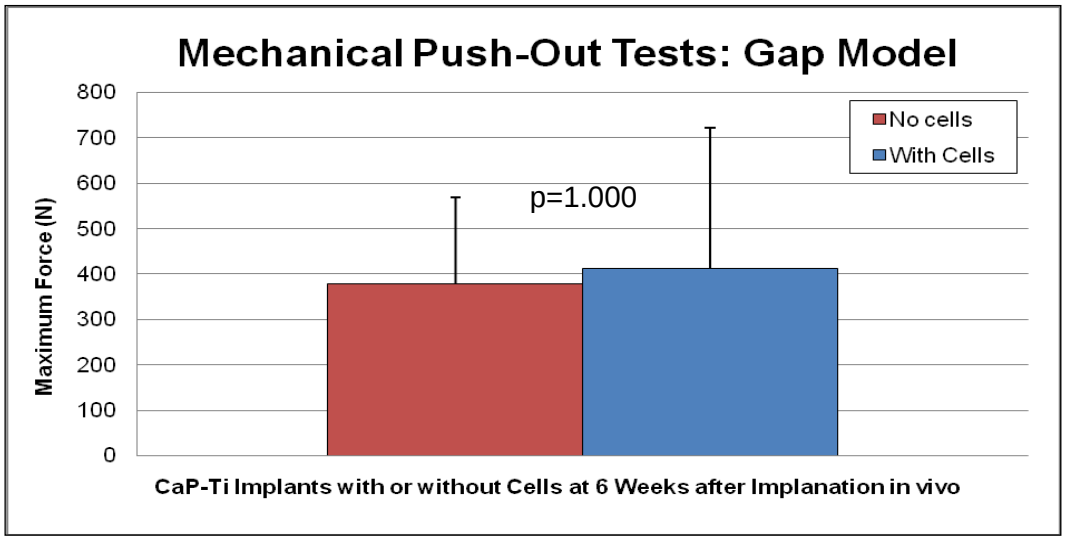

Figure 5.8 Gap model mechanical push-out tests results for CaP-Ti implants with or without cells at 6 weeks after implantation *in vivo*.

5.3.2 Histomorphometry: New Bone Formation

The results showed that there were no significant differences in new bone formation between the tissue-engineered and the non tissue-engineered implants ($p>0.05$). New bone formation was between 40% and 50% (Figures 5.9 and 5.11). For the gap model, new bone formation was lower but it was still over 20% (Figure 5.10 and 5.12).

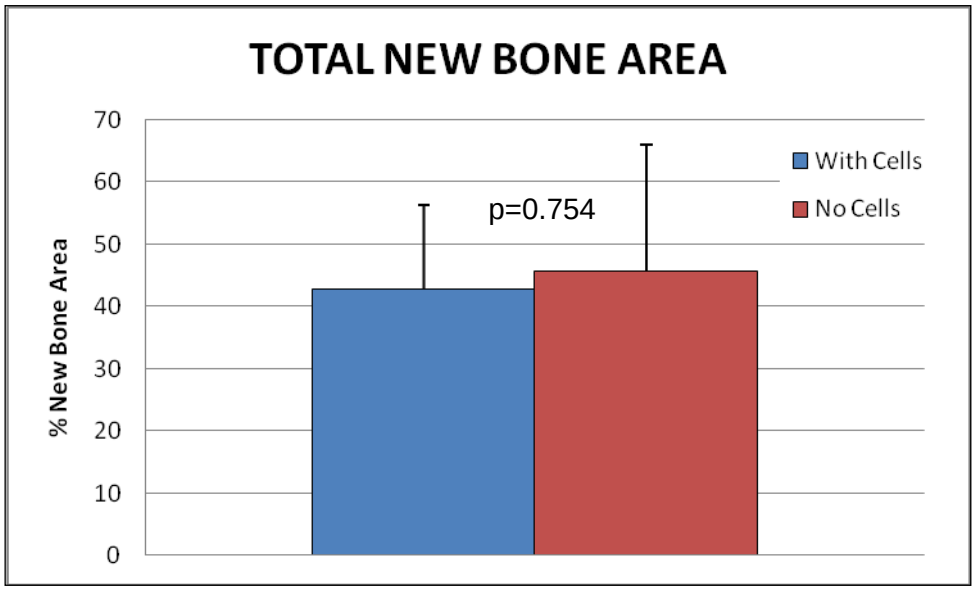

Figure 5.9 Comparison of total new bone area between tissue-engineered and non tissue-engineered constructs in the direct contact model, 6 weeks after surgery.

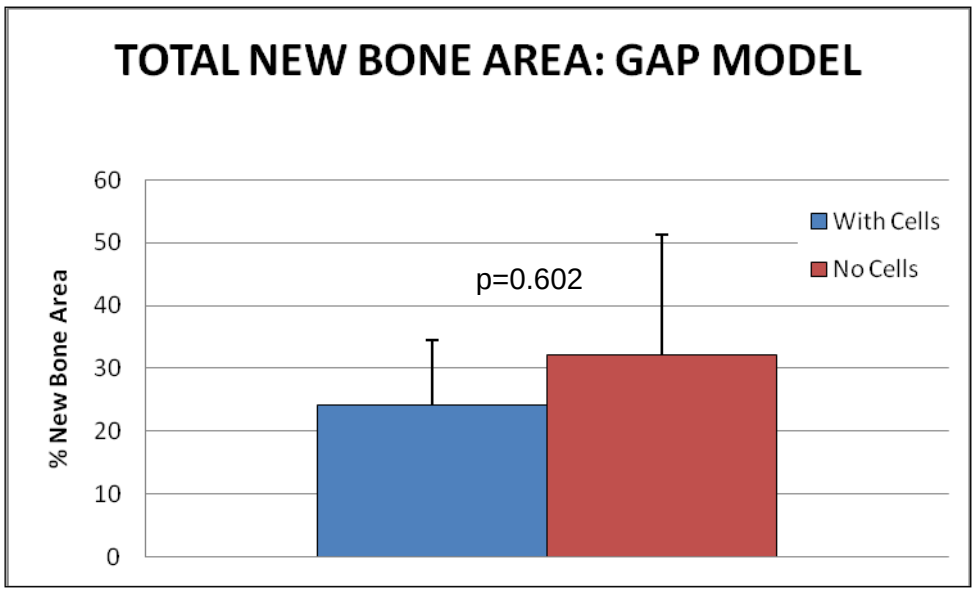

Figure 5.10 Comparison of total new bone area between tissue-engineered and non tissue-engineered constructs in the gap model, 6 weeks after surgery.

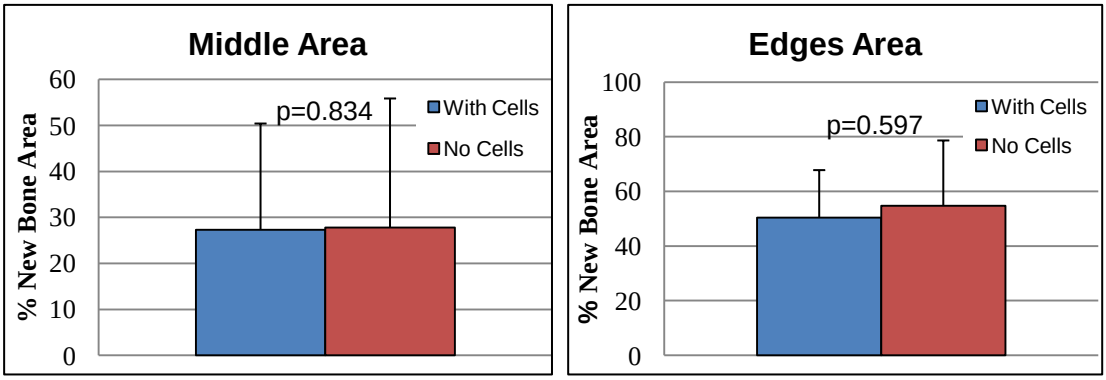

Figure 5.11 Comparison of new bone area at the middle (left) and edges of implants (right) between tissue-engineered and non tissue-engineered constructs in the direct contact model, 6 weeks after surgery.

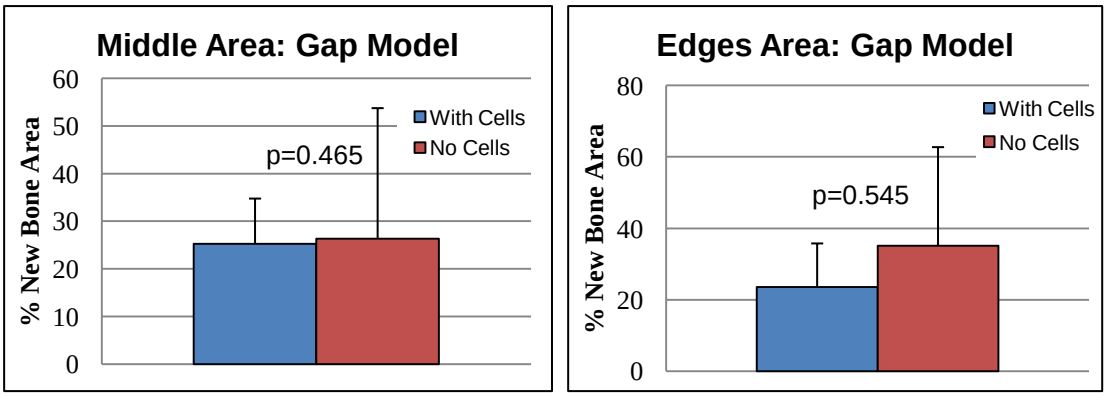

Figure 5.12 Comparison of new bone area at the middle (left) and edges of implants (right) between tissue-engineered and non tissue-engineered constructs in the gap model, 6 weeks after surgery.

5.3.3 Histomorphometry: Bone-Implant Contact

For bone-implant contact, both implants showed similar results with bone attached to over 50% of the implants' surface (Figures 13 and 15). However, no statistical differences were found between the two types of implants ($p>0.05$). In the gap model, the tissue-engineered implants showed slightly more bone contact than the non tissue-engineered implants but the difference was insignificant ($p>0.05$) (Figures 14 and 16). Overall, the new bone formation occurred more on the periphery of the implant than in the centre (Figures 15 and 16).

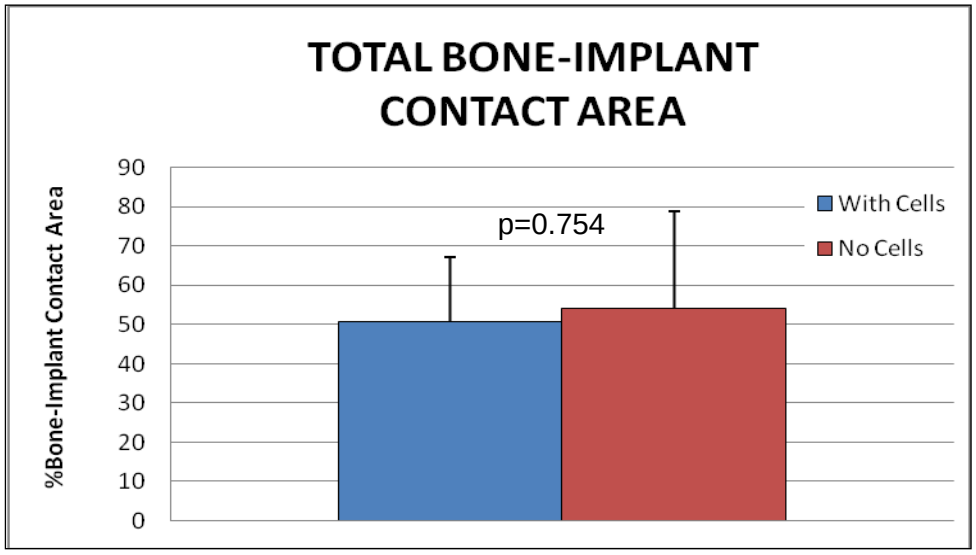

Figure 5.13 Comparison of total bone-implant contact area between tissue-engineered and non tissue-engineered constructs in the direct contact model, 6 weeks after surgery.

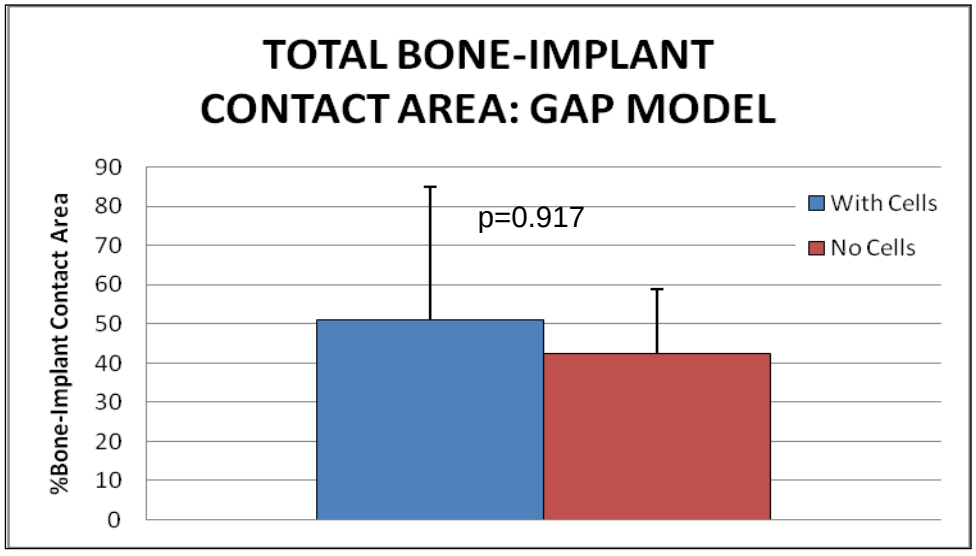

Figure 5.14 Comparison of total bone-implant contact area between tissue-engineered and non tissue-engineered constructs in the gap model, 6 weeks after surgery.

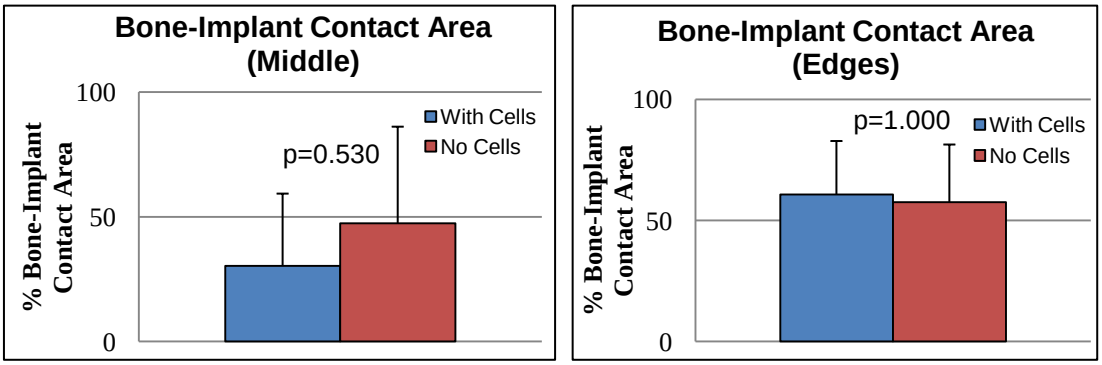

Figure 5.15 Comparison of bone-implant contact area at the middle (left) and at the edges (right) of implants between tissue-engineered and non tissue-engineered constructs in the direct contact model, 6 weeks after surgery.

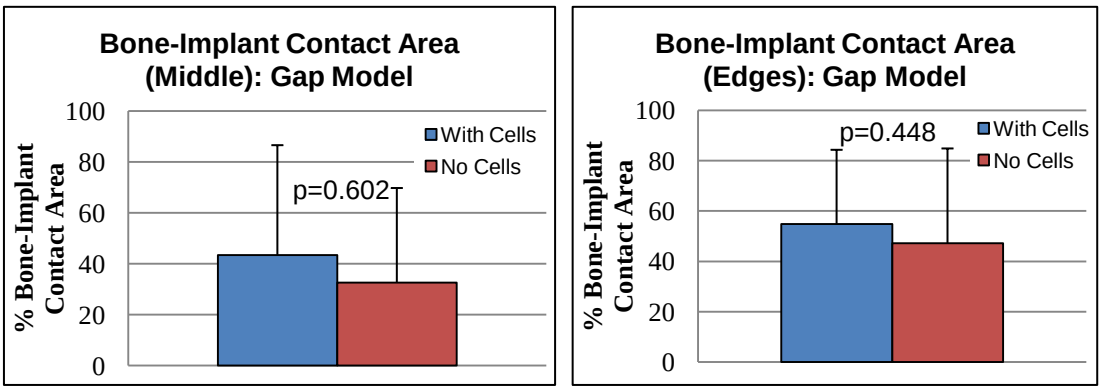

Figure 5.16 Comparison of bone-implant contact area at the middle (left) and at the edges (right) of implants between tissue-engineered and non tissue-engineered constructs in the gap model, 6 weeks after surgery.

5.3.4 Histological Analysis

For all the samples bone ingrowth into the pores was observed as well as direct bone-implant contact. The new bone tissue was well vascularised (Figures 17 to 20).

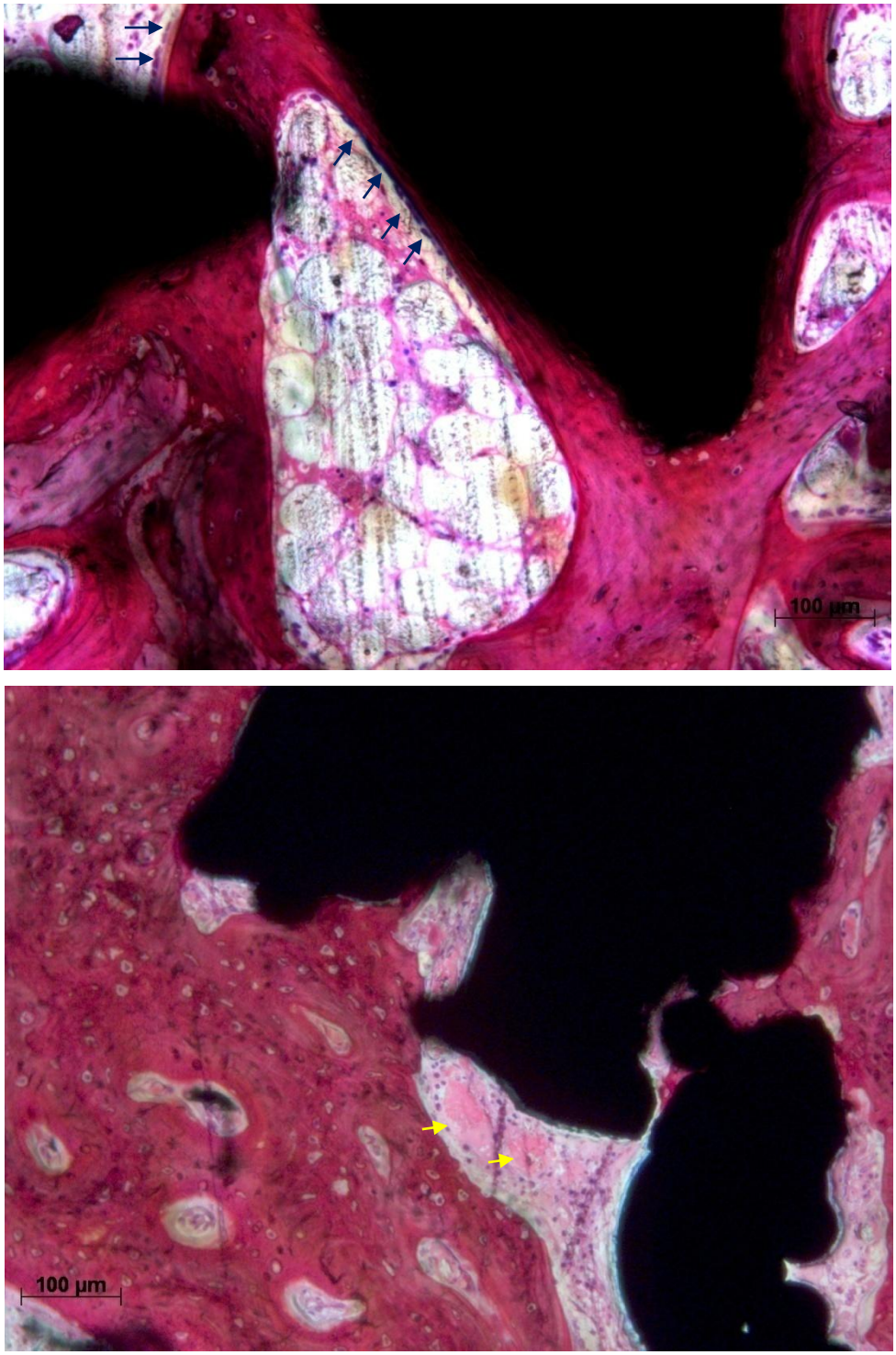

Figure 5.17 Histological analysis of non-tissue engineered (top) and tissue engineered (bottom) implants at the edge section. (Black: implant; bright pink: new bone; rest: soft tissue; yellow arrows: blood vessels; dark blue arrows: alignment of cells).

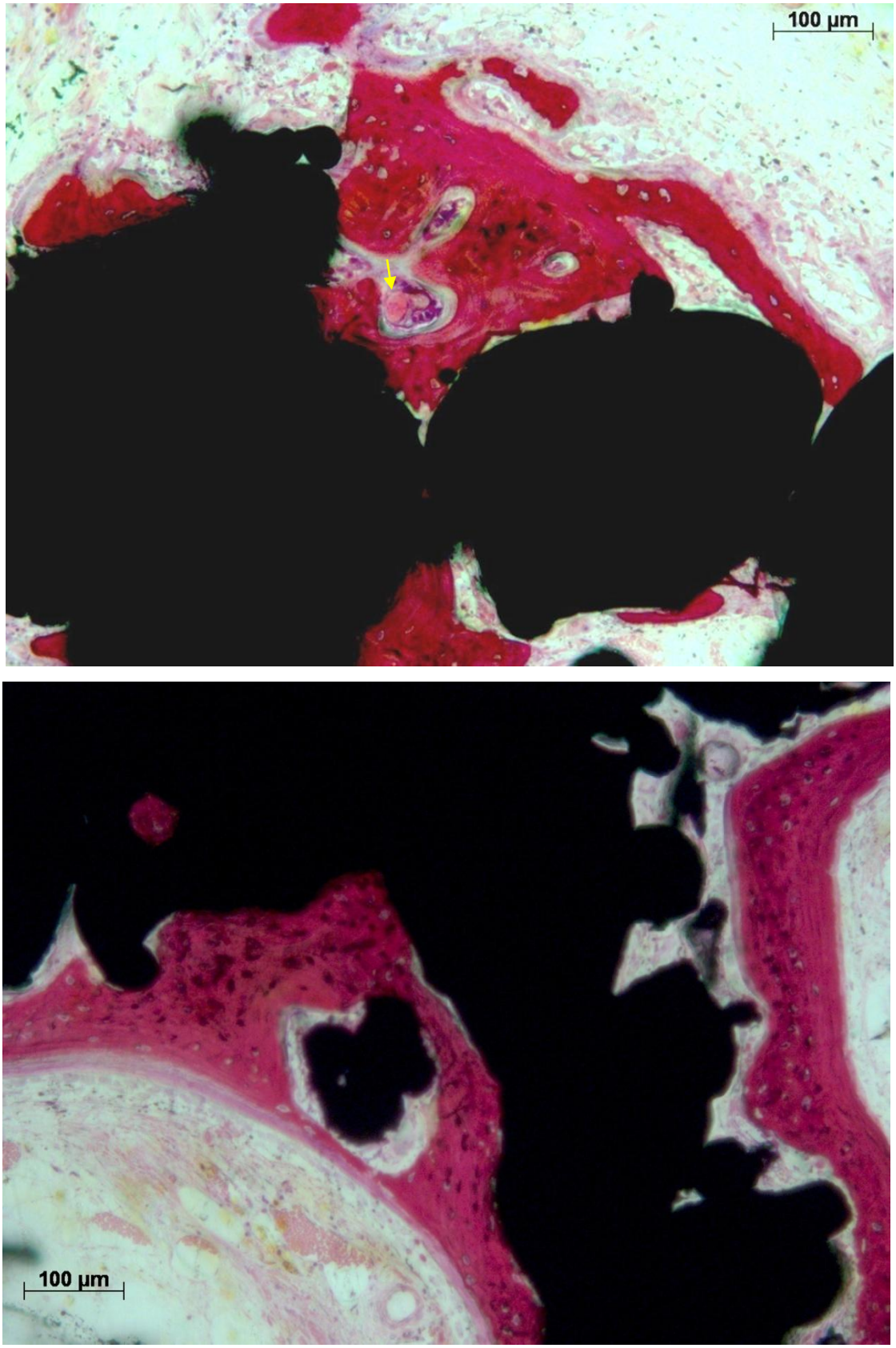

Figure 5.18 Histological analysis of non-tissue engineered (top) and tissue engineered (bottom) implants at the middle section. (Black: implant; bright pink: new bone; rest: soft tissue; yellow arrows: blood vessels).

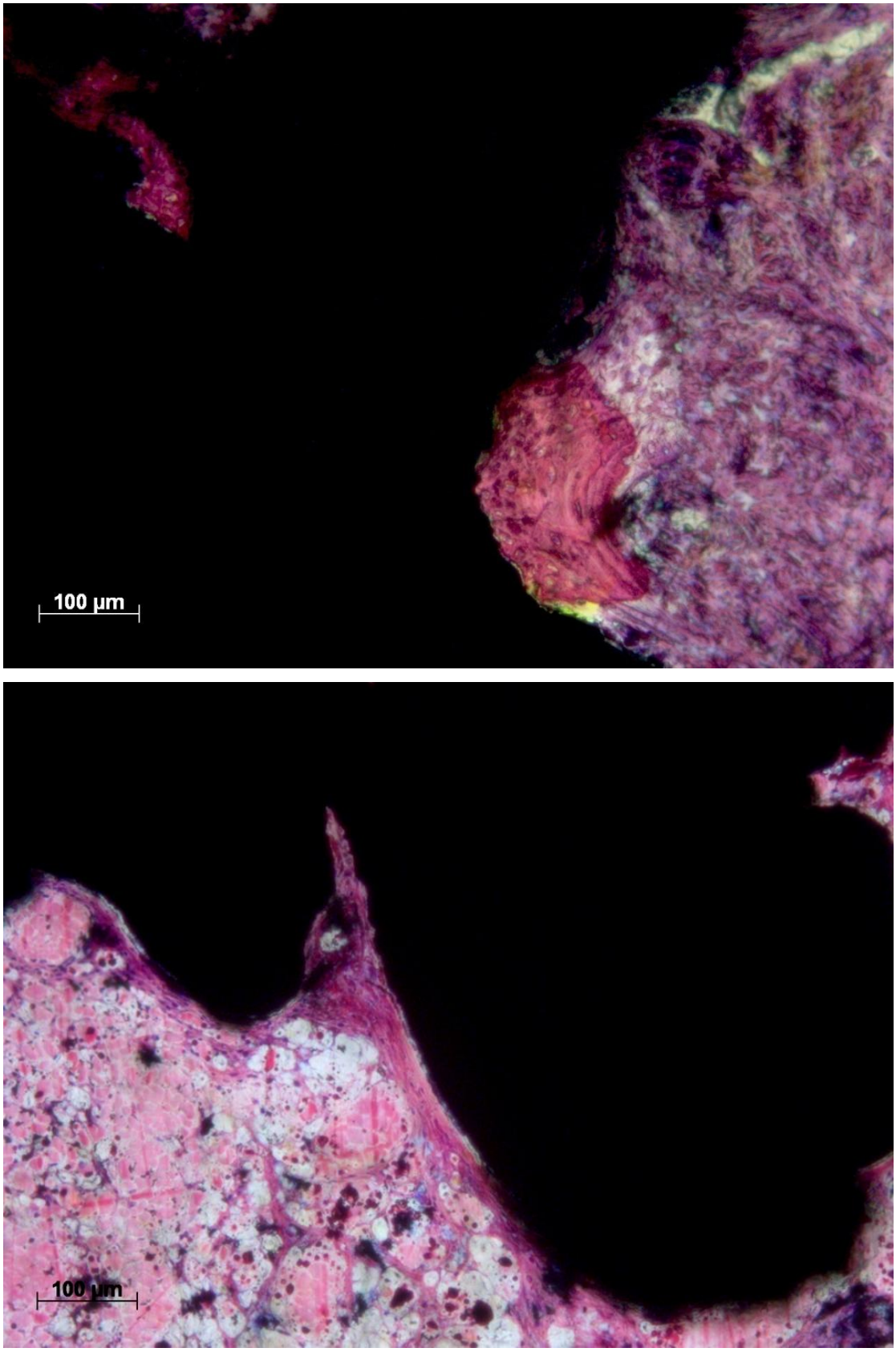

Figure 5.19 Histological analysis for the gap model of non-tissue engineered (top) and tissue engineered (bottom) implants at the edge section.
(Black: implant; bright pink: new bone; rest: soft tissue).

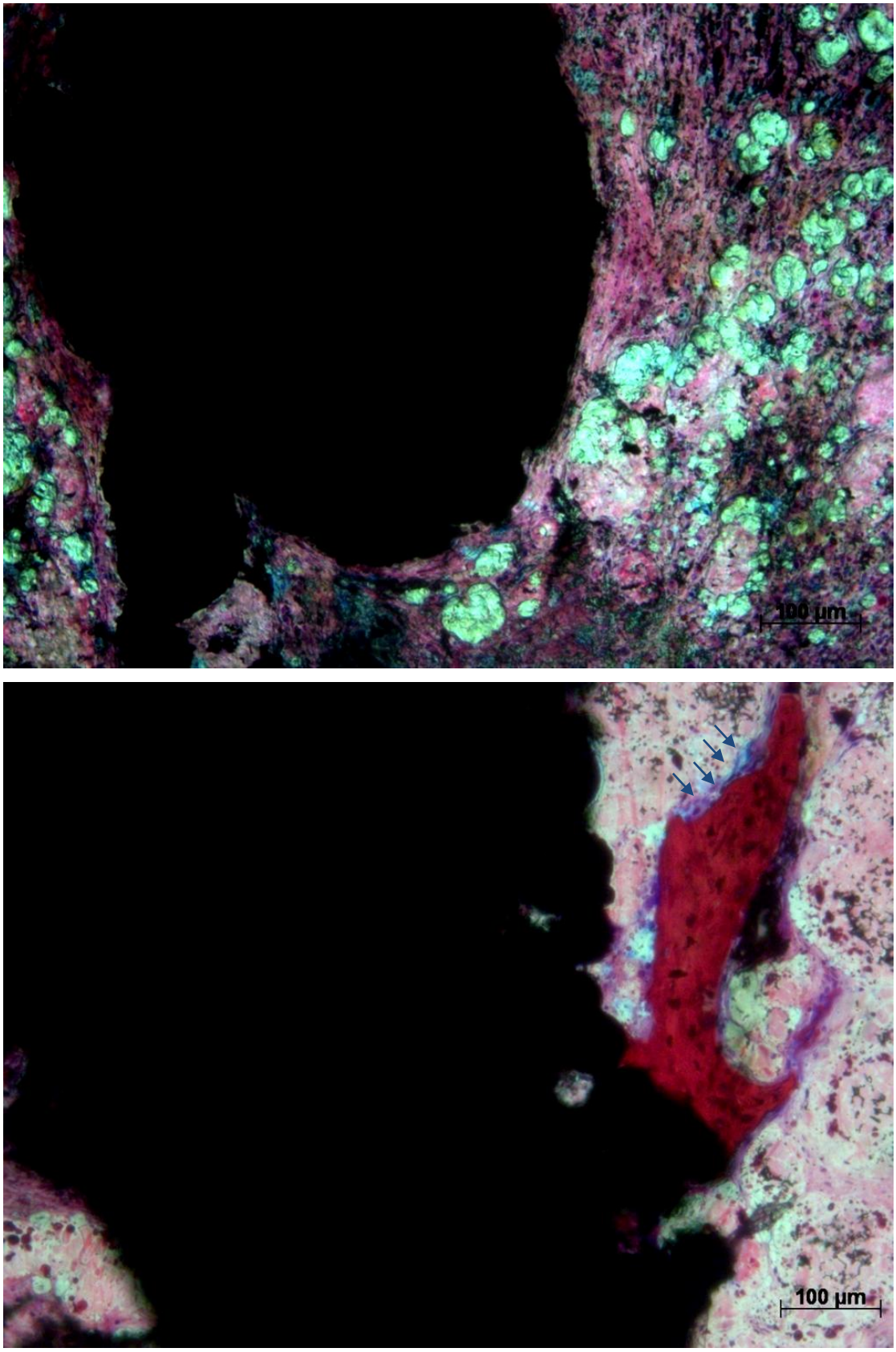

Figure 5.20 Histological analysis for the gap model of non-tissue engineered (top) and tissue engineered (bottom) implants at the middle section. (Black: implant; bright pink: new bone; rest: soft tissue; dark blue arrows: alignment of cells).

5.4 DISCUSSION

5.4.1 New Bone Formation and Ingrowth

In terms of new bone formation implants with no cells added showed a slightly higher percentage compared to tissue-engineered implants for both models of study. However, this was not significant. New bone formation was high, around 50% for the direct contact model and around 30% for the gap model. When Bobyn and colleagues implanted porous tantalum cylinders of two different pore sizes of 430 and 650μm in a transcortical canine model, percentages of 52.9% for the large pore size and 41.5% for the small pore size after 4 weeks of implantation were reported (Bobyn *et al*. 1999). These values are very similar to the ones found in my study.

Bone ingrowth into the porous implants, with or without cells, was demonstrated by the histological results (Bobyn *et al*. 1999; Ducheyne *et al*. 1990; Schliephake *et al*. 1991; Scliephake and Neukam 1991; Galois and Mainard 2004). Bone ingrowth potential is important for early implant fixation thus decreasing the incidence of implant loosening (Engh *et al*. 1987; Ducheyne *et al*. 1990; Bobyn *et al*. 1999). Ducheyne and colleagues demonstrated that the deposition of CaP coatings on titanium plugs increased bone ingrowth in the immediate post-operative period of 2, 4 and 6 weeks after surgery (Ducheyne *et al*. 1990). However, in my thesis implants without a CaP coating were not used and therefore it is not known whether the electrochemical deposition of a CaP layer on the surface of the porous Ti cylinders increased bone ingrowth.

The addition of MSCs to different materials has been shown to increase new bone formation and ingrowth as the added MSCs can differentiate into bone cells (Wolff *et al*. 1994; Petite *et al*. 2000; Eslaminejad *et al*. 2008; Kruyt *et al*. 2004). However, the results found in this chapter suggest that addition of MSCs to CaP coated porous Ti implants may not improve new bone formation and ingrowth into the implants. Location and vascularisation of the constructs, a decreased pore size and the length of the study may be the reasons why the added MSCs did not significantly contribute to new bone formation and ingrowth.

5.4.1.1 Location and Vascularisation of the Constructs

The diameter of the defects in the direct contact model was of 10mm and of 14mm in the gap model. Therefore the cells in the middle of the construct would be 5mm and 7mm respectively away from the nutrient supply in the adjacent host bone. In this situation the blood supply from the host is relatively accessible to the construct and therefore new bone formation by the added MSCs may have been masked by osteoconduction from the host (Kruyt *et al*. 2004). However, another explanation may be that vascularisation is more difficult in larger implants (Deleu and Trueta 1965) which would lead to a low oxygen tension and poor nutrient supply that may cause death of the MSCs in the tissue-engineered constructs.

5.4.1.2 Pore Size

The reduction in pore size after the addition of MSCs to the implants may also be accounted for the slight decrease in new bone formation shown by the tissue-engineered constructs compared with the non tissue-engineered ones. The original mean pore size of the CaP coated porous Ti cylinders was of 766µm. After the seeding and culture of MSCs for seven days using a perfusion bioreactor system the mean pore size of the constructs was of 611µm. Thus, a 20% reduction in pore size was exhibited by the tissue-engineered implants compared to the non tissue-engineered ones.

Several examples across the literature can be found showing that a reduction in pore size for a given material has an effect on bone ingrowth, with larger pore sizes showing more bone ingrowth. Schliephake and colleagues implanted HA blocks of 150 and 260µm pore sizes in alveolar ridge bone defects in minipigs. After five months, a high rate of implant loss was observed for the 150µm HA blocks and 260µm HA blocks showed three times more bone ingrowth than the HA blocks with smaller pore size (Schliephake *et al*. 1991). The same authors reported very similar results when the same HA blocks were used as bone graft substitutes in defects created in the endentulous mandibles of minipigs and fixed with two titanium screws. Histological analysis revealed that the HA blocks with larger pore size were evenly penetrated by bone that extended into the central pores while a high rate of implant loss occurred with the HA blocks with smaller pore size (Schliephake and Neukam 1991). Galois and Mainard implanted HA or TCP cylinders with pore sizes of 45-

80µm, 80-140µm, 140-200µm and 200-250µm in femoral condyles of rabbits. After 12 months the amount of newly formed bone was statistically smaller into the ceramic implants with 45-80µm pore size than with larger pore sizes (Galois and Mainard 2004). Finally, bone ingrowth into tantalum implants with different pore sizes of 430 and 650µm inserted in a transcortical canine model showed statistically significant more bone formation for the large pore size implants at 4 and 16 weeks after the surgical procedures (Bobyn *et al*. 1999).

5.4.1.3 Length of the Study

The question remains whether more bone formation in the tissue-engineered implants than in the non-tissue engineered ones would have been seen at a longer time point. In this study the samples were harvested at six weeks after surgery so that early bone ingrowth could be investigated, which is important for implant fixation. Other studies looking at tissue-engineered constructs to treat critical-size defects in large animals harvested their samples at 9 and 12 weeks (Kruyt *et al*. 2004) or 16 weeks (Bruder *et al*. 1998). Bruder et al. found that after 16 weeks of implantation the amount of bone was significantly greater in the tissue-enginereed implants than in the implants not loaded with cells when used in segmental defects in the femora of adult female dogs (Bruder *et al*. 1998). On the other hand, Kruyt and colleagues found significantly more bone apposition for the tissue-engineered constructs after 9 weeks of implantation while after 12 weeks the critical sized iliac wing defects created in goats were almost filled with bone with no significant advantage of the tissue-engineered constructs compared with the non tissue-engineered ones (Kruyt *et al*. 2004).

5.4.2 Implant-Bone Contact Area

In my study histological evidence of direct bonding between the implant and bone was found, thus demonstrating the osteoconductive potential of the CaP coating deposited on the surface of the porous metal Ti cylinders. CaP materials and coatings onto metal implants have long been regarded as osteoconductive in the literature. As in this chapter, Rivero and colleagues in 1988 demonstrated the osteoconductive properties of a CaP coating deposited on titanium fiber metal implants by bone forming in direct contact with the CaP coatings after implanted in the humeri and olecranons of adult dogs (Rivero *et al*. 1988). Similarly Geesink et al. also in 1988 found histological proof of direct bonding between bone and the apatite coating

deposited on cylindrical rods of TiAl6V4 alloy after inserted into canine femurs (Geesink *et al*. 1988). Buser and co-workers evaluated how different surface characteristics influenced bone integration of titanium implants. Six groups were studied with various surface modifications including a HA coating. The study showed the highest direct bone contact on the HA coated titanium group compared with any other surface modification (Buser *et al*. 1991).

Interestingly the addition of MSCs to the scaffolds appeared to improve bone-implant contact area in the gap model (Figures 5.14 and 5.16). In the gap model a 2.5mm gap was created between the implant and the surrounding bone tissue and thus the implant was not in direct contact with the existing bone tissue as in the direct contact model. The results suggest that in the defects with gap the MSCs added to the scaffolds differentiated to osteoblasts, with concomitant bone tissue formation on the surface of the implant taking place (Ohgushi *et al*. 1993; Ducheyne *et al*. 1990).

5.4.3 Implant-Bone Interface Fixation

The results showed no significant differences between the tissue-engineered implants and the implants without cells for both models (Figures 5.7 and 5.8). However, the addition of MSCs to the implants showed a beneficial trend on the mechanical performance in the gap model. These results agree with the observations discussed above for implant-bone contact area: as the MSCs added differentiated into osteoblasts subsequently forming bone on the surface of the implant the forces necessary to push the tissue-engineered implants out of the bone were higher than with the non tissue-engineered ones.

5.5 CONCLUSION

The addition of MSCs to a CaP coated porous Ti scaffold did not significantly increase new bone formation, implant-bone contact area or implant-bone fixation strength when implanted in defects created in the medial femoral condyle of sheep and compared to CaP coated porous Ti scaffolds without cells. Bone ingrowth into the porous implants was demonstrated by histology. Location and vascularisation of the constructs, a 20% reduction in pore size exhibited by the tissue-engineered implants compared to the non-tissue engineered ones and the length of the study may be accounted for the slight decrease in new bone formation shown by the tissue-engineered constructs.

Histological evidence of direct bonding between the implant and bone was found, thus demonstrating the osteoconductive potential of the CaP coating deposited on the surface of the porous metal Ti cylinders. In the defects with gap the MSCs added to the scaffolds differentiated to osteoblasts with concomitant bone tissue formation on the surface of the implant taking place, thus showing a higher implant-bone contact area than the non-tissue engineered constructs implanted in defects with gap. Therefore, the forces necessary to push the tissue-engineered implants out of the bone were higher than with the non tissue-engineered ones.

In conclusion, the two hypotheses explored in this chapter were not confirmed as tissue-engineered implants using a perfusion bioreactor system did not achieve greater osseointegration and implant-bone interface fixation when implanted *in vivo* than non tissue-engineered implants.

CHAPTER 6:

General Discussion and Conclusions

6.1 GENERAL DISCUSSION

Aseptic loosening of THRs due to osteolysis results in a reduction of the bone stock necessary for implant fixation in revision THRs (Cooper *et al*. 1992; Harris 1995; Harris 2001; Amstutz *et al*. 1992; Heisel *et al*. 2003). Several techniques such as impaction allografting are used today to overcome the problem associated with poor bone stock at revision operations. However, all of these the techniques present disadvantages, from limited bone supply and donor site morbidity to bacterial infection and immune response (Goulet *et al*. 1997; Moore *et al*. 2001). This thesis proposes bone tissue engineering (BTE) as strategy to address the issue of poor bone stock at revision THRs. BTE is a novel and promising research field which combines biomaterials science with cell biology techniques to generate bone tissue constructs *ex vivo* in order to replace damaged or lost bone (Salgado *et al*. 2004; Rose and Oreffo 2002; Karageorgiou and Kaplan 2005).

The aim of this thesis was to develop a bone-tissue engineered construct to enhance new bone formation in revision THR and the overall hypothesis was that the addition of MSCs to a porous metal scaffold coated with a CaP layer will enhance rapid formation of bone within the implant, thus repairing adjacent defect areas and increasing fixation strength at revision THRs. The main application of this thesis approach would be in acetabular cups, which could be made of porous metal, coated throughout with a CaP layer and seeded throughout with MSCs using a perfusion bioreactor system. Figure 6.1 shows the flow diagram for my thesis summarising the tissue engineering process to develop the bone tissue-engineered construct, the *in vitro* and *in vivo* phases of study and the questions and conclusions from each chapter that led to answering the overall hypothesis.

The first step of my thesis was to choose an appropriate material as scaffold for the bone tissue-engineered construct. As revision THR is a load-bearing application the excellent mechanical properties offered by metals such as TiAl6V4 (Ti) or tantalum (Ta) make them the ideal materials to be used as scaffolds in this thesis (Karageorgiou and Kaplan 2005; Niinomi 2008; Disegi 2000; Unger *et al*. 2005). Titanium and its alloys are widely used for biomedical applications because of their biocompatibility, strength, lightness and high resistance to corrosion, while porous

structures with similar material properties to those of bone have been developed (Niinomi 2008; Schuh *et al*. 2007). Similarly, a biomaterial made of porous tantalum, called trabecular metal has recently been developed and used in primary and revision THRs components with very promising early clinical results (Levine *et al*. 2006). Osteoconduction and bioactivity can be added to these metals scaffolds by coating them with a CaP layer (Karageorgiou and Kaplan 2005; Blockhuis *et al*. 2000). Plasma-spraying is the most common commercial method for coating metals with a CaP layer. However, this method takes place at high temperatures and does not allow the coating of complex shapes as it is a line-of-sight process. Several methods that overcome these disadvantages can be found in the literature in order to deposit a CaP layer on the surface of metal implants. Specifically the biomimetic and electrochemical methods allow the coating of complex shapes, such as porous structures, at low temperature and are economical. Biomimetic and electrochemical coatings onto metal implants have been used *in vivo* with promising results: Barrère and colleagues showed significantly higher bone contact for biomimetic CaP coated dense and porous metal implants compared to non-coated implants when implanted in the femoral dyaphisis of goats (Barrère *et al*. 2003) and electrochemically HA coated porous plugs implanted in the distal femoral metaphysic of pigs were shown to significantly increase bony ingrowth when compared with the uncoated implants (Redepenning *et al*. 1996). **Therefore, the first question to answer in my thesis was whether biomimetic and electrochemical methods can be applied to deposit a CaP layer on the surface of Ta and Ti discs.** In order to answer this question **Chapter two** was carried out using Ta and Ti discs with different topographical surfaces, polished and sand-blasted. They were CaP coated using the biomimetic coating process described by Habibovic *et al*. in 2002 and the electrochemical deposition process described by Redepenning *et al*. in 1996, using two different electrical currents of 20 and 6.5mA/cm^2 of surface area.

Data presented in **Chapter two** showed that biomimetic and electrochemical methods can be applied in order to deposit a CaP layer on the surface of metal discs. However, the biomimetic method did not deposit a uniform CaP layer on the surface of the discs while electrochemical coatings covered the whole surface. Surface topography and metal type do not affect the morphology and composition of the CaP coatings deposited by the same method. Biomimetic coatings are composed of a CaP phase or

phases that are very amorphous, composed of nano-sized crystals and Ca deficient (Wopenka and Pasteris 2005; Narasaraju and Phebe 1996; LeGeros 1993; Suryanarayana and Grant Norton 1998; Hammond 2001; Nishio *et al*. 2000). Mg may be incorporated into the biomimetic coatings, which is one of the reported substituting ions found in bone mineral (Wopenka and Pasteris 2005; LeGeros 1993; LeGeros 2008). Electrochemical coatings produced nano to micro crystals with different morphologies. They were also Ca deficient (Narasaraju 1996) with XRD patterns displaying a characteristic broad peak for HA, indicating it was amorphous (Suryanarayana and Grant Norton 1998; Hammond 2001). The XRD patterns also showed the electrochemical coatings were composed of HA as well as brushite, as peaks for this mineral remained after the ageing treatment. The coatings produced and characterised in Chapter two altered their morphology and composition when immersed in SBF, suggesting the three coatings would be bioactive bonding directly with bone when used *in vivo*, via dissolution and subsequent mineralisation incorporating suitable and available ions in the surrounding environment (Zhang *et al*. 2003). Therefore, by coating metal implants with a CaP layer by the methods used in this thesis osteconductive and bioactive properties would be added to the materials, both of them very important for implant fixation and osseointegration (Karageorgiou and Kaplan 2005; Salgado *et al*. 2004).

The next step of my thesis was to choose an appropriate source of cells for the bone tissue-engineering construct under development. The ideal source of cells for BTE should be easily explandable to high numbers, non-immunogenic and with a protein expression pattern similar to that of the bone tissue (Heath 2000; Salgado *et al*. 2004). Osteoblasts are the most obvious choice due to their immunogenicity, as they can be isolated from biopsies from the patients and expanded *in vitro*. However, relatively low numbers are yielded after the dissociation of the tissue and their expansion rates are relatively low (Heath 2000; Salgado *et al*. 2004). One promising possibility for BTE is to use stem cells, which are undifferentiated cells, capable of self-renewal and production of a large number of undifferentiated progeny (Blau *et al*. 2001; Lanza *et al*. 2000). Embryonic stem cells are pluripotent as they can differentiate into a wide range of cell types (Heath 2000; Salgado *et al*. 2004; Blau *et al*. 2001). However, it has been shown that when implanted *in vivo* undifferentiated embryonic stem cells give rise to teratomas and teratocarcinomas, thus showing

potential tumorogenicity, probably due to their unlimited proliferation potential (Wobus 2001). Adult stem cells, which are found in the fully differentiated tissues, are responsible for the regeneration of damaged tissues and therefore could be used for TE applications (Blau *et al*. 2001; Heath 2000). Specifically, for BTE purposes there is a special interest in the adult stem cells located in the bone marrow: mesenchymal stem cells (MSCs). MSCs are ideal candidates for developing bone tissue-engineered constructs as they have been shown to differentiate into bone, as well as other lineages of mesenchymal tissues (Caplan 1991; Jaiswal *et al*. 1997; Pittenger *et al*. 1999; Bosnakovski *et al*. 2005; Csaki *et al*. 2007; Janssen *et al*. 2006). Moreover, MSCs are already being used in clinical orthopaedic applications, such as non-union in long bone fractures where injection of concentrated bone marrow has been shown to be effective, with healing associated with the number of MSCs within the concentrated bone marrow (Sensebé *et al*. 2010). Therefore, MSCs were chosen as the source of cells in this thesis.

Once biomimetic and electrochemical CaP coatings had been deposited and characterised on the surface of Ta and Ti discs with different topographies, **the next question to answer in my thesis was how do MSCs grow and differentiate down the osteogenic lineage when cultured on these coatings? Chapter three** was carried out in order to answer this question by seeding and culturing MSCs for 4, 7 and 14 days on biomimetic and electrochemical coatings deposited on polished and sand-blasted Ta and Ti discs.

First of all MSCs were characterised by demonstrating their multipotency differentiating them down the osteogenic and adipogenic lineages (Pittenger *et al*. 1999; Erices *et al*. 2000; Rust 2003; Hara *et al*. 2008). After 21 days of culture under adipogenic conditions, Oil Red O staining showed the presence of lipids as well as a clear difference in morphology (Erices *et al*. 2000; Rust 2003). Changes in morphology were also observed in MSCs cultured under osteogenic conditions with cells becoming polygonal, an osteoblast feature (Vrouwenvelder *et al*. 1993). Mineral deposits, another osteoblastic feature, were stained in the osteogenic samples after 28 days (Erices *et al*. 2000). The osteogenic supplements added to the culture medium stimulated cell proliferation as well as differentiation (Jaiswal *et al*. 1997; Bruder *et al*. 1997). ALP/DNA of osteogenic cultures was higher at all time points, with a peak

in ALP activity observed at day 14 (Lian and Stein 1992; Jaiswal *et al*. 1997). Together, all the findings showed the multipotency of MSCs.

When MSCs were cultured on the coatings, the nano-sized crystals of the biomimetic coatings provided the best conditions for cell proliferation (Chen *et al*. 2007) compared to the crystals deposited by the electrochemical process and the uncoated discs. MSCs were also shown to proliferate more on polished discs than on sand-blasted ones (Anselme *et al*. 2000). All the coatings induced differentiation of MSCs down the osteogenic lineage, agreeing with the results of Ohgushi *et al*. 2003, Ohgushi *et al*. 2006 and Nishio *et al*. 2000. Osteogenic differentiation was greater on electrochemical coatings and complex topographies (Jäger *et al*. 2008). Finally, no significant differences were found between Ta and Ti discs in terms of MSCs growth and differentiation.

A perfusion bioreactor system is a valuable tool in BTE as it provides an optimised environment for functional 3D tissue development. It offers important advantages such as enhanced delivery of nutrients throughout the entire scaffold, which ultimately results in a construct with an even distribution of cells throughout, and mechanical stimulation to the cells by means of fluid shear stress, which enhances osteoblastic differentiation of MSCs (Bancroft *et al*. 2003; Martin *et al*. 2004; Sikavitsas *et al*. 2003). Once cells and scaffold had been characterised using a 2D experimental model in chapters two and three of this thesis, **the next step was to develop a 3D construct in which MSCs are uniformly distributed throughout the scaffold. The question to answer was whether a perfusion bioreactor system can be used in order to evenly culture MSCs throughout a porous CaP coated metal scaffold. Chapter four** was carried out in order to answer this question.

As Ta and Ti were shown on Chapter three to offer very similar characteristics for MSCs growth and osteogenic differentiation, Ti was chosen over Ta because of its proven biocompatibility, strength, lightness and high resistance to corrosion when used in orthopaedic applications (Niinomi 2008; Disegi 2000). An electrochemical CaP coating was chosen over a biomimetic one as the electrochemical method was able to coat the outside as well as the inside of the porous metal scaffold with a uniform CaP layer. The perfusion bioreactor system used in this thesis was designed

following the requirements outlined by Bancroft, Sikavitsas and Mikos in 2003 (Bancroft *et al*. 2003) and consisted of a multichannel peristaltic pump that allowed control of the flow rate, a bioreactor chamber with dimensions that optimised the delivery of the flow through the scaffolds, a medium reservoir with air ventilation and a tubing system that connected the different parts and sealed the system so it could be kept sterile. In this perfusion bioreactor system, seeded scaffolds were cultured for up to 14 days and cellular proliferation, osteogenic differentiation and the distribution of cells throughout the scaffold were compared to constructs cultured under static conditions.

First of all, a study in order to choose an appropriate flow rate for the perfusion bioreactor system designed was carried out. The perfusion flow rates study was based on the work conducted by Cartmell and colleagues, where the effect of four different perfusion flow rates (0.33, 3.3, 6.6 and 33mL/min/cm^3) on cell viability, proliferation and osteogenic differentiation of immature osteoblasts-like cells was assessed (Cartmell *et al*. 2003). However, 33mL/min/cm^3 was not investigated since Cartmell and co-workers reported that this flow rate resulted in substantial cell dead throughout the constructs. In my study, the higher flow rate of 6.6mL/min/cm^3 (1.4mL/min) cracked the bioreactor chamber after just one day of perfusion culture. The high shear forces generated by this flow rate may have sheared the cells off the scaffold, which blocked the outflow of the chamber resulting in an increment in pressure, which ultimately cracked the polycarbonate cylinder. The lower flow rate of 0.33mL/min/cm^3 (0.07mL/min) may not have been efficient enough in removing waste products and supplying fresh nutrients to the cells. Thus, the cells died and blocked the outflow of the bioreactor chamber, which ultimately cracked after 3-4 days of culture. The flow rate of 3.3mL/min/cm^3 allowed the system to run for up to 14 days and therefore was chosen to carry out the rest of the work presented in Chapter four. Furthermore, Zhao and Ma reported the highest seeding efficiencies when a flow rate of 3.77mL/min/cm^3 (0.79mL/min if used in my system) was assessed for the dynamic cell seeding of human MSCs on poly(ethylene terephthalate) (PET) fibrous matrices (Zhao and Ma 2005). This flow rate was also used in their next study to dynamically seed human MSCs on PET matrices, maintained for 20 days and compared to a perfusion flow rate of 56.6mL/min/cm^3. Increased cell numbers at the lower flow rate and increased ALP activity and calcium deposition, which are markers

for osteogenic differentiation, at the higher flow rate was observed (Zhao *et al*. 2007). The flow rate was further adjusted to 0.75mL/min in order to allow the construct to ideally renew the culture medium every minute. 0.75mL/min is in between 0.7mL/min (3.3mL/min/cm^3, Cartmell *et al*. 2003) and 0.79mL/min (3.77mL/min/cm^3, Zhao and Ma 2005; Zhao *et al*. 2007).

Results from the AlamarBlue® and DNA assays show that the constant supply of medium to and through the porous constructs has a beneficial effect on cell proliferation as constructs cultured under flow perfusion had an increased proliferation compared to constructs cultured under static conditions, as previously reported in the literature (Sikavitsas *et al*. 2005; Bjerre *et al*. 2008; Bancroft *et al*. 2002). Similarly, ALP showed an increased activity for the flow perfused constructs with a peak in activity at day 7. This may be associated with the faster rate of proliferation leading cells to differentiate quicker but could also be due to the fluid shear forces experimented by the cells cultured in the bioreactor system which may have had a mechanostimulatory effect enhancing their osteogenic differentiation (Sikavitsas *et al*. 2003; Sikavitsas *et al*. 2005; Zhao *et al*. 2007; Bancroft *et al*. 2002). Histology results showed that constructs cultured in the perfusion bioreactor developed a uniform cellular layer on the external as well as internal surfaces over time. Results showed that the chosen flow rate had a beneficial effect on cell proliferation and viability until day 7, as evidenced by the AlamarBlue® and DNA assays, but resulted in a decrease of cell viability between days 7 and 14 as shown by the AlamarBlue® assay (Cartmell *et al*. 2003). Under the conditions tested in this study, day 7 provided the best results for MSCs proliferation and differentiation as well as a uniform cellular distribution throughout the scaffold compared to static controls and the other time points. Therefore, this time point was chosen to carry out the next *in vivo* phase of this thesis.

Chapters two to four comprise the *in vitro* phase of this thesis (Figure 6.1), where the scaffold and cells chosen to develop a bone tissue-engineered construct to enhance new bone formation in revision THRs were characterised and studied. Furthermore, a 3D construct was developed in Chapter four, where a perfusion bioreactor system was designed and implemented for the culture of MSCs throughout CaP coated porous Ti scaffolds. During this *in vitro* phase growth was studied by DNA and AlamarBlue®

assays. Further analysis of viability could have been done with a live-dead assay which showed the percentage of live cells in the samples as it could have helped to further understand the toxicity of these coatings on MSCs. As it is well known that CaP materials and coatings promote MSCs differentiation down the osteogenic lineage (Ohgushi *et al*. 2003; Ohgushi *et al*. 2006; Nishio *et al*. 2000) and that the shear forces generated inside the perfusion bioreactor may also promote MSCs to differentiate down the osteogenic pathway (Sikavitsas *et al*. 2003; Sikavitsas *et al*. 2005; Zhao *et al*. 2007; Bancroft *et al*. 2002), in my project only one early marker for osteogenic differentiation was studied, ALP (Lian and Stein 1992). However, other markers of osteogenic differentiation such as osteocalcin or Runx2 could have been analysed in order to characterise the differentiation process of these cells along the osteogenic pathway in this *in vitro* phase of my thesis.

The last step in the development of bone tissue-engineered constructs is the evaluation of their performance on preclinical studies prior to evaluation in human subjects (Salgado *et al*. 2004; Goldstein 2002). **The final *in vivo* phase of this thesis was carried out to answer the question: can the tissue-engineered constructs generated using a perfusion bioreactor system achieve better osseointegration and therefore increase fixation strength than non tissue-engineered constructs when implanted *in vivo*?** The aim of **Chapter five** was to answer this question. Twenty skeletally mature mule sheep were used with two different models of study: a direct contact model with a defect of 10mm in which the constructs were in direct contact with the host bone and a gap model with a defect of 14mm in which a 2.5mm gap was created between the constructs and the host bone. The gap model simulates defects in revision THRs. Each sheep was implanted 2 constructs in both left and right medial femoral condyles, with one of them acting as control. Controls, or non tissue-engineered constructs, were acellular CaP coated Ti porous cylinders. Tissue-engineered constructs were seeded with autologous MSCs aspirated from the iliac crest about 2 months before implantation and cultured for 7 days in a perfusion bioreactor system. 6 weeks after the surgical procedures the sheep were euthanized, samples retrieved and either processed for hard grade histology or mechanical push-out tests.

Results showed that in terms of new bone formation implants with no cells added had a slightly higher percentage compared to tissue-engineered implants for both models of study. However, this was not significant. New bone formation was high, around 50% for the direct contact model and around 30% for the gap model, similar to values reported by other authors (Bobyn *et al*. 1999). Bone ingrowth into the porous implants, with or without cells, was demonstrated by histology (Bobyn *et al*. 1999; Ducheyne *et al*. 1990; Schliephake *et al*. 1991; Scliephake and Neukam 1991; Galois and Mainard 2004), which is important for early implant fixation thus decreasing the incidence of implant loosening (Engh *et al*. 1987; Ducheyne *et al*. 1990; Bobyn *et al*. 1999). Although the addition of MSCs to different materials has been shown to increase new bone formation and ingrowth (Wolff *et al*. 1994; Petite *et al*. 2000; Eslaminejad *et al*. 2008; Kruyt *et al*. 2004), the results found in this chapter suggest that addition of MSCs to CaP coated porous Ti implants may not improve new bone formation and ingrowth into the implants. Factors such as location and vascularisation of the constructs (Kruyt *et al*. 2004; Deleu and Trueta 1965), a decreased pore size for the tissue-engineered constructs (Schliephake *et al*. 1991; Schliephake and Neukam 1991; Galois and Mainard 2004; Bobyn *et al*. 1999) and the length of the study (Kruyt *et al*. 2004; Bruder *et al*. 1998) may affect bone ingrowth but were not studied in my project.

Histological evidence of direct bonding between the implant and bone was found, thus demonstrating the osteoconductive potential of the CaP coating deposited on the surface of the porous metal Ti cylinders (Rivero *et al*. 1988; Geesink *et al*. 1988; Buser *et al*. 1991). Interestingly the addition of MSCs to the scaffolds appeared to improve bone-implant contact area in the gap model, suggesting that in the defects with gap the MSCs added to the scaffolds differentiated to osteoblasts, with concomitant bone tissue formation on the surface of the implant taking place (Ohgushi *et al*. 1993; Ducheyne *et al*. 1990). The results from the mechanical push-out tests showed no significant differences between the tissue-engineered implants and the implants without cells for both models. However, the addition of MSCs to the implants showed a beneficial trend on the mechanical performance in the gap model, which agrees with the observations discussed for implant-bone contact area.

The work presented in this thesis did not confirm the overall hypothesis that the addition of MSCs to a porous metal scaffold coated with a CaP layer will enhance rapid formation of bone within the implant, thus repairing adjacent defect areas and increasing fixation strength, as no statistical differences were found between tissue-engineered and non tissue-engineered constructs in terms of new bone formation and implant-bone contact area. However, **in the defects with gap, the tissue-engineered constructs showed a higher implant-bone contact area and therefore higher forces were necessary to push the tissue-engineered implants out of the bone** than for the non tissue-engineered ones. Since the gap model is representative of the bone defects found in revision THRs the results suggest a beneficial trend in the addition of MSCs to porous CaP coated Ti scaffolds for the regeneration of the bone stock at revision THRs. **These results suggest that bone tissue engineering can be applied in order to develop constructs with a clinical application in rTHRs where a lack of bone stock is problematic.**

6.2 GENERAL CONCLUSIONS

- Biomimetic and electrochemical methods can be applied in order to deposit a CaP layer on the surface of tantalum and TiAl6V4 discs, where surface topography and metal type do not affect the morphology and composition of the CaP coatings deposited by the same method.

- The nano-sized crystals of the biomimetic coatings significantly increase MSCs growth compared to the electrochemical coatings and the uncoated discs.

- Biomimetic and electrochemical coatings induce MSCs differentiation down the osteogenic lineage, which was greater on electrochemical coatings and complex topographies.

- No significant differences were found between tantalum and TiAl6V4 in terms of MSCs growth and differentiation.

- 3D tissue-engineered constructs based on a CaP coated porous TiAl6V4 scaffold and cultured with MSCs using a perfusion bioreactor system for 7 days had increased proliferation and osteogenic differentiation as well as an even distribution of cells throughout the scaffolds compared to constructs cultured under static conditions.

- Tissue-engineered constructs did not significantly increase new bone formation, implant-bone contact area or implant-bone fixation strength when implanted in defects created in the medial femoral condyle of sheep and compared to non tissue-engineered constructs.

- In the defects with gap the MSCs added to the scaffolds differentiated to osteoblasts with concomitant bone tissue formation on the surface of the implant taking place, thus showing higher implant-bone contact area and interface fixation strength than the non-tissue engineered constructs.

6.3 FUTURE WORK

- A flow rates study in order to find out the optimum one for the perfusion bioreactor system designed in this thesis.

- An investigation into the optimum culture time inside the perfusion bioreactor system for the cells to deposit a mineralised extracellular matrix.

- Addition of osteogenic supplements to the culture medium used in the bioreactor system and study of the ostegenic differentiation of mesenchymal stem cells.

- Use of allogenic cells instead of autologous cells to eliminate donor-dependent factors.

- Implantation of constructs in an ectopic site to compare osteoinduction between tissue-engineered and non tissue-engineered ones.

- To choose a porous metal material with larger pore size to maximise cell growth.

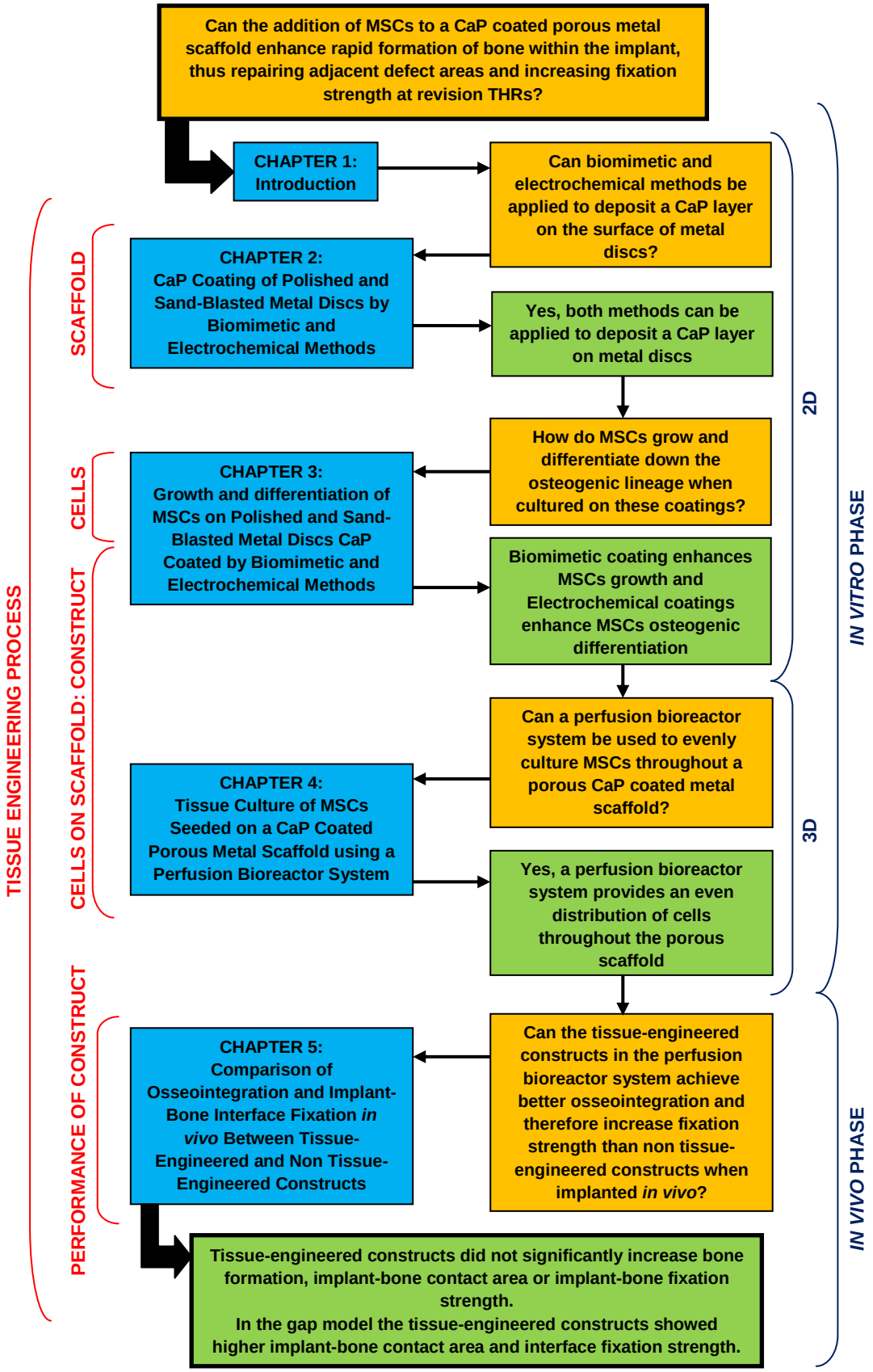

Figure 6.1 Thesis Flow Diagram

BIBLIOGRAPHY

Adams CS, Mansfield K, Perlot RL, Shapiro IM. (2001) Matrix regulation of skeletal cell apoptosis. *J Biol Chem* 23(8), 20316-20322.

Aerssens J, Boonen S, Lowet G, Dequeker J. (1997) Interspecies differences in bone composition, density and quality: potential implications for in vitro bone research. *Endocrinology* 139, 663-670.

Albrektsson T, Johansson C. (2001) Osteoinduction, osteoconduction and osseointegration. *Eur Spine J* 10, S96-S101.

Amstutz HC, Campbell P, Kossovsky N, Clarke IC. (1992) Mechanism and clinical significance of wear debris-induced osteolysis. *Clin Orthop Relat Res* 276, 7-18.

Amstutz HC, Grigoris P. (1996) Metal on metal bearings in hip arthroplasty. *Clin Orthop Relat Res* 329S, S11-S34.

An YH, Friedman RJ. (1998) Animal models in orthopaedic research. First Edition. CRC Press.

An YH, Woolf SK, Friedman RJ. (2000) Pre-clinical in vivo evaluation of orthopaedic bioabsorbable devices. *Biomaterials* 21, 2635-2652.

Anderson JM, Miller KM. (1984) Biomaterial biocompatibility and the macrophage. *Biomaterials* 5(1), 5-10.

Anselme K, Bigerelle M, Noel B, Dufresne E, Judas D, Iost A, Hardouin P. (2000) Qualitative and quantitative study of human osteoblast adhesion on materials with various surface roughnesses. *J Biomed Mater Res* 49(2), 155-166.

Athanasou NA. (1996) Current concepts review: cellular biology of bone-resorbing cells. *J Bone Joint Surg* 78A, 1096-1112.

Bancroft GN, Sikavitsas VI, Mikos AG. (2003) Design of a perfusion bioreactor system for bone tissue-engineering applications. *Tissue Eng* 9(3), 549-554.

Bancroft GN, Sikavitsas VI, van den Dolder J, Sheffield TL, Ambrose CG, Jansen JA, Mikos AG. (2002) Fluid flow increases mineralized matrix deposition in 3D perfusion culture of marrow stromal osteoblasts in a dose-dependent manner. *PNAS* 99(20), 12600-12605.

Barrère F, van der Valk CM, Meijer G, Dalmeijer RAJ, de Groot K, Layrolle P. (2003) Osteointegration of biomimetic apatite coating applied onto dense and porous metal implants in femurs of goats. *J Biomed Mater Res Part B Appl Biomater* 67B, 655-665.

Bensaïd W, Triffitt JT, Blanchat C, Oudina K, Sedel L, Petite H. (2003) A biodegradable fibrin scaffold for mesenchymal stem cell transplantation. *Biomaterials* 24, 2497-2502.

Bernardi G, Kawasaki T. (1968) Chromatography of polypeptides and proteins on hydroxyapatite columns. *BBA-Protein Structure* 160, 301-310.

Bharati S, Sinha MK, Basu D. (2005) Hydroxyapatite coating by biomimetic method on titanium alloy using concentrated SBF. *Bull Mater Sci* 28(6), 617-621.

Bjerre L, Bünger CE, Kassem M, Mygind T. (2008) Flow perfusion culture of human mesenchymal stem cells on silicate-substituted tricalcium phosphate scaffolds. *Biomaterials* 29, 2616-2627.

Bjornson CRR, Rietze RL, Reynolds BA, Magli MC, Vescoti AL. (1999) Turning brain into blood: a hematopoietic fate adopted by adult stem cells in vivo. *Science* 283, 534-537.

Blau HM, Brazelton TR, Welmann JM. (2001) The evolving concept of a stem cell: entity or function? *Cell* 105, 829-841.

Blokhuis TJ, Termaat MF, den Boer FC, Patka P, Bakker FC, Haarman HJThM. (2000) Properties of calcium phosphate ceramics in relation to their in vivo behaviour. *J Trauma Inj Inf Crit Care* 48(1), 179-186.

Bobyn JD, Stackpool GJ, Hacking SA, Tanzer M, Krygier JJ. (1999) Characteristics of bone ingrowth and interface mechanics of a new porous tantalum biomaterial. *J Bone Joint Surg* 81-B(5), 907-914.

Bohner M. (2000) Calcium orthophosphates in medicine: from ceramics to calcium phosphate cements. *Injury Int J Care Injured* 31, SD37-47.

Bosnakovski D, Mizuno M, Kim G, Takagi S, Okumura M, Fujinaga T. (2005) Isolation and multilineage differentiation of bovine bone marrow mesenchymal stem cells. *Cell Tissue Res* 319(2), 243-253.

Botchwey EA, Pollack SR, Levine EM, Laurencin CT. (2001) Bone tissue engineering in a rotating bioreactor using a microcarrier matrix system. *J Biomed Mater Res* 55, 242-253.

Bowers GN, McComb RB. (1966) A continuous spectrophotometric method for measuring the activity of serum alkaline phosphatase. *Clin Chem* 12(2), 70-89.

Brandoff JF, Silber JS, Vaccaro AR. (2008) Contemporary alternatives to synthetic bone grafts for spine surgery. *Am J Orthop* 37(8), 410-414.

Bruder SP, Jaiswal N, Haynesworth SE. (1997) Growth kinetics, self-renewal and the osteogenic potential of purified human mesenchynal stem cells during extensive subcultivation and following cryopreservation. *J Cell Biochem* 64, 278-294.

Bruder SP, Kraus KH, Goldberg VM, Kadiyala S. (1998) The effect of implants loaded with autologous mesenchymal stem cells on the healing of canine segmental bone defects. *J Bone Joint Surg Am* 80-A(7), 985-996.

Buma P, Gardeniers JWM. (1995) Tissue reactions around a hydroxyapatite-coated hip prosthesis. *J Arthroplasty* 10(3), 389-395.

Burg KJL, Porter S, Kellam JF. (2000) Biomaterial developments for bone tissue engineering. *Biomaterials* 21, 2347-2359.

Buser D, Schenk RK, Steinemann S, Fiorellini JP, Fox CH, Stich H. (1991) Influence of surface characteristics on bone integration of titanium implants. A histomorphometric study in miniature pigs. *J Biomed Mater Res* 25, 889-902.

Caplan AI. (1991) Mesenchymal stem cells. *J Orthop Res* 9(5), 641-650.

Caplan AI. (1994) The mesengenic process. *Clin Plast Surg* 21(3), 429-435.

Caplan AI. (2009) New era of cell-based orthopaedic therapies. *Tissue Eng: Part B* 15(2), 195-200.

Cartmell SH, Porter BD, Garcia AJ, Guldberg RE. (2003) Effects of medium perfusion rate on cell-seeded three-dimensional bone constructs in vitro. *Tissue Eng* 9(6), 1197-1203.

Chang YS, Gu HO, Kobayashi M, Oka M. (1998) Influence of various structure treatments on histological fixation of titanium implants. *J Arthroplasty* 13(7), 816-825.

Chen F, Lam WM, Lin CJ, Qiu GX, Wu ZH, Luk KDK, Lu WW. (2007) Biocompatibility of electrophoretical deposition of nanostructured hydroxyapatite coating on roughen titanium surface: in vitro evaluation using mesenchymal stem cells. *J Biomed Mater Res* 82B, 183-191.

Clohisy JC, Calvert G, Tull F, McDonald D, Maloney WJ. (2004) Reasons for revision hip surgery: a retrospective review. *Clin Orthop Relat Res* 429, 188-192.

Coathup MJ, Blackburn J, Goodship AE, Cunningham JL, Smith T, Blunn GW. (2005) Role of hydroxyapatite coating in resisting wear particle migration and osteolysis around acetabular components. *Biomaterials* 26, 4161-4169.

Colter DC, Class R, DiGirolamo CM, Prockop DJ. (2000) Rapid expansion of recycling stem cells in cultures of plastic-adherent cells from human bone marrow. *Proc Natl Acad Sci* 97, 3213-3218.

Conget PA, Minguell JJ. (2000) Adenoviral-mediated gene transfer into ex vivo expanded human bone marrow mesenchymal progenitor cells. *Experimental Hematology* 28, 382-390.

Constantz BR, Barr BM, Ison IC, Fulmer MT, Baker J, McKinney LA, Goodman SB, Gunasekaren S, Delaney DC, Ross J, Poser RD. (1997) Histological, chemical and crystallographic analysis of four calcium phosphate cements in different rabbit osseous sites. *J Biomed Mater Res (Appl Biomater)* 43, 451-461.

Cooper RA, McAllister CM, Borden LS, Bauer TW. (1992) Polyethylene debris-induced osteolysis and loosening in uncemented total hip arthroplasty. *J Arthroplasty* 7(3), 285-290.

Csaki C, Matis U, Mobasheri A, Ye H, Shakibaei M. (2007) Chondrogenesis osteogenesis and adipogenesis of canine mesenchymal stem cells: a biochemical, morphological and ultrastructural study. *Histochem Cell Biol* 128(6), 507-520.

Cuneyt Tas A, Bhaduri SB. (2004) Rapid coating of Ti6Al4V at room temperature with a calcium phosphate solution similar to 10× simulated body fluid. *J Mater Res* 19(9), 2742-2749.

Curtis A, Wilkinson C. (1997) Topographical control of cells. *Biomaterials* 18, 1573-1583.

Dalby MJ, Gadegaard N, Tare R, Andar A, Riehle MO, Herzyk P, Wilkinson CDW, Oreffo ROC. (2007) The control of human mesenchymal cell differentiation using nanoscale symmetry and disorder. *Nat Mater* 6(12), 997-1003.

Dalby MJ, McCloy D, Robertson M, Agheli H, Sutherland D, Affrossman S, Oreffo ROC. (2006) Osteoprogenitor response to semi-ordered and random nanotopographies. *Biomaterials* 27, 2980-2987.

De Bartolo L, Morelli S, Boder A, Drioli E (2002) Evaluation of cell behaviour related to physic-chemical properties of polymeric membranes to be used in bioartificial organs. *Biomaterials* 23(12), 2485-2497.

Deleu J, Trueta J. (1965) Vascularisation of bone grafts in the anterior chamber of the eye. *J Bone Joing Surg* 47B(2), 319-329.

Delloye C, Cornu O, Druez V, Barbier O. (2007) Bone allografts: what they can offer and what they cannot. J Bone Joint Surg 89B(5), 574-580.

Depprich R, Handschel J, Wiesmann HP, Jäsche-Meyer J, Meyer U. (2008) Use of bioreactors in maxillofacial tissue engineering. *British J Oral Maxillofacial Surgery* 46, 349-354.

Dewey MJ, Martin DW, Martin GR, Mintz B. (1977) Mosaic mice with teratocarcinoma-derived mutant cells deficient in hypoxanthine phosphoribosyltransferase. *Proc Natl Acad Sci* 74(12), 5564-5568.

Disegi JA. (2000) Titanium alloys for fracture fixation implants. *Injury* 31 Suppl 4, 14-7.

Ducheyne P, Beight J, Cuckler J, Evans B, Radin S. (1990) Effect of calcium phosphate coating characteristics on early post-operative bone tissue ingrowth. *Biomaterials* 11, 531-540.

Ducheyne P, Qiu Q. (1999) Bioactive ceramics: the effect of surface reactivity on bone formation and bone cell function. *Biomaterials* 20, 2287-2303.

Dvir T, Benishti N, Shachar M, Cohen S. (2006) A novel perfusion bioreactor providing a homogeneous milieu for tissue regeneration. *Tissue Eng* 12(10), 2843-2852.

Einhorn TA. (2003) Clinical applications of recombinant human BMPs: early experience and future development. *J Bone Joint Surg* 85, 82-88.

Engh CA, Bobyn JD, Glassman AH. (1987) Porous-coated hip replacement. *J Bone Joint Surg* 69B(1), 45-55.

Erices A, Conget P, Minguell JJ. (2000) Mesenchymal progenitor cells in human umbilical cord blood. *British Journal of Haematology* 109, 235-242.

Eslaminejad MB, Jafarian M, Khojasteh A, Abbas FM, Dehghan MM, Hassanizadeh R. (2008) In vivo bone formation by canine mesenchymal stem cells loaded onto HA/TCP scaffolds: qualitative and quantitative analysis. *Yakhteh Medical Journal* 10(3), 205-212.

Fakhouri SF, Zamarioli A, Wichr CRG, Araujo CA, Defino HLA, Shimano AC. (2011) Biomechanical study of the pullout resistance in screws of a vertebral fixation system. *Advances in Mechanical Engineering* 2011, 1-6.

Ferrari M, Corradi A, Lazzaretti M, De'Cilla M, Losi CG, Villa R, Lanfranchi A. (2007) Adult stem cells: perspectives for therapeutic applications. *Veterinary Research Communications* 31(Suppl. 1), 1-8.

Freshney RI. (2000) Culture of animal cells: a manual of basic technique. Forth Edition. Wiley-Liss.

Friedenstein AJ, Chailakhjan RK, Lalykina KS. (1970) The development of fibroblasts colonies in monolayer cultures of guinea-pig bone marrow and spleen cells. *Cell Tissue Kinet* 3, 393-403.

Friedenstein AJ, Deriglasova UF, Kulagina NN, Panasuk AF, Rudakowa SF, Luriá EA, Ruadkow IA. (1974) Precursors for fibroblasts in different populations of haematopoietic cells as detected by the in vitro colony assay method. *Exp Hematol* 2, 83-92.

Fröhlich M, Grayson WL, Wan LQ, Marolt D, Drobnic M, Vunjak-Novakovic G. (2008) Tissue engineered bone grafts: biological requirements, tissue culture and clinical relevance. *Curr Stem Cell Res Ther* 3(4), 254-264.

Fujita Y, Yamamuro T, Nakamura T, Kotani S. (1991) The bonding behaviour of calcite to bone. *J Biomed Mater Res* 25, 991-1003.

Galois L, Mainard D. (2004) Bone ingrowth into two porous ceramics with different pore sizes: an experimental study. *Acta Orthop Belg* 70, 598-603.

Geesink RGT. (2002) Osteoconductive coatings for total joint arthroplasty. *Clin Orthop Relat Res* 395, 53-65.

Geesink RGT, De Groot K, Klein CPAT. (1988) Bonding of bone to apatite-coated implants. *J Bone Joint Surg* 70B(1), 17-22.

Giannoudis PV, Tzioupis C. (2005) Clinical applications of BMP-7: the UK perspective. *Injury Int J Care Injured* 36S, S47-S50.

Gie GA, Linder L, Ling RS, Simon JP, Sloof TJ, Timperley AJ. (1993a) Impacted cancellous allografts and cement for revision total hip arthroplasty. *J Bone Joint Surg* 75B(1), 14-21.

Gie GA, Linder L, Ling RS, Simon JP, Sloof TJ, Timperley AJ. (1993b) Contained morselized allograft in revision total hip arthroplasty. Surgical technique. *Orthop Clin North Am* 24(4), 717-725.

Goldberg VM. (2000) Selection of bone grafts for revision total hip arthroplasty. *Clin Orthop Relat Res* 381, 68-76.

Goldstein SA. (2002) Tissue engineering: functional assessment and clinical outcome. *Ann N Y Acad Sci* 961, 183-192.

Gomes ME, Bossano CM, Johnston CM, Reis RL, Mikos AG. (2006a) In vitro localization of bone growth factors in constructs of biodegradable scaffolds seeded with marrow stromal cells and cultured in a flow perfusion bioreactor. *Tissue Eng* 12(1), 177-188.

Gomes ME, Holtorf HL, Reis RL, Mikos AG. (2006b) Influence of the porosity of starch-based fiber mesh scaffolds on the proliferation and osteogenic differentiation of bone marrow stromal cells cultured in a flow perfusion bioreactor. *Tissue Eng* 12(4), 801-809.

Goulet JA, Senunas LE, DeSilva GL, Greenfield MLVH. (1997) Autogenous iliac crest bone graft. *Clin Orthop Relat Res* 339, 76-81.

Grübl A, Chiari C, Gruber M, Kaider A, Gottsauner-Wolf F. (2002) Cementless total hip arthroplasty with a tapered, rectangular titanium stem and threaded cup: a minimum ten-year follow-up. *JBJS* 81-A(3), 425-431.

Guillemot F, Prima F, Bareille R, Gordin D, Gloriant T, Porté-Durrieu MC, Ansel D, Baquey C. (2004) Design of new titanium alloys for orthopaedic applications. *Med Biol Eng Comput* 42(1), 137-141.

Habibovic P, Barrère F, van Blitterswijk CA, de Groot K, Layrolle P. (2002) Biomimetic hydroxyapatite coating on metal implants. *J Am Ceram Soc* 85(3), 517-522.

Habibovic P, de Groot K. (2007) Osteoinductive biomaterials - properties and relevance in bone repair. *J Tissue Eng Regen Med* 1, 25-32.

Hallab N, Merritt K, Jacobs JJ. (2001) Metal sensitivity in patients with orthopaedic implants. *JBJS* 83-A(3), 428-436.

Hammond C. (2001) The basics of crystallography and diffraction. Oxford University Press.

Han Y, Fu T, Lu J, Xu K. (2001) Characterization and stability of hydroxyapatite coatings prepared by an electrodeposition and alkaline-treatment process. *J Biomed Mater Res* 54, 96-101.

Hara M, Murakami T, Kobayashi E. (2008) In vivo bioimaging using photogenic rats: fate of injected bone marrow-derived mesenchymal stromal cells. *J Autoimmunity* 30, 163-171.

Harper RA, Posner AS. (1966) Measurement of non-crystalline calcium phosphate in bone mineral. *Proc Soc Exp Biol Med* 122, 137-142.

Harris CT, Cooper LF. (2004) Comparison of bone graft matrices for human mesenchymal stem cell-directed osteogenesis. *J Biomed Mater Res* 68A, 747-755.

Harris WH. (1995) The problem is osteolysis. *Clin Orthop Relat Res* 311, 46-53.

Harris WH. (2001) Wear and periprosthetic osteolysis. *Clin Orthop Relat Res* 393, 66-70.

Harvey EJ, Bobyn JD, Tanzer M, Stackpool GJ, Krygier JJ, Hacking SA. (1999) Effect of flexibility of the femoral stem on bone-remodelling and fixation of the stem in a canine total hip arthroplasty model without cement. *JBJS* 81-A(1) 93-107.

Hayashi T. (1994) Biodegradable polymers for biomedical uses. *Prog Polym Sci* 19, 663-702.

Hayes WC, Bouxsein ML. (1997) Biomechanics of cortical and trabecular bone: implications for assessment of fracture risk. Second Edition. Lippincott-Raven Publishers, Philadelphia.

Haynesworth SE, Goshima J, Goldberg VM, Caplan AI. (1992) Characterization of cells with osteogenic potential from human marrow. *Bone* 13, 81-88.

Heath CA. (2000) Cells for tissue engineering. *Trends Biotech* 18, 17-19.

Heisel C, Silva M, Schmalzried TP. (2003) Bearing surface options for total hip replacement in young patients. *JBJS* 85A (7), 1366-1379.

Hilborn J, Bjursten LM. (2007) A new and evolving paradigm for biocompatibility. *J Tissue Eng Regen Med* 1, 110-119.

Hillsley MV, Frangos JA. (1994) Bone tissue engineering: the role of interstitial fluid flow. *Biotech Bioeng* 43, 573-581.

Hing KA. (2005) Bioceramic bone graft substitutes: influence of porosity and chemistry. *Int J Appl Ceram Technol* 2(3), 184-199.

Hing KA, Annaz B, Saeed S, Revell PA, Buckland T. (2005) Microporosity enhances bioactivity of synthetic bone graft substitutes. *J Mater Sci Mater Med* 16, 467-475.

Hing KA, Revell PA, Smith N, Buckland T. (2006) Effect of silicon level on rate, quality and progression of bone healing within silicate-substituted porous hydroxyapatite scaffolds. *Biomaterials* 27, 5014-5026.

Ho CY. (2011) Effects of stromal cell-derived factor-I on the differentiation of stem cells and their role in fracture healing. *Thesis* 1-159.

Holtorf HI, Sheffield TL, Ambrose CG, Jansen JA, Mikos AG. (2005) Flow perfusion culture of marrow stromal cells seeded on porous biphasic calcium phosphate ceramics. *Ann Biomed Eng* 33(9), 1238-1248.

Hu Y, Grainger DW, Winn SR, Hollinger JO. (2002) Fabrication of poly(alpha-hydroxy acid) foam scaffolds using multiple solvent systems. *J Biomed Mater Res* 59(3), 563-572.

Hulbert SF, Young FA, Mathews RS, Klawitter JJ, Talbert CD, Stelling FH. (1970) Potential of ceramic materials as permanently implantable skeletal prostheses. *J Biomed Mater Res* 4, 433-456.

Ikada Y. (2006) Tissue engineering: fundamentals and applications. First edition. Academic Press.

Jacobs JJ, Hallab NJ, Skipor AK, Urban RM. (2003) Metal degradation products: a cause for concern in metal metal bearings? *Clin Orthop* 417, 139-147.

Jäger M, Urselmann F, Witte F, Zanger K, Li X, Ayers DC, Krauspe R. (2008) Osteoblast differentiation onto different biometals with an endoprosthetic surface topography in vitro. *J Biomed Mater Res* 86A, 61-75.

Jaiswal N, Haynesworth SE, Caplan AI, Bruder SP. (1997) Osteogenic differentiation of purified, culture-expanded human mesenchymal stem cells in vitro. *J Cell Biochem* 64, 295-312.

Janssen FW, van Dijkhuizen-Radersma R, van Oorschot A, Oostra J, de Brujin JD, van Blitterswijk CA. (2010) Human tissue-engineered bone produced in clinically relevant amounts using a semi-automated perfusion bioreactor system: a preliminary study. *J Tissue Eng Regen Med* 4, 12-24.

Janssen FW, Oostra J, van Oorschot A, van Blitterswijk CA. (2006) A perfusion bioreactor system capable of producing clinically relevant volumes of tissue-engineered bone: In vivo bone formation showing proof of concept. *Biomaterials* 27, 315-323.

Javazon EH, Colter DC, Schwarz EJ, Prockop DJ. (2001) Rat marrow stromal cells are more sensitive to plating density and expand more rapidly from single-cell-derived colonies than human marrow stromal cells. *Stem Cells* 19, 219-225.

Kale S, Biermann S, Edwards C, Tarnowski C, Morris M, Long MW. (2000) Three-dimensional cellular development is essential for ex vivo formation of human bone. *Nature Biotechnology* 18, 954-958.

Kalyanaraman B, Supp DM, Boyce ST. (2008) Medium flow rate regulates viability and barrier function of engineered skin substitutes in perfusion culture. *Tissue Eng Part A* 14(5), 583-593.

Kang Q, Sun MH, Cheng H, Peng Y, Montag AG, Deyrup AT, Jiang W, Luu HH, Luo J, Szatkowski JP, Vanichakarn P, Park JY, Li Y, Haydon RC, He TC. (2004) Characterization of the distinct orthotopic bone-forming activity of 14 BMPs using recombinant adenovirus-mediated gene delivery. *Gene Therapy* 11, 1312-1320.

Karageorgiou V, Kaplan D. (2005) Porosity of 3D biomaterial scaffolds and osteogenesis. *Biomaterials* 26, 5474-5491.

Kasuga T, Maeda H, Kato K, Nogami M, Hata K, Ueda M. (2003) Preparation of poly(lactic acid) composites containing calcium carbonate (vaterite). *Biomaterials* 24, 3247-3253.

Kilpadi KL, Chang P, Bellis SL. (2001) Hydroxyapatite binds more serum proteins, purified integrins and osteoblast precursor cells than titanium or steel. *J Biomed Mater Res* 57, 258-267.

Kim S, Ahn K, Park MS, Lee J, Choi CY, Kim B. (2006) A poly(lactide-co-glycolide)/hydroxyapatite composite scaffold with enhanced osteoconductivity. *J Biomed Mater Res* 80A, 206-215.

Kim SS, Penkala R, Abrahimi P. (2007) A perfusion bioreactor for intestinal tissue engineering. *J Surgical Res* 1-5.

Knaack D, Goad MEP, Aiolova M, Rey C, Tofighi A, Chakravarthy P, Lee DD. (1998) Resorbable calcium phosphate bone substitute. *J Biomed Mater Res (Appl Biomater)* 43, 399-409.

Kohn DH, Sarmadi M, Helman JI, Krebsbach PH. (2002) Effects of pH on human bone marrow stromal cells in vitro: implications for tissue engineering of bone. *J Biomed Mater Res* 60, 292-299.

Kokubo T. (1998) Apatite formation on surfaces of ceramics, metals and polymers in body environment. *Acta Mater* 46(7), 2519-2527.

Kokubo T, Kim HM, Kawashita M, Nakamura T. (2001) Process of calcification on artificial materials. *Z Kardiol* 90(3), III/86-III/91.

Kokubo T, Kushitani H, Sakka S, Kitsugi T, Yamamuro T. (1990) Solutions able to reproduce in vivo surface-structure changes in bioactive glass-ceramic A-W. *J Biomed Mater Res* 24, 721-734.

Kruyt MC, Dhert WJA, Yuan H, Wilson CE, van Blitterswijk CA, Verbout AJ, de Brujin JD. (2004) Bone tissue-engineering in a critical size defect compared to ectopic implantations in the goat. *J Orthop Res* 22, 544-551.

Kuboki Y, Takita H, Kobayashi D, Tsuruga E, Inoue M, Murata M, Nagai N, Dohi Y, Ohgushi H. (1998) BMP-induced osteogenesis on the surface of hydroxyapatite with geometrically feasible and nonfeasible structures: topology of osteogenesis. *J Biomed Mater Res* 39(2), 190-199.

Lane JM. (2001) BMPs: why are they not in everyday use? *J Bone Joint Surg* 83, 161-162.

Langer R, Vacanti JP. (1993) Tissue engineering. *Science* 260, 920-926.

Lanza RP, Langer R, Vacanti J. (2000) Principles of tissue engineering. Second edition. Academic press.

Larsson C, Emanuelsson L, Thomsen P, Ericson LE, Aronsson BO, Kasemo B, Lausmaa J. (1997) Bone response to surface modified titanium implants-studies on the tissue response after 1 year to machined and electropolished implants with different oxide thicknesses. *J Materials Science: Materials in Medicine* 8, 721-729.

Larsson C, Thomsen P, Aronsson BO, Rodahl M, Lausmaa J, Kasemo B, Ericson LE. (1996) Bone response to surface modified titanium implants-studies on the early tissue response to machined and electropolished implants with different oxide thicknesses. *Biomaterials* 17, 605-616.

Le Blanc K, Pittenger MF. (2005) Mesenchymal stem cells: progress toward promise. *Cytotherapy* 7(1), 36-45.

Lee CH, Singla A, Lee Y. (2001) Biomedical applications of collagen. *International Journal of Pharmaceutics* 221, 1-22.

LeGeros RZ. (1993) Biodegradation and bioresorption of calcium phosphate ceramics. *Clinical Materials* 14, 65-88.

LeGeros RZ. (2008) Calcium phosphate-based osteoinductive materials. *Chem Rev* 108, 4742-4753.

Leopold SS, Jacobs JJ, Rosenberg AG. (2000) Cancellous allograft in revision total hip arthroplasty. *Clin Orthop Relat Res* 371, 86-97.

Levine B, Della Valle CJ, Jacobs JJ. (2006) Applications of porous tantalum in total hip arthroplasty. *J Am Acad Orthop Surg* 14, 646-655.

Levine BR, Sporer S, Poggie RA, Della Valle CJ, Jacobs JJ. (2006) Experimental and clinical performance of porous tantalum in orthopaedic surgery. *Biomaterials* 27, 4671-4681.

Li J, Liao H, Sjöström M. (1997) Characterization of calcium phosphates precipitated from simulated body fluid of different buffering capacities. *Biomaterials* 18, 743-747.

Li P, Kangasniemi I, de Groot K, Kokubo T. (1994) Bonelike hydroxyapatite induction by a gel-derived titania on a titanium substrate. *J. Am. Ceram. Soc.* 77, 1307-1312.

Lian JB, Stein GS. (1992) Concepts of osteoblast growth and differentiation: basis for modulation of bone cell development and tissue formation. *Crit Rev Oral Biol Med* 3(3), 269-305.

Ling RSM, Timperley AJ, Linder L. (1993) Histology of cancellous impaction grafting in the femur. *J Bone Joint Surg* 75B(5), 693-696.

Liu Y, Li JP, Hunziker EB, de Groot K. (2005) Incorporation of growth factors into medical devices via biomimetic coatings. *Phil Trans R Soc A* 364, 233-248.

Lopez-Heredia MA, Weiss P, Layrolle P. (2007) An electrodeposition method of calcium phosphate coatings on titanium alloy. *J Mater Sci Mater Med* 18, 381-390.

Ma J, Wong H, Kong LB, Peng KW. (2003) Biomimetic processing of nanocrystallite bioactive apatite coating on titanium. *Nanotechnology* 14, 619-623.

Maeda M, Hirose M, Ohgushi H, Kirita T. (2007) In vitro mineralization by mesenchymal stem cells cultured on titanium scaffolds. *J Biochem* 141, 729-736.

Mankani MH, Kuznetsov SA, Fowler B, Kingman A, Robey PG. (2001) In vivo bone formation by human bone marrow stromal cells: effect of carrier particle size and shape. *Biotechnol Bioeng* 72(1), 96-107.

Maquet V, Jerome R (1997) Design of macroporous biodegradable polymer scaffolds for cell transplantation. *Mater Sci Forum* 250, 15-42.

Martin I, Wendt D, Heberer M. (2004) The role of bioreactors in tissue engineering. *Trends in Biotechnology* 22(2), 80-86.

Matter P, Burch HB. (1990) Clinical experience with titanium implants, especially with the limited contact dynamic compression plate system. *Arch Orthop Trauma Surg* 109, 311-313.

McCarthy TL, Ji C, Chen Y, Kim KK, Imagawa M, Ito Y, Centrella R. (2000) Runt domain factor (Runx)-dependent effects on CCAAT/enhancer-binding protein delta expression and activity in osteoblasts. *J Biol Chem* 275, 21746-21753.

Moore WR, Graves SE, Bain GI. (2001) Synthetic bone graft substitutes. *ANZ J Surg* 71, 354-361.

Mygind T, Stiehler M, Baatrup A, Li H, Zou X, Flyvbjerg A, Kassem M, Bünger C. (2007) Mesenchymal stem cell ingrowth and differentiation on coralline hydroxyapatite scaffolds. *Biomaterials* 28, 1036-1047.

Nakamura K, Koshino T, Saito T. (1998) Osteogenic response of the rabbit femur to a hydroxyapatite thermal decomposition product-fibrin glue mixture. *Biomaterials* 19, 1901-1907.

Narasaraju TSB, Phebe DE. (1996) Some physico-chemical aspects of hydroxylapatite. *J Mater Sci* 31, 1-21.

Niinomi M. (2008) Mechanical biocompatibilities of titanium alloys for biomedical applications. *J Mechanical Behaviour Biomed Mater* 30-42.

Nishio K, Neo M, Akiyama H, Nishiguchi S, Kim HM, Kokubo T, Nakamura T. (2000) The effect of alkali-and heat-treated titanium and apatite-formed titanium on osteoblastic differentiation of bone marrow cells. *J Biomed Mater Res* 52(4), 652-661.

Nordström P, Pahjonen T, Törmälä P, Rokkanen P. (2002) Shear-load carrying capacities of the distal rat femora after osteotomy fixed with self-reinforced polyglycolic acid and poly-L-lactic acid pins. *J Mater Sci Mater Med* 13, 65-68.

Oh S, Oh N, Appleford M, Ong JL. (2006) Bioceramics for tissue engineering applications-a review. *A J Biochem & Biotechnol* 2(2), 49-56.

Ohgushi H, Dohi Y, Tamai S, Tabata S. (1993) Osteogenic differentiation of marrow stromal stem cells in porous hydroxyapatite ceramics. *J Biomed Mater Res* 27, 1401-1407.

Ohgushi H, Dohi Y, Katuda T, Tamai S, Tabata S, Suwa Y. (1996) In vitro bone formation by rat marrow cell culture. *J Biomed Mater Res* 32, 333-340.

Ohgushi H, Dohi Y, Yoshikawa T, Tamai S, Tabata S, Okunaga K, Shibuya T. (1996) Osteogenic differentiation of cultured marrow stromal stem cells on the surface of bioactive glass ceramics. *J Biomed Mater Res* 32, 341-348.

Oliveira AL, Malafaya PB, Reis RL. (2003) Sodium silicate gel as a precursor for the in vitro nucleation and growth of a bonelike apatite coating in compact and porous polymeric structures. *Biomaterials* 24(15), 2575-2584.

Oreffo ROC, Driessens FCM, Planell JA, Triffitt JT. (1998) Growth and differentiation of human bone marrow osteoprogenitors on novel calcium phosphate cements. *Biomaterials* 9, 1845-1854.

Osathanon T, Linnes ML, Rajachar RM, Ratner BD, Somerman MJ, Giachelli CM. (2008) Microporous nanofibrous fibrin-based scaffolds for bone tissue engineering. *Biomaterials* 29, 4091-4099.

Palmer LC, Newcomb CJ, Kaltz SR, Spoerke ED, Stupp SI. (2008) Biomimetic systems for hydroxyapatite mineralization inspired by bone and enamel. *Chem Rev* 108, 4754-4783.

Pastoureau PME, Arlot F, Caulin JP, Barier JP, Meunier PJ, Delmas PD. (1989) Effects of oophorectomy on biochemical and histological indices of bone turnover in ewes. *J Bone Miner Res* 4, 237.

Pearce AI, Richards RG, Milz S, Schneider E, Pearce SG. (2007) Animal models for implant biomaterial research in bone: a review. *Eur Cells Mat* 13, 1-10.

Peister A, Mellad JA, Larson BL, Hall BM, Gibson LF, Prockop DJ. (2004) Adult stem cells from bone marrow (MSCs) isolated from different strains of inbred mice vary in surface epitopes, rates of proliferation and differentiation potential. *Blood* 103, 1662-1668.

Petite H, Viateau V, Bensaid W, Meunier A, de Pollak C, Bourguignon M, Oudina K, Sedel L, Guillemin G. (2000) Tissue-engineered bone regeneration. *Nature Biotechnology* 18, 959-963.

Petrakova KV, Tolmacheva AA, Friedenstein AJ. (1963) Bone formation occurring in bone marrow transplantation in diffusion chambers. *Biull Eksp Biol Med* 56, 87.

Pittenger MF, Mackay AM, Beck SC, Jaiswal RK, Douglas R, Mosca JD, Moorman MA, Simonetti DW, Craig S, Marshak DR. (1999) Multilineage potential of adult human mesenchymal stem cells. *Science* 284, 143-147.

Platt JL. (1996) The immunological barriers to xenotransplantation. *Crit Rev Immunol* 16(4), 331-358.

Pongkao Kashima D, Rakngarm A. (2008) Calcium phosphate film coating on titanium substrate by electrochemical deposition. *J Metals Materials Minerals* 18(1), 27-31.

Ponsonnet L, Reybier K, Jaffrezic N, Comte V, Lagneau C, Lissac M, Martelet C (2003) Relationship between surface properties (roughness, wettability) of titanium and titanium alloys and cell behaviour. *Mater Sci Eng* 23(4), 551-560.

Porter AE. (2006) Nanoscale characterization of the interface between bone and hydroxyapatite implants and the effect of silicon on bone apposition. *Micron* 37, 681-688.

Posner AS. (1969) Crystal chemistry of bone mineral. *Physiological Reviews* 49(4), 760-792.

Predecki P, Stephan JE, Auslander BA. (1972) Kinetics of bone growth into cylindrical channels in aluminium oxide and titanium. *J Biomed Mater Res* 6, 375-400.

Rago R, Mitchen J, Wilding G. (1990) DNA Fluorometric assay in 96-well tissue culture plates using Hoechst 33258 after cell lysis by freezing in distilled water. *Analytical Biochemistry* 191, 31-34.

Redepenning J, McIsaac JP. (1990) Electrocrystallization of brushite coatings on prosthetic alloys. *Chem Mater* 2(6), 627-629.

Redepenning J, Schlessinger T, Burnham S, Lippiello L, Miyano J. (1996) Characterization of electrolytically prepared brushite and hydroxyapatite coatings on orthopaedic alloys. *J Biomed Mater Res* 30, 287-294.

Redepenning J, Venkataraman G, Chen J, Stafford N. (2003) Electrochemical preparation of chitosan/hydroxyapatite composite coatings on titanium substrates. *J Biomed Mater Res* 66A, 411-416.

Ripamonti U, Richter PW, Nilen RWN, Renton L. (2008) The induction of bone formation by smart biphasic hydroxyapatite tricalcium phosphate biomimetic matrices in the non-human primate Papio ursinus. *J Cell Mol Med* 12(6B), 2609-2621.

Rivero DP, Fox J, Skipor AK, Urban RM, Galante JO. (1988) Calcium phosphate-coated porous titanium implants for enhanced skeletal fixation. *J Biomed Mater Res* 22, 191-201.

Rocha LB, Goissis G, Rossi MA. (2002) Biocompatibility of anionic collagen matrix as scaffold for bone healing. *Biomaterials* 23, 449-456.

Rose FRAJ, Oreffo ROC. (2002) Bone tissue engineering: hope vs hype. *Biochem Biophys Res Commun* 292, 1-7.

Rubin PJ, Yaremchuck MJ. (1997) Complications and toxicities of implantable biomaterials used in facial reconstructive and aesthetic surgery: a comprehensive review of the literature. *Plast Reconstr Surg* 100(5), 1336-1353.

Rubin R, Strayer DS. (2007) Rubin's pathology: clinicopathologic foundations of medicine. Fifth edition. Lippincott Williams & Wilkins.

Rust PA. (2003) Human mesenchymal stem cells for tissue engineering bone. *Thesis* 1- 298.

Sachlos E, Czernuszka JT. (2003) Making tissue engineering scaffolds work: review on the application of solid freeform fabrication technology to the production of tissue engineering scaffolds. *European Cells and Materials* 5, 29-40.

Salgado AJ, Coutinho OP, Reis RL. (2004) Bone tissue engineering: state of the art and future trends. *Macromol Biosci* 4, 743-765.

Salgado CL, Turchetti-Maia RMM, Pereira MM, Salas CE, Francischi JN, Lopes MTP. (2006) Evaluation of biocompatibility for porous bioactive glass scaffolds. *Key Eng Mater* 309-311, 1035-1038.

Samizadeh S. (2010) Bone formation of calcium phosphate bone substitute materials. *Thesis* 1-205.

Santavirta S, Konttinen YT, Saito T, Grönblad M, Partio E, Kemppinen P, Rokkanen P. (1990) Immune response to polyglycolic acid implants. *J Bone Joint Surg Br* 72, 597-600.

Santoni BG, Hynes RA, McGilvray KC, Rodriguez-Canessa G, Lyons AS, Henson MAW, Womeck WJ, Puttlitz CM. (2009) Cortical bone trajectory for lumbar pedicle screws. *The Spine Journal* 9(5), 366-373.

Schieker M, Seitz H, Drosse I, Seitz S, Mutschler W. (2006) Biomaterials as scaffolds for bone tissue engineering. *European Journal of Trauma* 2, 114-124.

Schliephake H, Neukam FW. (1991) Bone replacement with porous hydroxyapatite blocks and titanium screw implants. *J Oral Maxillofac Surg* 49, 151-156.

Schliephake H, Neukam FW, Klosa D. (1991) Influence of pore dimensions on bone ingrowth into porous hydroxyapatite blocks used as bone graft substitutes. A histometric study. *Int J Oral Maxillofac Surg* 20, 53-58.

Schuh A, Luyten J, Vidael R, Hönle W, Schmickal T. (2007) Porous titanium implant materials and their potential in orthopaedic surgery. *Mat-wiss u Werkstofftech* 38(12), 1015-1018.

Sensebé L, Krampera M, Schrezenmeier H, Bourin P, Giordano R. (2010) Mesenchymal stem cells for clinical application. *Vox Sanguinis* 98, 93-107.

Shen Z, Crotti TN, McHugh KP, Matsuzaki K, Gravallese EM, Bierbaum BE, Goldring SR. (2006) The role played by cell-substrate interactions in the pathogenesis of osteoclast-mediated peri-implant osteolysis. *Arthritis Research and Therapy* 8(R70).

Sikavitsas V, Bancroft GN, Holtorf HL, Jansen JA, Mikos AG. (2003) Mineralized matrix deposition by marrow stromal osteoblasts in 3D perfusion culture increases with increasing fluid shear forces. *PNAS* 100(25), 14683-14688.

Sikavitsas V, Bancroft GN, Lemoine JL, Liebschner MA, Dauner M, Mikos AG. (2005) Flow perfusion enhances the calcified matrix deposition of marrow stromal cells in biodegradable nonwoven fiber mesh scaffolds. *Ann Biomed Eng* 33(1), 63-70.

Sikavitsas V, Bancroft GN, Mikos AG. (2002) Formation of three-dimensional cell/polymer constructs for bone tissue engineering in a spinner flask and a rotating wall vessel bioreactor. *J Biomed Mater Res* 62, 136-148.

Sikavitsas V, Temenoff JS, Mikos AG. (2001) Biomaterials and mechanotransduction. *Biomaterials* 22, 2581-2593.

Skoglund B, Aspenberg P. (2003) PMMA particles and pressure: a study of the osteolytic properties of two agents proposed to cause prosthetic loosening. *J Orthop Res* 21, 196-201.

Sloof TJJH, Huiskes R, van Horn J, Lemmens AJ. (1984) Bone grafting in total hip replacement for acetabular protrusion. *Acta Orthop Scand* 55, 593-596.

Suryanarayana X and Grant Norton M. (1998) X ray diffraction: a practical approach. Plenum Press, New York.

Svehla M, Morberg P, Zicat B, Bruce W, Sonnabend D, Walsh WR. Morphometric and mechanical evaluation of titanium implant integration: comparison of five surface structures. *J Biomed Mater Res* 51(1), 15-22.

Tisdel CL, Goldberg VM, Parr JA, Bensusan JS, Staikoff LS, Stevenson S. (1994) The influence of a hydroxyapatite and tricalcium-phosphate coating on bone growth into titanium fiber-metal implants. *JBJS* 76-A(2), 159-171.

Tiselius A, Hjertén S, Levin Ö. (1956) Protein chromatography on calcium phosphate columns. *Archives of Biochemistry and Biophysics* 65(1), 132-155.

Toma JG, Akhavan M, Fernandes KJL, Barnabé-Heider F, Sadikot A, Kaplan DR, Miller FD. (2001) Isolation of multipotent adult stem cells from the dermis of mammalian skin. *Nature Cell Biology* 3, 778-784.

Ullmark G, Linder L. (1998) Histology of the femur after cancellous impaction grafting using a Charnley prosthesis. *Arch Orthop Trauma Surg* 117, 170-172.

Unger AS, Lewis RJ, Gruen T. (2005) Evaluation of a porous tantalum uncemented acetabular cup in revision total hip arthroplasty: clinical and radiological results of 60 hips. *J Arthroplasty* 20(8), 1002-1009.

Urist MR. (1965) Bone: formation by autoinduction. *Science* 150(698), 893-899.

Urist MR. (2002) The classic. Bone: formation by autoinduction. *Clin Orthop Relat Res* 395, 4-10.

Urist MR, DeLange RJ, Finerman GAM. (1983) Bone cell differentiation and growth factors. *Science* 220(4598), 680-686.

Urist MR, Huo YK, Brownell AG, Hohl WM, Buyske J, Lietze A, Tempst P, Hunkapiller M, DeLange RJ. (1984) Purification of bovine bone morphogenetic protein by hydroxyapatite chromatography. *Proc Natl Acad Sci* 81, 371-375.

Vaccaro AR. (2002) The role of the osteoconductive scaffold in synthetic bone graft. *Orthopaedics* 25(5 Suppl), S571-578.

Verfaillie CM. (2002) Adult stem cells: assessing the case for pluripotency. *Trends Cell Biol* 12(11), 502-508.

Vitte J, Benodiel AM, Pierres A, Bongrand P (2004) Is there a predictable relationship between surface physical-chamical properties and cell behaviour at the interface? (2004*) Eur Cells Mater* 7, 52-63.

Vrouwenvelder WCA, Groot CG, de Groot K. (1993) Histological and biochemical evaluation of osteoblasts cultured on bioactive glass, hydroxylapatite, titanium alloy and stainless steel. *J Biomed Mater Res* 27, 465-475.

Vunjak-Novakovic G, Freed LE, Biron RJ, Langer R. (1996) Effects of mixing on the composition and morphology of tissue-engineered cartilage. *AIChE J* 42, 850-860.

Wang J, de Boer J, de Groot K. (2004) Preparation and characterization of electrodeposited calcium phosphate/chitosan coating on Ti6Al4V plates. *J Dent Res* 83(4), 296-301.

Wang Y, Uemura T, Dong J, Kojima H, Tanaka J, Tateishi T. (2003) Application of perfusion culture system improves in vitro and in vivo osteogenesis of bone marrow-derived osteoblastic cells in porous ceramic materials. *Tissue Eng* 9(6), 1205-1214.

Weiβenböck M, Stein E, Undt G, Ewers R, Lauer G, Turhani D. (2006) Particle size of hydroxyapatite granules calcified from red algae affects the osteogenic potential of human mesenchymal stem cells in vitro. *Cells Tissues Organs* 182, 79-88.

Weiner S, Wagner HD. (1998) The material bone: structure-mechanical function relations. *Annu Rev Mater Sci* 28, 271-298.

Wobus AM. (2001) Potential of embryonic stem cells. *Molecul Aspect Med* 22, 149-164.

Wolff D, Goldberg VM, Stevenson S. (1994) Histomorphometric analysis of the repair of a segmental diaphyseal defect with ceramic and titanium fibermetal implants: effects of bone marrow. *J Orthop Res* 12, 439-446.

Wopenka B, Pasteris JD. (2005) A mineralogical perspective on the apatite in bone. *Materials Science and Engineering* C25, 131-143.

Wozney JM, Rosen V, Celeste AJ, Mitsock LM, Whitters MJ, Kriz RW, Hewick RM, Wang EA. (1988) Novel regulators of bone formation: molecular clones and activities. *Science* 242(4885), 1528-1534.

Yamashita K, Yagi T, Umegaki T. (1996) Bonelike coatings onto ceramics by reactive magnetron sputtering. *J Am Ceram Soc* 79(12), 3313-3316.

Yang S, Leong KF, Du Z, Chua CK. (2001) The design of scaffolds for use in tissue engineering. Part I. Traditional factors. *Tissue Eng* 7(6), 679-689.

Yang XB, Roach HI, Clarke NM, Howdle SM, Quirk R, Shakesheff KM, Oreffo ROC. (2001) Human osteoprogenitor growth and differentiation on synthetic biodegradable structures after surface modification. *Bone* 29, 523-531.

Yang Y, Park S, Liu Y, Lee K, Kim H, Koh J, Meng X, Kim K, Ji H, Wang X, Ong JL. (2009) Development of sputtered nanoscale titanium oxide coating on osseointegrated implant devices and their biological evaluation. *Vaccum* 83, 569-574.

Yoon ST, Boden SD. (2002) Osteoinductive molecules in orthopaedics: basic science and preclinical studies. *Clin Orthop* 395, 33-43.

Yoon ST, Boden SD. (2004) Spine fusion by gene therapy. *Gene Therapy* 11, 360-367.

Young B, Lowe JS, Stevens A, Heath JW. (2006) Wheater's functional histology. A text and colour atlas. Fifth edition. Elsevier.

Yuan H, Yang Z, Li Y, Zhang X, De Brujin JD, De Groot K. (1998) Osteoinduction by calcium phosphate biomaterials. *J Mater Sci Mater Med* 9, 723-726.

Zhang Q, Chen J, Feng J, Cao Y, Deng C, Zhang X. (2003) Dissolution and mineralisation behaviours of HA coatings. *Biomaterials* 24, 4741-4748.

Zhang X, Zhou P, Zhang J, Chen W, Wu CA. (1992) Bioceramics and the human body, p408. Elsevier Applied Science, London.

Zhao F, Chella R, Ma T. (2007) Effects of shear stress on 3D human mesenchymal stem cell construct development in a perfusion bioreactor system: experiments and hydrodynamic modelling. *Biotechnol Bioeng* 96(3), 584-595.

Zhao F, Ma T. (2005) Perfusion bioreactor system for human mesenchymal stem cell tissue engineering: dynamic cell seeding and construct development. *Biotechnol Bioeng* 91(4), 482-493.

CONFERENCE PRESENTATIONS:

"Comparison of mesenchymal stem cells proliferation and differentiation between biomimetic and electrochemical coatings on different topographic surface" Garcia E, Hua J, Blunn G. TERMIS 2nd World Congress – September 2009, Seoul (South Korea).

"Effect of different calcium-phosphate coatings on different surfaces of titanium and tantalum on proliferation and differentiation of mesenchymal stem cells" Garcia E, Hua J, Blunn G. 56th Annual Meeting of the Orthopaedic Research Society - March 2010, New Orleans (Louisiana, USA).

"Electrochemical and biomimetic calcium-phosphate coatings on metal implants: how do they affect mesenchymal stem cells proliferation and differentiation?" Garcia E, Hua J, Blunn G. Surface Modification and Functionalization of Materials for Biomedical Applications BIOCOAT 2010 – June 2010, Zaragoza (Spain).

"Development of tissue-engineered bone constructs using a perfusion bioreactor system" Garcia E, Hua J, Rayan F, Blunn G. 57th Annual Meeting of the Orthopaedic Research Society - January 2011, Long Beach (California, USA).

"A perfusion bioreactor system for the development of tissue-engineered bone constructs" Garcia E, Hua J, Rayan F, Blunn G. TERMIS EU 2011 Annual Meeting - June 2011, Granada (Spain).